UNIVERSITY OF SOUTHAMPTON

FACULTY OF ENGINEERING, SCIENCE & MATHMATICS

School of Chemistry

Exploring the Influence of Structural Variation on the Solution and Solid-State Behaviour of Cyanine Dyes

By

Georgina Louise Hallworth

Thesis for the degree of Doctor of Philosophy

July 2008

UNIVERSITY OF SOUTHAMPTON

ABSTRACT

FACULTY OF ENGINEERING, SCIENCE & MATHMATICS

SCHOOL OF CHEMISTRY

Doctor of Philosophy

EXPLORING THE INFLUENCE OF STRUCTURAL VARIATION ON THE SOLUTION AND SOLID-STATE BEHAVIOUR OF CYANINE DYES

By Georgina Louise Hallworth

Cyanine dyes are well known and extensively studied molecules. The preparations and investigations of a wide range of dyes have been previously reported. Here several novel and known compounds have been synthesised to investigate the effect molecular structure has on their bulk-solution and solid-state behaviour. The preparations of sulfur-containing tri- and monomethine dyes were more reliable, hence the majority of these studies concerned sulfur analogues. Successful crystallisation of these products resulted in many novel crystal structures being obtained and compared. The monomethine dyes provided a simple, systematic study which could be analysed revealing relationships between the structures. The trimethine x-ray structural studies were less systematic but more varied. Despite many more structures being required, it appears that the prediction of packing structures may be possible from the molecular structure.

In aqueous solution cyanine dyes are known to form supramolecular-type aggregates with and without the presence of inorganic salts. The aggregation process of several trimethine dyes was found to be accelerated by the anion of inorganic salts with di- and trivalent anions being more efficient than monovalent anions. Simple oxygen containing dyes were found not to aggregate even in the presence of salts, this suggests that the heteroatom has a crucial role in the aggregation process. The aggregation process was affected by molecular structure but these effects were not noticeable when concerned with the fluorescence yield.

Electronic Lab Notebooks (ELN) have become successful in commercial companies but less so in academia. An ELN package designed primarily for use in a university research environment has been newly developed. This project involved trailing this product to test the system and provide feedback about the use. Several issues were recognized to affect the way the package functioned, but areas where improvements could be made were identified.

Contents

i. List of Tables

ii. List of Schemes

iii. List of Figures

.

iv. Acknowledgements

Firstly I would like to thank Martin and Jeremy for their supervision, guidance and optimism throughout this project. Next, thanks to all the Frey and Grossel group members past and present for their advice, company and chatter in the lab. Members including Chris, Dan, Polski, James, Alex, Franchesco, Jon, Andrew, Alan, Jamie and Wendy have all had a part to play in this PhD. Special thanks should go to Pete Horton and Alex Johnston; Pete for his constant help and patience with my many X-ray crystallography questions and problems, and Alex for all his support and proof reading.

I would also like to thank Neil Wells and Joan Street for their NMR help, John Langley and Julie Herniman for the Mass Spectrometry service upon which I relied, the entire X-ray crystallography group and Carl and the stores team for their friendly chatter and superb supply of stuff. Without these people the work would have been a lot more testing.

Finally I would like to thank all my family and friends whose unconditional love and support has carried me through. Mum, Dad, John and extended family for always being behind me a hundred percent. Simon for having a large part in my life but providing me with enough space to focus my attention. Sally for going through this with me day-to-day, sharing the ups and downs and being a great flatmate. Other friends including Becky, Claire, Laura, Rachel G, Caryl and Rachel T whose chatter and laughter at the end of the day was always very welcome.

v. Abbreviations

Solvents and Reagents

Methanol	MeOH
Acetonitrile	MeCN
Dichloromethane	DCM
Anhydrous sodium sulphate	Na_2SO_4
Deuterated chloroform	$CDCl_3$
Deuterated DMSO	DMSO-d_6
Deuterium oxide	D_2O
Deuterated methanol	d^4-MeOH
Diethyl ether	Ether
7,7',8,8'-Tetracyano-*p*-quinodimethane	TCNQ
Cyclodextrin	CD
Cucurbituril	CB

Miscellaneous

Room temperature	RT
Melting point	MP
Thin layer chromatography	TLC
Ultra violet and visible spectroscopy	UV-vis
Nuclear magnetic resonance spectroscopy	NMR
Singlet	s
Doublet	d
Triplet	t
Multiplet	m
Low resolution mass spectrometry	LRMS
High resolution mass spectrometry	HRMS
Electrospray	ES
Mass-to-charge ratio	m/z
Infrared spectroscopy	IR
Infra-red intensity: strong, medium, weak, broad	(s), (m), (w), (br)
Ultra-violet	UV
Electronic Laboratory Notebook	ELN

Chapter 1

Introduction

1.1 Supramolecular Chemistry

Supramolecular chemistry is a relatively modern area of chemistry which looks at the interactions between covalently and non-covalently linked molecules, incorporating aspects of organic, inorganic and bio-chemistry[1]. Some of the most commonly known supramolecular molecules include the mechanical rotaxanes and catenanes and the metal-binding crown-ethers, Figure 1.1. The properties and basic principles of these molecules range from selectively binding metal ions from mixed solution to being used as the basic components for molecular machines[1].

Supramolecular chemistry considers the behaviour of molecules both in solution and in the solid-state. The behaviour of a system can be very different in the solid-state compared with solution, making it important to study how the molecules behave in both phases and to find links between the two. Molecules such as porphyrins[2, 3] and dyes (including cyanine dyes) are known to self-associate (self-aggregate)[4], into supramolecular assemblies[5] in bulk solution with the resulting aggregates being thought of as intermediates between single molecules and bulk phases. This therefore makes them ideal models to study the effect of physical property changes both on the individual molecule and of their bulk property behaviour[6].

The study of supramolecular organised functional dyes is an essential part of miniaturising optoelectronic devices since they can then be fabricated on the basis of the bottom-up approach[7]. The bottom-up approach concerns the molecules that arrange themselves into more complex assemblies by looking at the interactions that cause spontaneous effects such as self-organisation (a modern research topic of particular interest). By using this approach greater understandings of the molecular properties can be achieved, leading to the potential of more devices[8]. Chromophores are ideal probes for the investigation of such effects because self-organisation generally corresponds to an electronic change and is accompanied by a characteristic alteration seen in UV-Visible spectroscopy.[9]

a)

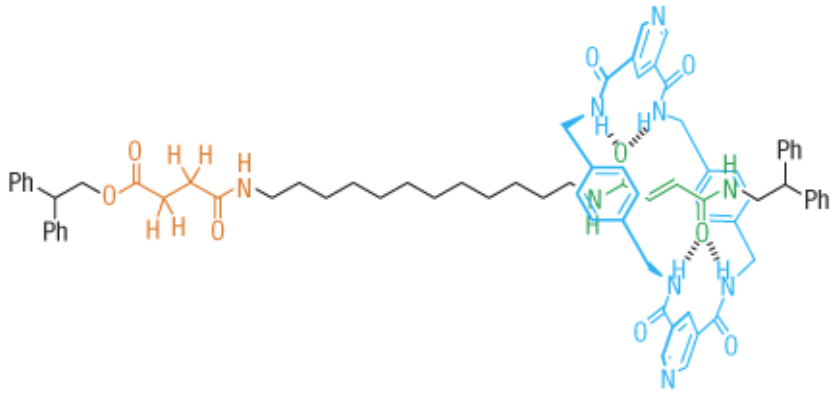

b)

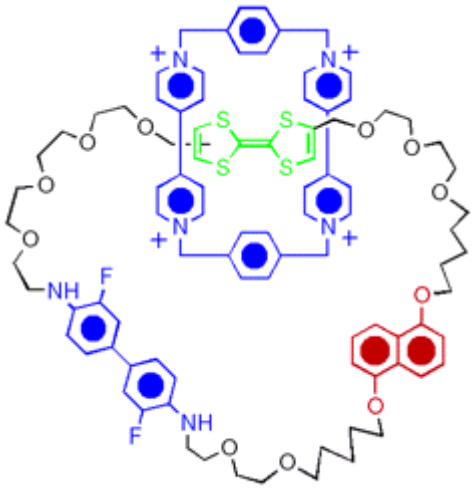

c)

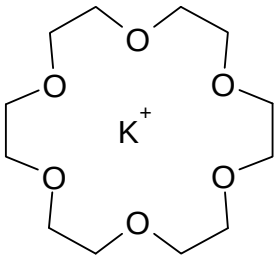

Figure 1.1. Examples of supra molecules. a) rotaxane[9.a] b) catenanes[10] c) crown ethers (18-crown-6). Molecules a and b have moving components which are ideal, if they can be controlled, for use in molecular motors and machines.

1.2 Cyanine dyes

Williams discovered the first cyanine dye, **1**, in 1856 other dyes soon followed with **2** being discovered in 1887 (initially thought to be a monomethine dye)[11]. It was only in the early 1900's that cyanine dyes were well recognised, mainly due to their aggregation properties[4].

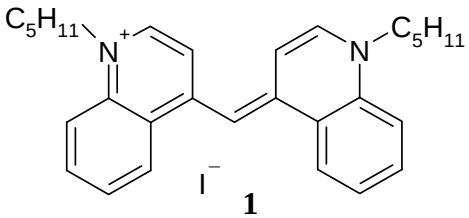

1

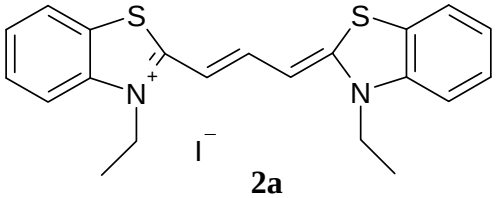

2a

Cyanine dyes have a general structure as shown in Figure 1.2 where two nitrogen atoms are separated by a methine chain of varying length. The positive charge on one nitrogen is delocalised through the methine chain to the other nitrogen[12]. The conjugated nature of this motif (and therefore the chromophore) remain even for a large number of double bonds.[11] The cyanine dyes commonly reported in literature are mono-, tri- and pentamethines. The conjugated nature of cyanine dyes result in intensely coloured crystals and solutions, Figure 1.3. Ironically, despite their name, they are not used for dying processes as they tend to break down in the presence of light[4] with aqueous solutions being particularly unstable in light because of the formation of aggregates which absorb at lower wavelengths[13]. The types of dyes presented in this thesis are symmetrical cyanine dyes, shown in Figure 1.2a.

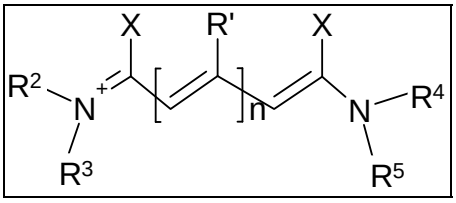

Figure 1.2. A generalised cyanine dye

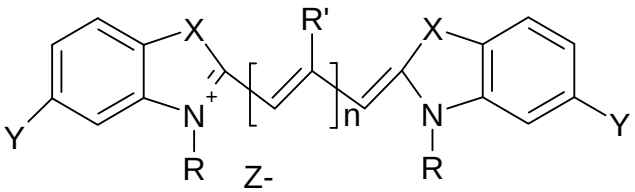

Figure 1.2a. A typical cyanine dye where:

X= O, N, Se, Si

R= alkyl group

R'= H, alkyl group

n= 0-3

Figure 1.3. The effect of small structural changes on the colour of these commercially available dyes

In 1936 Schiebe[14] and Jelly[15] independently discovered that cyanine dyes had very important aggregation properties. It was noticed that there was a dramatic change in the absorbance, with the λ_{max} shifting to the red end of the spectrum and the peak sharpening being attributed to the formation of a J-aggregate. A J-aggregate occurs in bulk solution when the dyes associate forming slipped stacks with an angle of slippage, α, $<32^{o}$, Figure 1.4. The angle of slippage is defined as the angle between a line joining centres of a column of dye molecules and the long axis of any one of the parallel molecules.

a) b)

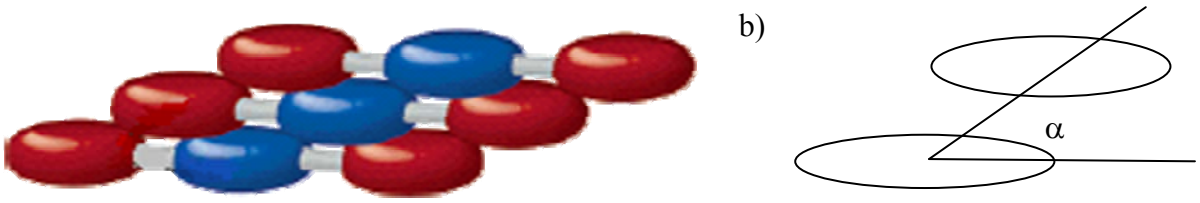

Figure 1.4. a) A cartoon representation of symmetrical cyanine dyes stacking in a J-aggregate[16] b) Schematic representation of cyanine dyes and how they stack resulting in a J-aggregate showing the angle of slip(α).

It was realised that certain dyes formed J-aggregates on the surface of silver halide crystals. Silver halides are only sensitive to blue light but the aggregates that form on the surfaces act like an antenna for the AgX crystals in the film[17]. The aggregates that formed on the AgX surfaces impart light sensitivity to the silver halide emulsions[4] and made these dyes ideal for use in photography by acting as a sensitizer to make film panchromatic. In more recent years cyanine dyes have been used for light harvesting, charge separation steps in photosynthesis and technological applications in terms of their structural and optical properties[18, 19].

The way that the dyes stack in solution defines which type of aggregate is formed. When the shallow stacks of dyes are formed, where $\alpha>32°$, the aggregates are known as H-aggregates[4]. H-aggregates result in an absorbance that is shifted to the blue end of the spectrum compared to the monomer. H-aggregation is thought to occur when the dyes that are aggregating are stacked one on top of another with only a small amount of slippage, as shown in Figure 1.5. These models for the J- and H-aggregates are widely accepted in the literature, however many of these models are based on indirect evidence such as X-ray structural studies of crystals [12].

Whilst all cyanine dyes are very similar in their basic structure, minor changes, such as modifying the aromatic rings, altering the carbon atoms linking the chromophores and introducing different counter ions, all alter the properties of the dyes in different ways including the absorption and aggregation properties.

a) 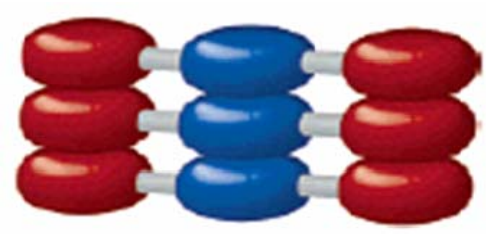 b) 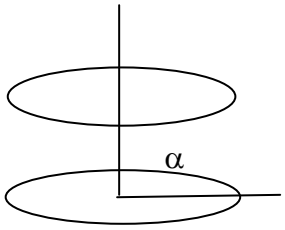

Figure 1.5. a) A cartoon representation of symmetrical cyanine dyes stacking in H-aggregate[16]. b) Schematic representation of cyanine dyes and how they stack showing angle of slip for a H-aggregate

Symmetrical cyanine dyes have high extinction coefficients[20] and typically a main absorbance with a shoulder on the shorter wavelength side, Figure 1.6. In dilute or alcoholic solutions, where aggregation is minimised, the shoulder on the shorter wavelength side of the main absorption band is considered to be the result of different vibronic transitions i.e. one absorbance being caused by the 0-0 transition and the other absorbance by the 0-1 transition[13]. Another suggested explanation is that stereoisomers are responsible for the two absorbances[21,22]. Suhyun *et al.*[22] describe how the two absorbances are a result of the syn- and anti- isomers of the cyanine dye under investigation, Figure 1.7.

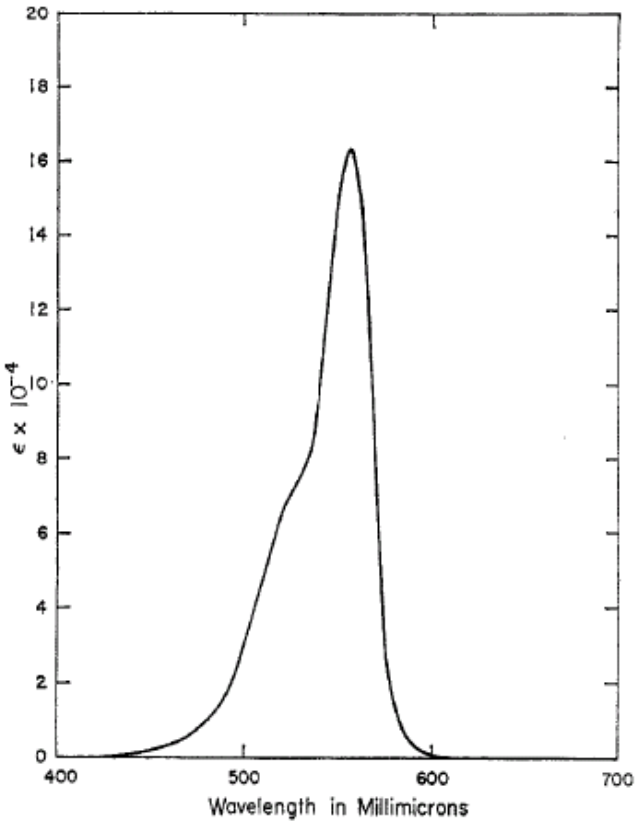

Figure 1.6 [13]. A plot of a typical UV-visible absorption of a cyanine dye. In this case it is the monomeric absorption of 3,3'-diethylbenzothiacarbocyanine p-toluenesulfonate, ***3b****, in MeOH.*

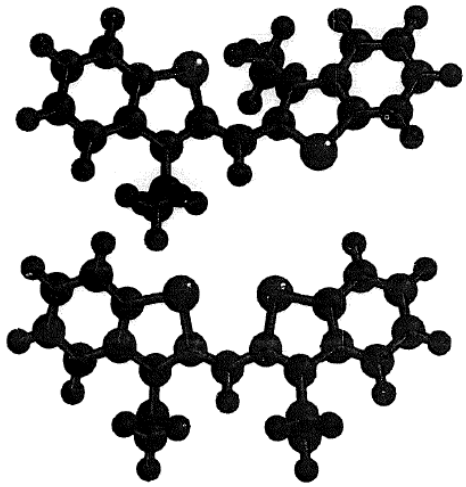

Figure 1.7. [22] Ball and stick representations of the cationic component of the monomethine dye which Suhyun et al. used to carry out their investigations of the anti- (above) and syn- isomers (below).

1.3 Aggregation Behaviour of Cyanine Dyes

Jelley *et al.*[15] showed that increasing the concentration of aqueous solutions containing cyanine dyes resulted in changes in the absorption spectra of the solution. A new, narrow, significantly red shifted peak was observed and attributed to the formation of J-aggregates. Many workers have since observed both this and other aggregation effects leading to extensive studies into the properties of J-aggregates because of their commercial value. H-aggregates have also become commercially more important in recent years. Figure 1.8 shows the change in the UV-visible spectrum of **6** as a result of the different aggregates formed in solution. The monomeric absorption is known as the M-band, dimers (the most simple aggregate) result in the appearance of the D-band and H- and J- aggregates result in H- and J-bands respectively. J-Aggregation leads to a shift towards the red and H-aggregates lead to a shift towards the blue[4].

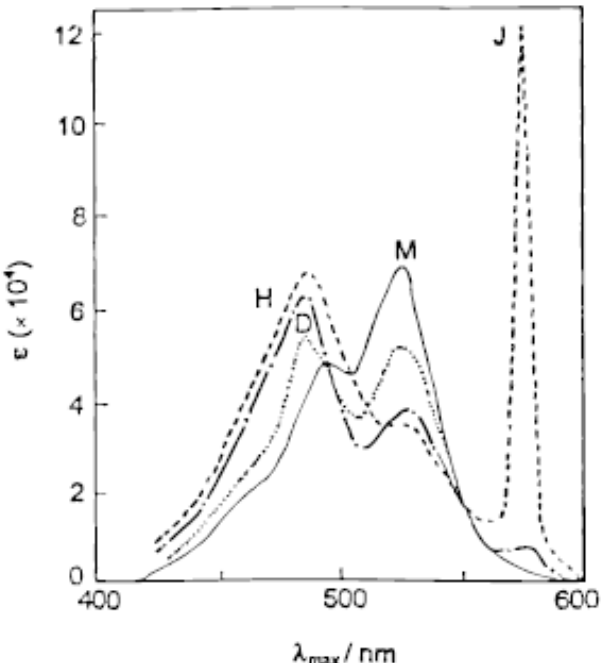

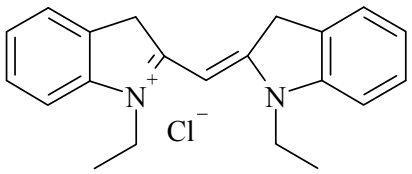

6

Figure 1.8[4]*. Absorption spectra of an aqueous solution of* ***6*** *at 25°C. H-band = H-shift, J-band= J-shift, M-band= absorption of the monomer, D-band= absorption of a dimer.*

It is the electronic coupling of the dye monomers within the aggregate which is thought to cause the distinct changes in their absorption band when compared to the monomeric species[4]. The aggregation process is driven by several factors, although there is much debate as to what is the dominating influence. The hydrophobic nature

of the molecular frame[23] is believed to be a major driving force. However, Harrison *et al.* have reported that aggregation is driven by intermolecular interactions because of short-range intermolecular attractive forces involving σ and π electrons and not the hydrophobic effect[12]. The fact that other dyes such as rhodamine 6G, Figure 1.9, also exhibit aggregation properties suggests that the factors that determine the association of the dyes are roughly independent of the structural details of the chromophore components[24].

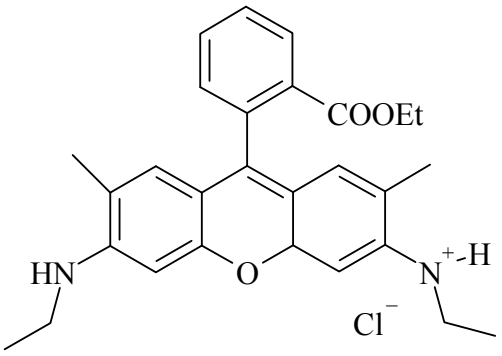

Figure 1.9. Structure of rhodamine 6G. This dye aggregates in bulk solution.

The aggregation of cyanine dyes can be controlled/determined by a range of factors including temperature[25], solvent[26], the presence and charge of metal ions[25] and dye structure[27].

Structure: The way that the molecules stack determines which type of aggregate occurs which is ultimately governed by the interactions formed and the shape of the dye. By substituting different groups into the basic structure (Figure 1.2a), the shape of the molecule can be altered which results in a degree of control of the favoured packing of these structures and hence their aggregation. To date, a huge library of cyanine dyes have already been prepared and studied [28], the main observations of these compounds are as following:

- Most structural variation arises from substitution of the 3-, 5- and 6-positions (positions shown in Figure 1.10). Substituents in the 5-position are known to affect the ease of aggregation, with electron withdrawing groups such as chlorine tending to promote aggregation[27]. Substituents on the nitrogen atoms (3-position) can control the solubility of the dye. By introducing bulky, aromatic groups the hydrophobicity can be increased which, as mentioned earlier, can accelerate the aggregation process[29]. However, introducing water

n

viour of the dye, but is also known to improve the photostability of the dye[31].

- Introducing bulky groups in the 9-position allows the angle of slippage to be controlled, although this is dependant on the shape and size of the group, as shown in Figures 1.11 and 1.12. Not only does this help control the angle of slip but it can increase the hydrophobicity, again increasing the likelihood of aggregate formation.[29] It has been noted that the introduction of a meso-group reduces the molar absorbance coefficient compared with that of a non-substituted dye[33], although there has been little explanation for this. Substituted dyes were also found, at low temperatures, to form two distinct absorbance bands because the stereoisomers exist as two separate species[34]. Even at higher temperatures, including room temperature, there is a distinct difference in the ratio of shoulder to the main peak between 9-substituted and non-substituted dyes.

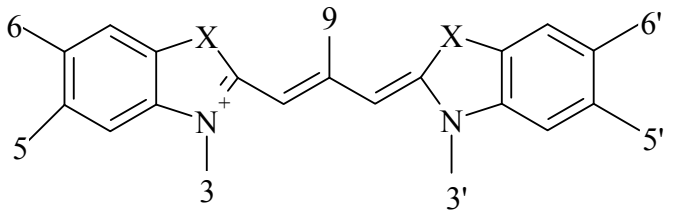

Figure 1.10. Trimethine dye with substituent positions numbered. Numbering applies for monomethine and pentamethine dyes also.

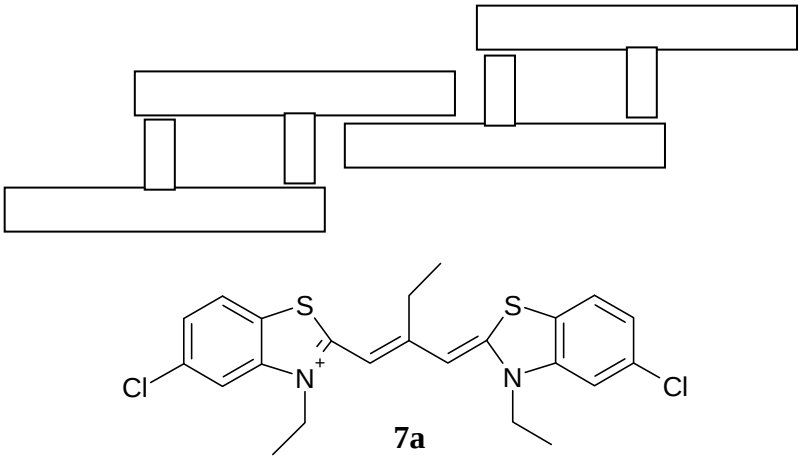

7a

*Figure 1.11. Schematic representation of the cyanine dye depicted in a modelled molecular arrangement in the aggregate[29]. View of **7** from above looking down from sulfur through to the nitrogen atoms with the 9-ethyl group perpendicular to the main body of the dye.*

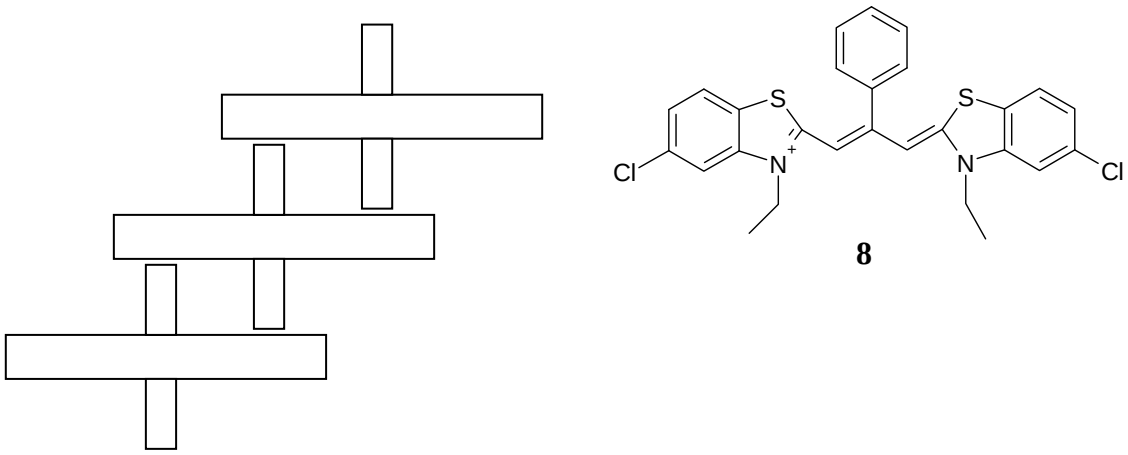

8

*Figure 1.12. Schematic representation of the cyanine dye depicted, in a modelled molecular arrangement in the aggregate[29]. View of **8** from above looking down from sulfur through to the nitrogen atoms with the 9-phenyl group perpendicular to the main body of the dye.*

Solvent and temperature: The solvent in which a dye is dissolved is known to greatly influence how the dye aggregates with West noting 'the peculiar solvent effects of water on the absorption spectra of dyes'[13]. Several groups have studied the effect of solvent[24,26,30] with much of the explanation lying with the fact that water has a high dielectric constant which effectively screens any charge repulsion between the dyes.

Berlepsch *et al.*[30] showed that increasing the percentage of methanol in an aqueous solution of a dye proportionally decreases the amount of aggregation. Slavnova *et al.*[26] noted that the formation of J-aggregates no longer occurs in alcohol concentrations above 30 vol%, at which point cyanine dyes are present in solvated monomeric form at room temperature. It is known that alcoholic solutions of the cyanine dyes follow Beer's law over a dye concentration range of at least 10^{-6} – 10^{-4} M [13] and therefore must not be aggregating under these conditions.

Studies into the effect of temperature such as that by Khairutdinov *et al.*[35] showed the dissolution (deaggregation) of J-aggregates as a solution of 1,1'-diethyl-2,2'-cyanine iodide (PIC) increased with increasing temperature from 15° to 55°, shown in Figure 1.13. Such studies also clearly demonstrated the reversibility of the aggregation process.

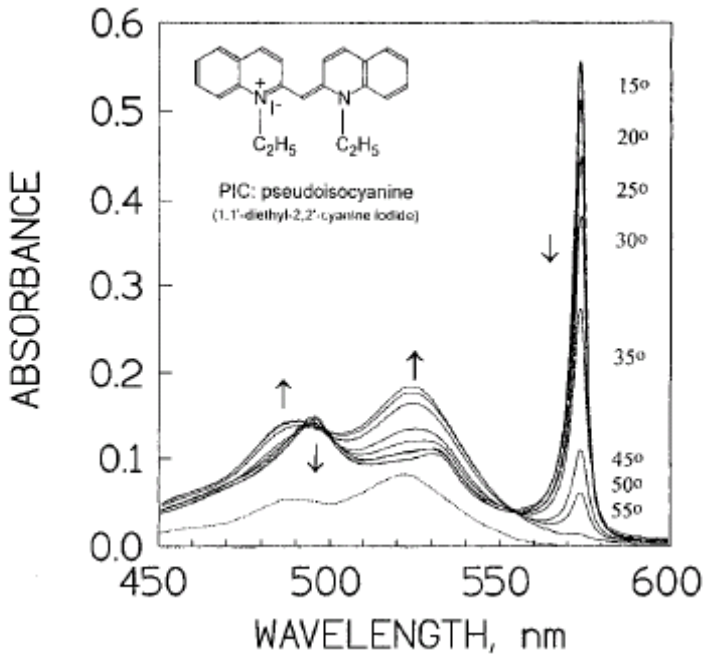

Figure 1.13. The absorbance spectra of an aqueous solution of PIC in the presence of NaCl at various temperatures[35].

Salt: Relating to the structure of the dye, it has been observed that certain dyes do not form J-aggregates in solution, only H-aggregates, that is unless additives such as salts are present[19]. The addition of inorganic salts to a cyanine dye solution appears to reduce the threshold concentration required for the appearance of the J-band[19,25-27,36-38,52]. One reason attributed to this fact is an increase in the screening factor (reducing

the repulsion experienced by molecules from like-charges) or effective dielectric constant of the medium promoting aggregation[6,39]. There have been several recent studies looking at the influence of different inorganic salts on the J-aggregation of cationic dyes (primarily dyes with sulfonate groups in the 3-position). In all of these studies the ability of the dye to co-ordinate with the metal ion was directly linked to the promotion of the aggregates. The principle mechanism of this salt-induced J-aggregation is reported to be the replacement of the cationic component of the cyanine dye by the metal ion present in the inorganic salt[6,23], Scheme 1.1. The mechanism has been reported to be independent of the anion used[19,25].

$$Na^+ \quad + \quad J_{dye}\text{-}[HN(C_2H_5)_3]^+ \longleftrightarrow \quad J_{dye}\text{-}Na^+ \quad + \quad [HN(C_2H_5)_3]^+$$

Scheme 1.1[6]. An expression of replacement of triethylammonium ion for Na^+ ions of dye ***9****.*

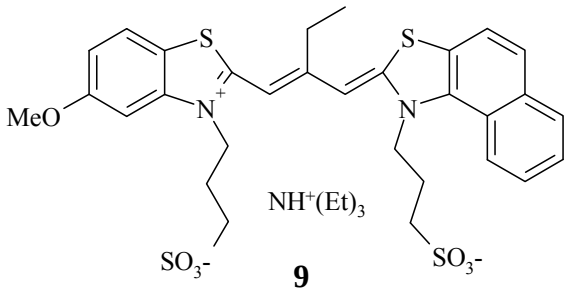

9

The formation of H- and J-aggregates can be readily identified and monitored by UV-visible spectroscopy and fluorescence spectroscopy but despite the ease of detection, there is still much discussion as to what a J-aggregate is. A major factor to this uncertainty is the large number of variables that affect aggregation. Slavnova *et al.* reported that resulting J-aggregates were polymer type assemblies which were composed of many thousands of dye monomers [25]. Takahashi *et al.* reported that their salt induced J-aggregates were oligomers comprising of 20- 80 monomer units [27]. On the other hand, Struganova[40] reported that J-aggregates of PIC were either simple chains containing as little as three dye molecules or packages of dye molecules containing the number of molecules within the unit cell of the dye. Harrison *et al.* reported that the solution J-aggregated state of several cyanine dyes is largely liquid crystalline in nature[12]. Work has also been carried out looking at mixed J-aggregates providing an interesting model of mixed molecular clusters and crystals[41].

1.4 Understanding the Aggregation Process of Cyanine Dyes

Historically, the interest to investigate J-aggregates was due to their role in sensitization of silver-halide photography[19]. More recently however, J-aggregates have been studied in order to better understand the mechanism and reaction pathway of aggregation[26]. At a basic level, the study of molecular aggregates enables intermolecular interactions with reduced degrees of freedom to be studied[42].

A significant proportion of the early work was performed with the purpose of discovering new dyes that possessed the desired properties for sensitisation of photographic film. Reich *et al.* realised that it was important to develop a rationale behind the aggregation process to increase the proportion of dyes synthesised that exhibited these desired properties[28]. Four hypotheses were put forward and investigated using thiacarbocyanines to try correlate structure with UV-visible spectral shifts. These were:

1) The dyes make ordered, epitaxial attachments to the AgBr surface.
2) The dyes tend to maintain an interplanar separation of the order of 3.37 Å (the graphitic distance).
3) Dyes such as these (which incorporate heterocyclic sulfur atoms) attach to the crystal surface with the formation of ligand bonds between sulfur atoms and silver ions.
4) The spectral shifts of the aggregate absorptions can be explained by simple coupling of oscillators through transition density formalism or other methods of calculation.

By using experiments, Reich *et al.* went on to rationalise each hypothesis with the overall conclusion being that the aggregation of these dyes was 'rational but not simple' and behaved mechanically like graphite. It was clear from their results that hypothesis 1 was the most difficult to prove because adsorption of the dye on the AgBr surface forces an aggregate which is unlike that of a free, bulk solution aggregate or in the crystal structure. With the lack of direct evidence i.e. AgBr crystal data with the adsorbed dye, indirect evidence was used including the partial absorption of polarised light.[28]

Many of the models for the behaviour of aggregating dyes have come from indirect results such as crystal structures with very little evidence to directly link solution

aggregates with packing structures. Continuing to understand the interactions, mechanisms and kinetics of the aggregation process is just as important today (despite classical photography being rapidly replaced with digital photography) for this reason and the various other applications of cyanine dyes. During the past couple of decades several studies have been carried out looking at the kinetics of the of aggregate formation[19,25,26,43]. Slavnova *et al.*[25] found that the rate of J-aggregation is non-linearly dependant on the dye concentration. The formation of J-aggregates is also thought to occur by the association of dimers at a critical concentration[44]. Khairutdinov *et al.*[35] concluded from their variable temperature studies that the results inferred the exothermic equilibrium shown in Scheme 1.2, depicting H-aggregates as the intermediate between monomers and J-aggregates.

Scheme 1.2. The exothermic equilibria found by Khairutdinov et al.[35].

It has been reported that H-aggregates are not only intermediates to J-aggregates but are easier to form and are more reproducible than J-aggregates[13,44-46]. Because of the reproducibility of H-aggregates, several groups have modelled H-dimers calculating dimerisation association constants, K_D. Takahashi *et al*. calculated[27] K_D for the range of dyes **10**- **16**, shown in Table 1.1.

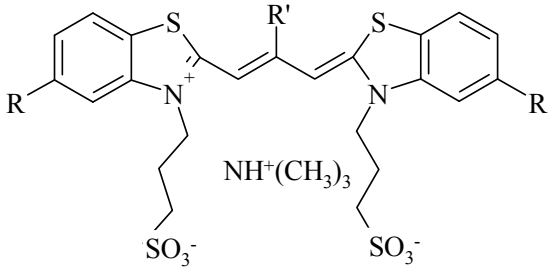

Dye	R	R'	K_D (dm^3mol^{-1})
10	Cl	C_2H_5	3.5×10^4
11	H	C_2H_5	1.24×10^4
12	CH_3	C_2H_5	4.58×10^4
13	OCH_3	C_2H_5	1.3×10^5
14	Cl	C_6H_5	3.69×10^4
15	Cl	CH_3	8.96×10^4
16	Cl	H	1.14×10^5

*Table 1.1. Dimerisation association constants calculated for the range of dyes **10-16**[27].*

Harrison *et al.* compared the equilibria shown in Scheme 1.2 to the equilibria of aqueous surfactant systems (Scheme 1.3), concluding that although similarities can be drawn, the equilibria are not completely analogous[12]. It has been reported in several instances that a solution containing J-aggregates which is left and shielded from the light results in a precipitate which can be isolated by centrifugation[12,27,37].

Monomer $\rightleftharpoons$ Micelle $\rightleftharpoons$ Mesophase

Scheme 1.3. Equilibria of aqueous surfactant systems. The Equilibria are comparable but not analogous to that in Scheme 1.2[12]

1.5 Fluorescence Behaviour of Cyanine Dyes

Because of their optical properties, cyanine dyes can be used for labelling molecules such as nucleic acids and proteins[47]. Owing to the importance of fluorescent probes and sensors in environmental and biological applications, it is important to be able to 'tune' fluorescent dyes in aqueous solution[48].

An ideal label in terms of fluorescence is that the dyes behave as they do with their absorption spectra where the more concentrated a solution the larger the absorption. This is, however, not the case as increasing the concentration of a solution of the majority of cyanine dyes leads to the dye self-quenching[29]. An additional problem is

that most H-aggregates, including dimers, are known not to be fluorescent [49] which is in contrast to J-aggregates which exhibit resonance fluorescence[50]. It is thought that upon dimerisation, the intersystem crossing (ϕ_{isc}) increases[49,50] which could explain the non-fluorescent behaviour of H-aggregates. Caselli *et al.*[45] however found that a series of water soluble oxacarbocyanines (**17-20**) formed H-aggregate dimers that were fluorescent and have emission quantum yields comparable to or even larger than those of the monomeric species in water.

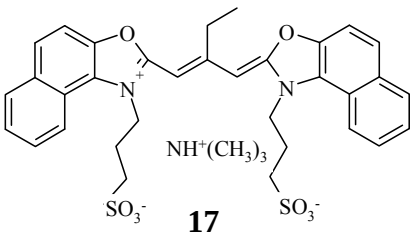

17

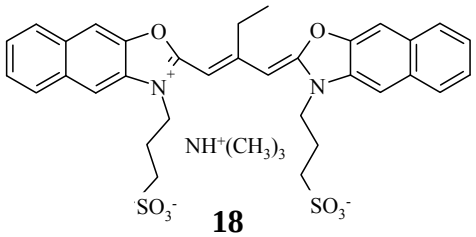

18

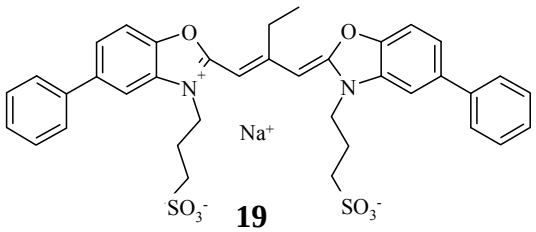

19

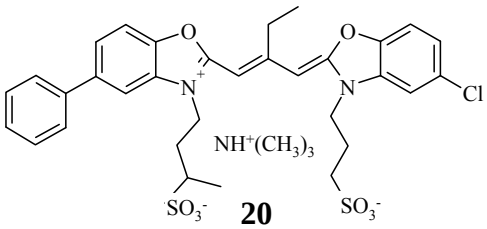

20

The encapsulation of cyanine dyes in cavity hosts such as cucurbituril (CB) and cyclodextrins (CD) (shown in Figure 1.14) is known to increase photostability and fluorescence yield[51]. Encapsulation can also improve the fluorescent yield by reducing the amount a dye can aggregate in solution[52]. Several groups have looked at the encapsulation in both CB[48] and CD[53-55] where cyanine dyes tend to bind to the cavity through hydrophobic binding[54]. Studies carried out by Huang *et al.* conversely showed that instead of enhancing the fluorescence, an unexpected quenching phenomenon was discovered because the dye was only partly encapsulated in β-CD, shown in Figure 1.15[53].

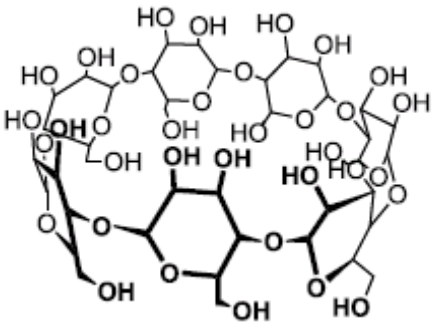

β-cyclodextrin

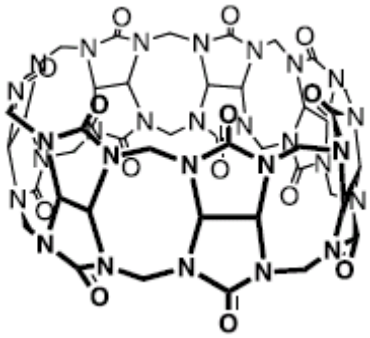

Cucurbit[7]uril

Figure 1.14.[48] *Two encapsulation molecules with comparable cavity sizes.*

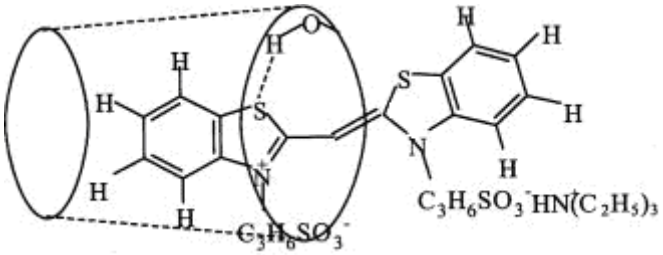

Figure 1.15.[53] *The partial encapsulation of cyanine dye leading to increased quenching*

1.6 Solid-state Behaviour and Studies of Cyanine Dyes

As with most supramolecular chemistry, changing the functional groups on the molecule leads to different types of intermolecular interactions. For example, the presence of aromatic rings allow for π–π interactions to occur, the anions introduce electrostatic interactions and inducible dipoles (Van der Waals) and the alkyl chains mean that C-H….π and C-H….I^- interactions can potentially occur. Very stable structures can be formed as a result of different interactions and this has been associated with the formation of crystals with high melting points.

There have been many X-ray structural studies carried out on cyanine dye crystals. The majority of the structures in literature include trimethine structures with a smaller number of monomethine structures (taken from Crystallographic Database version 5.29), Tables 1.2 and 1.3 respectively. Of these structures most of the dyes have simple counter ions but there are several structures that involve TCNQ, these are interesting due to their potential molecular electronic properties.

Early structural studies found distinct solvent of crystallisation to be present in crystals of most of the cationic dyes[11]. The ability to use X-ray crystallography to deduce a molecule's spatial arrangement is essential for this type of study although crystals have to be of a high enough quality to produce a good data set which can be an issue.

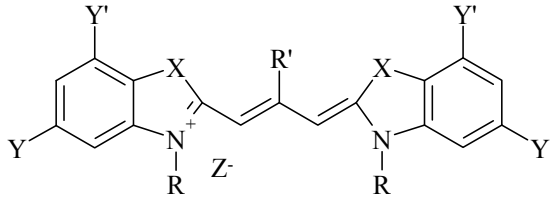

Dye	X	Y	Y'	Z	R	R'	Solvent of crystallisation
2b	S	H	H	Oxanol structure	Et	H	-
2c	S	H	H	$TCNQ^-$ & TCNQ	Et	H	-
2d	S	H	H	TsO^-	Et	H	H_2O
2e	S	H	H	$AuCl_2$	Et	H	-
2f	S	H	H	Br^-	Et	H	-
2f	S	H	H	Br^-	Et	H	EtOH
7b	S	Cl	H	Br^-	Et	Et	AcOH
21b	S	H	H	$TCNQ^-$ & TCNQ	Me	H	-
21a	S	H	H	Oxanol structure	Me	H	-
22	S	H	H	BF_4^-	Et	t-Bu	-
23	O	Ph	H	$MeO\text{-}SO_3^-$	Me	Et	MeOH
24	S	H	H	I^-	Et	Ph	MeOH
25	S	Me	Me	ClO_4^-	Et	Et	-

Table 1.2. Trimethine structures in the Cambridge Crystallographic Structural Database, version 5.29 (Nov. 2007) [56].

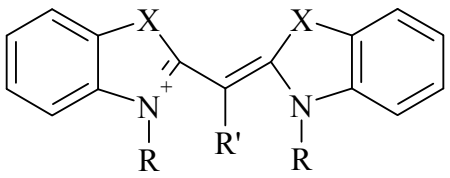

Dye	X	R	R'	Z
3c	S	Et	H	Br
3d	S	Et	H	$TCNQ^-$
3e	S	Et	H	$TCNQ^-$ & TCNQ
26	O	Et	H	$TCNQ^-$
27	S	Me	I	ClO_4^-

Table 1.3. Structures in the Cambridge Crystallographic Structural Database, version 5.29 (Nov. 2007) [56].

As part of understanding and describing the existing crystal structures a systematic approach is generally taken which considers the geometries of the molecule and dimers in the zero dimensions (0D), the formation of stacks in one dimension (1D), the planes in two dimensions (2D) and finally the three dimensions (3D) architecture. Within the molecule itself the three main properties of the dye that are considered include the orientation of the alkyl- and heterocyclic groups, the planarity of the dye and any intramolecular interactions:

- Cyanine dyes are known to twist along the methine chain. A review by Smith[57] found most dyes were nearly planar with angles of less than 15 ° between the planes defined by the heterocyclic rings. Smith concluded because the dyes are basically planar, they pack plane to plane with substituents determining the lateral displacement of adjacent rows and hence the slip angle[57].
- Cyanine dyes are planar with the exception of the alkyl groups in the 3-positions and substituents in the 9-position. This means that the alkyl groups are important in influencing the packing structures. The four geometries used to describe the molecules are Cis-Cisoid, Cis-Transoid, Trans-Cisoid and Trans-Transoid [58], Figure 1.16.
- Considering the length of the molecule from fixed points on each dye provides an indication of whether the heteroatoms are interacting with one another.

Sturmer *et al.* summarised[11] the common features of a range of crystal structures noting the presence of short S…S distances for the monomethine dyes (2.99 Å[59]) suggesting an interaction. The separation of the heteroatom by a trimethine chain means that the atoms are too far to interact with each other.

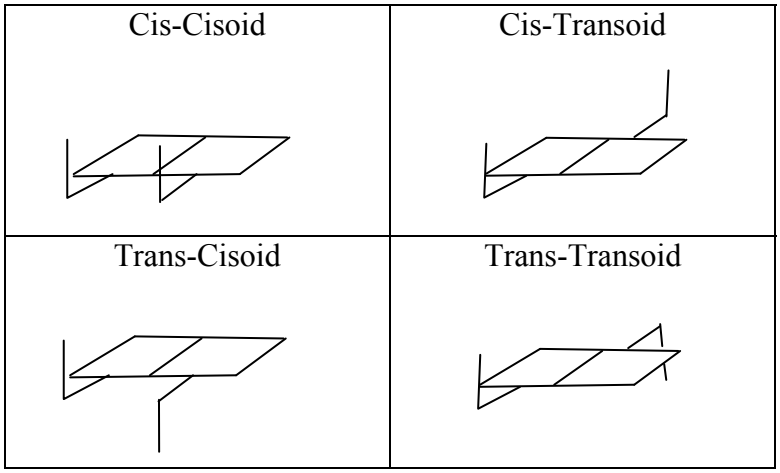

Figure 1.16. Schematic representations of the symmetrical cyanine dyes showing the different combinations of geometries defined by Horton[58].

The 2D and 3D architectures involve stacking in 2D arrays which then repeat into a 3D structure[58]. Czikkely *et al.*[60] observed the packing structures fit either 'brick work arrangement, ladder arrangement or a staircase arrangement', Figures 1.17, 1.18 and 1.19 respectively. These descriptions are commonly accepted and used by most groups [4,12,58,61]. It is these models that are directly linked to the aggregates formed in bulk solution with the brickwork being described as a J-aggregate, the ladder array as a H-aggregate and the staircase as both H- and J-aggregates depending on the angle of slip [5,12,62].

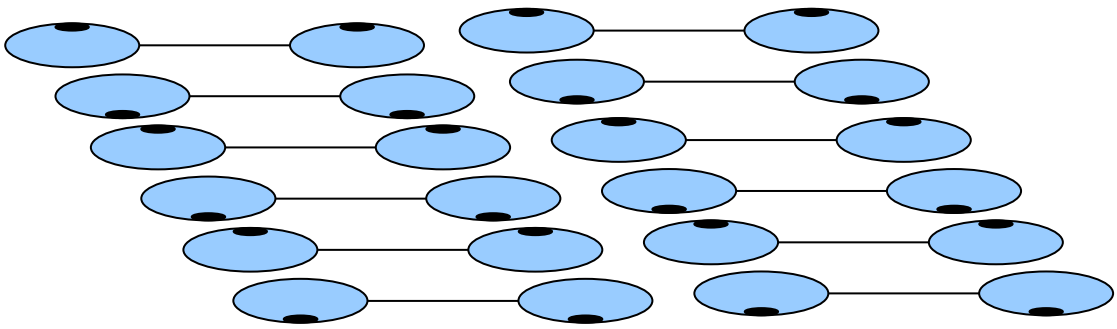

Figure 1.17. A schematic representation of symmetrical cyanine dyes in a staircase array. The dark spots represent the location of the alkyl groups.

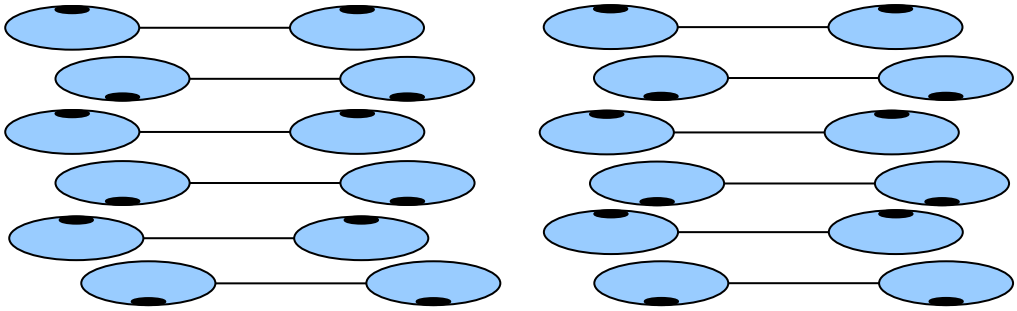

Figure 1.18. A schematic representation of symmetrical cyanine dyes in a ladder array. The dark spots represent the location of the alkyl groups.

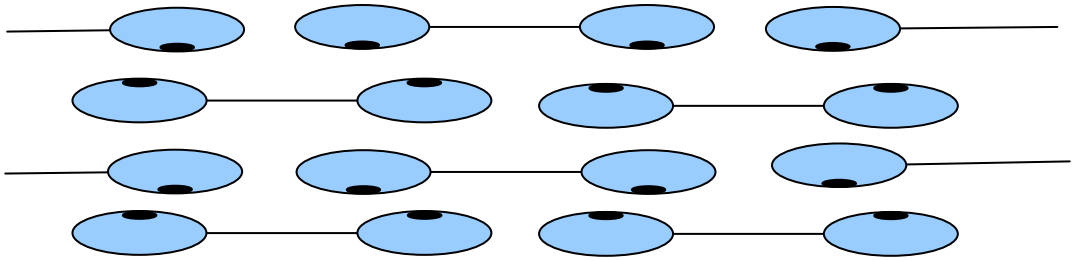

Figure 1.19. A schematic representation of symmetrical cyanine dyes in a brick work array. The dark spots represent the location of the alkyl groups.

1.7 Applications and Properties of Cyanine Dyes.

Through the extensive studies of these dyes for photographic applications, many other useful properties of cyanine dyes have been discovered. These include light harvesting, the probing of interfaces and the potential use of dyes in organic molecular electronics.

Organic solar cells are of interest because of their low cost and ease of manufacture but they are not as stable as more traditional inorganic solar cells. Several requirements that are important to classical photography also apply to organic solar cells including high extinction coefficients, tuneable absorption spectra and the possibility to form aggregates [20]. As we have seen, cyanine dyes posses all these essential characteristics. Applying the light energy conversion capability of cyanine dyes for use in photovoltaics means that TiO_2 nanocrystalline solar cells can easily be sensitised [31,63] as can thin film heterojunction photovoltaic devices[63a]. Because of their

high extinction coefficients it is possible to use thin films for efficient light harvesting[20].

As discussed, cyanine dyes have tuneable solubility properties making them ideal candidates to probe interfaces. Several different studies have been carried out ranging from studying the air-water interface and surface tension measurements to looking at the monolayers formed in the presence of template molecules such as hexadecane[64] and unsubstituted fatty acids[65]. Cyanine dyes can also easily be spin coated from solution which is of considerable technological interest[20].

Another aspect of this templating is in the solid state, where molecules that also form crystalline solids are mixed with the cyanine dyes. Some early work by Klanderman *et al.*[66] looked at how the electrical properties of complex radical-ion salts of TCNQ changed when mixed with various cyanine dyes. Small crystals containing both molecules resulted from the mixtures. Horton[58] also considered the interactions between cyanine dyes and TCNQ (neutral and as an anion) in the solid state. Several crystal structures resulted from these co-crystallisations which showed that in the case of cyanines and $TCNQ^{\cdot -}$, dimers formed with no extended stacking but in the case of diethyloxacarbocyanine $TCNQ^{\cdot -}$, **5b**, alternating monomers of $TCNQ^{\cdot -}$ and dye packed together in an almost herringbone-like array.

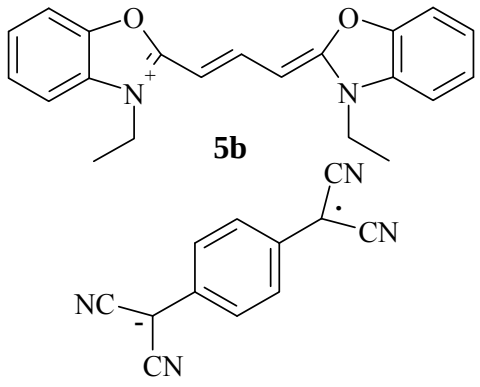

5b

1.8 Synthesis of Cyanine Dyes

Cyanine dyes have been known for over a century, with the significant amount of work on the development of the synthetic routes being established during early to mid-1900's. There has been relatively little recent work developing synthetic routes because these early methods were both useful and reliable. The majority of synthetic

work undertaken in recent years uses these routes with only subtle alterations depending on the desired dye. Most synthetic routes, whether for monomethines, trimethines or pentamethines, involve the reaction of a 2-methyl heterocyclic quaternary salt with another reagent in the presence of a basic condensing reagent.[67]

Monomethines

Several earlier synthetic routes involved two different quaternary salts producing both symmetrical and unsymmetrical dyes. These electrophilic routes used quaternary salts, Scheme 1.4, and reacted them with methylene bases to afford a variety of cyanines[11]. The method used for symmetrical dyes was developed by F M Hamer *et al.*[68,69] in which two identical methyl quaternary salts are reacted in the presence of amyl nitrite and acetic anhydride, Scheme 1.5. Koral *et al.* later adapted this route slightly, but found that this reaction resulted in the production of a triiodide counterion. Reduction with sulfur dioxide converted the triiodide to iodide[70].

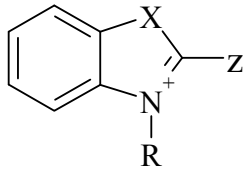

Scheme 1.4. [11] *Z= I, SR, SO_3^-, SO_2Me, OR, -CHNOR, CN*

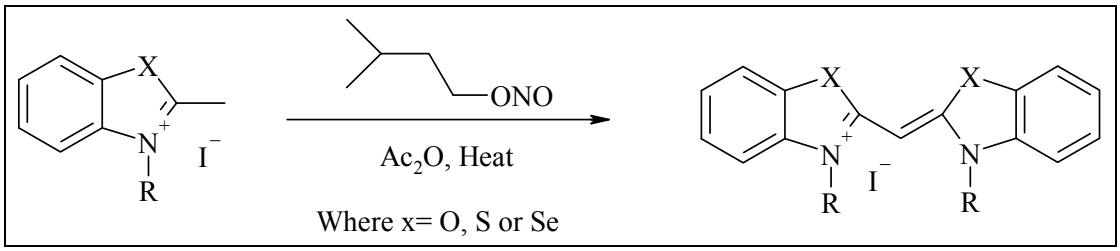

Scheme 1.5. The general oxidation reaction of an active methyl quaternary salt heated to reflux in the presence of acetic anhydride and amyl nitrite resulting in a symmetrical cyanine dye

Trimethines

The most useful and commonly used preparation for symmetrical trimethines is the method described by Ficken where of two equivalents of an active methyl quaternary salt react with an ortho-ester in the presence of pyridine, Scheme 1.6[67]. Hamer *et al.*[68] initially reported this condensation procedure and it was later adapted by Koral *et al.*[70]. The orthoester provides the central carbon in the methine chain. Brooker *et al.*

s

e was used as the solvent and the orthoester was present in 2-fold excess[71] as both a desiccant and a reactant. The range of dyes prepared are shown in Figure 1.20.

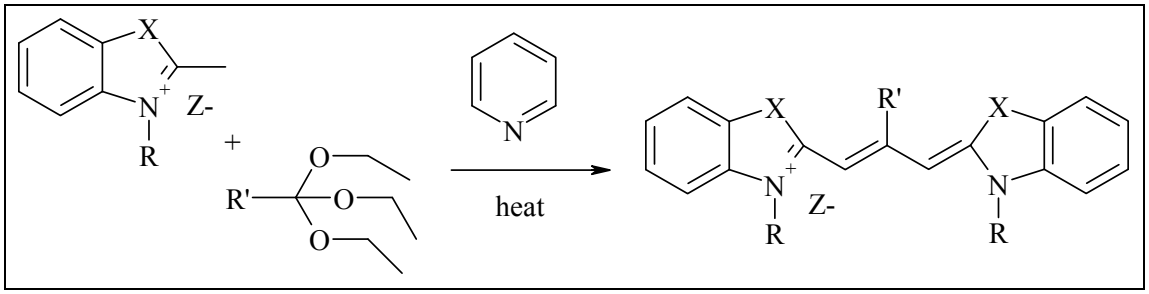

Scheme 1.6. The generalised condensation reaction of active methyl quaternary salt heated to reflux in the presence of pyridine and an orthoester resulting in a symmetrical carbocyanine

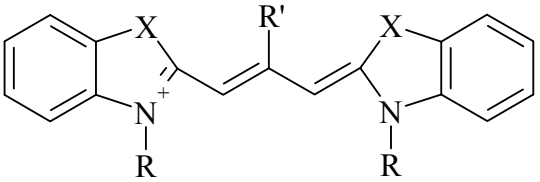

Where X= S, R= Me and Et

R'=	H	Me	Et	*n*-Pr	*n*-Bu	*n*-Am	*i*-Am	$PhCH_3$	$PhOCh_2$	Ph

Figure 1.20. Adapted from [71]. Meso-substituted carbocyanines prepared by Brooker et al.

Bistrimethines

Several groups[61,72,73] have prepared and investigated biscarbocyanines which possess two dye chromophores linked in a box-like structure. The cyclic biscyanines were prepared using the usual condensation method[72] although it was found that the highest yields resulted from using a pyridine:acetic anhydride (1:1) solvent, Scheme 1.7.

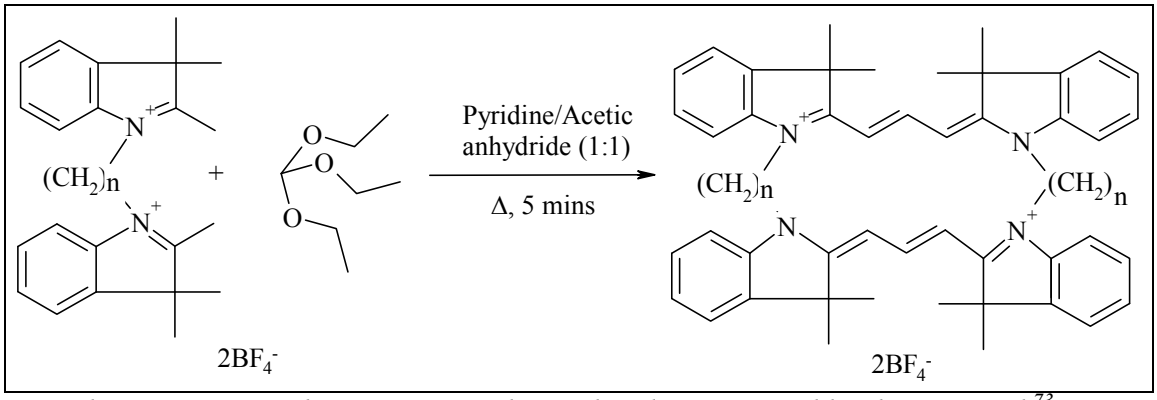

Scheme 1.7. Biscarbocyanines synthesised and investigated by Ibrayev et al.[73]. Method initially used by Mushkalo[72] n= 2 and 4.

Pentamethines

Synthetic routes used to prepare pentamethine dyes have been described by Kazymov *et al.*[74] where tetraethylacetals reacted with an active methyl quaternary salt in the presence of pyridine to produce a pentamethine, Scheme 1.8.

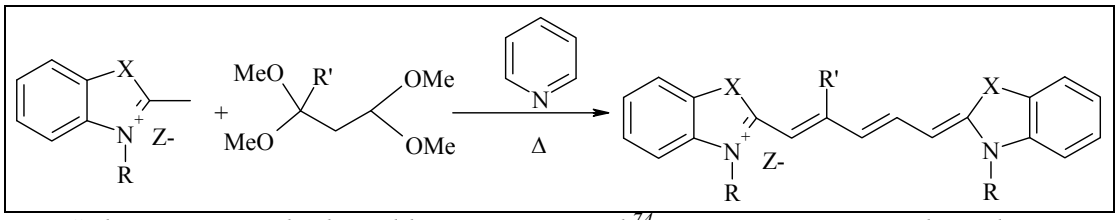

S*cheme 1.8. Method used by Kazymov et al.*[74] *to prepare pentamethine dyes.*

Chapter 2

Aims and Objectives

The following objectives were the focus of the study presented:

1) To prepare a range of cyanine dyes with various structures and obtain crystals of these dyes for structural determination using X-ray crystallography.
2) To study, compare and contrast the aggregation behaviour of these cyanine dyes in bulk solution with techniques including UV-visible spectroscopy and fluorimetry.
3) To investigate whether crystal structure data can be used to predict unknown packing architecture from the molecular structure and/or the relationships between packing structure and bulk solution aggregates.
4) To test an in-house designed Electronic Laboratory Notebook (ELN) in a research environment and by doing so, provide constructive criticism and suggestions for improvement.

Chapter 3

Synthesis

The synthetic strategies employed during this project for the heterocyclic quaternary salt dye precursors, monomethine dyes, trimethine dyes and pentamethine dyes are presented in this chapter. All methods have been previously reported with very few modifications made.

3.1 Preparation of the Heterocyclic Quaternary Salt Dye Precursors

Three different methods (methods I, II and III) were used to prepare a range of activated methyl quaternary amine salts (dye precursors) using nucleophillic substitution reactions between nitrogen heterocycles also containing a sulfur, selenium or oxygen atom in the ring and an appropriate alkyl halide or sultone.

Method I was adapted from Koral *et al*[75] involving the reaction of an alkyl halide in the presence of catalytic NaI with a benzothiazole in anhydrous MeCN, (Scheme 3.1). This method resulted in the highest yields for salts **28**- **34**, with yields ranging from 15% to 91%. Introducing benzyl groups in the 3-position (**32** and **34**) almost doubles the yield in comparison to the ethyl analogues **31** and **33**, suggesting that the benzyl group introduces favourable interactions.

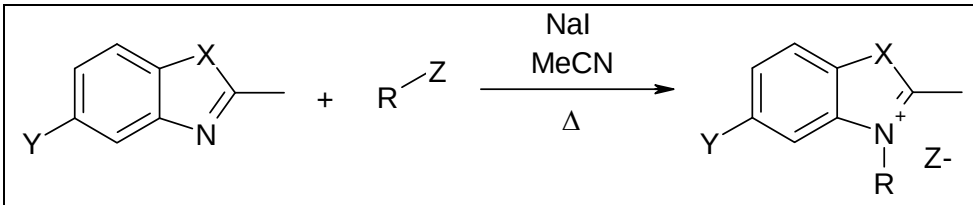

Precursor	X	R	Y	Z	Yield (%)
28	S	Benzyl	H	Br	16
29	S	2-bromo-benzyl	H	Br	15
30	S	4-bromo-benzyl	H	Br	61
31	S	Ethyl	F	I	47
32	S	Benzyl	F	Br	91
33	S	Ethyl	Cl	I	15
34	S	Benzyl	Cl	Br	31

Scheme 3.1. Method I. Nucleophillic substitution involving nitrogen heterocycles and alkyl halide in MeCN catalysed by sodium iodide.

Method II involved reacting the heterocycle and the alkyl halide in the absence of a solvent[76], (Scheme 3.2) which resulted in yields ranging from 39% to 98% for dyes **35- 38**.

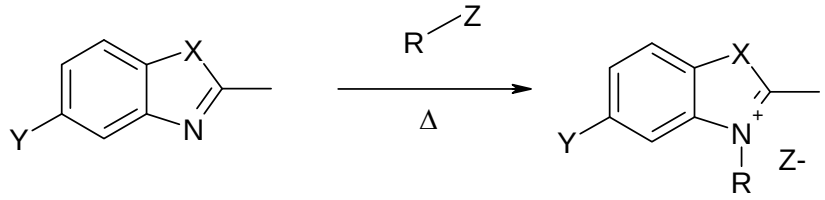

Precursor	X	R	Y	Z	Yield (%)
35	O	Methyl	H	I	39
36	S	Phenethyl	H	Br	61
37	S	2'-methyl-3'-hexyl-benzothiazolium	H	2 Br	98
38	S	Naphthyl	H	Br	78

Scheme 3.2. Method II. Nucleophillic substitution involving a nitrogen heterocycle and an alkyl halide.

The preparation of the water soluble, zwitterionic, sulfo-precursors **39- 42** involved a method adapted from Galin *et al*[77], (Scheme 3.3) which was carried out in anhydrous MeCN. The yields of precipitated product ranged from 25% to 53%.

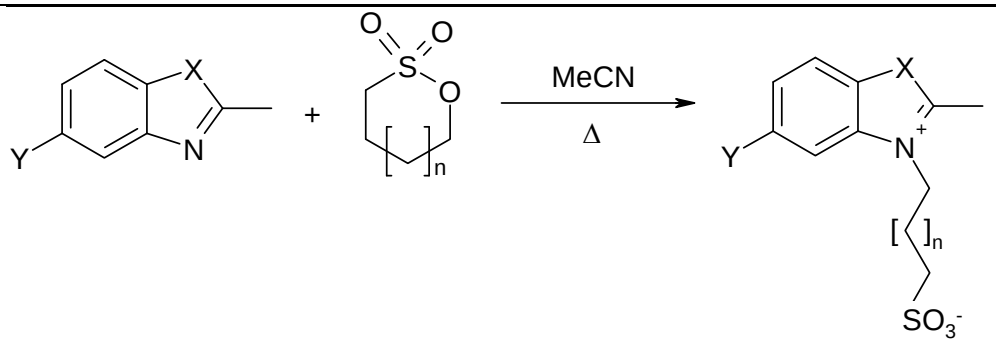

Precursor	X	n	Y	Yield (%)
39	S	2	H	35
40	S	1	H	53
41	S	1	Cl	25
42	Se	1	H	16

Scheme *3.3. Method III. Reaction of a nitrogen heterocycle with sultone in dry acetonitrile.*

For all three methods, the product generally formed a precipitate and could be easily isolated by filtration. The purification of all quaternary salts was achieved by crystallisation from polar solvents such as MeCN, MeOH and EtOH. Compounds **30**, **34-36** and **39** formed crystals of a high quality enabling X-ray structural studies to be carried out. Compounds **29**, **31-33** and **38** formed crystals which eventually turned cloudy upon isolation, possibly due to loss of solvent, and compounds **40- 42** formed micro-crystalline solids.

The method shown for a given molecule was the method which resulted in the highest yield for that product. For each compound different methods were investigated but there did not appear to be a correlation between structure and which method (I or II) would be more efficient for which alkyl quaternary amine.

The majority of the quaternary salts successfully prepared contain sulfur because the oxygen and selenium analogues, benzoxazole and benzoselenazole, were much less

reactive than the sulfur analogues. The extended reaction times employed (>5 days compared with 1-2 days for the sulfur analogues) still resulted in the recovery of large quantities of unreacted starting material.

3.2 Monomethine Dyes

Using a method adapted from Koral *et al* [70], a range of monomethine dyes were prepared, Scheme 3.4, and the conversion of the iodide counterion to triiodide also resulted. The products prepared from our work showed that this conversion was less than 100% however, forming a mixture of both iodide structures and triiodide structures. In all cases the two counterions resulted in distinctly different crystals after purification, the triiodide monomethine salts formed large dark blocks or needles whereas the iodide analogues formed small yellow/green needles. In some cases isolation of the triiodide/iodide dyes could be achieved by visual identification and separating them by hand. This was not possible however when both the iodide and triiodide structures were needles, therefore requiring a further reaction to convert the triiodide product to iodide. Koral *et al*[70] reported that bubbling sulfur dioxide through a solution of the dye salt reduced the triiodide to iodide. A simple method was employed in our work which used sodium metabisulfate to reduce the triiodide to iodide simply and cleanly (Scheme 3.5). The MeCN/H_2O mix ensured solubility of both dye and sodium metabisulfate.

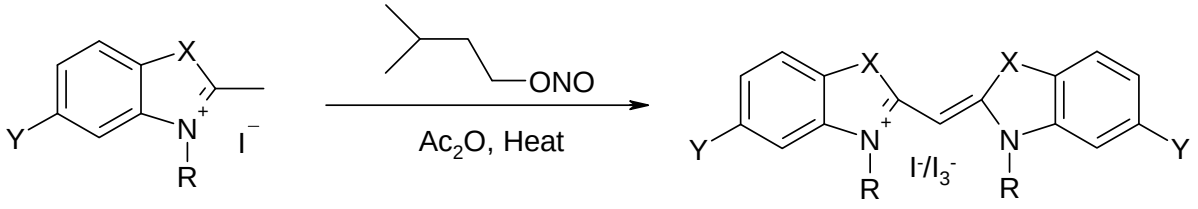

Compound	X	Y	R
3a/3f	S	H	Et
44a/44b	O	H	Et
45a/45b	S	Cl	Et
46a/46b	S	F	Et

Scheme 3.4. General oxidation reaction of an active methyl quaternary salt heated to reflux in the presence of acetic anhydride and amyl nitrite resulting in a symmetrical cyanine dye. Yields not shown because of mixed counter ions.

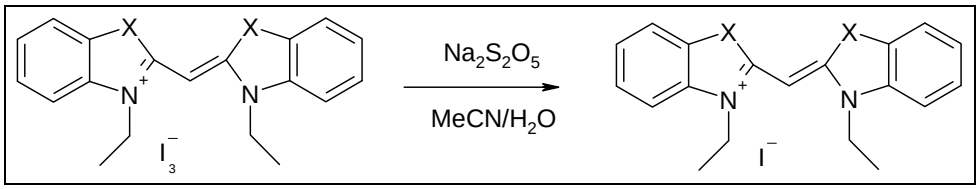

Scheme 3.5. The reduction of monomethine counterions from triiodide to iodide using sodium metabisulfite.

The purification of the monomethine dyes was achieved through crystallisation in single solvent systems such as MeCN and MeOH. All crystals were of a high quality which enabled X-ray structural studies to be carried out on all triiodide and iodide monomethine dyes prepared (Chapter 5).

The preparations of monomethines with alkyl groups other than ethyl via the method outlined in Scheme 3.4 were found to be unsuccessful, possibly because of steric hindrance. This resulted in the majority of the monomethine dyes studied in this project having an ethyl group in the 3-position with the exception of compound **47** which was formed as the unintended product of a reaction to prepare a 9-substituted trimethine. Very little of the crystalline compound **47** was isolated with a few of the crystals being of a suitable quality for X-ray structural studies as is discussed in more detail in Chapter 5.

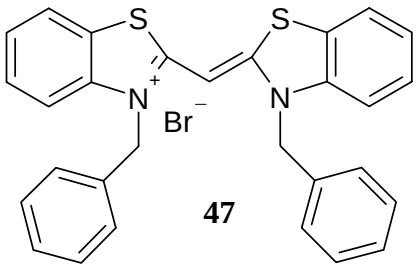

47

3.3 Trimethine Dyes

The method used in the preparation of trimethine dyes was also adapted from a reaction described by Koral *et al*[70] shown in Scheme 3.6 with yields ranging from 4% to 98% for dyes **2a**, **5a**, **11** and **48- 59**. In a similar fashion to the preparations of the quaternary salts, the sulfur analogues were much easier and more reliable to synthesise than the oxygen and selenium analogues. The preparation of trimethine

dyes was also more successful for the sulfur analogues. This resulted in the majority of the trimethine dyes studied being sulfur analogues. It seems that oxygen and selenium atoms not only have an effect on the nucleophillic properties of the nitrogen atom but also the reactivity of the methyl group.

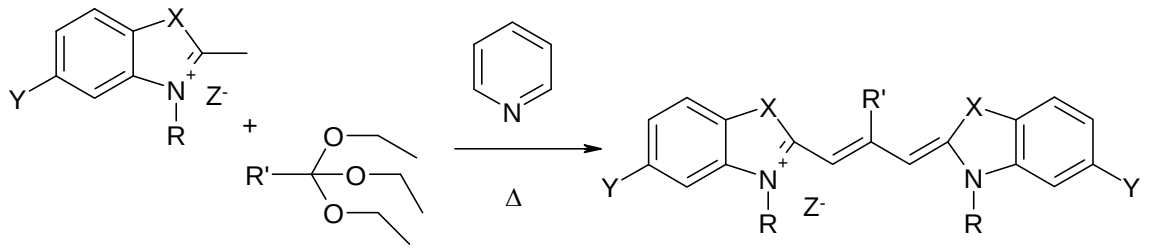

Dye	X	Y	Z	R	R'	Yield (%)
2a	S	H	I	Ethyl	H	88
5a	O	H	I	Ethyl	H	42
11	S	H	*	$(CH_2)_3SO_3^-$	Et	04
48	O	H	I	Methyl	H	69
49	S	H	Br	Benzyl	H	74
50	S	H	Br	Phenethyl	H	82
51	S	H	Br	Naphthyl	H	73
52	S	H	Br	4-Bromobenzyl	H	75
53	S	Cl	I	Ethyl	H	54
54	S	Cl	Br	Benzyl	H	29
55	S	F	I	Ethyl	H	60
56	S	F	Br	Benzyl	H	49
57	S	H	*	$(CH_2)_4SO_3^-$	H	98
58	S	H	*	$(CH_2)_3SO_3^-$	H	63
59	S	H	I	Ethyl	Et	35

** = Unknown counter-ion*

Scheme 3.6. Condensation reaction of active methyl quaternary salt heated to reflux in the presence of pyridine and an orthoester resulting in a symmetrical carbocyanine

The counterions for the cationic sulfo-dyes **11**, **57** and **58** have not been identified. Similar dyes in literature have been reported to have organic ammonium or pyridinium ions as the counterions[6, 12]. There has been no spectroscopic evidence to

suggest this is the case in the present study. Crystal structures of **57** show no organic counter-ion but the electron density suggests the presence of a simple proton although this is unconfirmed.

Surprisingly the synthesis of **60** was unsuccessful when the isomeric **52** was successfully prepared and crystallised. The reaction of the precursor **29** as described by Scheme 3.6 resulted in a dark, oily product that could not be purified and no dye component could be identified by NMR or mass spectrometry. The positioning of the bromine atoms appears to have a significant effect controlling whether the reaction can proceed as desired.

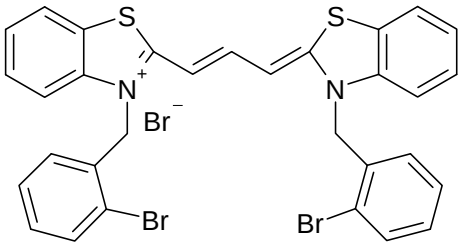

60

3.3.1 Meso-Substituted Trimethine Dyes

The preparation of meso-substituted trimethine dyes proved more difficult than reported in literature by Brooker *et al*[71]. Following literature procedures all attempts to produce the phenyl- or ethyl-substituted trimethine dyes resulted in a monomethine (**3a**) and a 9-methyl trimethine (**61**) in a mixed yield of 23%, Scheme 3.7. To understand why this was the case, a control reaction was carried out without any orthoester which also resulted in molecules **61** and **3a**. This lead to the conclusion that the formation of the **61** was a result of a starting material **62a**, when in the presence of a base, being susceptible to attack from water which leads to the reaction with other molecules of **62a**, although the mechanism for the formation of **3a** remains unclear.

The orthoester shown in Figure 3.1 when R= H is hygroscopic. When in excess, it desiccates the reaction mixture as well as reacting with starting material, which is why the preparation of unsubstituted meso-dyes are unaffected by the presence of trace amounts of water. When R = Me or a larger group however, the orthoester is no longer hygroscopic and so ceases to desiccate the reaction mixture, leaving water present to react catalytically with the starting material. This problem was overcome

by adding molecular sieves to the reaction mixture which successfully aided the preparation of the ethyl-substituted dye **59**, but not the intended meso-phenyl dye **63**. Monomethine dyes (**3a, 47** and **64a**) were successfully isolated from the attempts to produce **63**.

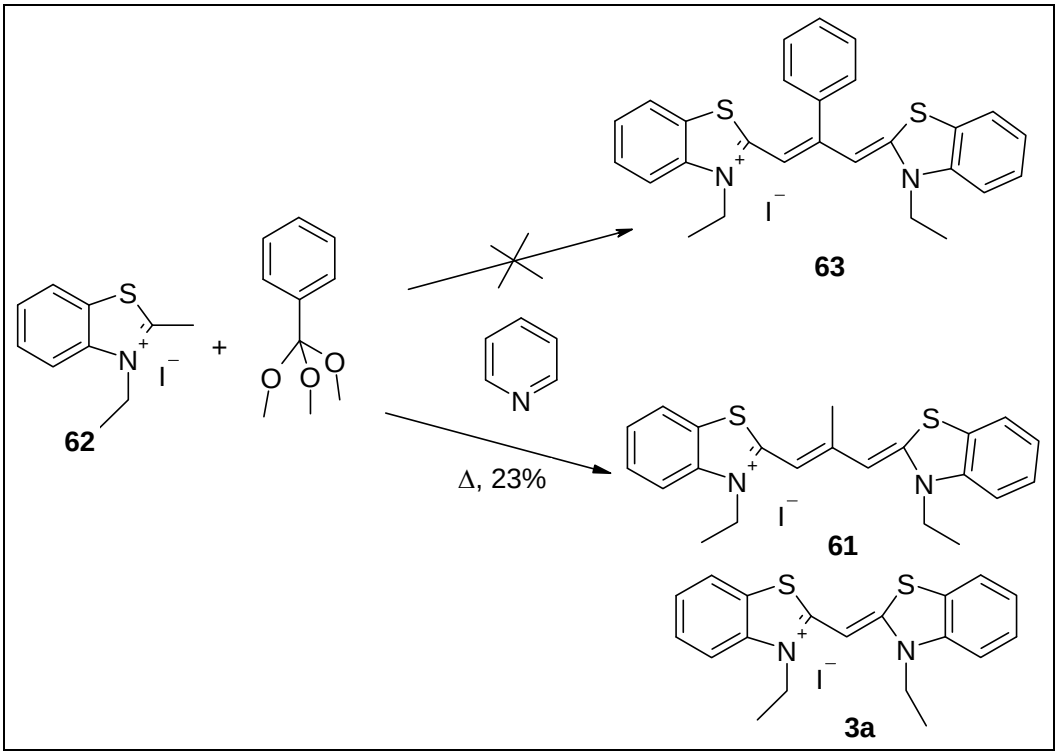

*Scheme 3.7. The attempted synthesis of **63** using an orthoester and an active methyl quaternary salt (**62**) in anhydrous pyridine.*

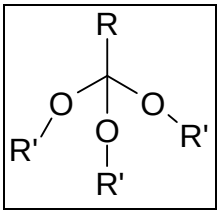

Figure 3.1. Orthoester starting material.

R = H, Me, Et, benzyl

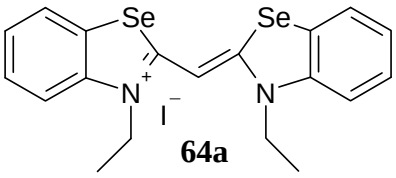

Purification of these compounds by column chromatography was not possible as the dyes were prone to bleaching on a silica column and the products co-eluted in a range

of solvent systems on an alumina column. Crystallisation was therefore the only practical purification technique despite unreacted starting materials co-crystallising with the dye resulting in a mixture of crystals. This problem was overcome by dissolving the crude product in an excess of solvent and performing fractional crystallisations. Both of these techniques reduced the yield, but resulted in purer compounds as identified by ESMS.

3.3.2 Water-Soluble Dyes

Purification of the sulfo-dyes was achieved using a mixture of EtOH/ toluene, but unlike traditional mixed solvent crystallisations, the product was dissolved in an excess of EtOH with only several drops of toluene present and allowed to evaporate over an extended period of time (weeks). In the case of **11** only the first crop of crystalline product was pure dye, resulting in very poor yields, Scheme 3.6.

A problem that became an issue when preparing meso-substituted **11** was the low solubility of the sulfo-precursors **39** and **40** in pyridine. This resulted in the recovery of large amounts of unreacted starting material, making purification of dye **11** problematic because of the similar physical properties of the dye and starting material. In an attempt to increase the solubility of the starting material investigations were performed using different ratios of MeOH/pyridine as the reaction solvent. However, reactions using these mixed solvent systems resulted in a dark product which could not be characterized due to its insolubility in a range of common solvents. Using pyridine as the single solvent resulted in any lumps of starting material becoming coated in purple signifying the formation of the desired product but the core remaining unreacted suggesting that increasing the surface area of the starting material would result in a higher yield. The starting material was ground into a fine powder before use which did result in a higher conversion of starting material to dye going from <1% to 4%.

The sulfo-dyes **16** and **65** were prepared, but characterisation of the crude products showed a significant amount of unreacted starting material. The several different techniques explored to isolate the desired product were unsuccessful. Crystallisation was not possible as the dyes were only soluble in H_2O but concentrated H_2O solutions

resulted in the formation of J-aggregates (visible by a colour changed from purple to blue) which eventually precipitated out.

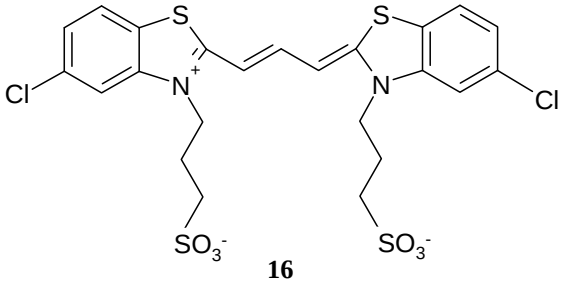

16

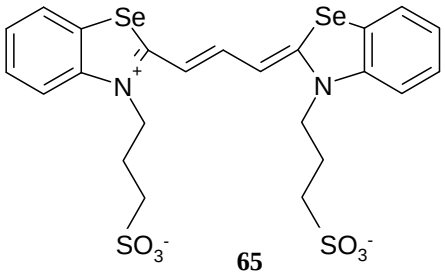

65

3.4 Biscarbocyanine Dyes

Preparation of the biscarbocyanine **66** was investigated using the same method for the trimethine dyes, (Scheme 3.8). The product, **66**, was a dark purple solid that was only very partially soluble in water, which did allow for a dilute UV-Vis spectrum to be obtained. This corresponded to the spectra observed by Hetz *et al*[37] suggesting the presence of the desired product but it was not possible to determine its level of purity. Solid state NMR spectra were acquired but these proved to be inconclusive and nothing was observed by electrospray mass spectrometry. This dye was insoluble in a wide range of common solvents and so it was not possible to observe the behaviour of the dye in solution, and in particular to investigate the behaviour of a fixed dimer.

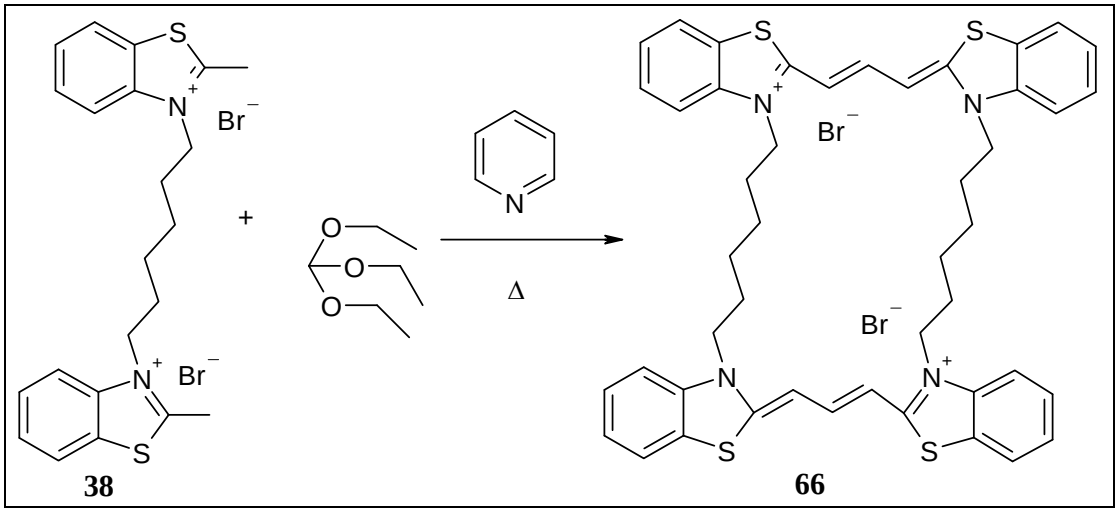

38 **66**

Scheme 3.8. Condensation reaction with orthoester in the presence of pyridine to produce a cyclic-bistrimethine dye.

3.5 Pentamethine Dyes

Pentamethine dyes were prepared using a simple condensation reaction shown in Scheme 3.9[74]. This method had to be carefully monitored by UV-Visible spectroscopy by monitoring the ratio of peaks at ~560 nm and ~650 nm (~480 nm and ~580 nm for oxapentamethines). If the reaction was left on for too long and the ratio of these peaks started to decrease, an insoluble, uncharacterisable product resulted.

After several attempts to purify these compounds by crystallisation, mass spectrometry still indicated the presence of starting material in all cases, meaning that none of the dyes could be used for physical studies, other than for rough comparisons. The yields using this method ranged from as little as 5% to a maximum of only 30%.

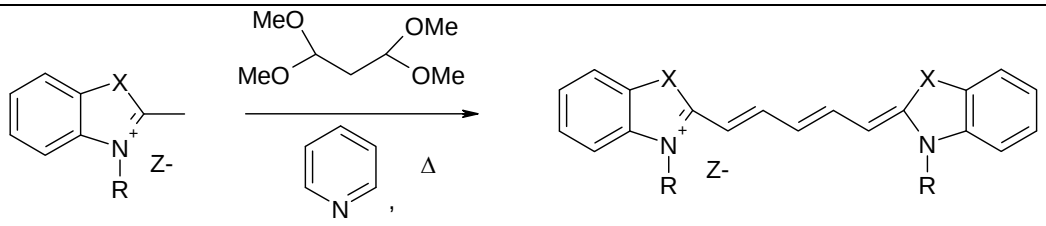

Dye	X	R	Z	Yield (%)
4	S	Ethyl	I	05
67	O	Ethyl	I	06
68	S	Benzyl	Br	22
69	S	Phenethyl	Br	30
70	S	4-Bromobenzyl	Br	29

Scheme 3.9. Condensation reaction of active methyl quaternary salt heated to reflux in the presence of pyridine and an tetraethylacetal resulting in a symmetrical dicarbocyanine

3.6 Inclusion of Dyes into Cyclodextrins

Several attempts were made to insert cyanine dyes into cyclodextrin cavities to try and isolate and study a restricted monomer or dimer. Initial attempts involved stirring several of the cyanine dyes, **2a**, **49** and **50**, in the presence of β-cyclodextrin in water. These hydrophobic dyes were expected to insert into the hydrophobic CD cavity but no change in the absorbance of the dye occurred indicating no interaction between the

dye and the CD. The second method used involved stirring the dyes in the presence of cyclodextrin in MeCN, this being compatible with both the dye and CD. This was the most successful method with a new peak forming on the crude UV-vis spectrum but unfortunately it was not possible to separate the mixture of uncomplexed dye, the cyclodextrin and any dye-cyclodextrin complex. The problem with both of these methods, as reported in literature, is the reversibility of dye/cyclodextrin complexation[54]. Buston *et al*[54] prepared a non-symmetrical cyanine dye in the presence of the cyclodextrin which resulted in a mixture of dye and dye-CD complex. Our attempts to synthesise the dyes in the presence of a CD resulted in a dark solid, the characterisation of which was not possible due to its insolubility in most common solvents. It was therefore not possible to determine if formation of the dye or its complexation with the cyclodextrin had occurred.

3.7 Spectroscopic Techniques

The most reliable method for measuring purity of the precursor, desired dye and any unwanted dye structures was electrospray mass spectrometry. The dyes and the precursors flew well and showed up easily. A sample with a high proportion of unreacted starting material present in it could easily be identified by NMR methods, in which case further purification was required. When a small amount of starting material was present (~ 2 or 3 %) only mass spectrometry was sensitive enough to detect it. Although UV-visible spectroscopy cannot differentiate between dye and unreacted starting material, it is a useful method for the detection of dye by-products along with mass spectrometry. UV-visible spectroscopy provided a quick and reliable method for following the pathway of a reaction especially in the cases of meso-substituted trimethine dyes and pentamethine dyes.

3.8 Conclusions

A range of compounds have been prepared and purified. The synthesis of these compounds was relatively simple as the same procedure could be used for each dye with only slight modification. Achieving purity suitable for the physical-type studies (primarily identifiable by ESMS) was often problematic especially as the starting material, the desired dye and any unwanted dyes had similar properties. The reactions were carried out on a small scale (~1 g), as scaling up to larger quantities resulted in higher proportions of unreacted starting material. Because of the difficulties in

purification, it was more sensible to do several small-scale reactions to obtain the same amount of product than one larger scale preparation.

The preparations of oxygen- and selenium-containing quaternary salts and dyes were slow and low yielding, therefore the majority of compounds prepared were the sulfur analogues. The monomethine dyes have small systematic changes enabling direct comparisons to be made as to the effect of each change. The trimethine dyes prepared have a wider range of variations making the study less systematic than the monomethines.

These structures have been written up in the traditional manner in the experimental section but as mentioned in Chapter 8 some of the data is available on an ELN package. Several of these structures have been reported previously in the literature but their characterisation is incomplete[70] because of the limited characterization techniques available at the time of reporting. In the present study each structure is characterised fully irrespective of whether it has been previously reported or is a novel compound to ensure the availability of a complete data set.

Chapter 4

Solution Studies

The aggregation properties of a range of cyanine dyes will be presented in this chapter, focusing on the effect of the molecular structure on these aggregates. The effect of the molecular structure on the chromophore will firstly be discussed followed by the properties of the water soluble dyes and finally the hydrophobic dyes. The main methods used in literature to detect any aggregation in bulk solution include UV-Visible spectroscopy[78], Fluorimetry[33] and NMR studies[79]. UV-Visible spectroscopy provides a quick and easy way of analysing the aggregation behaviour by the appearance and disappearance of absorption bands. As mentioned earlier, based on the shift of the new band in comparison with the monomeric band/species, we gain an insight into the nature of any aggregation structures therefore the behaviour of these dyes has been monitored using UV-Visible spectroscopy together with some emission spectroscopy. Earlier related work is described along with the behaviour of several novel dyes as part of a large comparative study.

Throughout these experiments it is worth noting, solvent along with the ions present play a key role in controlling what properties can be investigated. As mentioned previously, cyanines dyes generally form aggregates in aqueous solution. This is because of the charge screening effect of water as a result of the high dielectric constant (~80)[80] which encourages aggregation. Additives that increase the effective dielectric constant can further reduce repulsion between similarly charged organic ions and thus facilitate their interaction. The opposite effect can be expected from compounds that diminish this constant[37].

To study the properties of the chromophore and minimise the formation of aggregates it is important to use a solvent that the majority of dyes are soluble in but which has a low charge screening effect. To study aggregation properties the dyes need to be soluble in water. Dyes which have low solubility in water therefore require the presence of a water miscible solvent to aid dissolution before further dilution with water. Methanol was the appropriate choice for both conditions as it ensured

maximum solubility but minimised aggregation where appropriate (dielectric constant of ~33)[80].

4.1 The Effect of Molecular Structure on the Chromophore

The following section investigates the effect of the molecular structure on the chromophore of a range of trimethine dyes. Several pentamethine and monomethine dyes are also included in these investigations as a comparison.

4.1.1 Extinction coefficients

To minimise the effect of aggregation but to ensure the maximum solubility, the extinction coefficients, ε, were measured in MeOH at room temperature. As discussed in Chapter 1, using a non-aqueous solution limits the amount of aggregation and therefore enables Beer-Lambert Law behaviour to be observed. It is known that aggregating dyes do not obey this rule[13] because of the different species formed as concentration is increased. Figure 4.1 shows some examples of how the absorbance at λ_{max} changes with increasing concentration. The change in the absorbance with increasing concentration results in straight lines indicating that no aggregation is occurring. Using the following equation meant that the gradient of the plot of the absorbance, A, at λ_{max} vs. concentration, c, resulted in ε, shown in Table 4.1.

$$\varepsilon = \frac{A}{cl} \quad \text{where l= path length}$$

The monomethine dyes have extinction coefficient values roughly half those of the trimethines and the pentamethines are roughly double the trimethines, showing that the increase in the conjugation improves ε of the dyes, as expected.

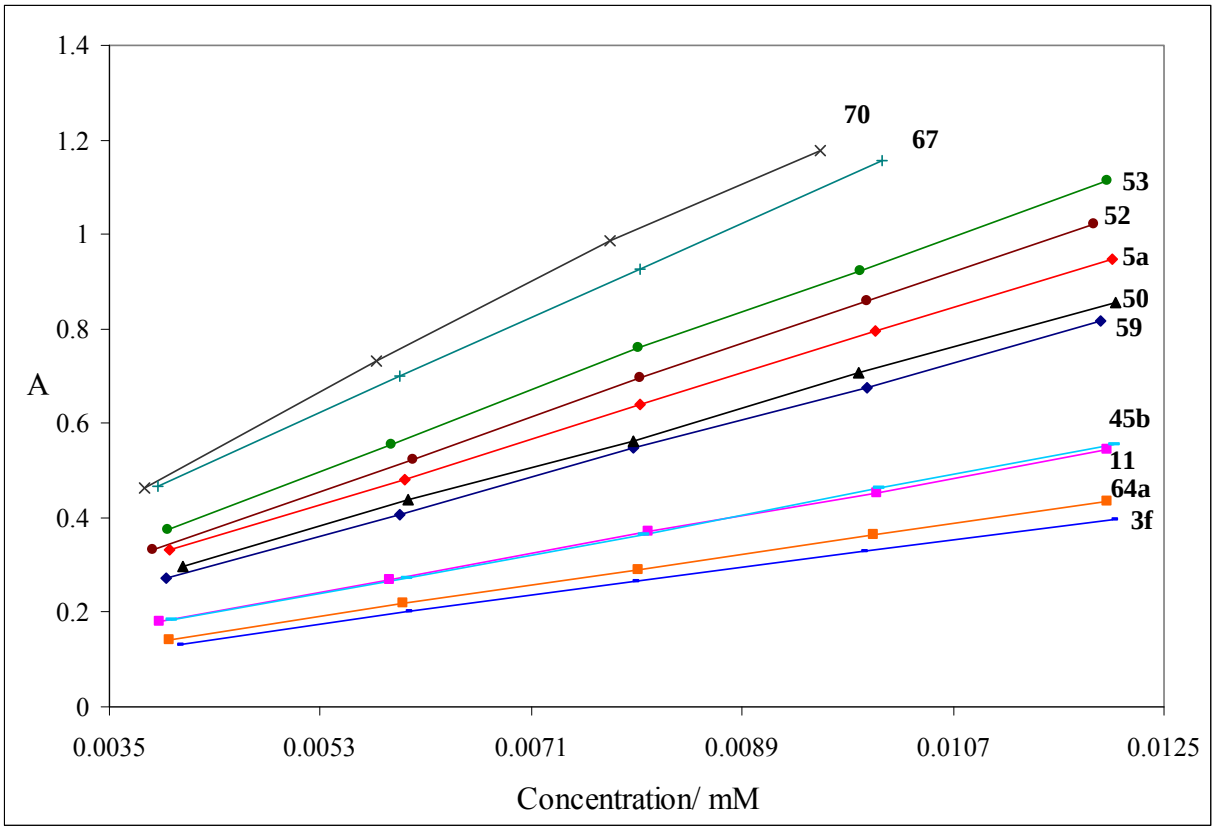

Figure 4.1. A plot showing how the λ_{max} absorbances of a range of dyes in MeOH increase as a function of concentration (over the range 0.004 mM to 0.012 mM). The data was then used to calculate the extinction coefficients shown in Table 4.1. Pathlengths of 5 mm used.

Molecule	ε/ $M^{-1}cm^{-1}$	λ_{max}
2a	126000	556
3f	66000	423
5a	154000	482
11	90000	548
45b	93000	428
46a	104000	426
48	152000	481
49	168000	560
50	140000	561
51	159000	561
52	172000	561
53	188000	561
54	166000	566
55	177000	561
56	172000	566
57	123000	558
58	134000	558
59	137000	546
64a	73000	430
68	>260000*	658
67	>223000*	584
70	>239000*	659

*Table 4.1. Extinction coefficients calculated from MeOH solutions ([dye]= 0.004 to 0.012 mM). A pathlength of 5 mm was used to measure the absorbance of these solutions. *Pentamethine ε values approx values as compound not pure, Chapter 3.*

As expected the ε of the 9-substituted derivative **11** is considerably lower than that of the majority of the unsubstituted trimethine dyes, with a value similar to the monomethine dyes i.e. an order of magnitude lower. Kabatc *et al.* report that the value of the ε for alkyl substituted *meso* dyes is about one order of magnitude lower than that for non-substituted dyes[33]. Interestingly however the 9-substituted derivative **59** has a ε_{eff} value which is similar to that of the unsubstituted dyes. It appears in this case that the 9-substituent has very little effect on the chromophore of the dye.

It is not realistic to make generalised observations in terms of the effect of the heteroatom on ε because so few oxygen dyes were prepared and studied. What can be said in the case of both trimethines, **5a** and **48,** they exhibit larger ε values than their sulfur analogues. The oxygen containing monomethine **44b** could not be measured in this manner because of its low solubility in MeOH. Introducing halogen atoms in the 5-positions and 3-alkyl substituents also increased the ε values when compared with the non-halogenated analogues indicating that these atoms have an effect on the chromophore of the dye. Because of the different positions of the halogen substituents it is difficult to say whether the effect is electronic or steric.

In summary, increasing the length of the methine chain has the most dramatic effect on the absorption of the dyes but ε can be tuned with small structural changes. Introducing aromatic groups in the 3-position and halogens in the 5-position tend to increase ε and as we will see they also increase the resistance of the dye to photodegradation.

4.1.2 Photostability

Photostability is an important aspect of these dyes especially in solution. To use the dyes in any application where they will be exposed to light, it is important to know the durability of a dissolved molecule as the degradation process normally results in a reduced ability of the molecule to be detected. It is therefore important to investigate the effect different groups have on the photostability of cyanine dyes. Chen *et a.l*[31] describe how the presence of large benzyl groups attached to the nitrogen improved the photostability of a cyanine dye.

Early qualitative experiments investigated the effect of exposing a range of dyes to light of 254 nm. Acetonitrile proved to be the solvent dyes were most soluble in (monomethine **44b** was not very soluble in MeOH) and ensured no aggregates could form. These solutions were then exposed to the light using quartz cells and monitored by UV-visible spectroscopy at regular intervals to measure the degradation of the solution. Solutions of dyes **2a**, **49**, **61** and **50** were exposed to the light and a noticeable change had occurred after <4 hours. The intensity of **2a** decreased by 30%,

49 by 18%, **61** by 10% and **50** by 2% with **50** the most resistant to degradation and **2a** the least i.e. **50**> **49** > **61** > **2a**. This shows that having larger groups in the 3-position and alkyl substituents in the 9-position improves resistance to photodegradation of a carbocyanine.

Comparing trimethine dyes to the shorter monomethine dyes shows that, at this wavelength of light, the monomethine dyes are more resistant to photobleaching. For an exposure period of <4 hours the absorption of the dye **3f** and **44b** had only decreased by 1% and <1% respectively.

There are two hypotheses as to why this photobleaching process occurs; the first is the rearrangement of the molecule as a direct result of the light and the second involves the dye being broken down by singlet oxygen. Generally the occurrence of degradation by rearrangement results in the intensity of one peak decreasing as additional bands form when monitored by UV-Visible spectroscopy. This was not observed leading to the conclusion the degradation of these dyes is due to singlet oxygen. Other studies have shown that cyanine dyes are very susceptible to degradation by the addition of singlet oxygen generated in-situ (Scheme 4.1) across the methine chain[81] resulting in photobleaching. As a control experiment, crystals of both **2a** and **49** were exposed to the same light source as had been used in the solution experiments whilst monitoring any colour loss and/or change. No change in the crystals occurred when exposed for a substantial duration supporting the view that it is because the dyes are in solution they are being bleached.

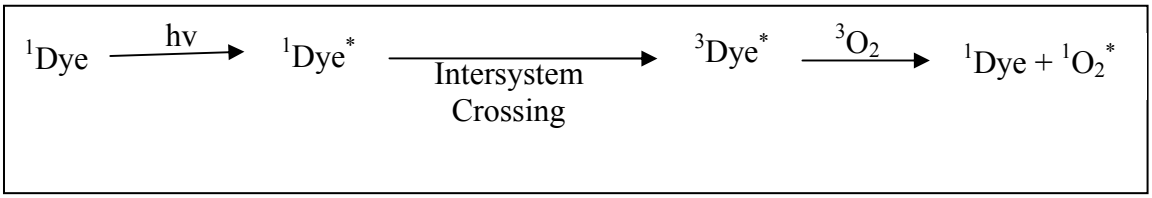

Scheme 4.1.[81] Photochemical production of singlet oxygen ($^1O_2$) from fluorescent dyes

4.1.3 Fluorescence

The fluorescence of cyanine dyes can be affected by both the process of self-quenching as a function of the concentration and the type of aggregates formed (this will be discussed later in the chapter). At low concentrations the fluorescence emission increases proportionally to the concentration but, at a certain point

(dependant on the dye structure) the dye self-quenches dramatically decreasing the emission. By studying the effect of structure on the fluorescence behaviour in non-aggregating dyes, quenching can be reduced.

The emission spectra of a range of trimethine dyes were studied in alcoholic solution in order to minimise aggregation and investigate the effect of the structure on the fluorescence yield and self quenching. As expected initially the concentration of a cyanine dye is increased with a corresponding increase in the fluorescence emission followed by a decrease because of quenching by the molecules. Figure 4.2 and Table 4.2 illustrate the results. It is clear to see the following general trends:

- The intensity of the emission of the oxygen containing dyes is larger than that for the sulfur containing analogues.
- The introduction of a 9-substituent greatly reduces the intensity. This is not entirely surprising with the exception of **59** which, when compared to ε, had a value much larger than expected.
- Introducing fluorine substituents in the 5-position (**56** & **55**) has little effect compared to the analogous unsubstituted dyes **2a** and **49** whereas the intensity of 5-chloro dyes, **53** and **54**, is increased in both cases. The 5-chloro groups also appear to have the effect of reducing the concentration at which the dyes start to self-quench, **54** being most prominent.
- Introducing bulky groups in the 3-position only separated by one carbon atom from the nitrogen atom of the core (e.g. benzyl and naphthyl) increases the emission intensity.

By scanning over different ranges of wavelengths it was observed that the dyes exhibited resonance fluorescence. Resonance fluorescence has an identical wavelength to the radiation that caused the fluorescence[82] because the system is losing very little energy. As a result, all of the scanning ranges start below the excitation wavelength. Another observed effect is the shifting of the λ_{max} to longer wavelengths as the concentration of the dye is increased.

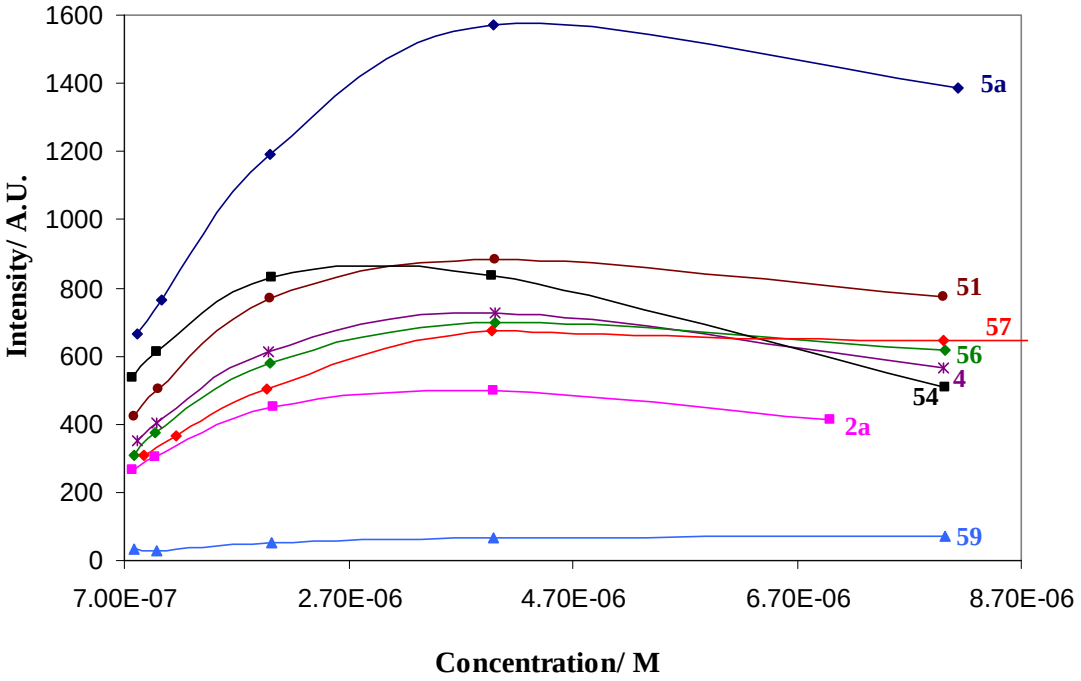

Figure 4.2. The intensity measured at the maximum emission of various dyes in MeOH as a function of concentration.

Dye	Shift λ_{max}/ nm	Max emission/ A.U.
2a	7	501
5a	5	1570
11	8.5	71
48	5	1218
49	6.5	726
50	7	485
51	7	883
52	6	778
53	7	649
54	7.5	833
55	7	498
56	6.5	700
57	7	675
58	6	638
59	10.5	69

Table 4.2. The maximum emissions and shift of λ_{max} for a range of monomethine and trimethine dyes

4.2 Aggregation Behaviour of Water Soluble Dyes

To better understand, quantify and therefore reduce the effect of methanol as the solvent on the aggregation process, the deaggregation of aqueous solutions of **57** were investigated with increasing concentrations of methanol ranging from 0 – 80%. Figure 4.3 clearly shows that, as the amount of MeOH is increased, the D-band decreases with a corresponding increase in the M-band as the dimer deaggregates. It is important to be aware that there are two effects occurring with increasing concentrations of methanol; firstly deaggregation and secondly a solvent shift which is most obvious from the M-band.

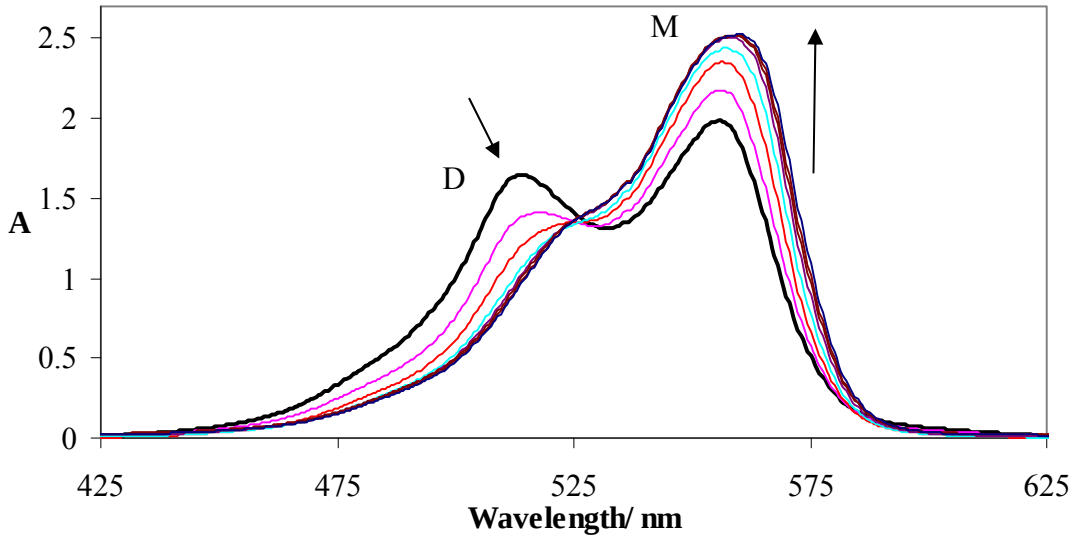

Figure 4.3. Absorption spectra of ***57*** *in water/MeOH mix. [****57****] 0.025 mM. Percentage MeOH: 0 - 80 vol% Insert showing the change as function of the concentration MeOH. The heavy line is the absorption of the dye in 100 % water.*

4.2.1 Aqueous Aggregation Studies

As expected, studying the water soluble dyes **11**, **57** and **58** in aqueous solution showed the clear formation of a dimer D-band as the concentration of the dye increased. An example of this is shown in Figure 4.4 demonstrating how, even at high concentrations, **11** does not form more extensive H- or J-aggregates than a H-dimer. It is known that structures similar to these only form H-dimers in bulk aqueous solution[27]. The formation of a distinct isosbestic point in the examples shown

indicates a simple mechanism of one species directly converting to another, suggesting a monomer to a dimer. In the cases where different species exist in solution the term effective extinction coefficient shall be used, ε_{eff}.

a)

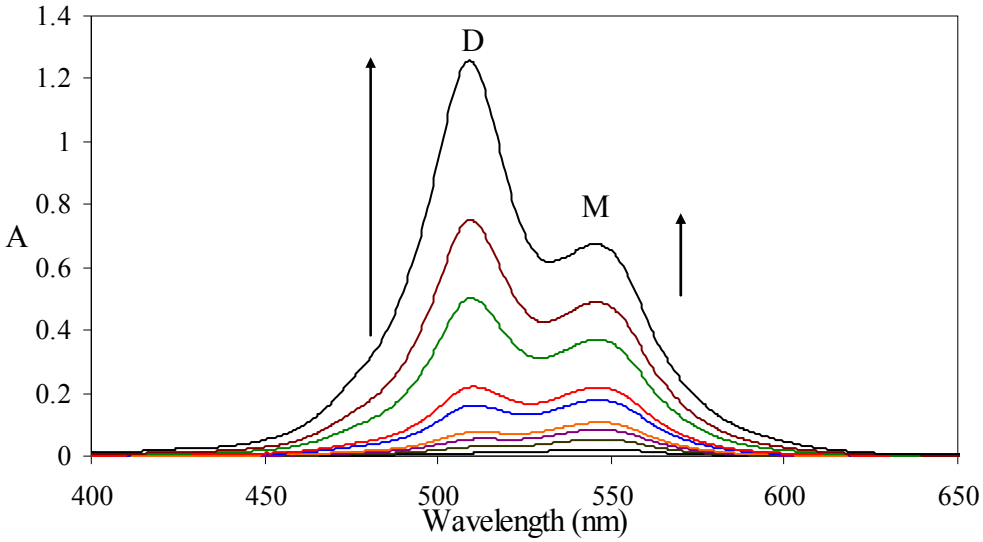

b)

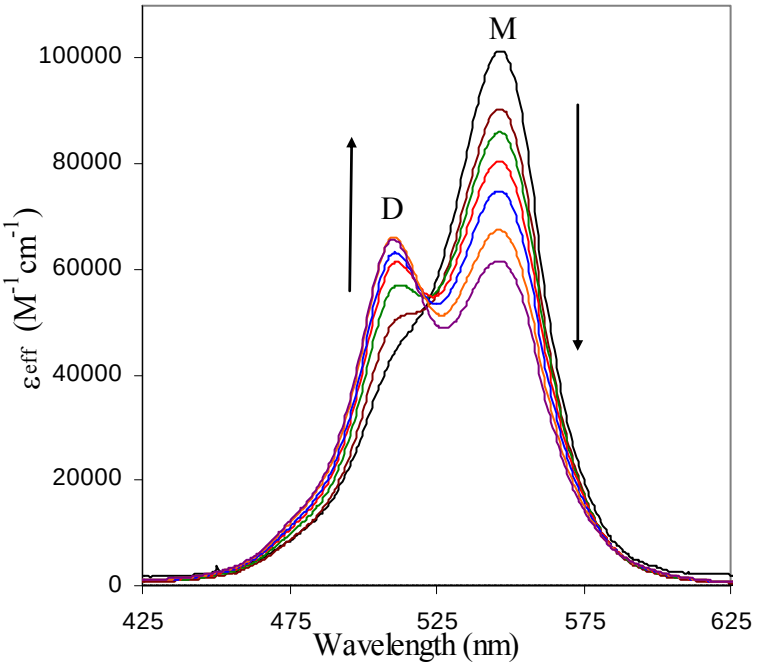

*Figure 4.4. Absorption spectra of **11** in aqueous solution. a) Increasing concentrations from 2 μM to 0.12 mM. Absorption measured using 1 mm path length cuvettes. b) Change in effective extinction coefficient, ε_{eff}, of **11** as the dye concentration is increased. Data set different to that shown in a) to illustrate the isosbestic point. Concentrations of **11** ranged from 2 μM to 0.04 mM. Absorbance measured in 5 mm cuvettes.*

The unsubstituted **57** and **58** demonstrate similar behaviour to that of **11** with the monomeric absorption decreasing and a corresponding increase in the dimeric absorption with increasing concentration, shown in Figure 4.5. Like **11**, higher concentrations (<0.1 mM) of **57** and **58** were investigated. These unsubstituted analogues were found to form further H-aggregates. In the case of **58**, as shown in Figure 4.6, increasing the concentration of the dye lead to the formation of a D-band whilst the monomeric absorption decreases. Unlike **11** however, further H-aggregates start developing at 0.25 mM (shoulder at ~450- 490 nm) but because of the strong absorption of the dye even using the 1 mm pathlength, the spectrum distorts above this concentration.

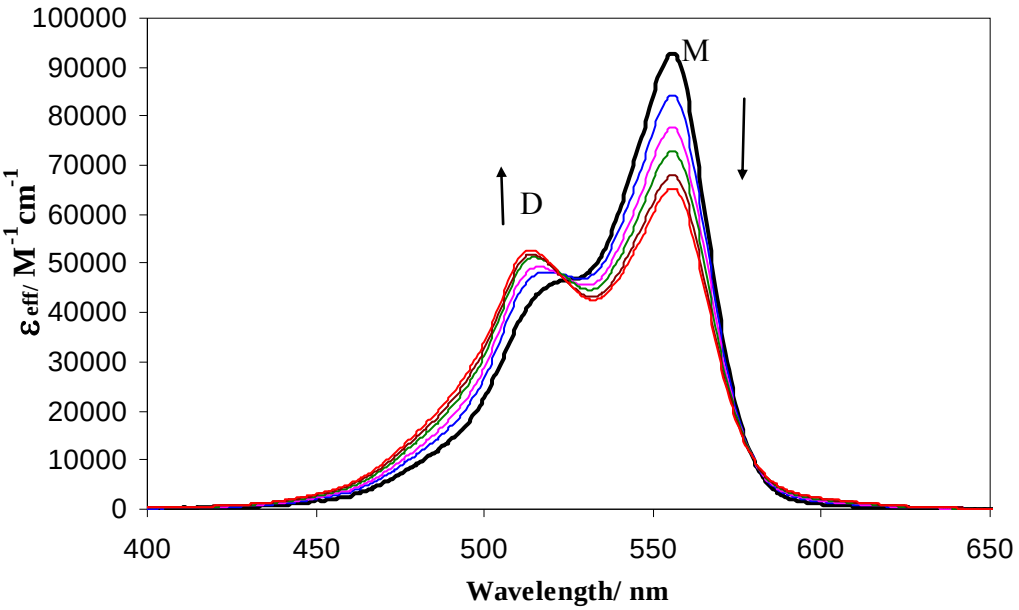

*Figure 4.5. The normalised UV-Vis absorbance of **58** in water. The absorbances at 509 and 545 nm change relative to one another with an isosobestic point indicating the conversion of one species directly to another. The simplicity of the conversion suggests the presence of a monomer → dimer equilibrium. The concentrations range from $3.9x10^{-6}$ – $2.9x10^{-5}$M.*

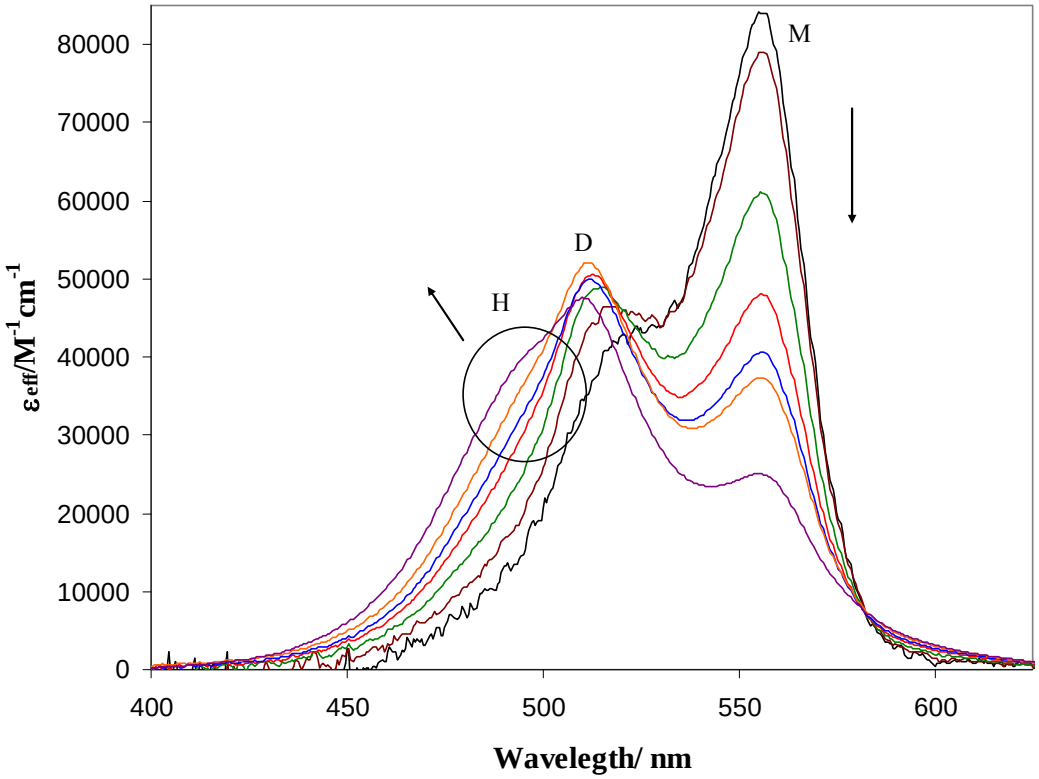

Figure 4.6. Change in normalised absorption of **58** *as the concentration of the dye is increased. 1 mm cuvettes used. At the higher concentrations an extra shoulder starts developing (circled).*

The number of molecules involved in an aggregation as a result of increasing concentration can be calculated using UV-Visible data by comparing the absorbances of the aggregate versus the monomer. By plotting log $A_{monomer}$ vs. log $A_{Aggregate}$ the gradient of the slope gives the number of molecules involved in an aggregation i.e. 2 represents a dimer and 3 a trimer[27]. When these were calculated for **11**, **57** and **58** using experimental data the resulting gradients were ~1.3 for all three compounds, Figures 4.7. This does throw into doubt whether this method is suitable for these dyes without taking into consideration the overlap of the monomeric and dimeric absorptions, discussed in more detail below.

a)

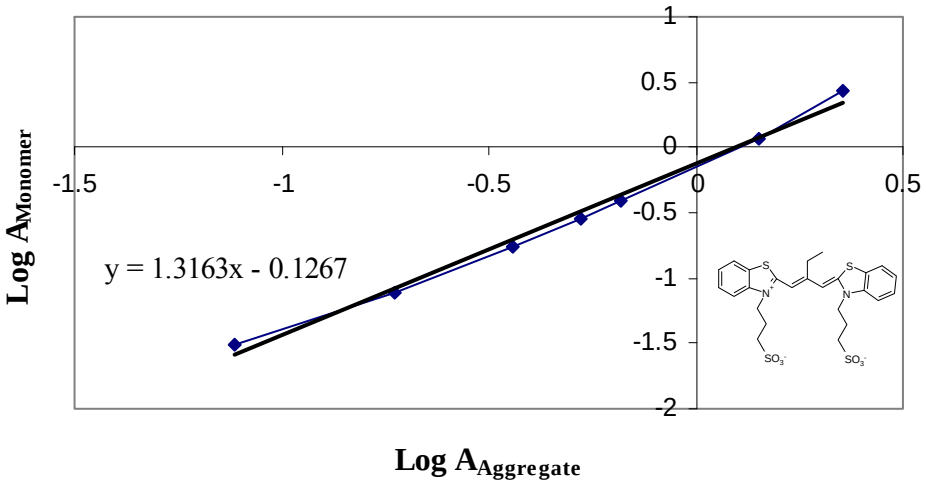

b)

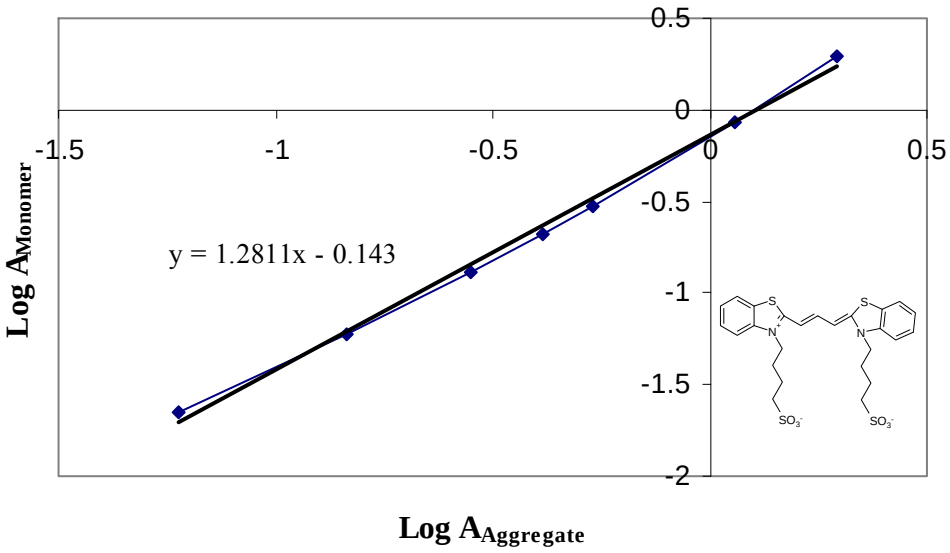

c)

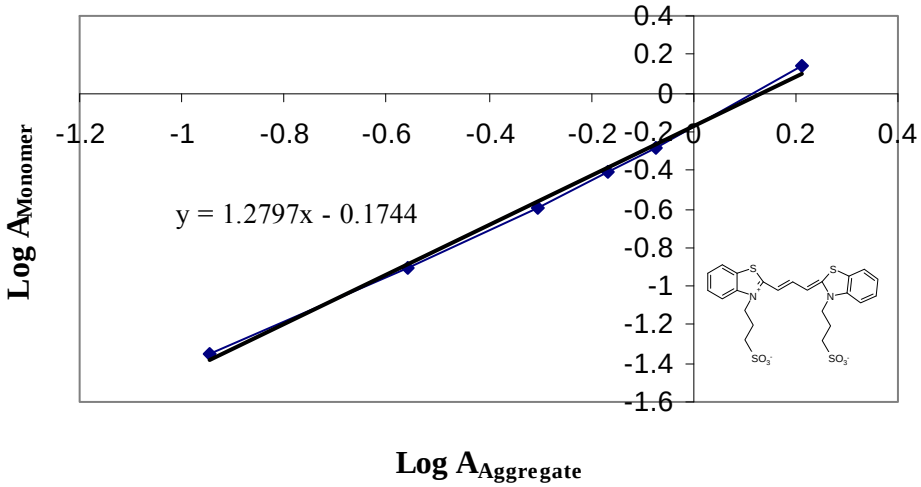

Figure 4.7. Plot of the log A_{dimer} vs log $A_{monomer}$ of a) **11**, b) **57** and C) **58** *which are known to demonstrate the number of molecules involved in the aggregate*[33].

Even when absorbance of these dyes is measured in methanol or very dilute concentrations, when aggregation can be considered minimal, there is a distinct shoulder (as discussed in Chapter 1) at shorter wavelengths in the region where H-dimers absorb. For this reason it is important when considering kinetic calculations the monomeric component of the dimer absorption is taken into account.

As shown in Figure 4.4 the absorbance spectrum of **11** (0.01 mM) in distilled water shows a monomer band at 545 nm with a shoulder resulting from the dimer at 509 nm. As the concentration of the dye increases there is a conversion of the monomer to the dimer. In this case where only dimerization needs to be considered, the UV/Vis spectra can be deconvoluted to give the proportions of the monomer and dimer species. At higher concentrations both species contribute and the spectra overlap to some degree, so that is it better to attempt to deconvolute the spectrum rather than assume that at specific wavelengths only the monomer or the dimer contribute to the observed absorbance.

The following calculations and results were facilitated by Frey[83]. With the concentration of monomer C_M and the dimer C_D, the conservation of the monomers means that the total concentration of monomer, C_0, is related by,

$$C_0 = C_M + 2 * C_D$$

The observed absorbance is made up of two terms

$$A(\lambda) = \varepsilon_M(\lambda) C_M l + \varepsilon_D(\lambda) C_D l$$

and the effective absorption coefficient is

$$\varepsilon(\lambda) = {A(\lambda)}/{C_0 l} = \alpha_M \varepsilon_M(\lambda) + \alpha_D \varepsilon_D(\lambda)$$

where the α are the mole fractions of the species in the mixture, so that

$$\alpha_M = C_M / C_0$$
$$\alpha_D = C_D / C_0$$
$$\alpha_M + 2\alpha_D = 1$$

Using the low concentration spectrum to determine $\varepsilon_M(\lambda)$ and the highest concentration (before any significant J-aggregates are formed) to then derive the dimer spectrum, the fractions of monomer and dimer were then determined for each measured spectrum.

The equilibrium is

$$M + M \rightleftharpoons D$$

With equilibrium constant,

$$K = \frac{[D]}{[M]^2} = \frac{C_D}{C_M^2} = \frac{\alpha_D}{\alpha_M^2 C_0}$$

so a plot of $\frac{\alpha_D}{\alpha_M^2}$ *vs.* C_0 should be a straight line with zero intercept, with a slope of *K*.

For the dye **11** the plot in Figure 4.8 shows the quality of the data and a linear least-squares fit gives

$K = 15150 \pm 350\ M^{-1}$

$\Delta G^{\theta} = -24.0 \pm 0.15$ kJ/mol (95% confidence limits)

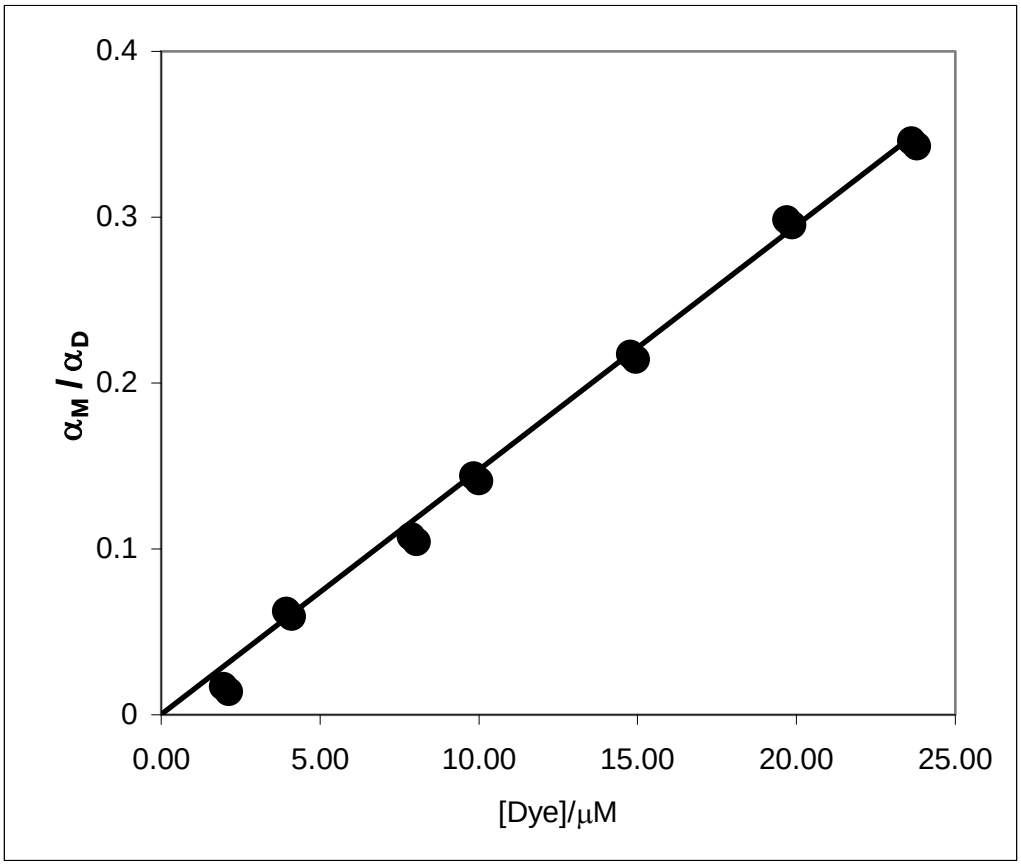

*Figure 4.8. Data used to calculate K for **11**, showing the quality of the data. The line goes through the origin indicating high quality data.*

As discussed in Chapter 1, Takahashi *et al.*[27] calculated the dimerisation association constants for a range of dyes including **11** for which $K_D = 1.24 \times 10^4$ dm^3mol^{-1}. This value is slightly different from the value obtained from the results obtained above (1.52×10^4 dm^3mol^{-1}) but this is not surprising as it does not appear that Takahashi *et al.* take into consideration the overlap of the M-band and the D-band.

4.2.2 Salt-induced Aggregations of Water Soluble Dyes

As we have seen so far, dyes **11**, **57** and **58** only form H-dimers in aqueous solution allowing us to control the formation of higher aggregates with salts.

It was noted that, in the presence of Na_2SO_4, solutions of aqueous **11**, **57** and **58** all changed colour with the UV-Visible absorption of these solutions showing the formation of distinct J-bands. Dye **11** was used for the subsequent studies for the following two reasons; 1) the non-substituted **57** and **58** were very susceptible to

photodegradation, more so than the 9-substituted **11** (these results are comparable to photostability experiments discussed earlier in this chapter), and 2) **11** formed distinct D- and J-bands as a result of the 9-substituent unlike **57** and **58** which form other aggregates including higher H-aggregates, as seen in Figure 4.6.

To ensure that the dyes were exposed to the salt for the same duration, and to minimise photobleaching and differences in solubility, the salt was dissolved in the minimal volume of water, the dye solution was then added in the dark and quickly made up to the mark before running the absorption spectrum. The average time taken to start the absorption scan was ~40 seconds but, for consistency and to minimise any human errors, spectra were measured after 60 seconds. Initial experiments showed that after 60 seconds no more aggregates formed, with measurements taken earlier being unreliable.

Figure 4.9 shows the effect of increasing the salt concentration; initially there is the formation of the dimer (~510 nm) with a corresponding decrease in monomer peak (546 nm), the dimer peak then starts decreasing with the eventual appearance of a J-band (620 nm) as a result of J-aggregation at ~0.5 M salt. A clearly defined isosbestic point occurs at 522 nm indicating the monomer directly converts to the dimer (comparable result when increasing dye concentration without the presence of salt, Figure 4.4). A less clearly defined isosbestic point arises at 569- 575 nm suggesting that the dimer/monomer species convert to the J-aggregate. Figure 4.10 shows the colour change that occurs upon addition of the salt as a result of the predominant species in solution. Using UV/ Vis absorption to observe the progression of the aggregation, one cannot tell whether the dimer dissociates and then forms the aggregate or whether it just slides into the lowest energy configuration and forms the aggregate. Several groups[44-46] describe the dimer as being an intermediate to the J-aggregates.

It is important to note, at the concentration of dye used in these experiments (0.01 mM), there is already a portion of dimer existing in solution before the salt is added. The results from this experiment seem in agreement with the literature where the absorbance of J-band increases with increasing salt concentrations[6,38]. The salt-dye solution was then protected from light for two days which resulted in the

disappearance of the M-, J- and H-bands as the solution became colourless and exhibited an apparently stable (as long as shielded from light) solid precipitate. This behaviour was also observed by Herz[37] and Takahashi *et al.*[27], as discussed in Chapter 1. Unfortunately, the solid was not identified in the present study. Future work could investigate this further.

a)

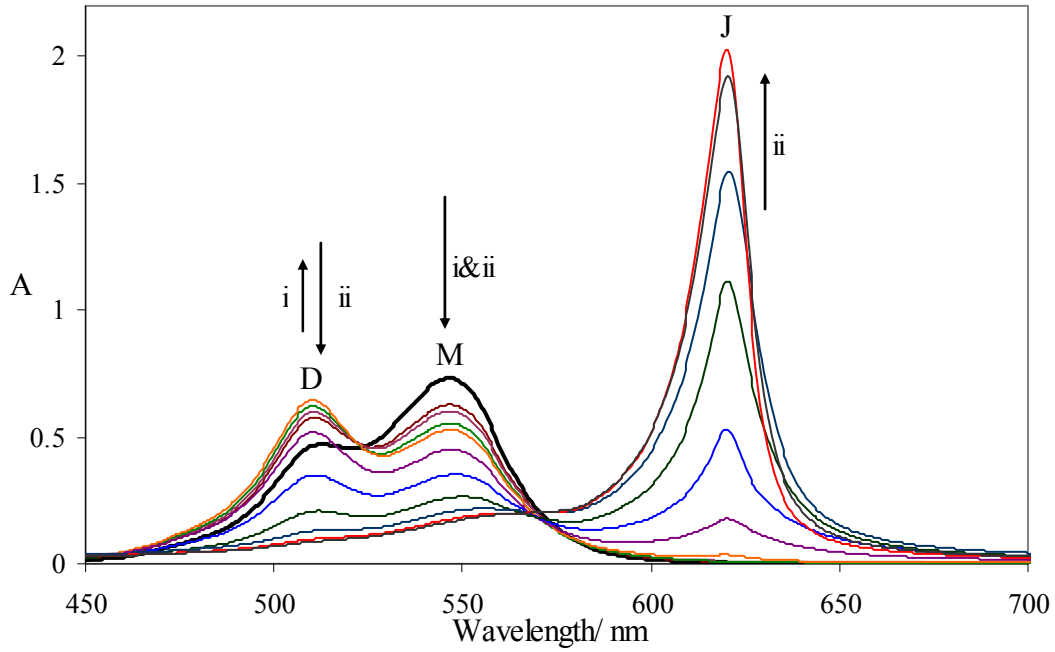

b)

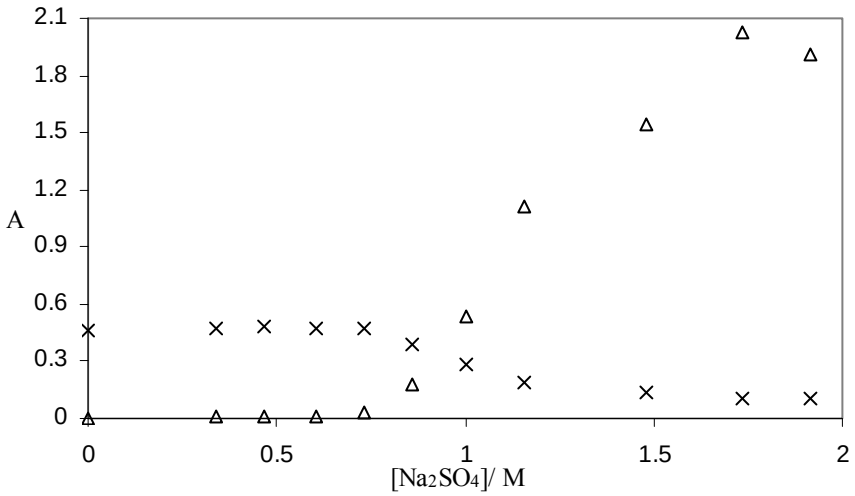

*Figure 4.9. a)Absorption spectra of aqueous **11** with various concentrations of Na_2SO_4 at 25 °C. As increasing concentration of Na_2SO_4 the absorbance the D-band initially increases (i) then decreases (ii), the M-band (546 nm) decreases throughout and the J-band (620 nm) increases when enough salt is present. Na_2SO_4 concentrations ranged from 0 - 1.9 M. The heavy line is the absorption of dye alone.*
*b) Changes in the absorbance of **11** at the J-band at 620 nm (△) and 522 nm (X) as a function of Na_2SO_4 concentration.*

*Figure 4.10. Photographs demonstrate the colour changes of **11** as a result of the addition of Na_2SO_4.*

These Na_2SO_4 experiments were carried out at two other dye concentrations. It was found that, at lower dye concentrations, more salt was needed to induce the aggregate, as shown in Figure 4.11.

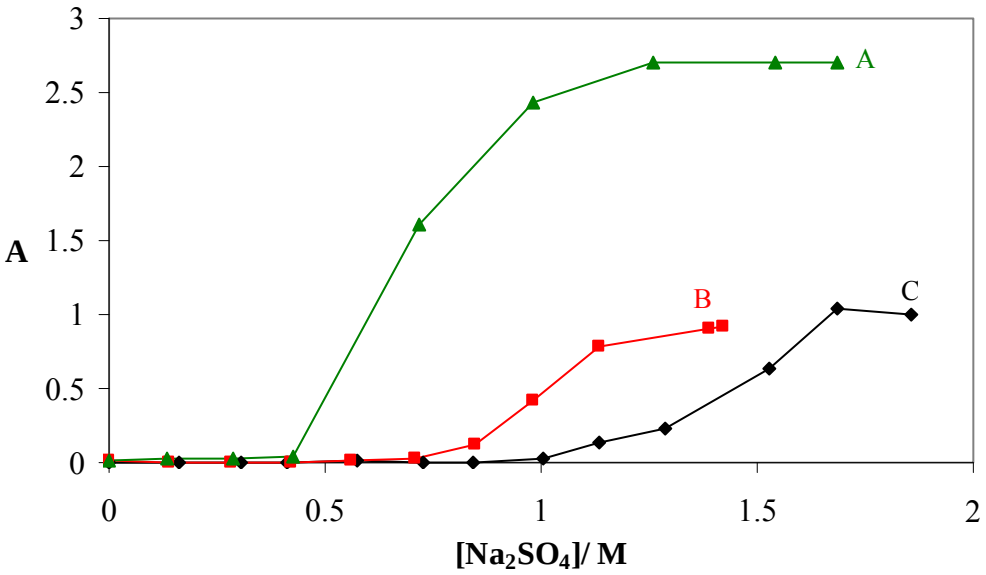

*Figure 4.11. Change in absorbance of **11** at 621 nm (aggregate peak) at different concentrations on addition of Na_2SO_4. A=2.5x10^{-5} M, B=1x10^{-5} M, C=5x10^{-6} M*

It was noted that during the experiment at high enough concentrations of salt, the aggregates that formed in solution appeared to be surface active. Patches of blue film appeared on the surface of any bubbles that formed. A blue film also appeared to

deposit on the surface of the pipette suggesting that the solubility of the J-aggregates in water is low which is reinforced by the formation of a stable J-aggregate precipitate. Shielded from light this solid lasted in solution for several months, even shaking the solution did not make the precipitate redissolve. This behaviour has been observed by several groups[27,37] with isolation of this precipitate by centrifuge. As discussed in Chapter 1, Harrison *et al.*[12] made the analogy of the aggregation behaviour of cyanine dyes to that of aqueous surfactant systems, shown in Scheme 1.3. The fact that a precipitate results from the induction of the aggregates does tend to suggest that some kind of destabilisation/insolubility processes are occurring and the behaviour is comparable to the destabilization of colloids with salts[84].

It was observed in early screening experiments that a few chloride salts did not induce any J-aggregates. NaCl was further investigated in some detail as a comparative study. By adding **11** to aqueous solutions of NaCl (0 – 5.3 M) different aggregation behaviours were observed to those resulting from the addition of Na_2SO_4, shown in Figure 4.12. The H-band increased, whilst the M-band decreased, however, even at very high NaCl concentrations (~5 M) no J-band was observed. In the presence of NaCl no distinct isosbestic point was observed. At higher concentrations of the dye it appeared from solution colour changes that the aggregation process when induced by NaCl is more complicated and slower compared to Na_2SO_4.

a)

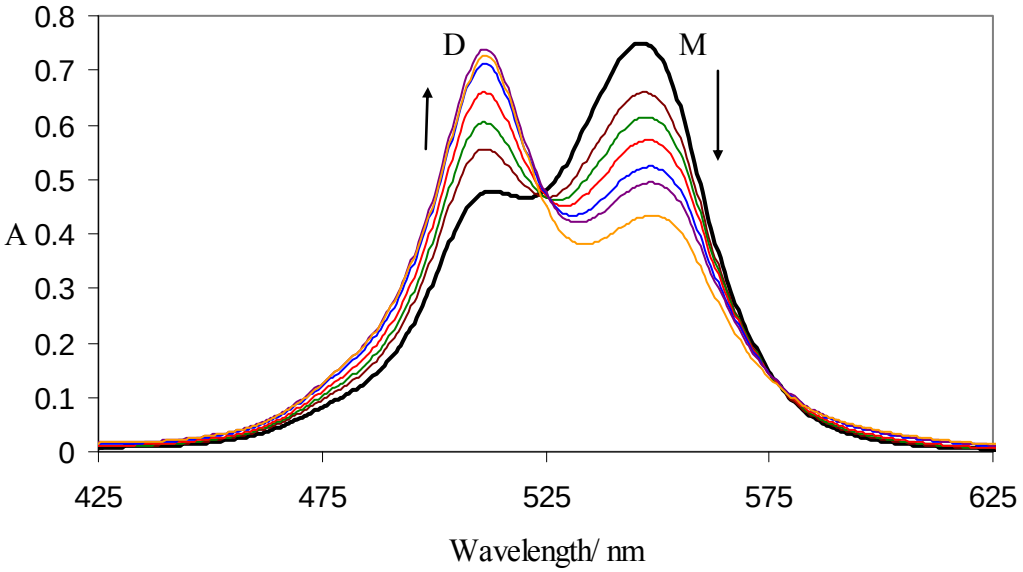

b)

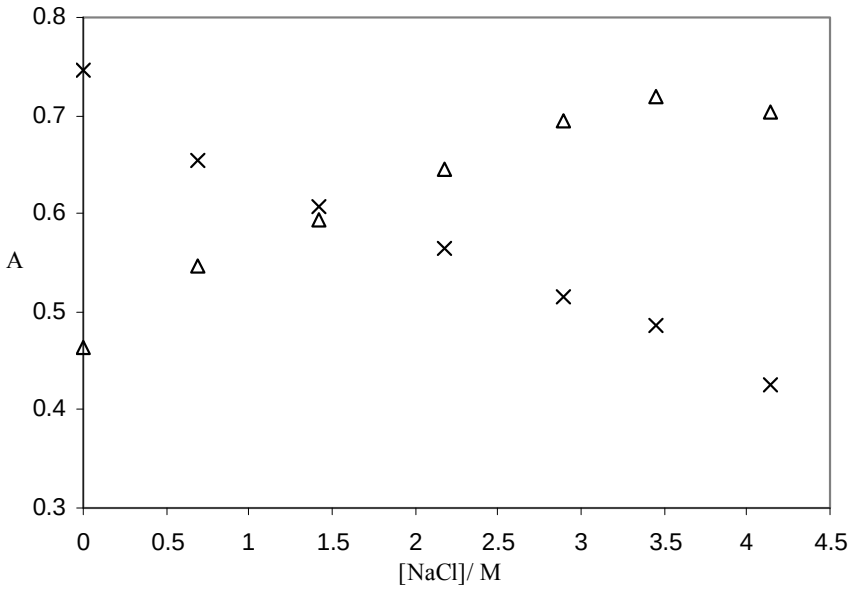

*Figure 4.12. Absorption spectra of aqueous **11** solutions a) different concentrations (0 - 4.14 M) of NaCl at 25 °C (b) Absorbances taken from λ_{max} of the H-band at 510 nm (△) and M-band at 545 nm (X).*

To rule out the effect of ionic strength on the observed aggregation differences experiments in which the ionic strength was maintained but using varying ratios of Na_2SO_4/NaCl were carried out. The results of these are shown in Figure 4.13. Na_2SO_4 has an ionic strength 3 times greater than NaCl so the ratios of salts were adjusted accordingly. Ionic strength is calculated using the formula:

$$I = \frac{1}{2}\sum Cz^2$$

Where I= ionic strength, C= concentration and z = charge of each component.

The absorbance of **11** changed markedly as the solutions varied from 100% Na_2SO_4 to 100% NaCl. In the presence of 100% Na_2SO_4 J-aggregates were the predominant species but as Na_2SO_4 was replaced with NaCl the J-band disappeared and the H- and M-band appeared. Even at the very low concentrations Na_2SO_4 is having a more significant effect on the aggregation of the dye than NaCl as going from 20% to 0% there is little change in the absorbance. This transition of J-band into H-band upon varying the salt from Na_2SO_4 to NaCl can be looked upon as a type of molecular switch or the dye behaving as a type of sensor. A similar observation was reported recently by Zhang *et al.*[38] but for a different type of study where the transition of J-aggregates into H-aggregates was brought about by removal of the potassium ion responsible for the J-aggregation using a complexation procedure.

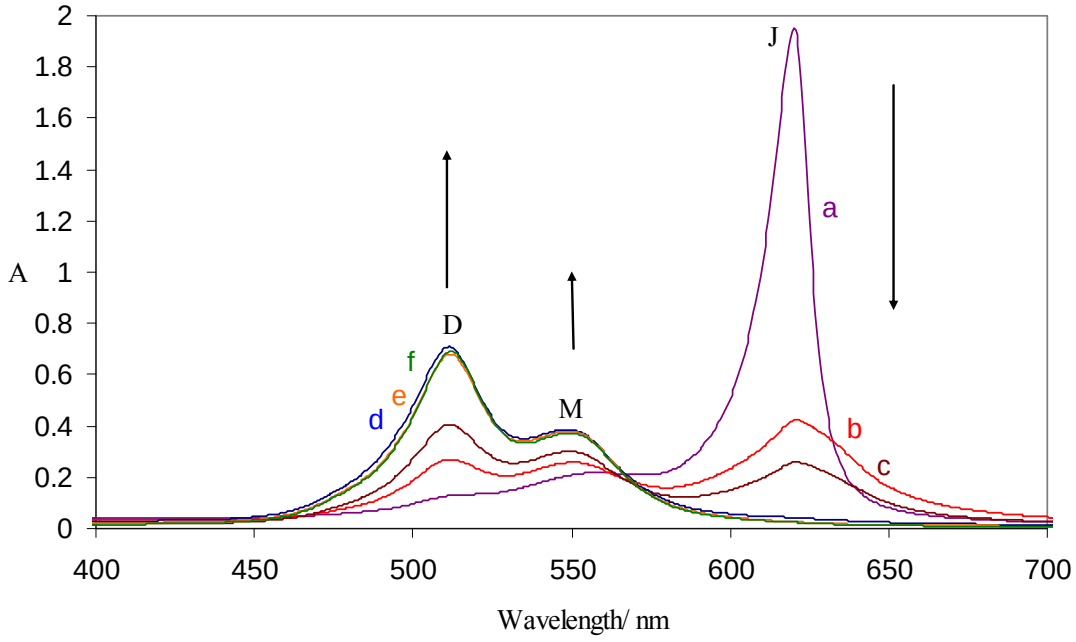

*Figure 4.13. Absorbance spectra of aqueous **11** in the presence of mixtures of Na_2SO_4/NaCl:* a) 1.61/ 0 M, b)1.28/ 0.97 M, c) 0.96/ 1.93 M, d) 0.64/ 2.90 M, e) 0.32/ 3.86 M and f) 0/ 4.83 M *at 25 °C. The ionic strength of the solution was maintained throughout.*

Several literature reports state that it is the metal ion that induces the aggregation with the anion being redundant.[6,19,23,25] From our results it is clear that the anion does play

a dominant role in the case of these dyes. A systematic salt study was carried out to investigate the effect of various salts on the absorbance of **11** as shown in Table 4.3. Here we show that whilst all the salts tested resulted in the promotion of H-bands only anions with a negative charge greater than 1 resulted in the formation of J-aggregates. Monovalent anions appear to be less efficient than di- and trivalent anions at inducing J-aggregation at the concentrations of **11** used even when the ionic strength of the salts are comparable. The fact that ammonium and metal salts have resulted in similar behaviour effects on the dyes further discounts recent theories that the key component in the induction of the aggregation process is a cationic metal, again with charge being important rather than the chemical characteristics of the components.

Salt	**Presence of J-band**
NH_4Cl	No
$(NH_4)_2SO_4$	Yes
NH_4NO_3	No
Na_2CO_3	Yes
$NaClO_4$	No
Na_2SO_3	Yes
K_2SO_4	Yes
KCl	No
K_3PO_4	Yes
$MgCl_2$	No
$MgSO_4$	Yes
$CaCl_2$	No

*Table 4.3. Effect of various salts on **11** in aqueous solutions at 1 x 10^{-5} M*

As mentioned above, it is important to note that the concentration of the dye solution is very important; Figure 4.11 showed that increasing the concentration of a dye solution reduces the amount of salt needed to induce any aggregation. At the dye concentrations considered earlier, a saturated solution of NaCl does not result in the formation of J-aggregates. If however the concentrations of the dye solutions are increased then eventually monovalent anions do result in the induction of J-aggregates

suggesting that the higher the charge, the more efficient the anion is at inducing aggregation such that monovalent < divalent < trivalent anions in terms of efficiency.

It is important to note that to rule out this behaviour being a result of the sulfonate groups or the meso-ethyl group, the salt-induced aggregation properties of **2a**, **58** and **59** were also investigated. It was important to show that the behaviour of **11** was not a result of interactions between the sulfo-groups and the anion but was behaviour common to this type of dye. This was observed with all four dyes showing the patterns observed for **11**.

At room temperature the formation of salt-induced aggregates was found to be dependant on the concentration of the dye, the salt and the charge of the anion. The aggregation process was determined to be complicated but, under the right conditions, can be finely tuned suggesting there may be potential for these cyanine dyes in a type of sensory role.

4.2.3 Fluorescence

Increasing the concentration of **58** was shown to result in the formation of H-dimers (Figure 4.5). The emission spectra of this aggregating solution was investigated and compared to the non-aggregating solution discussed in Section 4.1.3. The aqueous solution of **58** showed the normal behaviour of decreasing intensity due to self-quenching and a shift to longer wavelengths as the concentration is increased (0.004 – 0.011 mM) shown in Figure 4.14. There is little difference in the fluorescence behaviour between the non-aggregating and aggregating solution suggesting that there is little effect on the emission from the formation of H-aggregates (dimers in this case) but that the dominant effect in the reduction was the self-quenching. Dyes **11** and **57** showed similar behaviour.

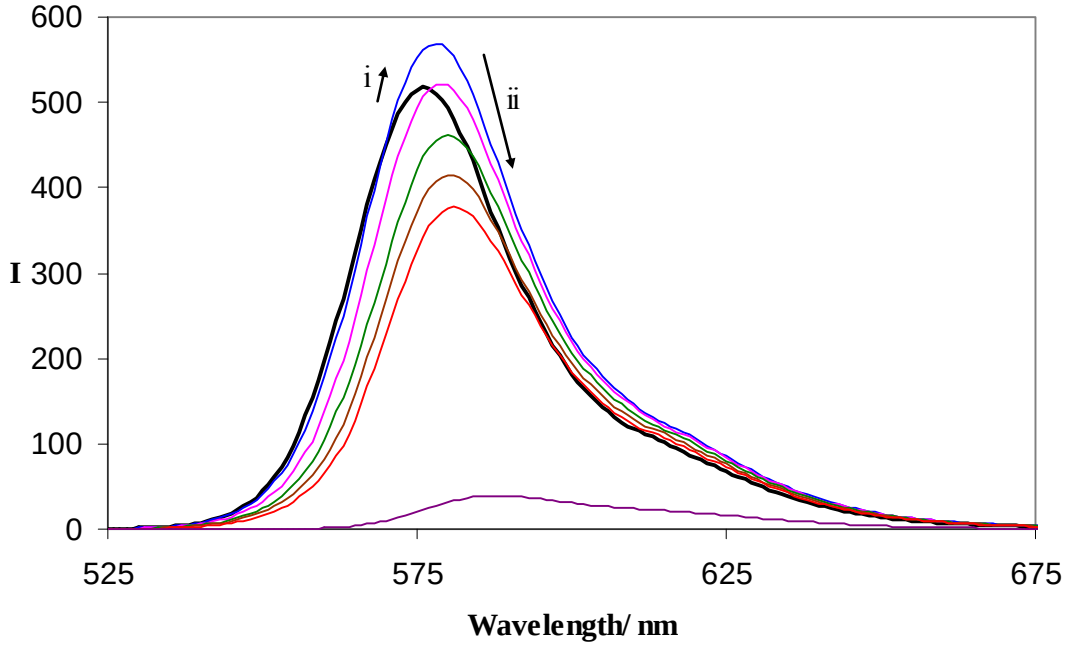

*Figure 4.14. Emission spectra of **58** over a range of concentrations (0.0039 – 0.011 mM). Bold line indicates the lowest concentration. The intensity increases initially (i) followed by a decrease (ii) as a result of self-quenching.*

4.3 Aggregation Behaviour of N-Alkyl Substituted Dyes

The decreased solubility of dyes with N-alkyl groups in aqueous solution meant that MeOH was required to dissolve the dye initially and dilute further with water. Preparing samples via dilution from a bulk solution can lead to experimental problems where concentrations of MeOH vary; as the concentration of a dye increases so does the concentration of MeOH. As we have seen, aggregation is inversely proportional to the amount of MeOH resulting in the more MeOH present, the less aggregates that form. It is therefore essential that all samples are topped up with MeOH to ensure the same MeOH% in the final solution, making the experiments comparable.

The data generated from the absorbances of dyes that are only minimally soluble in water can only be used in a qualitative manner. Quantitative studies were not possible because the minimal solubility of the dyes in aqueous solution meant the dyes did not remain in solution for long, sticking to the glassware and resulting in the

concentrations not being accurate. The solutions were made up and analysed as quickly as possible to minimise the precipitation of dye.

4.3.1 UV-Visible Studies of the Aggregation of N-alkyl Dyes

Studying the concentration profiles of a range of dyes resulted in the following observations. Dyes with N- benzyl substituents form aggregates more readily especially with the incorporation of chlorine or fluorine substituents in the 5-position. When dyes **49**, **52**, **54** and **56** were compared in 10% MeOH/H_2O solution they showed the following results (their absorbance spectra shown in Figures 4.15, 4.16, 4.17 and 4.18). Dye **49** formed a D-band on increasing concentration but no J-band however; dyes **52**, **54** and **56** did form J-bands. These results suggest that the halogens have a role to play in the aggregation process with the influence of a chlorine atom in the 5-position being greater than that of a fluorine substituent as a direct comparison. The bromine-substituent of **52** does again appear to play a role in the aggregation process but cannot be directly compared to the fluorine and chlorine substituents because it is not in the same position. Unlike the water soluble dyes the transition from monomer to dimer does not create an isosbestic point in the absorbances of these dyes. This could be because of the fluctuations in dye concentration as a result of the precipitation onto the glass or even the MeOH interfering with the dimerisation process. The occurrence of other isosbestic points in the spectra suggests, as shown in Figure 4.18, that it is the formation of dimers that is particularly sensitive to these conditions.

The spectra of **54** are complicated even at very low concentration with monomer, H-dimer, J-aggregates and higher H-aggregates coexisting in the solution. A relatively clear isosbestic point occurs at ~520 nm (circled on Figure 4.18) suggesting that the H-dimers are directly converting into higher H-aggregates, as one might expect.

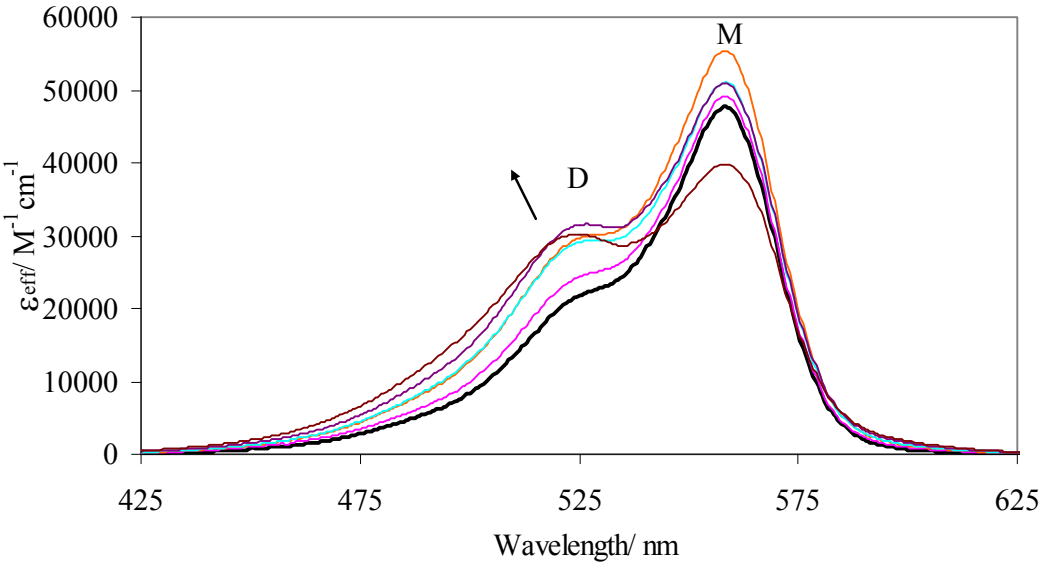

*Figure 4.15. ε_{eff} of **49** with increasing concentration, ranging from 0.004- 0.04 mM (10%vol MeOH). Bold line indicates initial absorption measured.*

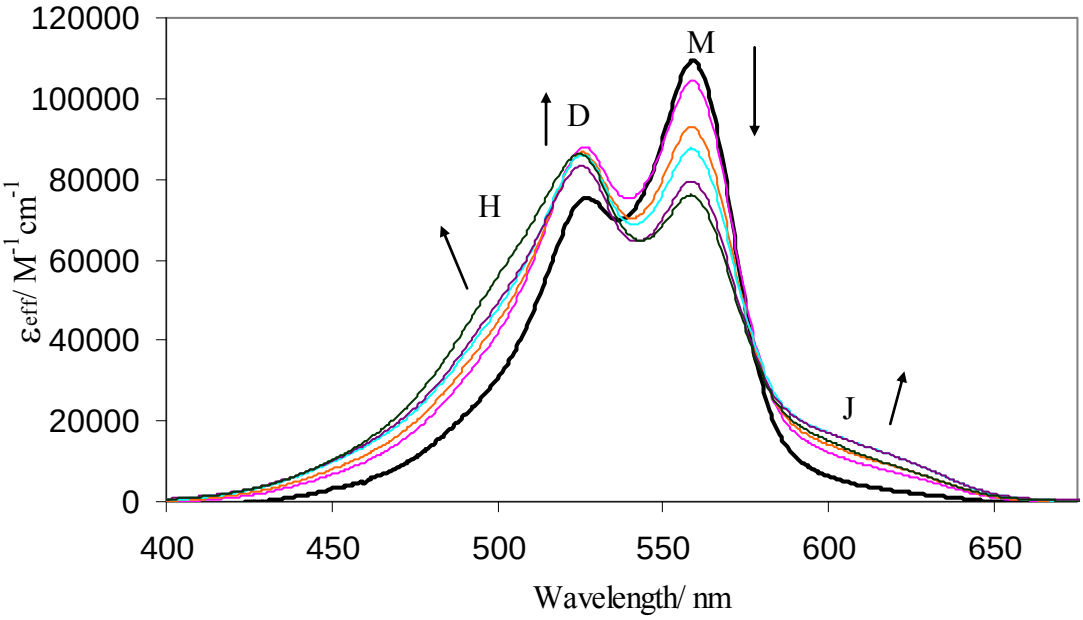

*Figure 4.16. ε_{eff} of **52** with increasing concentration, ranging from 0.004- 0.04 mM (10%vol MeOH). Bold line indicates initial absorption measured.*

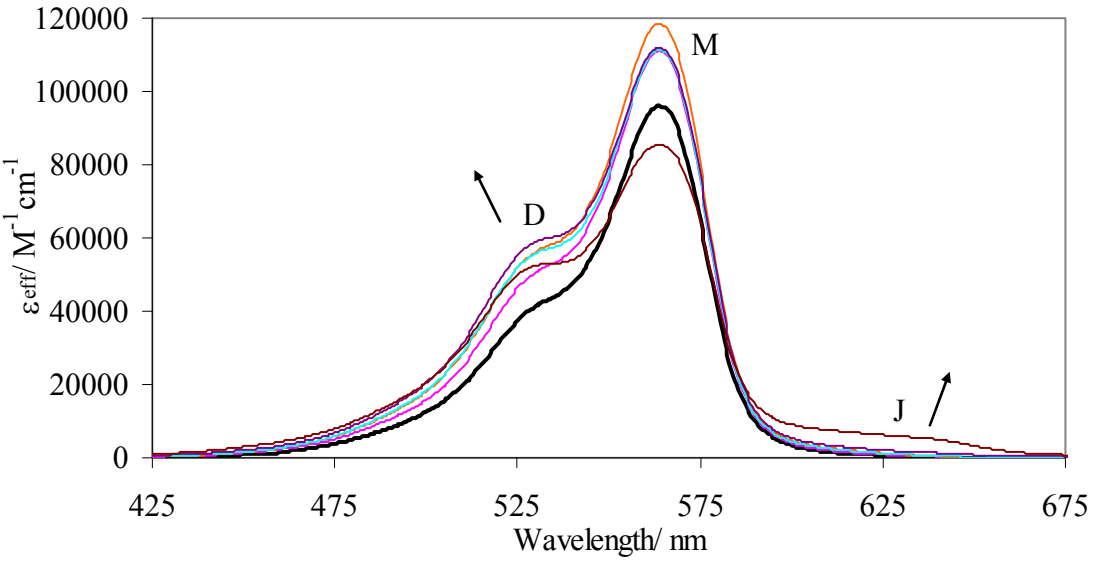

Figure 4.17. ε_{eff} of ***56*** *with increasing dye concentration, ranging from 0.004- 0.04 mM (10%vol MeOH). Bold line indicates initial absorption measured.*

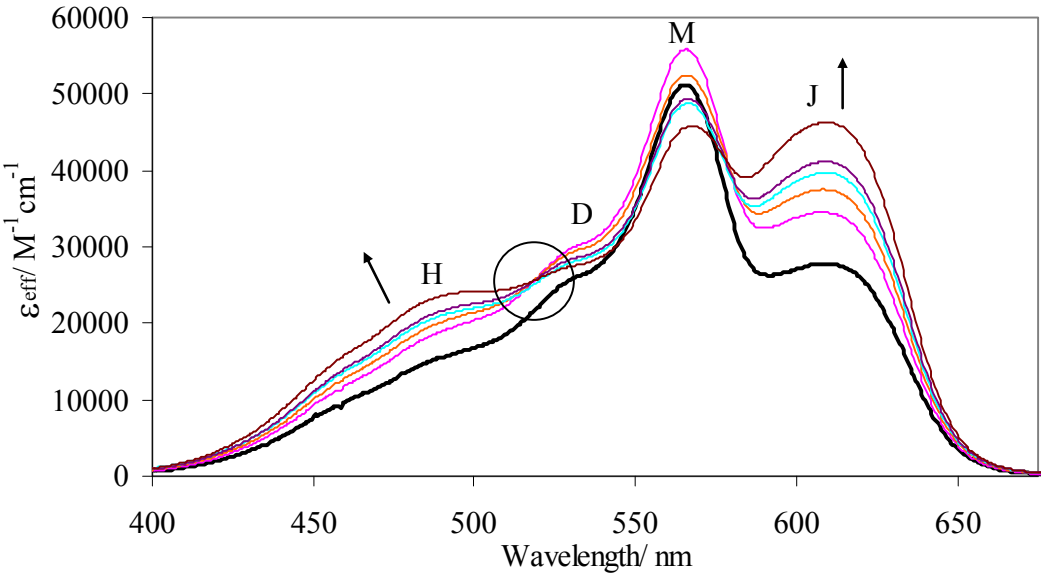

Figure 4.18. ε_{eff} of ***54*** *with increasing dye concentration, ranging from 0.004- 0.03 mM (10%vol MeOH). Isosbestic point circled. Bold line indicates initial absorption measured.*

Comparing sulfur-dye, **2a** and the oxygen-dye, **5a**, in MeOH/H_2O solutions, **2a** showed the formation of the D-band with a corresponding decrease in the M-band, Figure 4.19. The analogous **5a** however did not aggregate even at high concentrations

of 0.0045- 0.05 mM. The naphthalene-containing dye **51** also showed no signs of aggregating at the concentration range 0.004- 0.06 mM. This either suggests that the threshold concentration for the **51** is higher than we can study even with a path length of 1 mm or that these structures do not readily form aggregates.

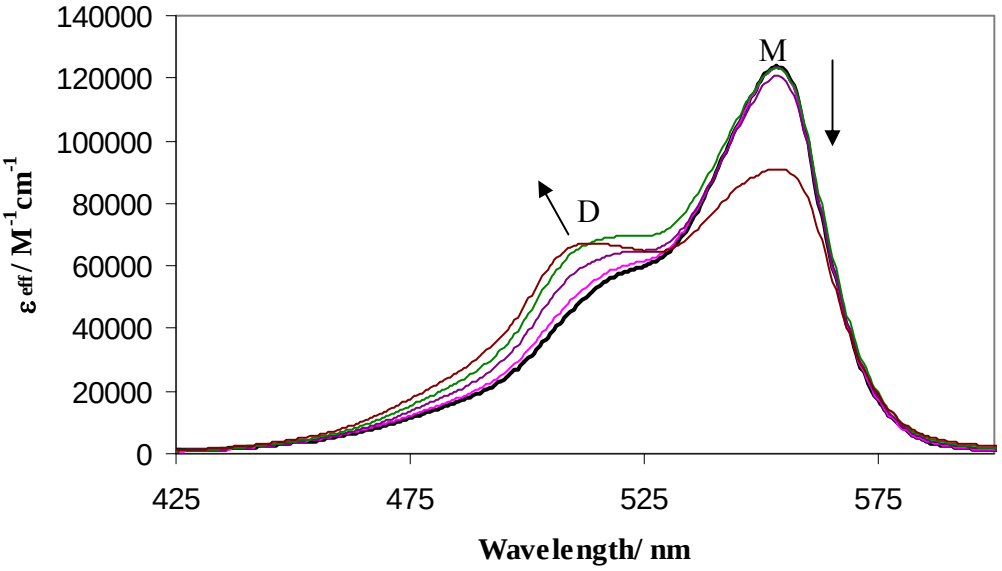

Figure 4.19. The æff of ***2a*** *as it changes with increasing concentration.*

In the presence of increasing amounts of Na_2SO_4 the absorbances of **2a** and **5a** again behave very differently with **2a** forming higher aggregates and **5a** not even forming dimers, shown in Figure 4.20. Like **5a**, the naphthalene dye did not form aggregates in aqueous solution however **51** did form aggregates in the presence of ammonium sulfate, as shown in Figure 4.21. The salt has lowered the aggregation threshold concentration sufficiently for us to study this dye which was not possible without the presence of salts. The interesting questions that arise from this are: 1) why does **51** not aggregate readily when it appears that the hydrophobic nature of a molecule has a large part in determining whether it will aggregate; and 2) why do the oxacarbocyanines not aggregate at all? A possible suggestion for **51** not aggregating as readily as the majority of the thiacarbocyanines could be interactions between the naphthalene groups, although fluorescence studies did not show evidence for any such interactions.

a)

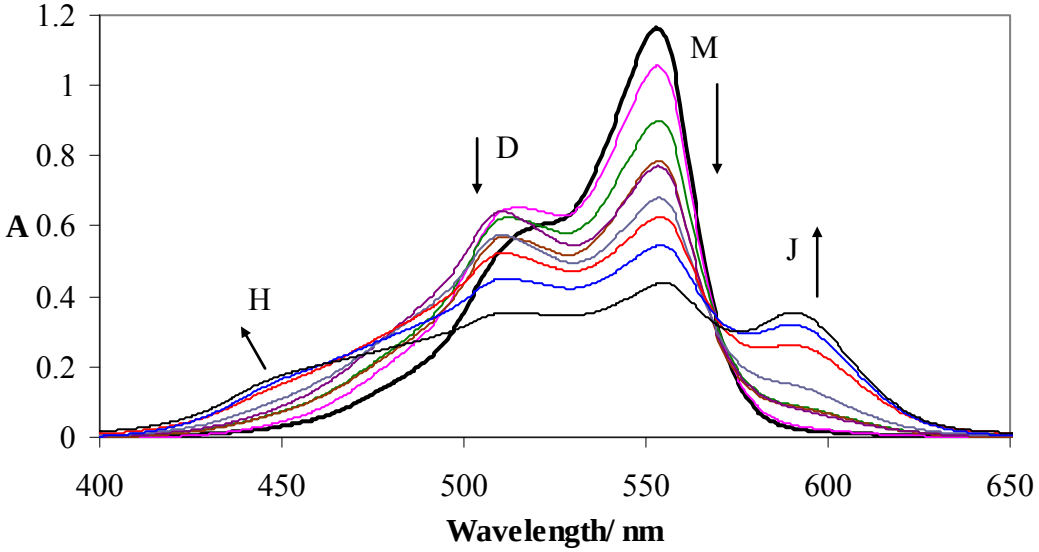

b)

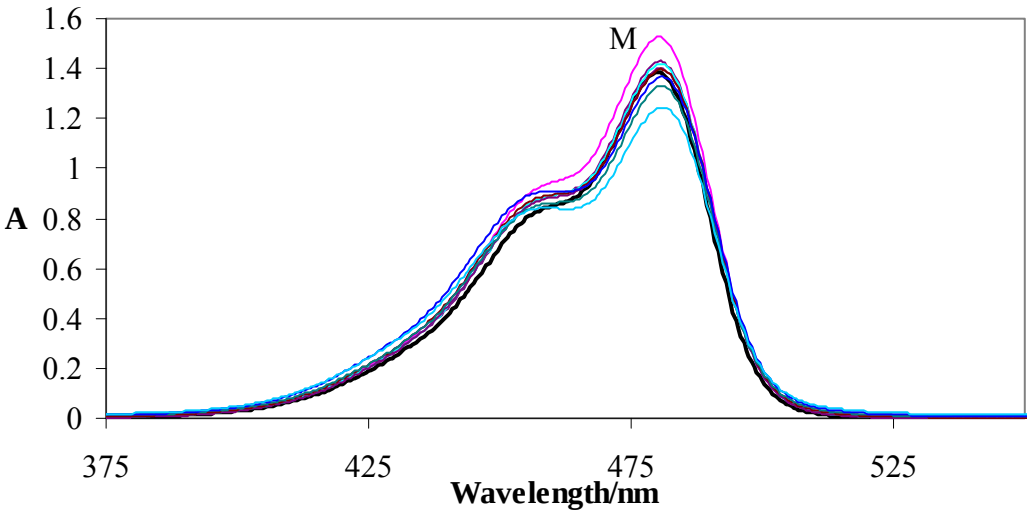

Figure 4.20. Absorption of a) ***2a*** *and b)* ***5a*** *in 3% MeOH aqueous solution as the concentration of Na_2SO_4 is increased. Bold line is the dye without any salt.*

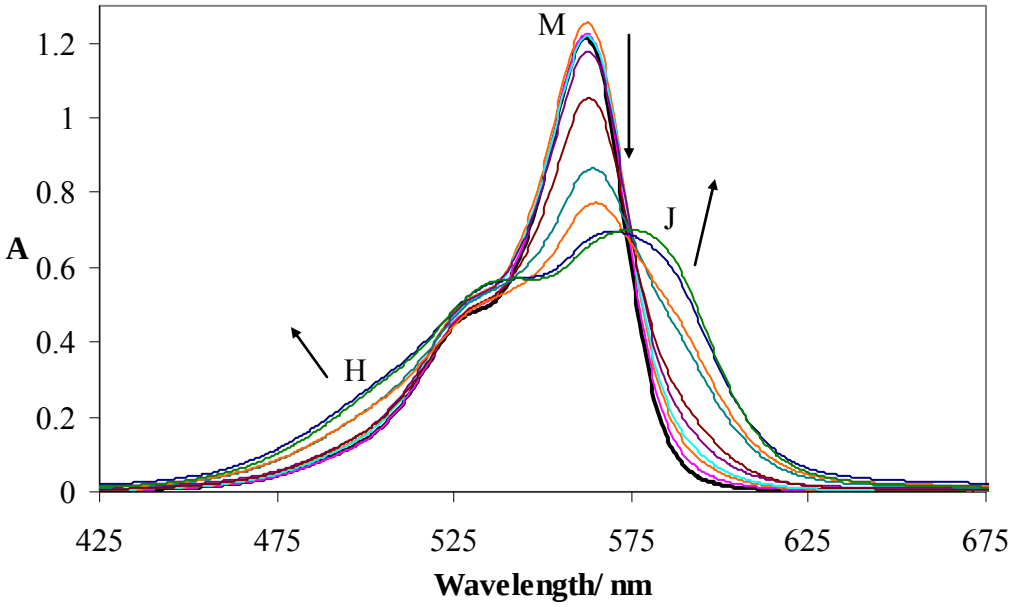

Figure 4.21. Absorption of ***51*** *(0.01 mM) as $(NH_4)_2SO4$ increased (0- 1.82 M) in 25 % MeOH aqueous solution. Bold line is absorption of dyes without any salt.*

Adding sulfate salts to solutions of these dyes induced further aggregates for all dyes (with the exception of **5a** discussed above). In the case of **54,** H- and J-aggregates form even at very low concentrations without any salt, the addition of salt induced the precipitation of the J-aggregates. Addition of salt reduces the threshold concentration of the different phases of the aggregation process acting in an almost catalytic role, accelerating the next stage of aggregation.

From these results it appears as though the formation of aggregates has a high dependence on solubility. Dyes that have bulkier groups tend to form aggregates more readily especially if halides are present. The heteroatom has a large influence on whether a dye will aggregate. The presence of groups such as naphthalene that are capable of additional interactions seem to take control and seem to have a relatively high threshold concentration at which aggregation occurs.

4.3.2. Fluorescence

To investigate if the varying aggregation behaviours of N-alkyl cyanine dyes affected the emission spectra of these molecules the three dyes **5a**, **48** and **51**, were studied. These dyes which showed less evidence for aggregation were expected to show

different patterns of behaviour to the rest of the dyes; this was not the case however. It appears that the dominant effect is self quenching i.e. for a dye less prone to aggregation there is little change in the fluorescence behaviour as self-quenching is dominant.

Adding ammonium sulfate to a solution to induce further aggregation has the effect shown in Figure 4.22. The fluorescence of **51** shows clearly how, as the higher aggregates form, the intensity of this sharpens and increases.

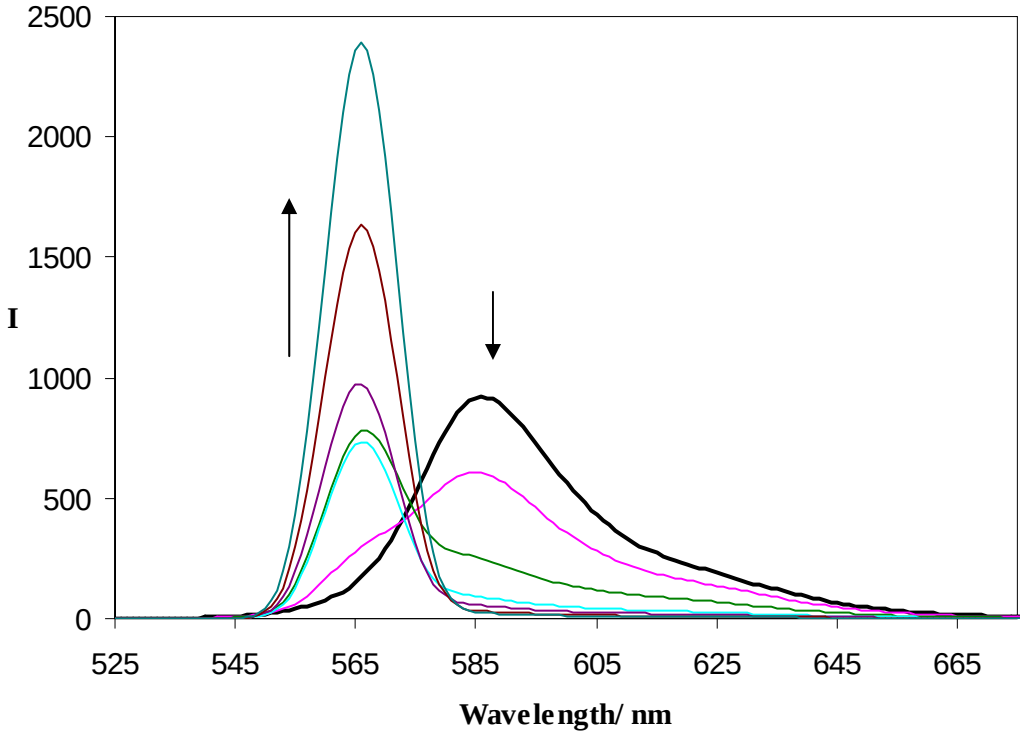

*Figure 4.22. Emission of **51** with increasing $(NH_4)_2SO_4$. Excitation at 561 nm*

4.4 Surface Tension

As mentioned earlier, it was noted that the formation of salt-induced J-aggregates resulted in the formation of patches of a surface active solid on the surface of the bubble. The surface tension of the dye was measured resulting in strange results. The method used is known not to be good for cyanine dyes because of the adsorption of the dye onto the paper. A more suitable method involves a drop of the solution[85] and therefore removes this adsorption effect but time and equipment constraints meant that this property could not be measured. Future work would need to continue with this.

4.5 Conclusions

Studying a range of dyes in MeOH allowed the effect of the dye's molecular structure on the chromophore to be investigated, the results of this study showed:

- Increasing the length of the methine chain increased both the extinction coefficient and the fluorescence emission.
- Oxygen dyes were found to have both higher extinction coefficient and fluorescence emissions than the sulfur analogues.
- Introducing bulky groups in the N-position (such as benzyl and phenethyl) increased the extinction coefficient
- Photostability experiments showed an improvement in resistance to photodegradation for dyes with a 9-substituent and bulky N-alkyl groups.

The majority of trimethine dyes formed aggregates in aqueous solution, with and without the presence of inorganic salts. An ethyl-substituent in the 9-position appeared to reduce the formation of higher H-aggregates, resulting in very distinct H-dimers and J-aggregate absorptions. The oxygen containing dyes **5a** and **48**, however did not form any type of aggregate at the concentration levels studied even in the presence of salts. This suggests that the heteroatom has a crucial role to play in the aggregation process.

The effect of the N-substituent can dramatically affect the aggregation properties. Introducing water solubilising groups enabled the aggregation behaviour of the dyes to be easily studied. Without the presence of salts, the water soluble dyes **11**, **57** and **58** formed only H -aggregates in the aqueous solution, this enabled the dimerisation constant to be calculated in the case of **11**. In the presence of inorganic salts however these dyes formed both H-and J-aggregates. Upon further investigation it became apparent that it was the anion that controlled the aggregation process. This is contrary to reports in literature which claim the anion has a redundant role[6,19,23,25].

Dyes with large N-alkyl groups formed J-aggregates readily in a MeOH/ water solution, with the exception of the N-naphthalene dye, **51**, which only formed aggregates in the presence of salts by lowering the threshold concentration of the dye.

Using UV-visible spectroscopy subtle differences were observed in the aggregation of a range of dyes related to the molecular structure. The emission spectra however showed no evidence of the aggregates having an effect and were dominated by self-quenching.

Chapter 5

Solid-State Studies

5.1 Introduction

As discussed in Chapter 1, there have been a large number of studies on cyanine dyes concerning their aggregation behaviour in bulk solution, but relatively fewer studies into the behaviour of these dyes in the bulk solid. A search of crystallographic structure database[56], CSD, shows that the majority of the known cyanine crystal structures are of trimethine dyes, as shown in Figure 1.2, with very few examples of monomethine dyes, Figure 1.3, and dye precursors (Figure 5.1 shows the only three known quaternary salts of this type). Only one monomethine structure is known that possesses a simple inorganic counterion found by Nakatsu *et al.*[59] in 1972. However, there are several structures that incorporate TCNQ monomer and dimer counterions as shown in Table 1.3.

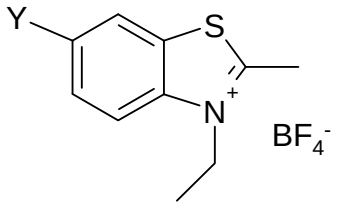

Y = H, OMe, NO_2

Figure 5.1. Structures in crystallographic database, version 5.29 (Nov. 2007) [56].

Two possible reasons for the small number of structural studies compared to the large library of compounds that exist are: 1) a large proportion of the cyanine dyes were made before X-ray crystallography was a readily available technique; and 2) it is notoriously difficult to isolate cyanine dye crystals of a high enough quality for X-ray structural studies. Cyanine dyes normally result in intensely coloured, often metallic-looking crystals that can appear opaque making the prediction of crystal quality by microscopy difficult. Thus, the screening process has to occur on the diffractometer which can be time consuming and often very impractical.

During this project structural studies have been carried out on a range of precursor, monomethine and trimethine structural salts. These results clearly show that whilst all cyanine dyes are very similar in their basic structure, minor structural modifications can result in significant changes in the solid-state architecture. Understanding the effect of small structural changes on the solid-state architecture may help establish links between the molecular and supramolecular structure. It is therefore important to understand influences that control the solid-state architectures in order to design dyes with specific properties i.e. to 'tune' the properties. The correlation of these properties with the behaviour of the dyes in bulk solution is also fundamental alongside the comparison of the solid-state structure with solution aggregate architecture.

As mentioned in Chapter 1, the descriptions of a packing architecture can be broken down into the molecular (the dye itself), the 0-D (dimers and pairs), the 1-D (stacks or chains), the 2-D (planes) and finally the 3-D structure. Each crystal structure has been considered in this manner with examples being used throughout this chapter to illustrate the main and most interesting points. All the crystal data is included on the supplementary compact disc.

5.2 Packing Structures

There are the three types of solid-state assemblies generally seen for cyanine dyes; brickwork, staircase and ladder arrays. Examples of each of these are shown in Figure 5.2. These models are sufficient for describing the individual stacks, but in cases where the stacks pack in different orientations relative to one another, a different type of architecture results where the existing descriptors fall short. Viewing such structures down the axis of the stacks an obvious herringbone arrangement of the stacks can often be observed. Such architectures can therefore be described using herringbone as the suffix i.e. staircase-herringbone or ladder-herringbone arrays. An example of a staircase-herringbone array is also shown in Figure 5.3.

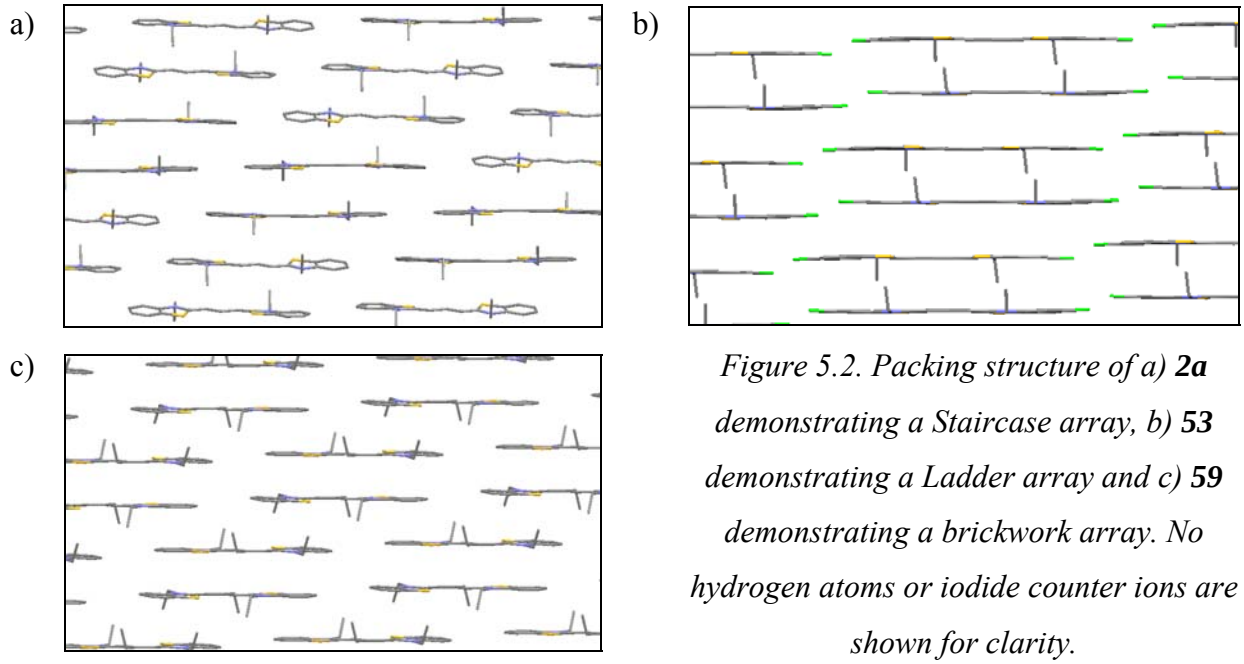

*Figure 5.2. Packing structure of a) **2a** demonstrating a Staircase array, b) **53** demonstrating a Ladder array and c) **59** demonstrating a brickwork array. No hydrogen atoms or iodide counter ions are shown for clarity.*

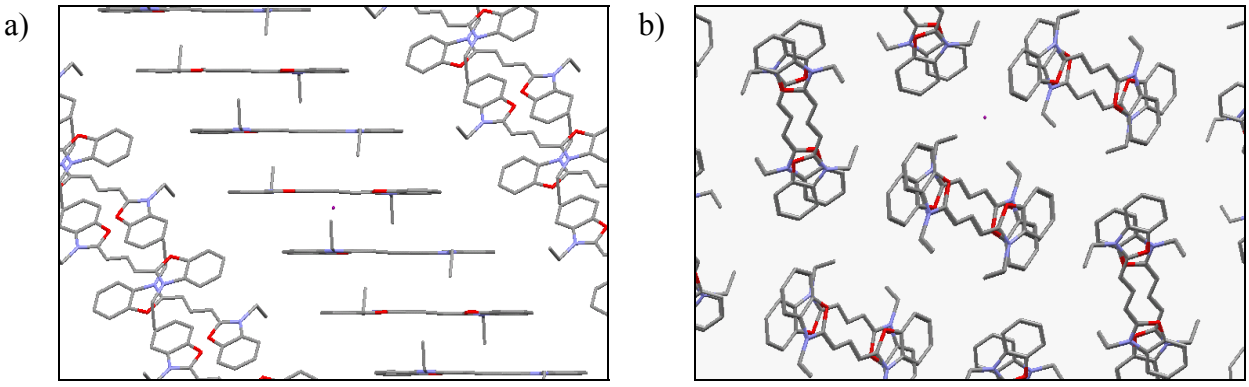

*Figure 5.3. Packing structure of **5a** demonstrating a Staircase-Herringbone array. Hydrogen atoms and iodide counter ions are omitted for clarity.*

The majority of the structures obtained during this project can be described using these five arrays and the few examples that do not will be discussed later in the chapter. It is worth noting that a brickwork array can almost be viewed as an exaggerated staircase array. In some cases it is therefore unclear as to which array the architecture is best described by. There is no defining angle that separates brickwork and staircase arrays currently in literature. In these cases, if it is uncertain which direction of slipped stack the dimers are part of, then this type of architecture will be described as a brickwork array.

5.3 Dye Precursors

Activated methyl quaternary salts do not form aggregates in bulk solution and therefore have not been of particular interest. Their solid-state behaviour, however, is important to help understand the key interactions and to what extent the extra conjugation of the dyes has on the overall structure. Ideally, X-ray structural studies would have been carried out on all precursors prepared. In reality, however, not all compounds resulted in crystals of a suitable quality for structural studies. As previously discussed, several compounds (**29-33**, **37** and **38**) appeared to lose solvent from within the crystal lattice upon removal from the mother liquor (crystals turned opaque) thereby breaking up the crystal structure. X-ray structural studies have been carried out on the compounds shown in Table 5.1 which allows some initial tentative conclusions about the structural effect on the overall architecture. The R-values have been shown to give an idea of the quality/reliability of the structures. All data is very good with the exception of **35** which has a higher R-value, therefore making the data less reliable than the other examples.

The solid-state architecture of 3-ethylbenzothiazolium with a BF_4^- counter ion, **62b**, has been previously reported[86], shown in Figure 5.4a. In the present study we have obtained the structure with an iodide counter ion, **62a** shown in Figure 5.4b. These figures show that **62b** forms stacks of molecules all in the same orientation with the adjacent stack the inversion of this. Dye precursor **62a** forms a stack of dimers. The difference in these packing structures shows that exchanging the counterion from a large BF_4^- to a smaller spherical I^- can have a significant effect on the overall architecture. The crystal structures of dye precursors presented in this thesis have not been previously reported in literature.

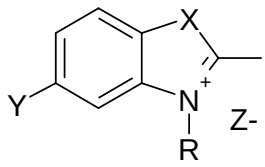

Precursor	X	Y	Z	R	R-value
28	S	H	Br	Benzyl	2.92
30	S	H	Br	4-Bromo-benzyl	2.82
34	S	Cl	Br	Benzyl	3.08
35	O	H	I	Me	8.42
36	S	H	Br	Phenethyl	2.15
39	S	H	-	$(CH_2)_4SO_3^-$	2.88
62a	S	H	I	Et	2.23
71	Se	H	I	Et	2.55

Table 5.1. Quaternary salt crystal structures obtained in this project.

a)

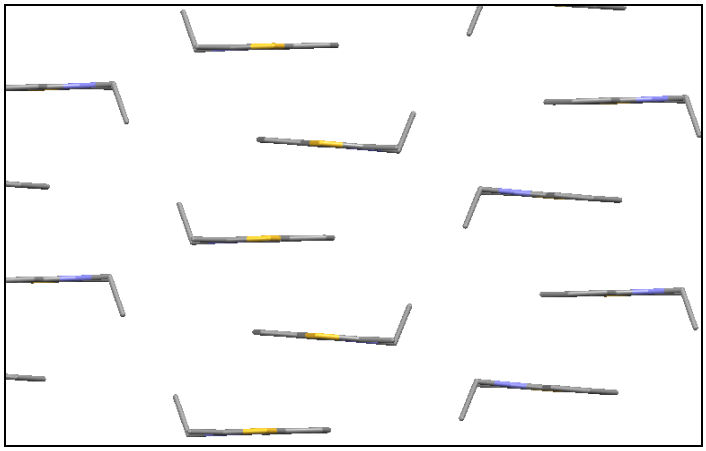

b)

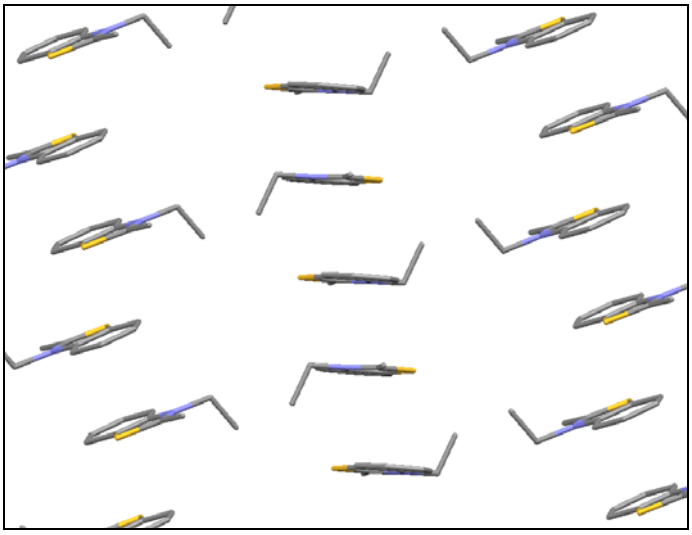

Figure 5.4. Packing structures of a) ***62b*** *obtained by Srenger et al.*[86] *and b)* ***62a****. Hydrogen atoms and counterions omitted for clarity.*

Studying the architectures of the remaining quaternary salts has shown that these structures generally form dimers in the solid-state which then either pack as isolated dimers (**28** and **34**), shown in Figure 5.5, or form stacks of dimers (**30**, **39, 62a** and **71**). Figure 5.6 shows **39** as an example of the type of stacks formed. The formation of stacks comprising of dimers is analogous to the stacks formed by the majority of the monomethine and trimethine dyes, as will be discussed later in the chapter. This suggests that the majority of the interactions to form the dimers is determined by the benzoheterocycle.

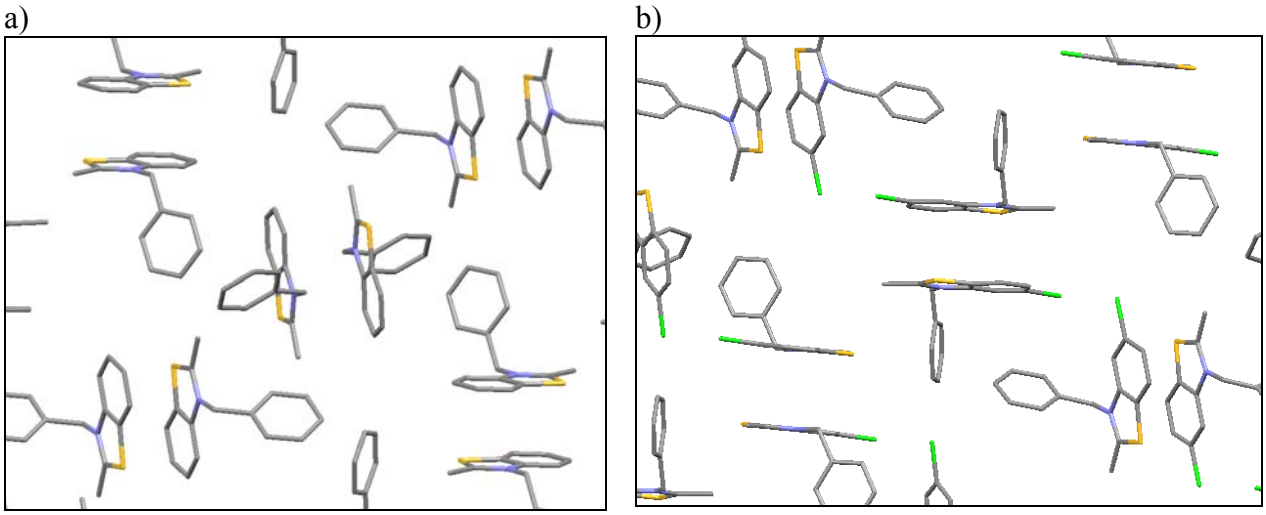

*Figure 5.5. Packing structures of **28** and **62a** showing a) isolated dimers and b) stacks of dimers respectively. Hydrogen atoms and counter ions omitted for clarity*

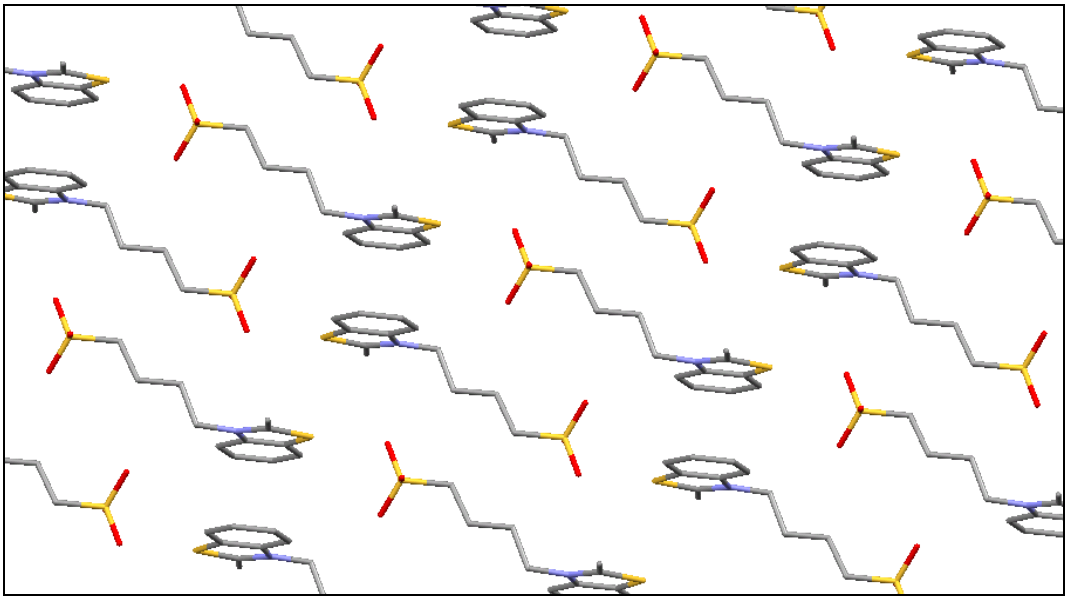

*Figure 5.6. Packing structure of **39** as an example of the formation of stacks. The sulfo-groups orientate towards the adjacent stacks.*

Table 5.2 shows the separation between the molecules in the dimer and the distance separation between the next dimer in the stack. The separation between the planes of the benzoheterocycles range from 2.89 to 3.56 Å. Molecule **30** has double the separation (7.7 Å) between two dimers compared to **39**, **62a** and **71** (3.4 -3.5 Å) because of the large N-bromobenzyl groups interacting with one another, shown in Figures 5.7 and 5.8.

			Distance between		
Salt	**X**	**R**	**dimer planes**	**Dimer 1 & 2**	**Type of stack**
28	S	Benzyl	3.395 Å	-	Isolated dimers
30	S	4-Bromo-benzyl	3.555 Å	7.724 Å	Ladder
34	S	Benzyl	3.443 Å	-	Isolated dimers
39	S	$(CH_2)_4SO_3^-$	3.402 Å	3.406 Å	Very slipped staircase
62a	S	Ethyl	3.385 Å	3.500 Å	Ladder
71	Se	Ethyl	3.394 Å	3.518 Å	Ladder

*Table 5.2. The distances within and between adjacent dimers and a description of the architectures of the individual stacks or dimers of **28**, **30**, **34**, **39**, **62a** and **71***

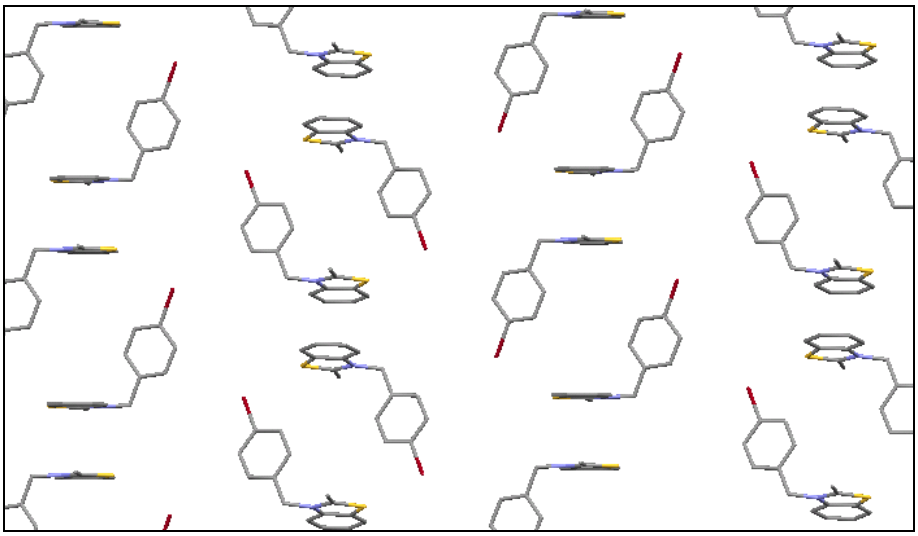

*Figure 5.7. Structure of **30**, showing the stacks of dimers. Hydrogen atoms and counterions omitted for clarity.*

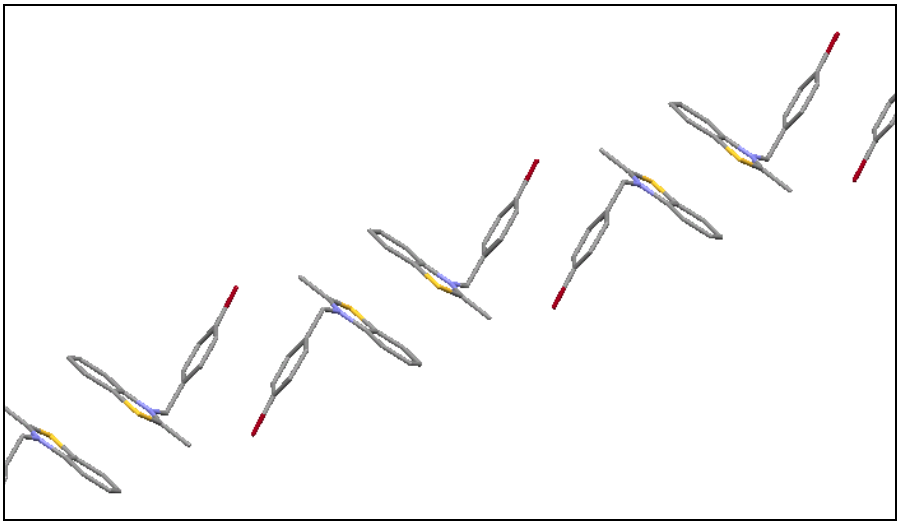

*Figure 5.8. Showing a single tape-like structure of **30**. Hydrogen atoms and counterions not shown for clarity*

The benzyl groups of **30** clearly form face-to-face π-π interactions with a contact distance of 3.44 Å. As a result it is difficult to conclude whether the architecture is made up of stacks of dimers (Figure 5.7) or tapes of dimers (Figure 5.8). Like **30**, **34** also has halogen substituents but these structures cannot be directly compared because of the different positions of these substituents. Neither structure forms any Cl-Cl or Br-Br interactions respectively. However, there appears to be interactions between the halogen and the bromide counter ion in both structures with distances of Br-Br$^-$ 3.48 Å and Cl-Br$^-$ 3.54 Å. One would expect the Br-Br$^-$ contact to be longer than that of the Cl-Br$^-$ [87] but this is not the case. Both **30** and **34** can however be compared to **28**.

Both **28** and **34** have similar overall architectures; packing as dimers that do not form extended stacks, shown in Figure 5.5. The benzyl groups in both **28** and **34** are positioned to optimise interactions with both the benzo- and benzyl groups of an adjacent molecule shown in Figures 5.9 and 5.10. The benzyl substituent of **28** forms an off-set edge-to-face π-π interaction with the benzyl group of an adjacent molecule. Molecule **34** also forms these types of interactions but the benzyl group is at more of an angle from the benzo- and benzyl-group of the adjacent group. This increased angle is likely to be because of the size of the chlorine groups. From this it appears that the chlorine in the 5-position does not have a significant effect on the packing structure compared to the non-substituted architecture.

The packing structure of **30** is significantly different to that of **28** (and therefore **34**) suggesting that the bromine does effect how the molecule packs. Altering the steric or electronic properties of the benzo- and benzyl groups by the introduction of halogen atoms leads us to the conclusion that the benzyl-group is more influential on the packing than the benzo-group.

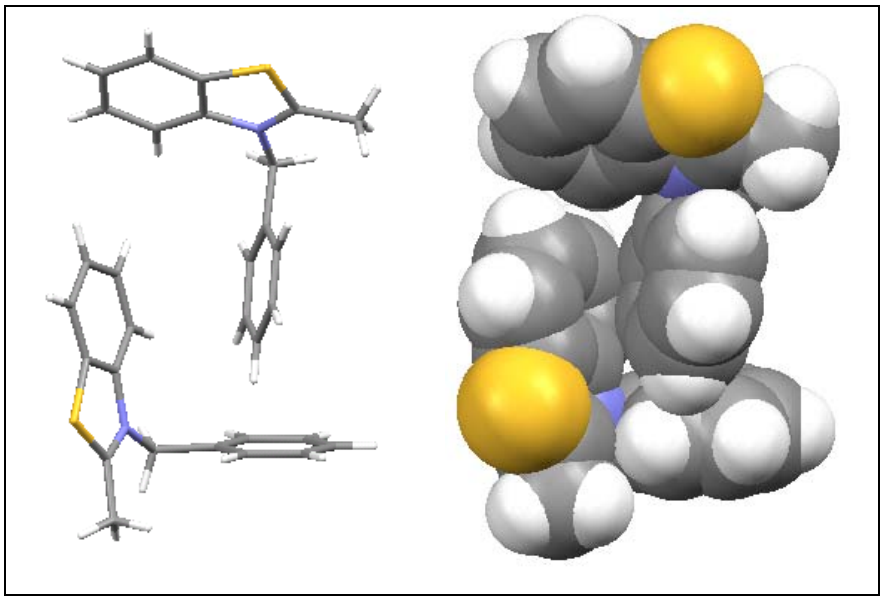

Figure 5.9. Two representations of a pair of interacting molecules of ***28****. Counterions have been omitted for clarity*

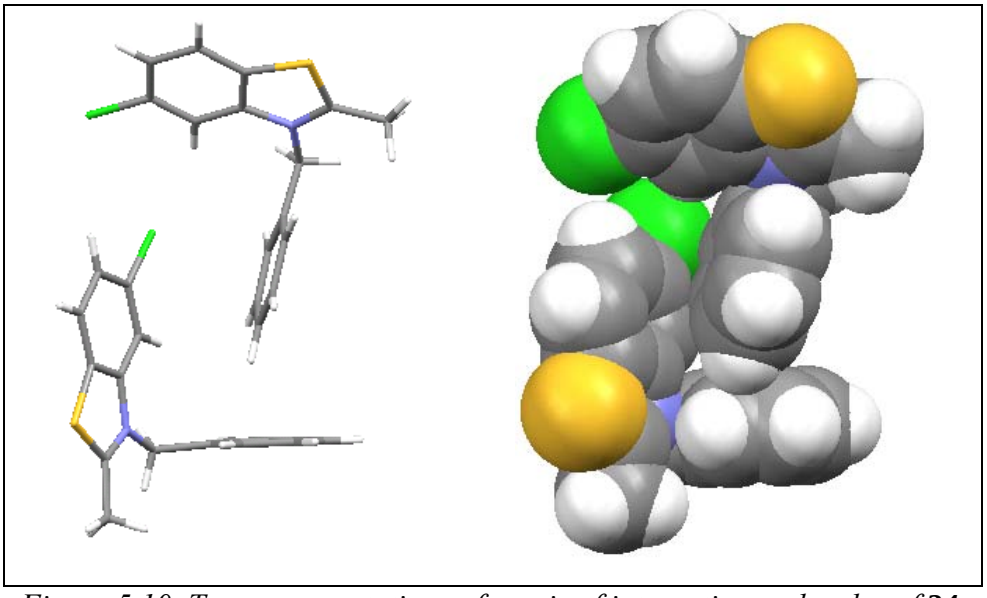

Figure 5.10. Two representations of a pair of interacting molecules of ***34****. Counterions have been omitted for clarity*

Molecules **35** and **36** do not form dimers, **36** form tapes of monomers as shown in Figure 5.11 and **35** forms stacks of monomers which have a slight overlap with adjacent stacks, as shown in Figure 5.12. The phenethyl substituent of **36** exhibit face-to-face π-π association with an interaction distance of ~ 3.3 Å to the adjacent benzo-group. It is also the only quaternary salt structure with one molecule in the unit cell and forms a very different structure to the other quaternary salts. The trimethine analogue of this structure, **50**, interestingly also forms a different architecture compared to the other dyes.

a) b)

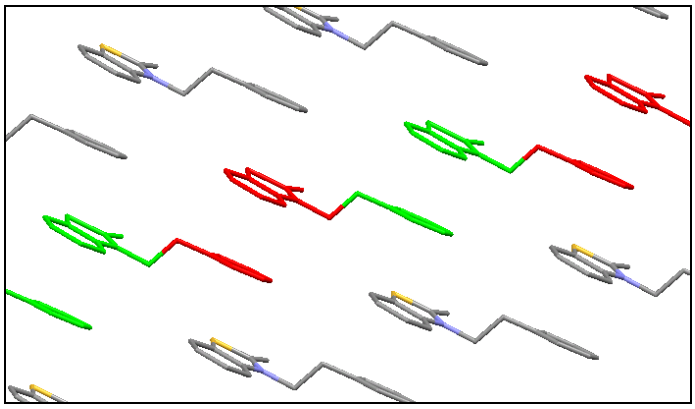

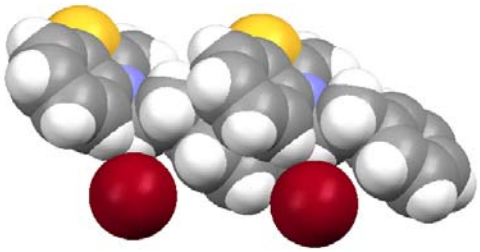

*Figure 5.11. a) View of **36** showing how molecules form tape-like structure. Like colours indicate the interacting components which form the tape. Hydrogen atoms and bromide counter ions omitted for clarity b) Two spacefilled molecules of the tape.*

a)

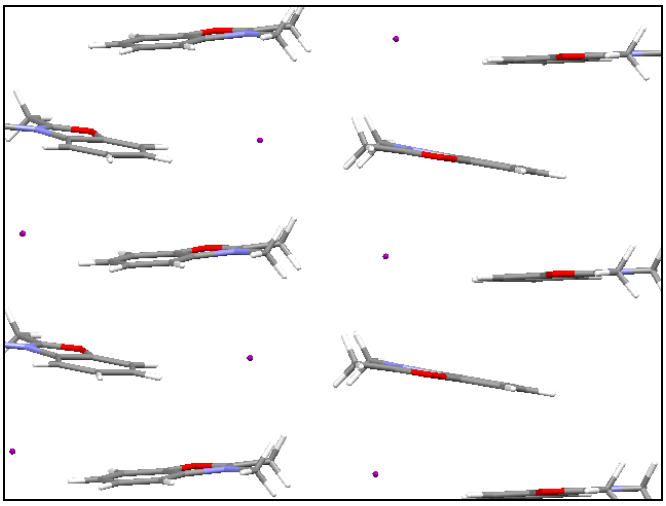

b)

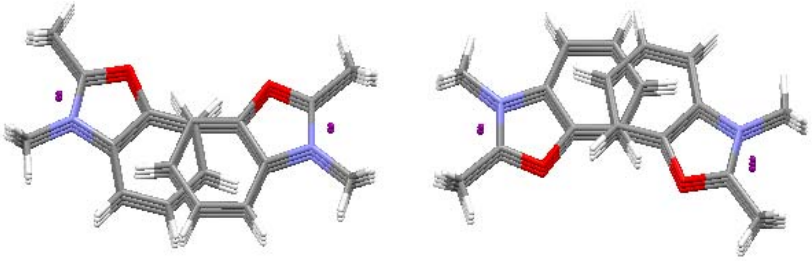

Figure 5.12. a) packing structure of ***35*** *showing no dimers with stacks directed around the iodide counter ion. b) Looking down the axis of the stacks, showing the slight overlap with the adjacent inversed stacks.*

In summary the behaviour of this set of quaternary salts has been studied, comparing the effects of the molecular structure on the packing architectures. The set does not directly correlate with the structures of mono-and trimethine dyes that will be discussed later but there are sufficient dye precursors to provide some trends of the types of interactions present from a bottom-up approach.

5.4 Monomethines

The nature of the changes in the monomethine dye structures prepared and crystallised has enabled a systematic study to be carried out, concentrating primarily on the effect of the heteroatom, the counter ion and the substituent in the 5-position. Table 5.3 shows the compounds for which X-ray structural studies were carried out during this project and the corresponding R-values to give an estimate of the quality of the structures. All of these structures have an R-value that is very good; this is with the exception of a polymorph of **3a**, indicating that the majority of the data collected is very reliable.

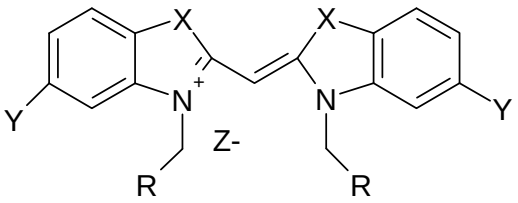

Dye	X	Y	Z	R	R-value
3a	S	H	I	Et	11.28 & 2.56 (Polymorphs)
3f	S	H	I_3	Et	2.77
44b	O	H	I_3	Et	3.97
44a	O	H	I	Et	2.15
45a	S	Cl	I	Et	4.31
45b	S	Cl	I_3	Et	3.50
46a	S	F	I	Et	2.15
46b	S	F	I_3	Et	2.83
47	S	H	Br	Bnz	3.57
64a	Se	H	I	Et	3.65

Table 5.3. X-ray structural studies of monomethine dyes presented in this thesis. The R-values provide an indication of the quality of the data.

Table 5.4 describes the properties of the individual dye molecules as calculated using Wingx[88] and Mercury[89]. There is a distinct difference in the length of the oxamethine dye compared to the S and Se analogues, shown in Figure 5.13. Initially it appears as if the oxygen atoms are pulling in towards one another as the O-O, S-S and Se-Se distances are 2.67, 3.00 and 3.06 Å respectively. On further investigation, considering the angle of the methine carbon it appears that the S and Se atoms are actually pushing further apart. The angles for the central methine carbon, $\alpha 1$, for **3a**, **44a** and **64a** are shown in Table 5.5. One would expect an sp^2 carbon angle to be 120°, suggesting that the S and Se results in a greater strain on this angle than the oxygen atoms possibly because of the size difference between selenium and sulfur compared to oxygen (atomic radii O is 0.66 Å whereas S and Se are both 1.04 Å[90]). Comparing $\alpha 1$ with the angle that the central methine carbon forms with the benzo-carbons adjacent to the heteroatom, $\alpha 2$, confirms that this observation is likely to be a result of the size difference between oxygen and sulfur/selenium. It is also interesting that the

angles α1 and α2 of **3f**, **44b** and **64b** shown in Table 5.5 are greater compared to the iodide analogues suggesting that the counterions have not only an effect on the architecture but the geometry of the dye also.

The torsion angles along the long axis of dyes **3a**, **3f**, **44a, 44b**, **45a, 45b, 46a, 46b**, **47** and **64a** range from 0.88 – 5.39° with no obvious correlation between molecular structure and the resulting torsion angle. This is probably because this will be greatly affected by the close contacts formed as well as the sterics.

	Relative Orientation		
Dye	**Of R groups**	**Torsion angle of dye**	**Long axis length**
3a (i)	Cis	3.20 (0.07)°	11.725 Å
3a (ii)	Cis	0.88 (0.16)°	11.697 Å
3f	Trans	4.60 (0.09)°	11.703 Å
44a	Cis	3.36 (0.08)°	10.814 Å
44b	Cis	5.39 (0.19)°	10.835 Å
45a	Cis	3.24 (0.08)°	11.702 Å
45b	Trans	1.43 (0.13)°	11.698 Å
46a	Cis	3.18 (0.06)°	11.694 Å
46b	Cis	4.06 (0.03)°	11.691 Å
47	Cis	3.18 (0.11)°	11.685 Å
64a	Cis	1.84 (0.10)°	11.897 Å

Table 5.4. Properties of dyes. The torsion angles were calculated using the planes of the benzo-groups (Wingx[88]) and the length was measured from carbon- carbon in the 5-positions (Mercury[89]).

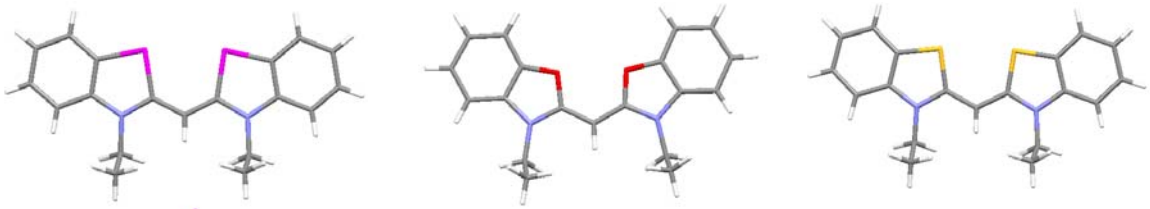

*Figure 5.13. Se, O and S containing monomethine dyes **64a**, **44a** and **3a** from left to right. Counterions omitted for clarity.*

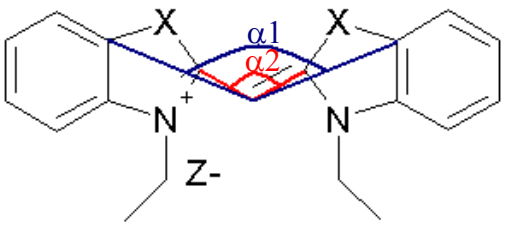

	Z	X= O	X= S	X= Se
α1	I	123.9°	126.1°	126.2°
α2	I	99.4°	113.1°	116.0°
α1	I_3	125.2°	126.5°	128.0
α2	I_3	100.6°	112.9°	116.5°

*Table 5.5 Measured angles of the central carbon for dyes **3a**, **44a** and **64a** and **3f**, **44b** and **64b***

It is worth noting that the only monomethine dyes to have solvent of crystallisation incorporated in their architectures are the 5-substituted derivatives **45a**, **46a** and the benzyl dye **47**. Both **45a** and **46a**, along with most of the other dyes were crystallised from MeCN but the halogen substituents, in the presence of the iodide counter ions, create a void suitable for MeCN. Strumer *et al.* reported that distinct solvent of crystallisation was found to be present in crystals of most of the cationic dyes[11] which seems not to be the case here, with a larger portion of the dyes studied not having any solvent of crystallisation.

The N-benzyl derivative **47** is the only dye successfully prepared with a group in the 3-position larger than an ethyl group. Figure 5.14 shows **47** in its Cis-Cisoid geometry with a benzene ring which is rotationally disordered about the CH_2-Ar bond. To reduce steric hindrance, one might predict the benzyl groups would be trans or the dye would have a transoid structure but this is not the case. The cis geometry is somewhat surprising for this reason but could be explained by looking at the orientations of the benzyl groups (for the smaller proportion of molecules) which are close enough to interact with one another and form a T-shape enabling edge-face π-stacking to occur with a CH-π distance of ~ 2.8 Å.

The 1-D and 2-D structure comprises of stacks which are roughly perpendicular to one another so however the structure is rotated the same axis of all the stacks cannot be viewed simultaneously, shown in Figure 5.15. This structure therefore does not fit any of the models described in Figures 5.2 & 5.3 but could be described as a Perpendicular-Ladder array.

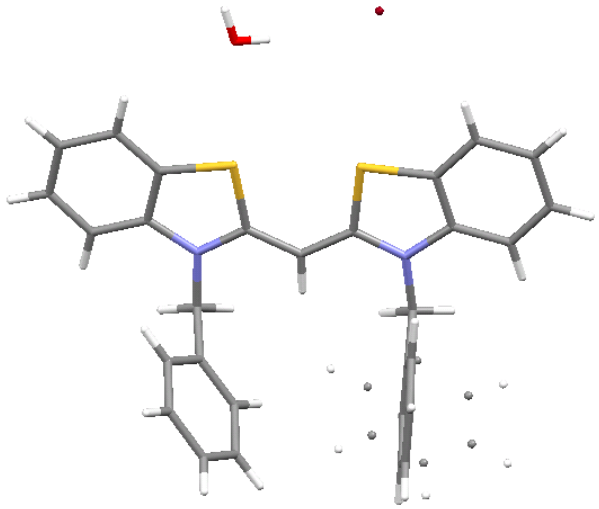

*Figure 5.14. Structure of **47** with the two positions of the disordered benzyl group shown.*

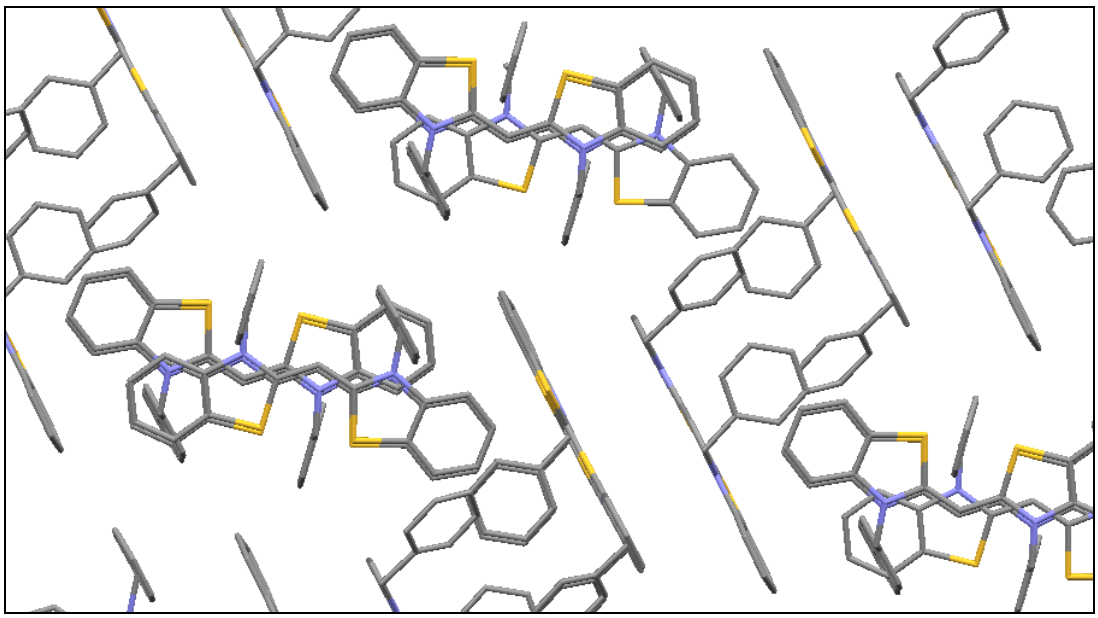

*Figure 5.15. The packing structure of **47.** Looking down the axis of a stack shows the stacks of dimers perpendicular to one another, resulting in a perpendicular-ladder array. Hydrogen atoms, bromide counterions and disordered benzene ring are not shown for clarity.*

The 1- and 2-D architectures of the 3-ethyl monomethines clearly illustrate the effect of the counter ion and substituents in the 5-position on the overall architectures. Figure 5.16 illustrates the differences between **3a** and **3f** as a result of the effect of the iodide and triiodide counterions. The polymorphic architectures of **3a** (Figures 5.16a&b) are also shown.

Monomethine **3a** (polymorph i) has been found to be isostructural with the bromide version of this dye, **3c**, found by Nakatsu *et al.*[59]. This combined with the formation of polymorphs of **3a** suggests that spherical counterions such as iodide and bromide do not control the architecture whereas larger counterions with less symmetry have a greater effect. This in theory means that exchanging iodide to bromide and vice versa will not make a difference to the overall packing structure. To prove this however many more architectures would need to be studied.

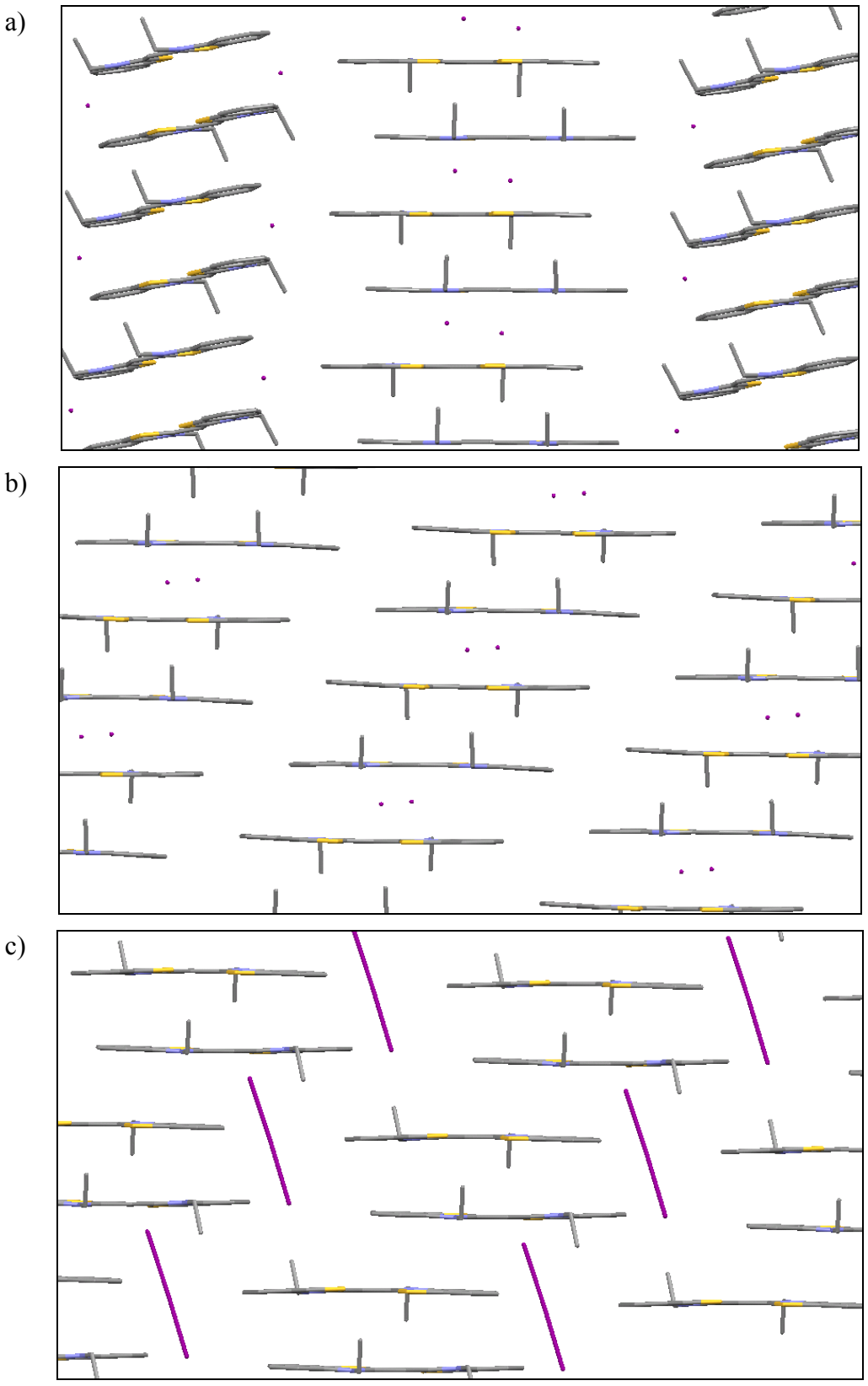

*Figure 5.16. Showing the effect of counter ion on **3**. a) I⁻, Ladder-Herringbone array, **3a** b) I⁻, Staircase array, **3a** and c) I_3^-, Brickwork array, **3f**. Hydrogen atoms omitted for clarity.*

The triiodide counter ions of **3f**, **44b**, **45b** and **64b** orientate perpendicular to the long axis of the dye as depicted in Figure 5.16. For **46b** however, the triiodide lies parallel to the dye and forms part of the stack resulting in dimers being sandwiched in a stack by chains of end-to-end triiodide pairs as shown in Figure 5.17 with I_3^--I_3^- pair contact of 3.68 Å. Kazheva *et al.* found triiodide ions to form chains of pairs similar to this with I_3^--I_3^- pair contact of 3.81 Å[91]. Table 5.6 shows the distances and angles between the dimers and stacks for this dye and the other structures. In all cases the intermolecular distances are ~ 3.5 Å. The majority of the distances between the dimers are again ~ 3.5 Å with two exceptions, **46b** and **47** which are separated by double this distance. In the case of **46b** this is because the dimers are separated by triiodide pairs but the dimers of **47** are separated by the large benzyl groups.

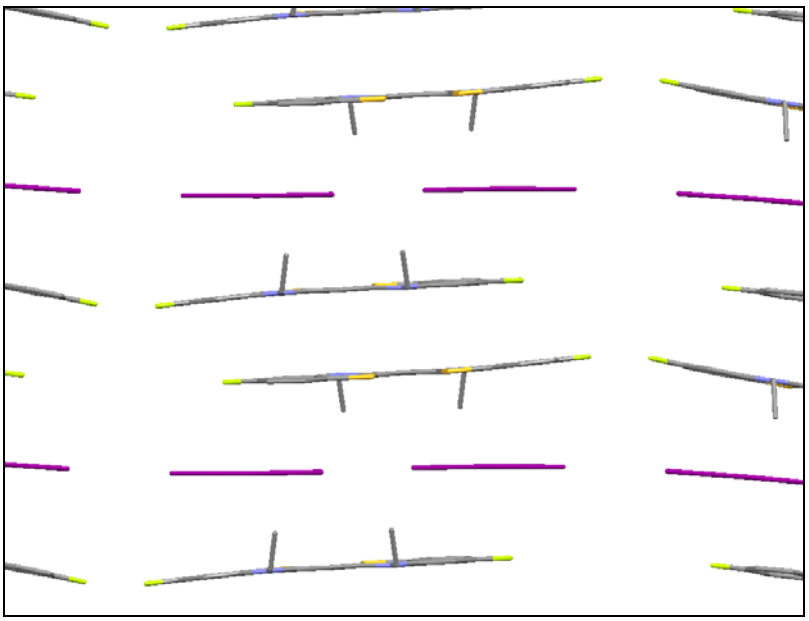

*Figure 5.17. Packing structure of **46a** with stacks of dimers sandwiched between pairs of end-to-end triiodide molecules.*

Dye	Distance between dimer planes/ Å	Distance between dimer 1 and dimer 2/ Å
3a (i)	3.42	3.47
3a (ii)	3.45	3.4
3f	3.53	3.34
44a	3.36	3.21
44b	3.31	Brickwork
45a	3.52	3.54
45b	3.52	3.29
46a	3.47	3.36
46b	3.4	7.46
47	3.52	7.56
64a	3.41	3.57

Table 5.6. Showing the values calculated for the dimers and stacks for a range of monomethine dyes.

The values in Table 5.6 have been calculated using the centroid, as generated in Mercury[89], of the roughly planar NNXX framework. Figure 5.18 shows the order in which the molecules were considered to arrive at the values. P. Horton[92] was involved with these calculations, the spreadsheet used to calculate all the values can be found in the supplementary data on compact disc attached to cover.

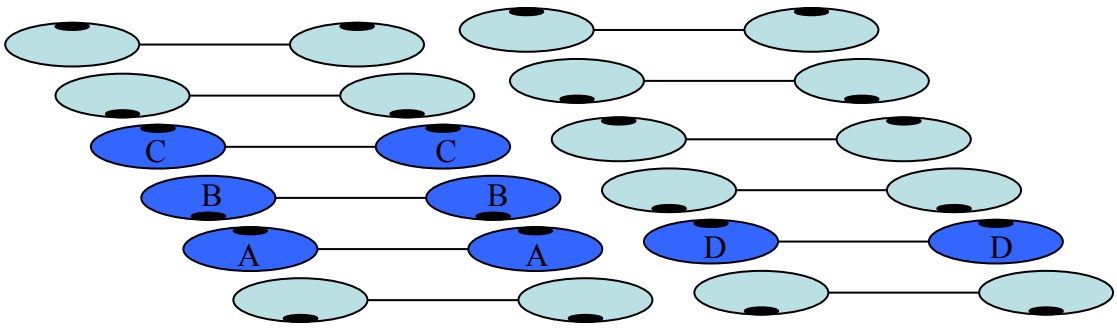

Figure 5.18 Cartoon representation of cyanine dyes. Illustrates the molecules involved to calculate the values in Table 5.6. A-B make up dimer, C represents the next dimer in the stack and molecules A and D are components of stacks 1 and 2 respectively.

Unlike the quaternary salts, monomethine dyes with halogen atoms in the 5-position form X-X interactions. Structures **46b** and **45a** form dye-based halogen contacts with F-F 2.93 Å (2.8 -3.6 Å [93]) and Cl-Cl 3.5 Å (3.2-3.6 Å[87]) respectively. Structure **46a** does not form any direct F-F interactions but forms instead two short H-F interactions of 2.73 Å (3.02 Å and 2.63 Å[93a]). Molecule **45b** also does not form any Cl-Cl interactions but does form dye-counterion interactions with a Cl-I distance of 3.59 Å (which is likely to be van der Waals radii[87]), Figure 5.19 highlights these main interactions.

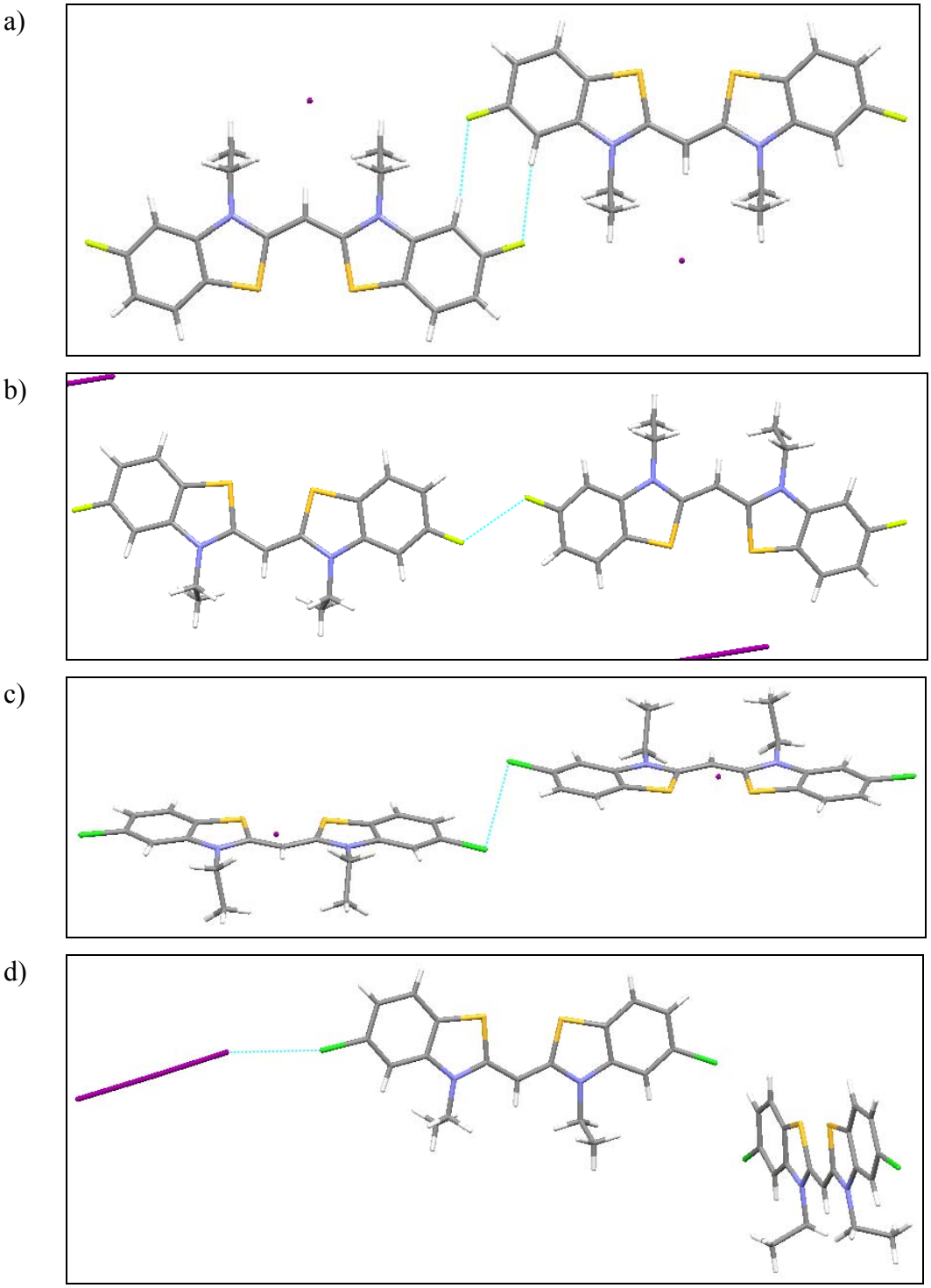

Figure 5.19. Main halogen interactions for monomethine dyes a) ***46a****, b)* ***46b****, c)* ***45a*** *and d)* ***45b****. Blue dashed lines indicate interactions*

Because of the systematic nature of this monomethine study, these structures could be analysed using the software package, XPac, which can be used to identify similar supramolecular constructs[94]. The results have been summarised in the Hasse diagram[92], shown in Figure 20. This type of diagram depicts relationships by

connection with a solid line. The nodes that make up the first line represent the 3-D structure, the nodes in the second line represent the 2-D structure i.e. planes and the third row represents the 1-D structures i.e. rows or vectors. Compounds within the same node have been found to be isostructural. For example the solid-state architectures of **3a** and **64a** are isostructural and have been found to be related to the architecture of **45a** by the 001 and $00^{-}1$ planes respectively. Molecules **47** and **44b** are the only monomethines that are not related to any other structures by their 2-D architecture, having only rows or stacks in common with other compounds. The results from this analysis far out do the relationships that at can be identified with out the software[94]. Future work should involve analysing all known cyanine dyes.

All monomethine dyes have been found to form dimers which could have been represented by a fourth line of nodes as the 0-D. This fourth line of nodes however has been omitted because many of the structures were related, making the Hasse diagram very complicated whilst not really adding any extra information.

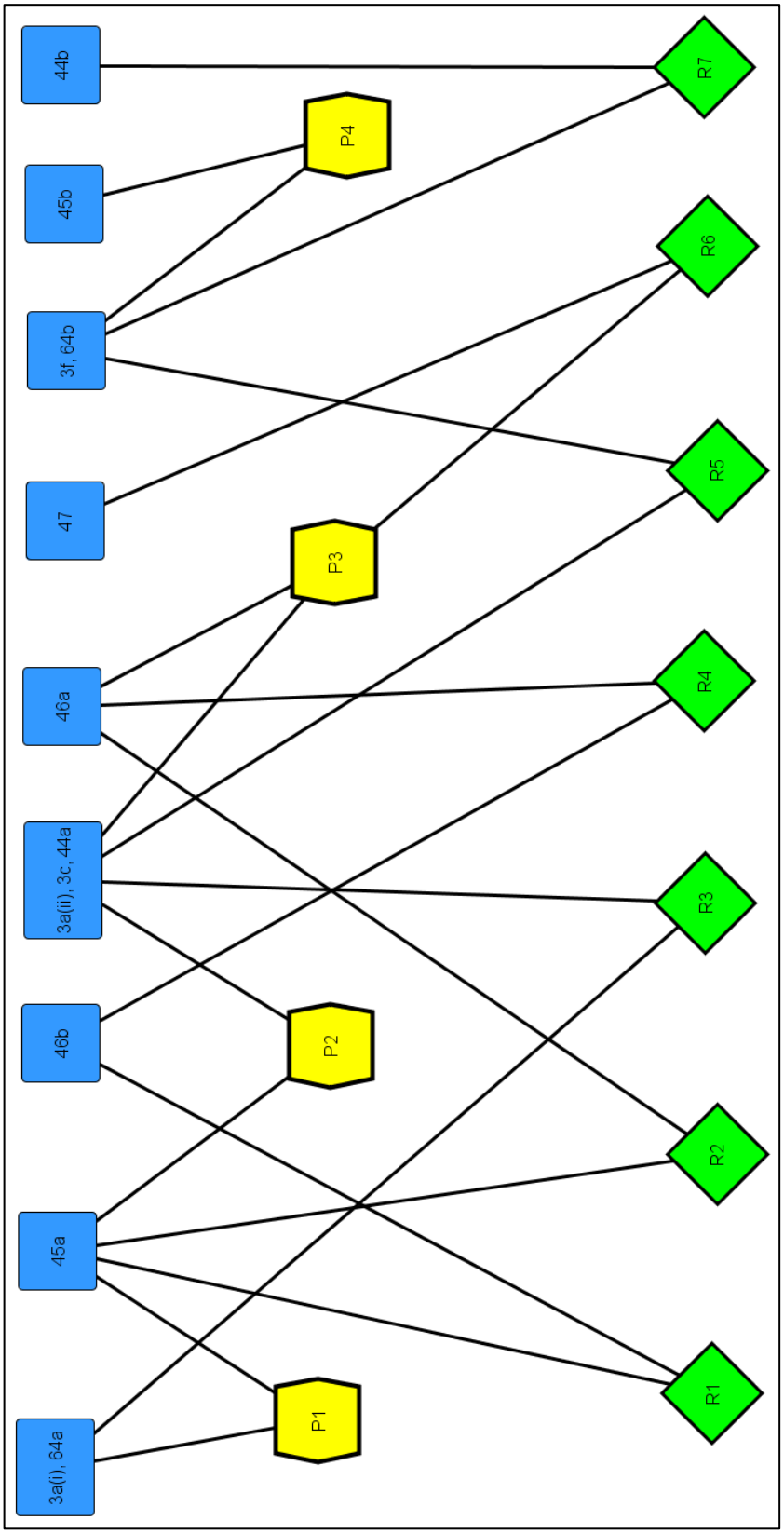

Figure 5.20. A Hasse diagram showing the relationships between packing structures of monomethine dyes ***3a****,* ***3c****,* ***3f, 44a****,* ***44b, 45a****,* ***45b, 46a****,* ***46b, 47, 64a*** *and* ***64b.*** *The blue nodes represent the 3-D, the yellow the 2-D and the green nodes the 1-D*[92].

5.5 Trimethine Dyes

The trimethine dyes prepared during this project resulted in structures and crystals which provided a larger number of structural variations, more so than that of the monomethines, making this study less systematic but more diverse, see Table 5.7. This range of variations allows us to describe the effect these structural changes have on how these dyes pack. Direct comparisons are possible between some dyes but in several instances where there are two or more variables i.e. both structural changes and different counter ions, it may not be possible to make reliable direct comparisons. In these instances however, the difference in spherical counterion can be considered as minimal because the effect of exchanging bromide for iodide on monomethine **3** was negligible (the packing architectures being isostructural).

The data, indicated by the R-value, for the structures shown in Table 5.7 are generally good with the exception of **50**. The structure has a high R-value but this is likely to be because of the disordered solvent molecules rather than the dye structure being unreliable. Dyes **5a**, **51** and **57** have slightly higher R-values than that of the remainder of dyes.

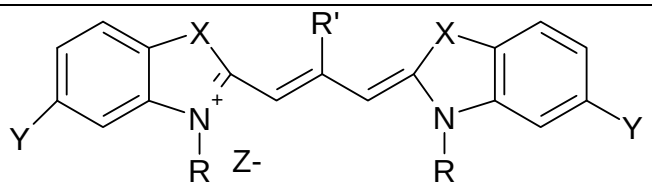

Dye	R	R’	X	Y	Z	R-factor
2a	Et	H	S	H	I	4.31
5a	Et	H	O	H	I	7.09
49	Benzyl	H	S	H	Br	3.43
50	Phenethyl	H	S	H	Br	17.61
51	Naphthalene	H	S	H	Br	7.20
52	4-Bromo-benzyl	H	S	H	Br	3.95
53	Et	H	S	Cl	I	3.38
54	Benzyl	H	S	Cl	Br	4.07
55	Et	H	S	F	I	5.77
56	Benzyl	H	S	F	Br	5.05
57	$(CH_2)_4SO_3^-$	H	S	H	-	6.33
59	Et	Et	S	H	I	4.09
61	Et	Me	S	H	I	2.63

Table 5.7. The range of trimethine dyes X-ray structural studies were performed on. R-values shown as an estimate on the structure quality.

By looking at molecules **61** and **59** (Figure 5.21) it can be shown how the geometry of the molecule changes from cisoid to transoid when the 9-substituent is changed from a methyl to an ethyl group respectively. All monomethine and trimethine structures take on the cisoid geometry which is known to be the most stable conformation[4] with the exception of dyes with 9-substituents such as **59**. Table 5.8 summarises the key properties of the various trimethine dyes. Once again the oxatrimethine dye is the shortest of the cisoid structures. This again suggests that the geometry of the 5-membered heterocycle is sensitive to the heteroatom present and results in the varying long-axis lengths.

a) b)

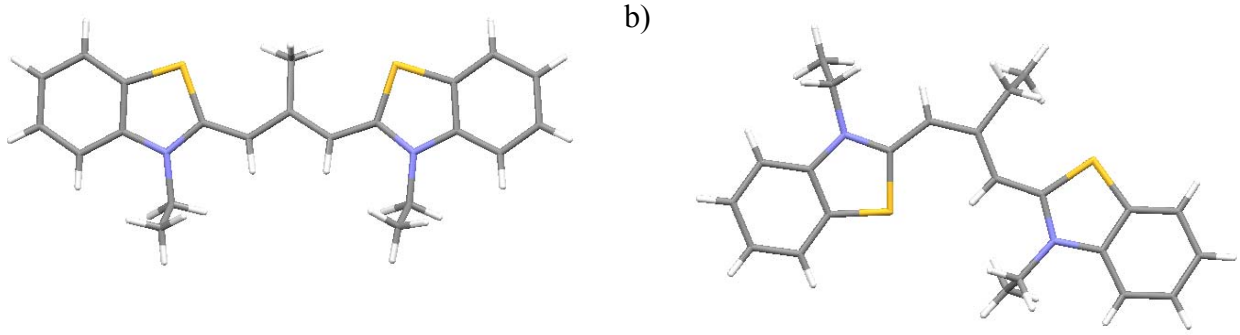

*Figure 5.21. a) Cis-cisoid geometry of **61** b) Cis-Transoid geometry of **59**.*

Dye	Relative Orientation Of R Groups	Relative Orientation of Heteroatoms	Torsion Angle of Dye (estimated error)/ °	Long Axis Length/ Å
2a	Trans	Cis	8.05 (0.08)	14.141
5a	Trans	Cis	3.30 (0.13)	13.454
49	Trans	Cis	11.01 (0.07)	14.152
50	Cis	Cis	*2.61 (0.59) A/ 12.55 (0.52) B	*14.078 A /13.758 B
51	Cis	Cis	2.04 (0.17)	14.020
52	Cis	Cis	2.87 (0.09)	14.331
53	Cis	Cis	0.98 (0.07)	14.156
54	Cis	Cis	3.52 (0.10)	13.949
55	Cis	Cis	1.25 (0.14)	13.783
56	Trans	Cis	18.21 (0.08)	14.199
57	Trans	Cis	3.57 (0.08)	13.936
59	Cis	Trans	4.33 (0.09)	13.316
61	Cis	Cis	3.62 (0.06)	14.391

*Table 5.8. Molecule structural information on a range of dyes. The torsion angles were calculated using the planes of the benzo-groups (Wingx[88]) and the length was measured from carbon- carbon in the 5-positions (Mercury[89]). *Two molecular geometries resulted.*

As discussed in Chapter 1, cyanine dyes often show a twist along the methine chain which can be as large as 15° [57]. Here we describe the effect of various groups on the twists of the dyes prepared during this project. Table 5.8 shows the calculated values

of the torsion angles with estimated errors for all the dyes and Figure 5.22 depicts four of these examples that illustrate the effect of different substituents. The incorporation of large groups in the 3-position (**49** and **50**) increases the torsion angle whereas introducing chlorine atoms in the 5- position (**53** and **54**) can reduce the torsion angle. Conversely, introducing fluorine atoms in the 5-position resulted in a dramatic increase in the twist for **56**. When we compare **54** with **49** and **56** we can see that the larger twist result when the benzyl groups are trans to one another. Dye **52** is another example of a dye which has bulky groups in the 3-position but because the groups are cis to one another, the torsion angle is small. It appears that when the groups in the 3-position are trans to one another, the planarity of the dye is reduced resulting in more twisted structures. From these and the monomethine structures discussed earlier, there does not appear to be an obvious trend as to whether R-groups will be cis or trans. It is important to note that that the sterics of the groups cannot be considered alone, external interactions play a crucial role in determining the geometry of the molecule as these molecules are flexible.

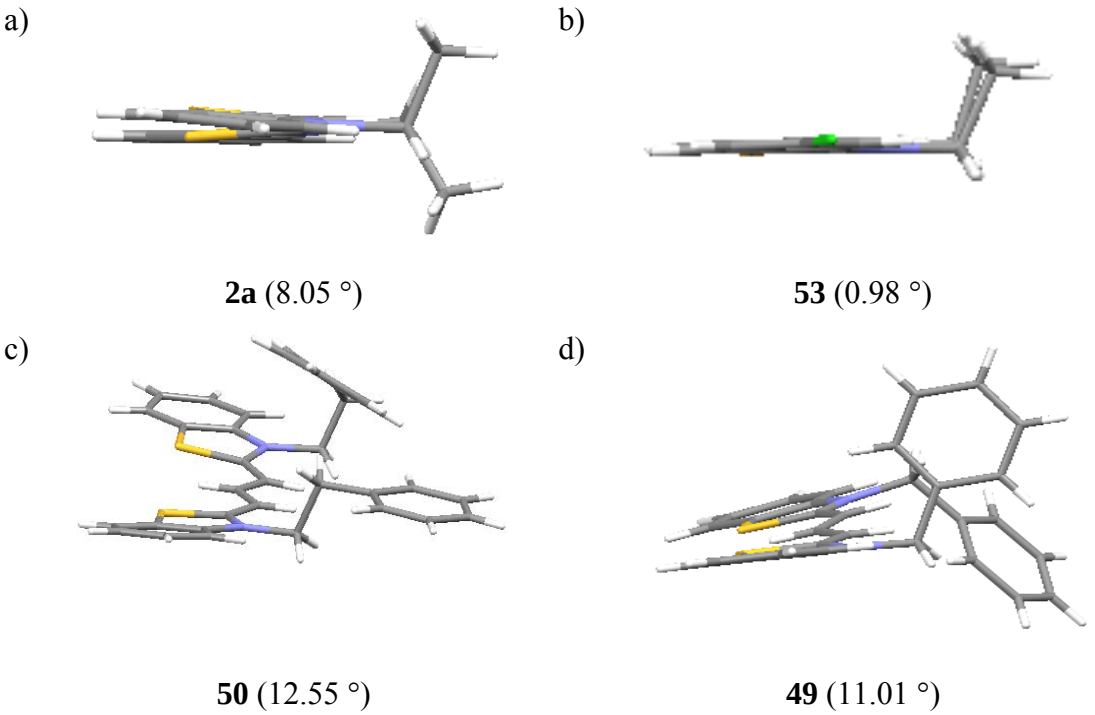

Figure 5.22. Four examples of how structure can affect torsion angles of a dye a) ***2a*** *b)* ***53*** *c)* ***50*** *d)* ***49****. Torsion angles written in brackets*

It was hoped that introducing bulky groups such as naphthalene or p-xylene would exaggerate the torsion further and to see how much twist a dye would tolerate before becoming a transoid structure. Trimethine **51** was the only dye with large, bulky groups to be successfully prepared. X-ray structural studies were carried out, the resulting structure shown in Figure 5.23 but as is clearly shown, the torsion angle (2.04 (0.17) °) is dramatically less than **49** and **56**. A possible explanation for this can be found; the naphthalene groups are cis to one another and they appear to be interacting with naphthyl groups of another dye by lining up (with a distance of ~3.8 Å between the groups), shown in Figure 5.23, supporting the importance on intermolecular interactions. Muro *et al.* reported face-to-face π-π interactions with distances of 3.45 Å[95] suggesting the naphthalene interactions are weaker than this.

a) b)

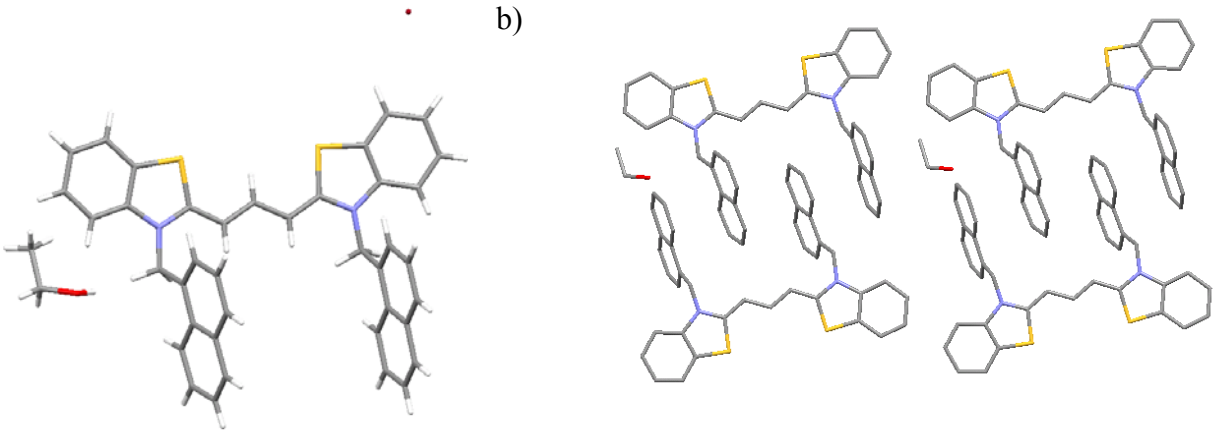

*Figure 5.23. Views of **51**. a)Cis-Cisoid geometry of **51** b)Naphthalene groups interacting (hydrogen atoms omitted for clarity).*

The only trimethine structure to form intermolecular dye halogen-halogen contacts is **54**. Figure 5.24 shows the Cl atoms forming relatively short and therefore strong interactions. The staggered Cl-Cl interactions shown in Figure 5.24 have a contact distance of 3.347 Å which is shorter than the expected values of 3.6 Å based on Pauling's van der Waal's radii[87]. It has been found that 4-chloroenzoic acid formed short Cl-Cl contact of 3.441 Å[87]. Dyes **53**, **55** and **56**, which have either Cl or F in the 5-positions, do not form any direct halogen-halogen interactions which is again surprising as interhalogen contacts are thought to stabilise crystal structures[87].

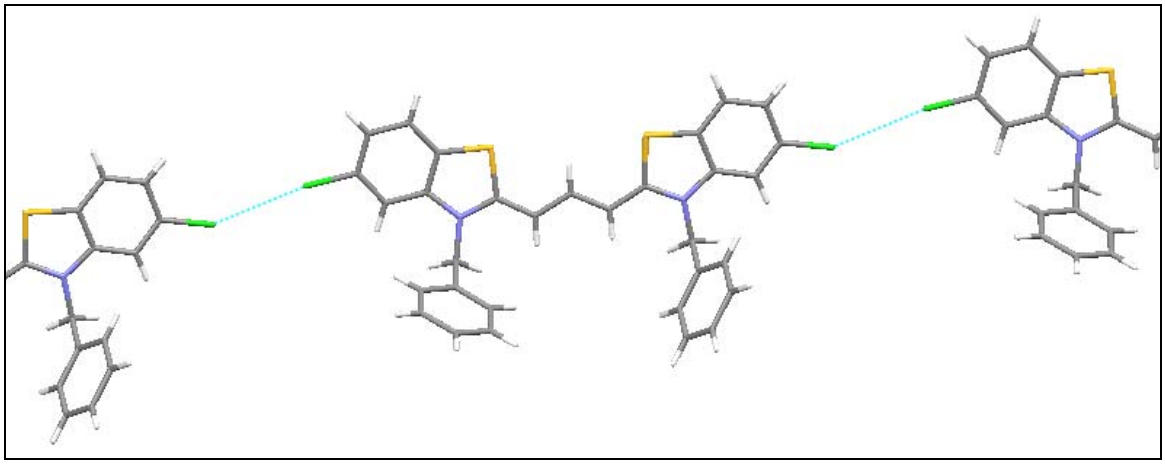

Figure 5.24. Dye ***54*** *forming staggered dye Cl-Cl interactions in packing structure.*

As with the monomethines, the trimethine dyes form dimers which then pack in stacks or brickwork arrays. In some instances, especially staircase-arrays, it is difficult to tell which pairs are the dimers as the structure looks like a stack of monomers. An example of this is shown in Figure 5.25 with separations of 3.48 and 3.58 Å. Only when calculations are used does it become clear where the dimers are. Table 5.9 summarises the information calculated to find out how the dimers and stacks relate to one another.

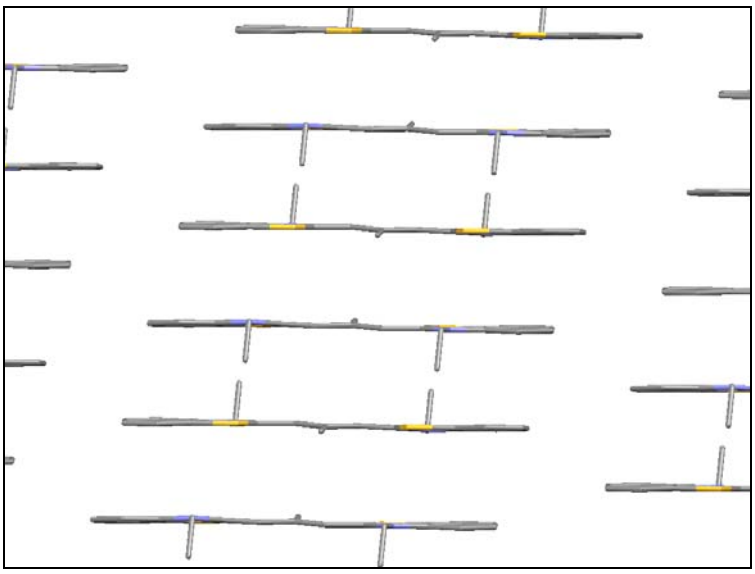

Figure 5.25. Packing structure of ***61****, demonstrating a Ladder-array where dimers are not easily distinguished.*

Dye	Distance between dimer planes/ Å	Distance between dimer 1 and dimer 2/ Å
2a	3.48	3.49
5a	3.26	3.26
49	3.55	3.73
50	3.36/ 3.40	-
51	3.20	7.29
52	3.36	3.45
53	3.44	3.51
54	3.51	3.30
55	3.42	3.51
56	3.27	3.29
57	3.54	3.41
59	3.48	3.46

Table 5.9. Structural information about dimers and stacks of a range of trimethine dyes

The architecture of **50** is quite different from that of the other trimethine dyes. Unlike other dyes this compound results in two different dye architectures, in one of which a phenethyl-group twists over the methine chain whereas in other the geometry the phenethyl-group twists over the benzo-group, shown in Figure 5.26. The difference in the positioning of the phenethyl-group results in two torsion angles; 12.55 ° (shown in Figure 5.22) and 2.61 ° respectively. The two different molecules form separate dimers but not stacks of these dimers, assembling in a herringbone type array shown in Figure 5.27, more like the architectures seen for the quaternary salts earlier in this chapter.

a) b)

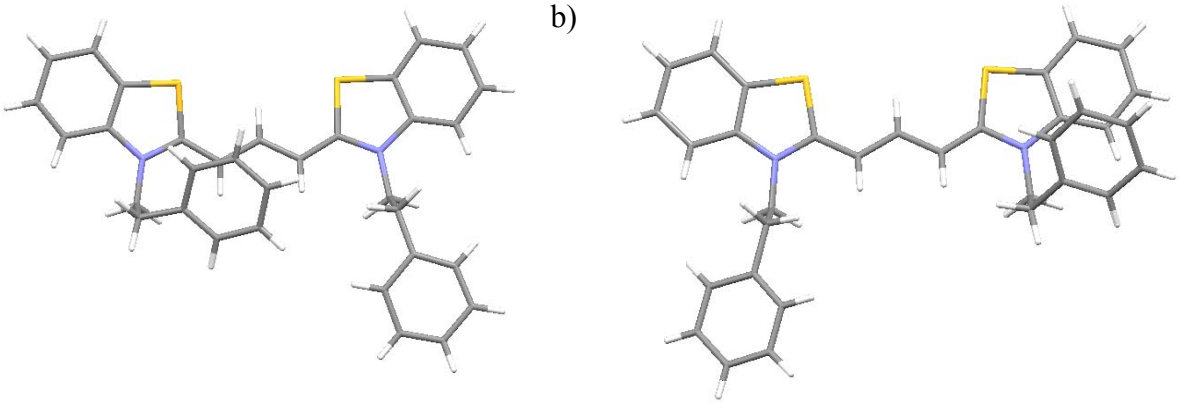

Figure 5.26. Showing the two architectures for ***50****. The phenyl groups orientate over the methine chain or benzo-group resulting in different torsion angles.*

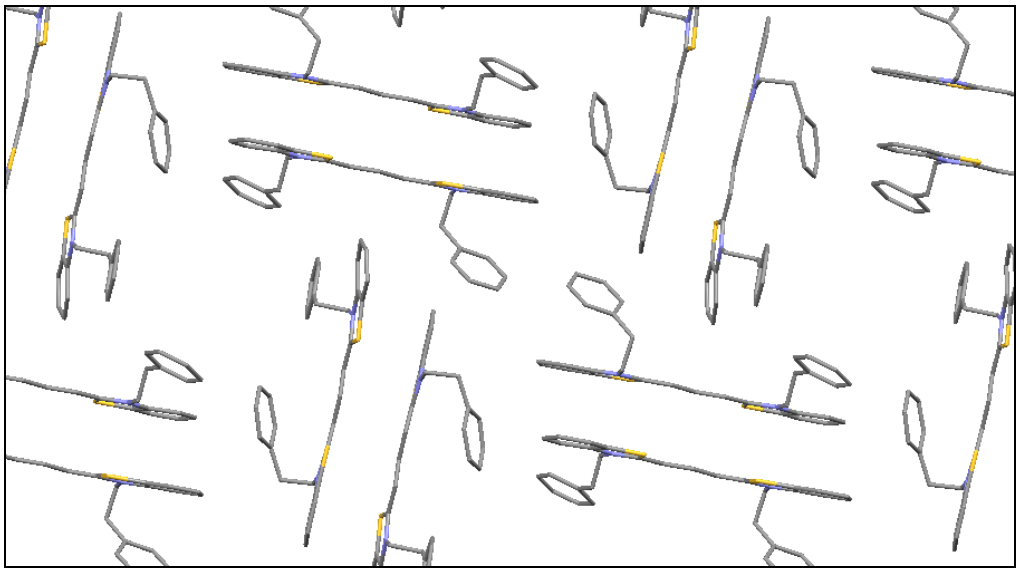

Figure 5.27. Packing structure of ***50****. Dimers form a herringbone-type array but no stacks. Hydrogen atoms, bromides and solvent molecules omitted for clarity.*

It was important to carry out structural studies on **11**, **57** and **58** to try and establish a link between the packing structure and the large number of solution studies carried out using these dyes. Unfortunately, **11** and **58** upon purification only resulted in very fine microcrystalline products, both compounds diffracted very poorly. The water soluble **57** did however result in large crystals suitable for X-ray structural studies, suggesting that the extra carbons in the 3-position of **57** compared with **11** and **58** have a large influence on the crystallinity of the compound. Figure 5.28 shows the trans-cisoid geometry of the molecule and 2-D brickwork array formed by **57**. As discussed in Chapter 3, most of the water soluble dyes seen in the literature have ammonium or pyridinium counter ions[6, 12]. The X-ray data of this compound shows no such counterion which is also backed up by the MS and NMR. The remaining electron density which was not accounted for suggests that there could be either a H^+ or Na^+ as the counterion.

a) b)

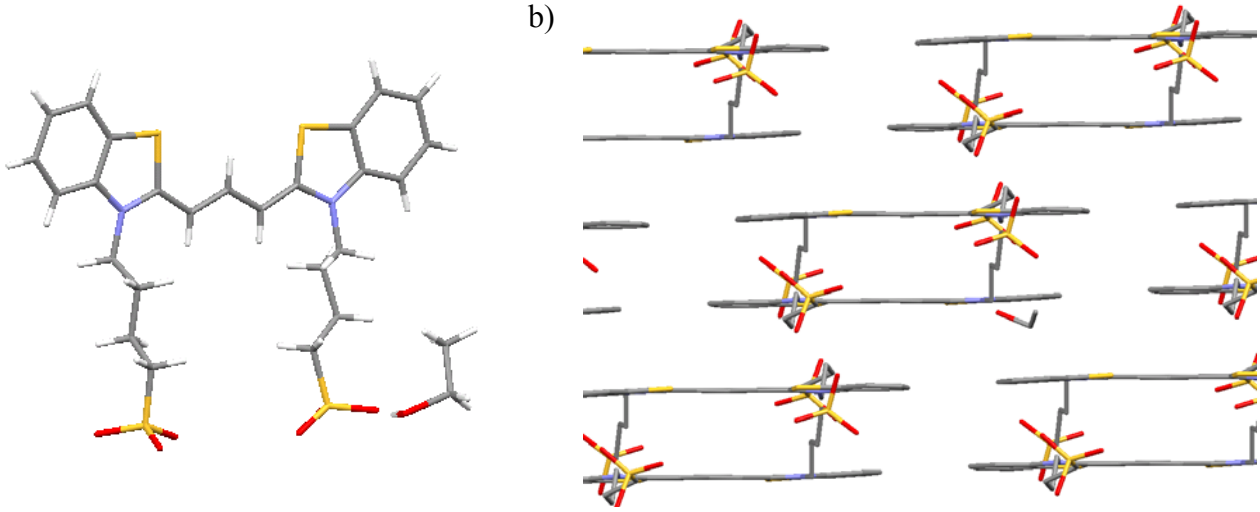

Figure 5.28. Solid-state structure of ***57****. a) Solvent molecule clearly shown hydrogen bonding with the sulfo-group. b) How the dyes pack forming a brick-work array. Hydrogen atoms and majority of solvent molecules not shown for clarity.*

5.6 Prediction of Crystal Structures from the Molecular Structure

From the monomethine analysis and comparison of the trimethine structures it can be seen that there are systematic patterns linking the structural changes which influence the packing structure. This study has only considered a limited number of dyes compared to the known cyanine dye compounds, but even within this small study the appearance of these systematic differences does suggest that the prediction of a crystal structure from the molecular structure may be possible. At this point it seems that we could predict a change if one structural component exchanged for another but reliably predicting the packing structure from a totally different molecular structure would be difficult. This study needs to be extended to a larger library of compounds before further progress can be made in this area.

5.7 Can we Link Solution and Solid Studies?

Before the solid-state behaviour can be linked directly to the solution studies, much larger libraries and more systematic studies need to be carried out. At the moment one can only really explain any abnormalities in solution by then looking at the structures. For example, the fact that the naphthalene dye, **51**, does not aggregate as readily as other hydrophobic dyes without the presence of a salt could be explained by looking at the packing structure where the naphthalene groups have been seen to interact with one another therefore limiting aggregation. Dyes with halogens incorporated into the

molecular frame have shown a tendency in solution to aggregate more readily than dyes without halogens but there is no consistent evidence looking at the crystal structures as to why this might be, so the link between solid and solution states falls short here.

5.8 Conclusions

Structural studies have been carried out on a range of compounds, showing the effect small changes in the molecular structure can have on the packing structure of a dye. The structures were grouped together as quaternary salts, monomethine dyes and trimethine dyes and compared relative to one another. Links were also made, where appropriate, between the three groups. The main findings were:

a) General

- The main descriptors used in the literature to describe the packing structure were staircase-, ladder- and brickwork-arrays. These sufficed for the description of the stack but not for how the stacks relate to one another. The descriptors were therefore extended to staircase-herringbone and ladder-herringbone arrays. It was also noted that in some instances it was difficult to distinguish between staircase- and brickwork-arrays.
- All dyes form packing structures that can be described by one of these five main descriptors with the exceptions dyes **47** and **50**.
- The oxygen containing dyes have a shorter long-axis length than the S and Se analogues. By considering angles of the methine carbon it has become clear that the effect of Se and S on the geometry of the 5-membered heterocycle results in a greater strain on the methine chain compared to the oxygen analogues.

b) Quaternary salts

- All quaternary salts formed dimers with the exception of **35** and **36**
- Two of the six structures that form dimers, **28** and **34**, do not formed stacks of dimers, they pack as isolated dimers.

c) Monomethine dyes-

- The majority of the monomethine structures adopted solid-state architectures that did not incorporate solvent of crystallisation which is contrary to early literature reports.

- The isostructural **3a** and **3c** and polymorphic **3a**i and **3a**ii suggest that when the counterion is relatively small and spherical it does not have a large influence on the packing structure. When the symmetry of the counterion is reduced and the size is increased the counterion does impact the solid-state architecture.
- Dye **47** was the only monomethine structure to have groups other than ethyl in the 3-position. In this case the benzyl groups were disordered.

d) Trimethine dyes-

- The torsion angle of the dyes ranged from 0.98°- 18.21° with the trans-geometry generally resulting in a larger twist along the methine chain. The introduction of halogen atoms in the 5-position also has a dramatic effect on the torsion angle. There seems to be little correlation between the alkyl groups and the formation of the cis- or trans-geometry therefore resulting in little correlation with which groups will result in large torsion angles.
- Dye **50** was the only trimethine dye to not form stacks.
- A range of different interactions were observed as a result of the N-substituent. Naphthalene dye **51** clearly demonstrated face-to-face π-π interactions.

The systematic nature of the structural changes to the monomethine dyes enabled these packing structures to be analysed to a further level using Xpac[94]. The results from this analysis showed the architectures of several of the structures could be linked by supramolecular constructs leading to the conclusion that there is the potential to predict the packing structure from the molecular structure. Because there are so many variables that affect the packing structure, many more structures need to be analysed to make this prediction effective.

Linking this prediction to the behaviour of cyanine dyes in solution, is more difficult because of the complicated nature of the aggregation process. Many more studies need to be carried out but there does appear to be the potential to design a dye for a specific role by predicting its solution and solid-state properties from the molecular structure.

Chapter 6

The Electronic Laboratory

6.1. Introduction

An Electronic Laboratory Notebook (ELN) is essentially a computer program designed to replace the traditional laboratory notebook where COSHH assessments, notes, details and measurements of experiments are recorded. ELNs are becoming increasingly popular because they are capable of combining the flexibility of paper with the ability to access data and information from an advanced computer network, therefore saving time reporting and searching for information. The time saved and the potential improvement in quality of research means that the keyboard is becoming mightier than the pen.

ELNs are a relatively new technology, being commercially sold from the early 1990s with investment increasing significantly recently[96] because of the great number of potential benefits they can offer an organisation. The range of disciplines within science is great which means ELN packages have to be tailored not only for the discipline but the organisation's needs and requirements also. There are many commercially available ELN packages, Scientific Computing World[97] describes the products shown in Table 6.1 as 'worthy of note'.

As mentioned, commercial ELN systems can offer many positive attributes, including searching facilities which can increase productivity and efficiency by improving data accessibility, promoting knowledge sharing across an organization, and minimizing duplication of work[96, 98]. By having experimental information available to all, experiments can be recycled and data collated therefore minimising the time wasted working on problems already solved elsewhere. ELN systems can also be designed to take proactive roles alerting scientists of the arrival of chemicals and deliveries or when an experiment has met certain parameters (providing the technology is available), enabling the researcher to use their time more constructively in and outside

the lab. It is important that an organisation, especially commercial, gets something back in terms of productivity.

Company	Product Name	Focus
IDBS	BioBook	Biologists
Labtronics	Nexxis qELN	(Web based) QA/QC
Studylog Systems	Study Director	Animal studies
Waters	eLab Notebook Software	Chemists
Infotrieve	Infotrieve/ELN	Cross-discipline
Contur	ConturELN	Cross-discipline
Kalabie	Kalabie ELN	Cross-discipline
Tripos	Benchware Notebook	Drug discovery
Mettler Toledo	VirtualLab	Chemists
CambridgeSoft	E-Notebook	Chemists
Symyx	Symyx ELN	Cross-discipline
Axiope	Catalyzer	Biologists
NoteBookMaker	NoteBookMaker	Scientists, engineers and lawyers
iAdvantage Software	eStudy	Cross-discipline

Table 6.1. Information taken from Scientific Computing World[97] about commercially available ELN packages

Lab notebooks have many roles, one such role requires its use as a legal document to situate and date intellectual property claims[99], this therefore means ELNs have to also take this role. IP protection and patent interference are of main concern in order to protect the possibility of future patenting[100] especially as it is becoming increasingly likely that electronic data will be used as evidence for federal laws in civil procedures[96]. It is also important that commercially sensitive work has restrictions placed upon it to prevent access by unauthorised persons with any amendments/tampering being traceable. This can now be achieved through electronic digital signatures and time stamps which are legally accepted[96].

Many organisations, whether academic or commercial, have some type of system to manage their data ranging from basic spreadsheets to more sophisticated in-house

programs (commercially known as Lab information management systems{LIMS})[97]. This means that commercial ELNs have to provide more than a LIMS to be worth the investment by offering database search facilities. The cost of ELN packages are significant considering the software licence, the equipment, training requirements and time taken to get the system right for the organisation costs can often be higher than originally planned. Despite the high initial costs the systems can offer huge benefits especially in quality, time and money[100].

6.2. ELN Industry vs. Academia

There has been more interest in ELNs from industrial companies than academic institutes[101] which has led to more packages being aimed towards commercial businesses. There are subtle differences in how commercial and academic institutes operate but there are many underpinning similarities so if ELN systems are suitable for industry, why have they not taken off in universities?

Academia has many of the same issues as industry except less available financial and dedicated IT resources[96]. Technology in industry changes rapidly because of money and time available to invest in developing this area whereas finances in academia are often allocated, making investment in new systems like ELNs a low funding priority. Both academic and corporate research laboratories require safeguards in terms of security and authenticity although those for industry are stricter than in academia for confidentiality and competitiveness reasons[100].

Researchers employed in industry do not generally publish results outside the company to protect commercial interests, it is therefore crucial that within the company, experiments and results are available for co-workers to access. Electronic systems of recording experiments and associated data have proven to be an excellent way to share valuable research within companies[96].

Academic researchers by contrast are often free to publish their research. Whilst this provides a means of sharing successful work and successful experiments, very little information is therefore available concerning unsuccessful experiments, often the

most time consuming part of research. An electronic system that allowed researchers to see all selected experiments, both successful and unsuccessful, could save time and effort especially when repeating work previously established by others.

Academic institutions may have been discouraged from investing in ELNs, electronic recording and storage of research data because of the high capital costs. For any investment in such systems, it would have to do much more than replace a lab book because of the reduced financial availability in academia compared to industry. There may also be a lack of faith in the new methods especially when traditional methods have worked successfully in conjunction with simple in-house systems of data handling for many years. The use of an ELN within a university in their everyday work could open up the world of research with quick, on hand information linked to other workers in the chosen field of interest.

It seems that a major problem for those in academia is that existing systems are not intuitive and do not focus on the interface enough to make them worth the investment[101]. Jeremy Frey *et al.*[99] set about developing a program for the use in a academic chemistry laboratory environment that is innovative and focuses on the interface. The front-end includes the tablet PC, preloaded software and web browsers for the planning and entering of analysis results and the back-end is concerned with how the data is handled. The back-end of the system is generally of little interest to the customer, but is very important in terms of planning and designing a system capable of storing and retrieving large amounts of data. This research project involves trialling and feeding back the findings of this ELN in terms of planning, recording, reporting and publishing of experiments as well as storing associated spectra and analysis data.

6.3. The Designing Process

Although the basic principles of an ELN are the same, there are many areas within the package that need to be considered and varied to result in a suitable product for a desired consumer. A paper lab notebook is flexible, portable, robust and can be used as a legal document[99]. For an ELN package to be successful it needs to encompass all

of these qualities and more. Having a flexible package can be an attractive feature to customers enabling them to reduce the cost by removing unwanted/unnecessary features. Options including the use of the pilot, purchasing by user licence or per institute licence and finer details within the package such as a single share point for several users can provide some cost reductions.

Paper lab notebooks are cheap to purchase in comparison to the software and computers involved in an ELN package. To promote use within academic institutes the cost of the ELN package needs to be minimised, not only because the initial costs need to be considered, but storage and maintenance have an impact on the costs also. Running costs of a lab book are nil but need physical storage space (for a minimum duration for legal reasons[100]), computers on the other hand use electric and require fixing whenever problems occur but a single server can store a vast number of experiments requiring very little physical room.

The process of carrying out a COSHH assessment for an experiment is an important part of managing safety in the laboratory. The hazards associated with each chemical, and the control measures to mitigate the risks related with their use are determined by researching catalogues and safety data sheets. The act of copying out this data by hand into a traditional lab book forces the researcher to focus on understanding the hazards but can therefore be a time consuming process. Providing it does not compromise hazard awareness, an ELN could speed up this process by taking a proactive role flashing up reminders to remind/warn the chemist to take particular care.

Because of the high security requirements of the large pharmaceutical companies compared to the smaller companies where the security does not need to be as strict, it is important to have a flexible package where security features can be removed/added as desired, which as mentioned can also reduce the cost of the package. Depending on the needs of the organisation, different levels of security can be implemented including network, application and project access control. Experimental notes can be required to site intellectual work, it is therefore important that the process to record data is traceable and would stand up in the eyes of the law. A higher security level would result in heavier access control but it is crucial that even very basic security

levels cover legalities. Work can be secured in terms of access and storage by implementation of passwords, traceability and the backing up of data providing a higher security than a traditional paper lab notebook.

Chemistry is a very broad area so having one package that can handle the majority of these areas would be advantageous. It is useful to know where the software's capabilities lie, to know where it can be marketed hence a trialling/improvement process will ensure the maximum capabilities are realised and implemented. ELNs are by nature systematic and require processes to be adhered to therefore making them not as flexible as traditional methods but this can have its advantages. For example, in QA/QC-type organisations it is important that certain procedures are exactly followed. By constraining a package a degree of control over the procedures can be implemented.

The lab is a relatively harsh environment, paper as the information storage is a robust way to ensure the document will remain legible for the legal duration required and longer[96]. In a lab environment, the ELN hardware needs to be resistant to any chemicals that it comes in contact with as it is expensive to replace. It is important to have a system that stands a better chance of surviving than a paper lab book although the data which will be stored on a remote server is likely to remain intact. In terms of a fire, experiments entered into an ELN system would be more likely to survive especially if a remote server was used to backup the data whereas paper lab books would be very unlikely to survive.

6.4. Understanding the Experimental Process

To translate the process of a chemist recording their experiment into a piece of software required careful consideration. A common approach to designing new software is the 'user- centred design' involving a user community trialling a set of techniques against their needs in order to produce a prototype which is again trialled. Frey *et al.* found these human computer interaction methods unsuitable for the development of the ELN software due to the non-systematic nature of chemistry

experiments which were found to be “highly expert, loosely structured and of potentially long duration”[99].

To therefore fully understand the experimental process the software engineers took the simple procedure of making a cup of tea and made it into an experiment by dividing it into stages in a scientific manner. This procedure was then carried out and monitored closely to provide the basic structure for the experimental work flow. The first release of the software was called ‘SmartTea’ after the experiment it was designed around. Although the experiment design was crucial for the project as we have seen, it was not the only aspect of importance to the package.

6.5. The Product

Due to the dynamic nature of research it was important any recording medium was portable and could be moved to wherever necessary. A Tablet PC is heavier than a notebook, but is still light enough to carry around. A traditional lab book is fairly robust and has few constraints as to what is written on the paper. The option of using a desktop PC was discounted to enable maximum flexibility and portability. As mentioned, a tablet PC was chosen as the media carrier in the lab to ensure the project reached its maximum potential in terms of combining the contrasting and varied nature of this and other projects.

The knowledge and experience gained from the lab environment and experimental process was then used to produce a basic interface to be improved upon through a trial and feedback process. Snapshots of the first version of the software, SmartTea, are shown in Figure 6.1. The product was then trialled and feedback used to refine the product resulting in a new release entitled ‘MoreTea’, of which snapshots are shown in Figure 6.2.

As with any experiment, the first stage is planning and considering the hazard data in the form of a COSHH assessment. In the case of the SmartTea software the main steps involved with this were:

i) entering the chemical name

ii) the amount of the chemical
iii) the COSHH information associated with the chemical
iv) the process involved with the step e.g. filtering, refluxing, stirring, recrystallising etc

Repeating this process for each reagent allowed a method to be built up. Steps could easily be added and removed at any time.

Once the plan had been entered the experiment could be run in the lab using the bench station where experimental details such as accurate weights and observations were added. Observations were drawn, hand written using the stylus or typed. The experimental notes and observations associated with each step could then be observed at any point before, during or after the experiment in a separate browser called 'viewer0'.

a)

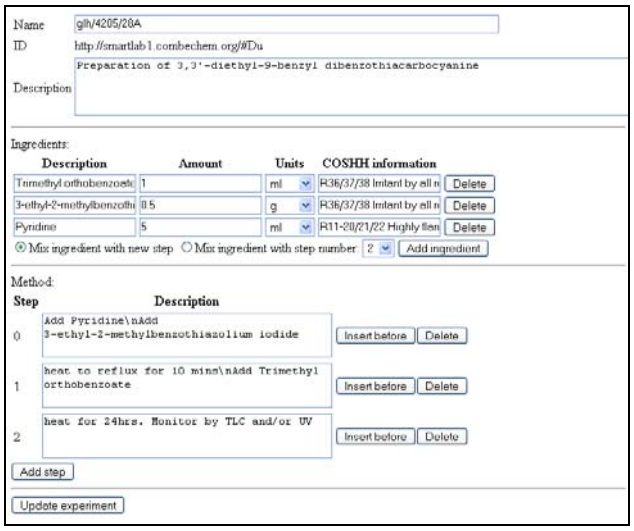

b)

c)

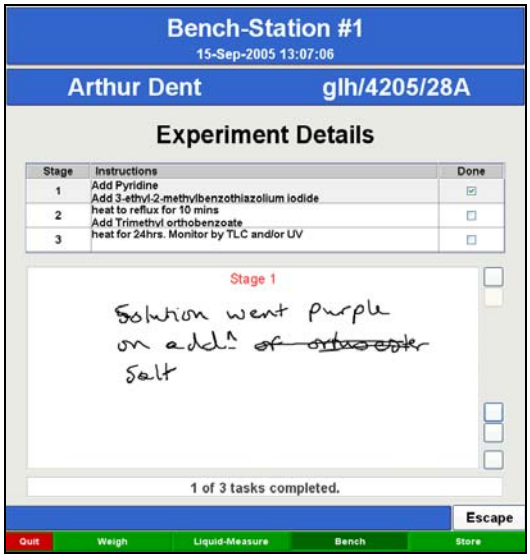

d)

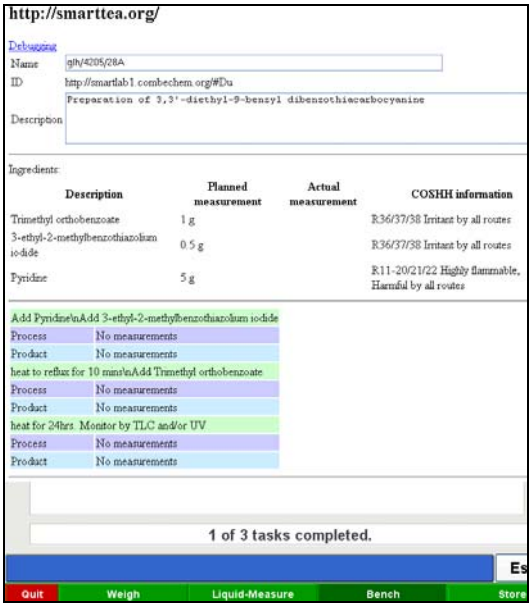

Figure 6.1. Four snapshots of the different aspects of the original ELN software a) planning screen, 'Planner0'. The details of an experiment are shown as they are being entered into the appropriate boxes with a method building up as the reagents are entered. b) 'Weigh-Station'. This part of the interface records measurements of reagents used during the experiment c) 'Bench-Station'. This provides experimental steps to follow and observations are written and recorded here. d) 'Veiwer0', showing all details of the experiment which can be checked at any point for a summary of the reaction.

MoreTea, the later, more refined version of the software, has fewer components to the package as the experiment can be planned and viewed in the experiment browser. The compound details and experimental method (again in steps) were entered into the 'experiment browser'. The experimental notes and observations were then entered into the 'LabTool' as the experiment progressed. It was possible to view the different steps in the experiment browser at any time because the components were linked and refreshed frequently.

a)

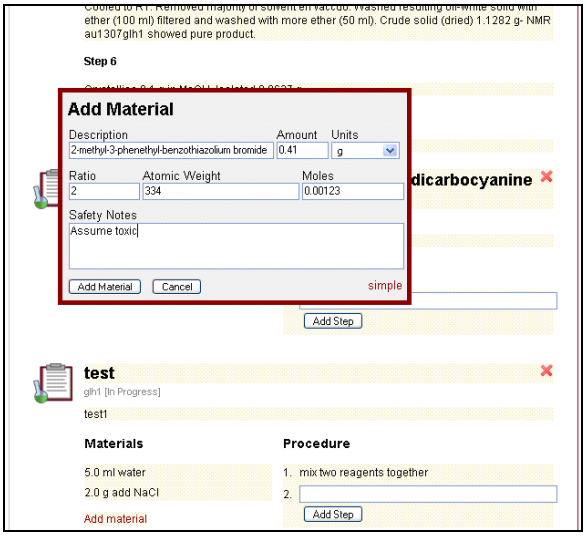

b)

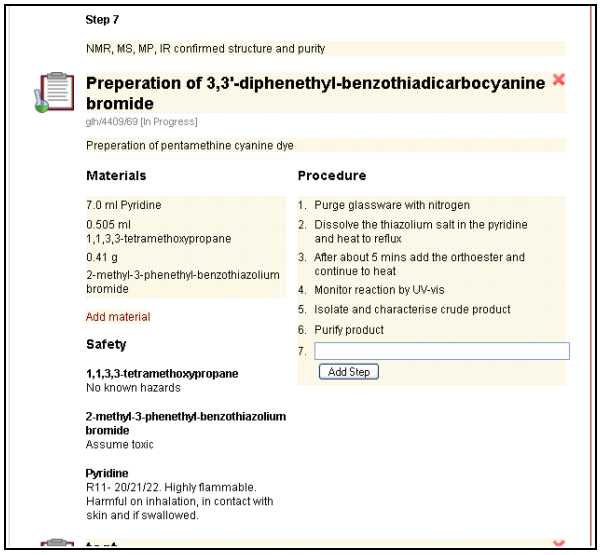

c)

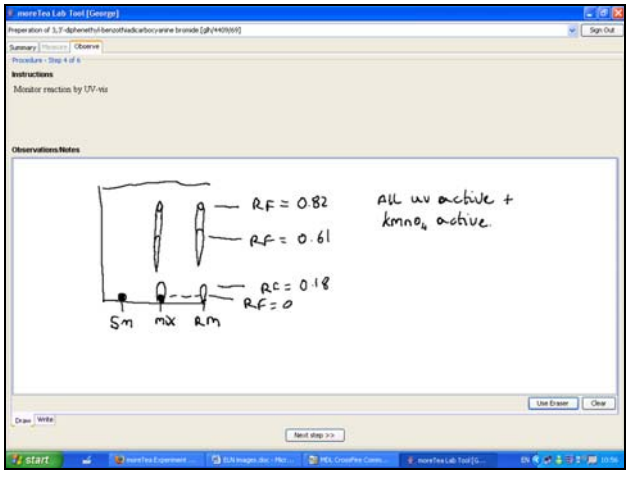

d)

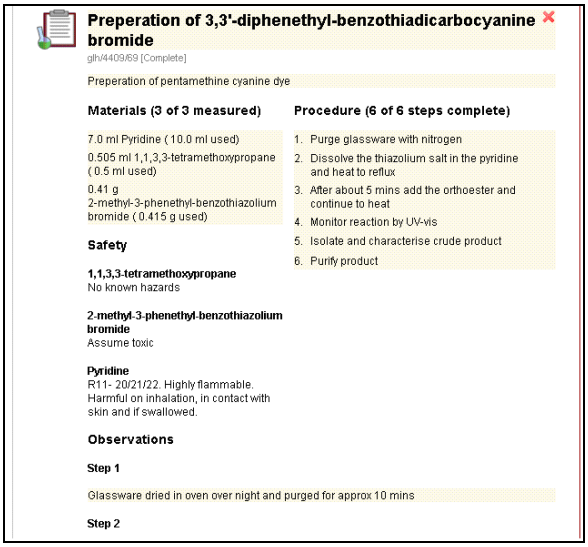

Figure 6.2. Showing snapshots of the newest version of software, MoreTea. a) Entering details of the chemicals b)Entering the steps c)making notes in the Labtool d)Viewing the plan and notes of the experiment

To connect the front- and back-ends, a tool where spectra could be uploaded and associated with an experiment was used, known as Repository for Laboratories (R4L)[102] The R4L has been trialled during this project to see how all the components to this package meshed together but the designing and background is discussed by Coles *et al.*[103].

The R4L browser required the input of a chemical structure and any associating spectra data or additional experiments. Spectra associated with the experiments were then uploaded into the R4L web browser by giving the molecule a code (same as the code assigned to the experiment) and drawing the structure of the molecule generated an unique identifier (an inchi code). Spectra files are then uploaded onto the site. Figure 6.3 shows some snapshots of R4L in use.

a) b)

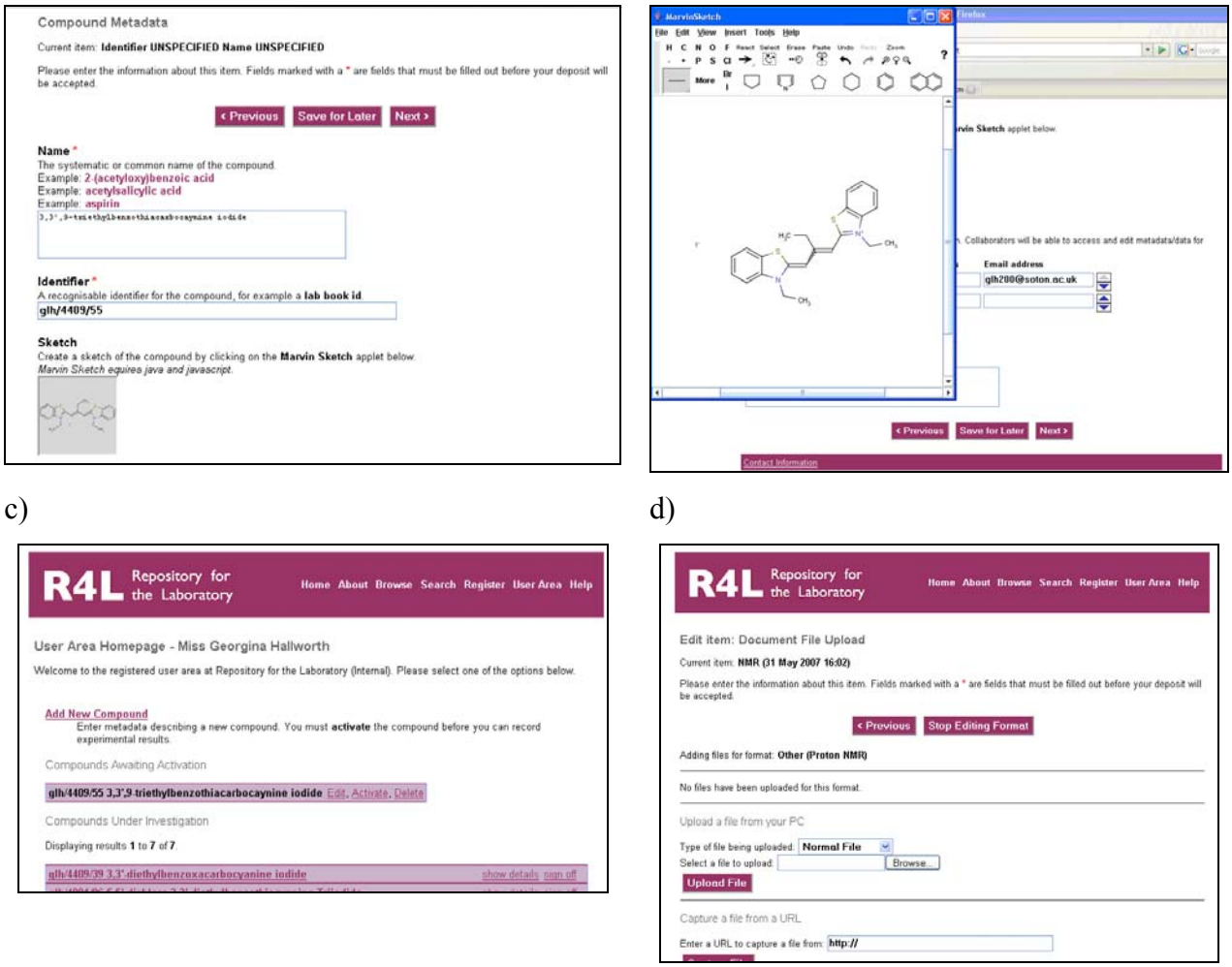

c) d)

Figure 6.3. Four snapshots of the R4L software. a) input of chemical information b) generation of inchi code c) activation of compound and finally d) the uploading of data.

6.6. Results and Discussion

It was important to establish not only how the system coped in real time but also how it dealt with a large number of experiments and data. Several experiments were therefore carried out in real time but to ensure a relatively large volume of experiments and data, old experiments were entered into the system as if run in real time. It was also important to trial a range of experiments to establish if the subtle differences in the basic principles of a synthetic experiment compared to a physical-type experiment affected how the requirements of software changed. Testing the system in this manner allowed all components of the package to be tested including the back-end.

Repeating the process of trialling the package and feeding back comments not only for numerous experiments but different types of experiments including synthetic and physical-type studies allowed any software bugs and any practical difficulties to be identified and corrected. Any suggestions for improvement of the package were also noted down and reported back to the software engineers for consideration. Noting down and prioritising the problems meant the software engineers could focus on remedying important issues that immediately prevented the system from working as it should.

The software worked well and was simple to use. It became apparent during the trialling process that every chemist has their own way of doing things so an ELN package cannot meet every individual's needs and preferences but there were some crucial findings as summarised below.

The robustness of the tablet PC and hardware in a lab became an issue when the scribe came into contact with solvent for a short period which resulted in it partially dissolving. Contamination of the hardware was also a problem as to financially make the most of the tablet PC it was used both inside and outside a lab potentially resulting in the transportation of chemicals from 'dirty' to 'clean' areas. By purchasing or engineering a frame for the Tablet PC to be mounted, any spilt chemicals could drain or be brushed away easily and a plastic keypad covering would provide a certain amount of protection against contamination from the surface of gloved hands and again, spilt chemicals.

Several bugs have been identified whilst trialling SmartTea and MoreTea. An example of this involved the information about amounts and units of reagents/solvents not being transferred between the different components of the package i.e. the default, grams, repeatedly appeared instead of mLs and drops. Another example concerns the chemical name which included apostrophes i.e. 3,3'-diethyl-benzocarbocyanine; the program did not accept this nomenclature and entered a large number of back-slashes which increased each time a step was added. Bugs such as these cannot be predicted but trialling a system can help find these errors before commercialisation/final product.

There were occasional problems recovering and saving the data entered into the planner although these were promptly resolved. Problems like these on the final product could lead to frustration and mistrust of the software resulting in abandoning the ELN in favour of the traditional paper method or duplicating work by creating a hard copy also.

Due to the fact the programme was not written by chemists and the nature of the trial experiment (making tea in a scientific way), phrases such as 'ingredient' were used instead of 'reagent' in the SmartTea version. Other details which could be easily corrected and significantly improve the professionalism of the product included the area where the formula weight was entered being labelled as 'Atomic weight' and the MoreTea package did not take into the consideration the density when entering the details of a compound if a liquid.

When entering details into the experiment browser for MoreTea each new stage added resulted in the screen refreshing and returning to the top of the page. The experiments were listed alphabetically by title so each new step or reagent addition resulted in the user having to scroll through all the listed experiments until the current one was found. The list of experiments looked very similar resulting in a time consuming process which could be avoided if the experiments were listed in order of time or date. Another solution which would aid recognition of the experiments but also add to the quality of the overall ELN product, would be an area under the title where the chemical compounds/reaction schemes could be drawn out. This would also be of benefit if/when the package was be used to generate basic reports form the information entered into the system.

The quality of reagents purchased or prepared in-house can vary from batch to batch making it useful to have somewhere to enter the batch codes of the reagent, which might explain anomalies in products. For in-house compounds it would be useful to note this somewhere with the code/experiment it relates to. A function that links the current experiment with the experimental data from the preparation of the reagents would also improve the system.

Experiments are very fluid processes with aspects and outcomes that cannot always be predicted and need to be solved e.g. the production and therefore necessary separation of unknown by-products. In these cases it is very much a case of trial and error but it is crucial everything is recorded. In terms of then generating a report (which is a time consuming process) the chemist interprets the experimental observations and filters out unnecessary steps by not including them in the final report. Because the procedure by which observations are recorded in both SmartTea and MoreTea is not constrained it may be difficult to get the ELN package to generate a comprehensive report.

Whilst carrying out experiments in real time and making experimental notes it was noticed that there was no method to move between steps in the both versions of the lab tool- the user could only move forward onto the next step. The flow of the product is therefore very rigid but in reality a chemist is likely to do a few steps before recording anything resulting in bits being potentially missed out and therefore the need to go between steps. Anything that had been entered into the final step had to be saved by closing the experiment even if there is more to do i.e. potential extra crops from recrystallisations. An experiment is only finished when a product has been identified, purified and fully characterised. To allow for the final step to be revisited there needs to be some sort of save function and a finished experiment option.

Using the package did require some adjustments to working habits. In the first instance, whilst designing/planning the experiment it was required that the process was divided into suitable stages to enter into the ELN as the plan which was easier for known experiments compare to novel reactions. In the cases where novel reactions were being attempted, thinking of the experiment in stages was difficult and often led to large, very general steps being used. Secondly, the fact that the reactions could be potentially viewed by others without consultation required notes to be clear, concise and legible which is ultimately of considerable benefit. Often, when using personal paper lab notebooks the notes are made quickly and little thought goes into how interpretable these observations are resulting in the user having to translate the notes at a later date into a useable form. In terms of safety, there was no change to working practice and using the ELN had no detrimental effect to the awareness of the potential hazards of the chemicals being used which was an essential criterion.

Using the ELN package required more time and thought to be put into the planning of the experiment. As a result of this, it became very obvious that the extra effort in the planning stages resulted in a considerable time saving in the later stages of the experiment. The process of thinking of 'what path the experiment could take' meant that the user was prepared, whereas with paper notebooks very little thought goes into the outcome and is dealt with as and when it occurs. Obviously some outcomes or experimental results are unpredictable but these were equally likely whether using traditional paper lab notebooks or the ELN package. Generally, what can be predicted is dealt with more proactively whilst using an ELN.

6.7. Conclusions and Further Work

The project is in its early stages and much more work is required on the user interface, hardware and the underlying software to handle all the data needs. Questions that arisen from the trialling process as points of discussion and need further attention include:

- It is important to develop a system that associates a compound with the corresponding spectra. Is there a way of linking the compound to the spectra before? The spectra are generated remotely so is it possible that these spectra will go straight into a folder?
- We know that paper provides us with long term storage of information as paper has been shown to have survived through centuries. It is not clear however what the long-term data storage properties of computers are because of the relatively recent development of computers.
- How should searching facilities be managed? Searching for reactions entered by names, structures or inchi codes? Problems arise when searching by name as spellings can be wrong and systematic names are not always used. Also should the ELN provide a database-type searching facility or is it better that existing ones are used?
- Work also needs to be carried out looking at whether reports can be generated from the information entered into the system. Would a more realistic function one that summarizes the analytical data?

It was important that whilst using the software that some of the main criteria of this ELN package were kept in mind; the product had to flexible, innovative, useful and reduce time wasted on duplicating work and processes that could be aided by a proactive system. The ELNs package developed here has proven to currently be a highly developed experiment manager. At present, MoreTea may not be a saleable product in its own right considering there are increasingly sophisticated ELN products out on the market but it could easily be incorporated and enhance an existing product. Another marketing option could be that the basic software is offered as a free package with the choice of higher security and more functions being available at a cost should an organisation desire.

Chapter 7

Conclusions and Future Work

A range of novel and known cyanine dyes were prepared using a series of condensation reactions. The conditions of the reaction remained constant for each type of dye with the exception of the activated quaternary salt. The reactivity of 3-methylbenzothiazole was greater than that of the oxygen and selenium analogues resulting in the majority of the dyes containing sulfur. Purification was achieved through fractional crystallisation for most of the dyes. Electrospray mass spectrometry was found to be the most suitable technique for detecting any unreacted starting material remaining in the sample.

As expected the majority of trimethine dyes formed aggregates in aqueous solution, with and without the presence of inorganic salts. The oxygen containing dyes **5a** and **48**, however did not form any type of aggregate at the concentration levels studied, even in the presence of salts. This suggested that the heteroatom had a crucial role to play in the aggregation process. Aqueous solutions of dyes **11**, **57** and **58** formed J-aggregates in the presence of salts. Upon further investigation it became apparent that the anion was inducing and therefore controlling the aggregation process. This is contrary to findings in literature which report the anion having a redundant role[6,19,23,25]. Subtle differences in the aggregation behaviour related to the molecular structure when monitored by UV-visible spectroscopy were not apparent in the emission spectra of these molecules, with self quenching being the dominant effect.

A large number of previously unknown crystal structures were determined of quaternary salts, monomethine and trimethine dyes during this project. Despite the precursor set being incomplete compared to the corresponding dyes, these structures provided information into the effect of the extra conjugation. Because of the systematic nature of the changes in monomethine molecular structures successfully prepared, crystallised and studied, this provided an ideal set to be analysed in more depth using a computer program known as Xpac[94]. The results of this study showed

there were systematic correlations between molecular structure and the packing structure, therefore suggesting a potential to predict how a dye may pack from the molecular structure. The differences in the trimethine molecular structure were less systematic but more diverse therefore resulting in a diverse set of crystal structures that were analysed.

The bulk solution and solid-state behaviour of many more cyanine dyes need to be compared and analysed. By collecting more data, in the future it may be possible to predict how a dye will pack in the solid-state. Forming links between the solid-state and the bulk-solution behaviour is a little more tenuous. In some cases the solid-state behaviour is in agreement with the solution behaviour but in other instances the solid-state observations do not reinforce the bulk solution behaviour.

More trialling work needs to be carried out on the ELN package designed within the department. Early signs are showing that the product is a sophisticated experiment manager that can potentially reduce the time wasted on redoing work. Using the package in the lab brought some problems to our attention which were then reported to the software engineers to be corrected. The trialling processes also showed how the ELN altered the way experiments were carried out.

Chapter 8.

Experimental

8.1 General Methods and Instrumentation

Commercial compounds were purchased from Acros, Avocado, Fluka, Lancaster or Sigma-Aldrich and used without further purification. The following solvents were purified and dried according to known literature procedures and distilled immediately before use.

- Acetonitrile (MeCN) was dried over calcium hydride and distilled before use
- Acetone was dried over calcium sulphate and distilled before use
- Diethyl ether (Et_2O) was dried over sodium wire and was freshly decanted
- Ethanol (EtOH) was dried over calcium sulphate and distilled before use
- Methanol (MeOH) was dried over calcium sulphate and distilled before use
- Pyridine was dried over calcium hydride and distilled before use
- Toluene was dried over calcium hydride and distilled before use

Characterisation methods

- Melting points were measured on an Electro-thermal melting point apparatus and are uncorrected.
- IR spectra were obtained using a Golden Gate Attenuated Total Reflection (ATR) sampling attachment on a Mattson Satellite 3000 FTIR spectrometer.
- ^{1}H and ^{13}C NMR solution spectra were recorded on a Bruker AV300 spectrometer at 300.13 and 75.42 MHz respectively.
    - Multiplicities are quoted as s-singlet, d-doublet, t-triplet, q-quartet, qu-quintet and m-multiplet; coupling constants (J) are quoted in Hz.
    - ^{13}C NMR spectra were fully decoupled. Peaks are quoted in p.p.m. (δ) and are referenced to residual solvent.

- ^{1}H and ^{13}C NMR solution spectra were also recorded on a Bruker AM400 spectrometer when required at 400.13, 100.62 MHz respectively

- Electrospray mass spectra were recorded on a Micromass Platform II single quadrapole mass spectrometer.

    - The instrument is calibrated with a mixture of sodium and caesium iodide, the operating conditions were capillary 3.50kV, HV lens 0.5kV, cone voltage 20V, source temperature 110ºC, ES eluent: 100% acetocyano at 100µl min^{-1}, nitrogen drying gas 3001h^{-1} and nebulising gas 201h^{-1}

    - 10µl injections of c.a. 1-10 µl ml^{-1} solutions were made using a Hewlett-Packard HP1050 auto-sampler.

    - Negative ion data were recorded under identical conditions except for different polarity voltages and capillary voltages of 3.0 kV.

- Single Crystal X-ray structural analyses were made using a Nonius Kappa CCD diffractometer and Nonius FR591 rotating anode X-ray generator.

    - The data was processed using the *Collect*[104], *HKL*[105] and *maXus* software[106]

    - Structures were solved using *SHELX*[88] in the *WinGX*[107] suite of programs.

    - All H atom fixed at idealized positions, with a riding model and fixed thermal parameters [$U_{ij} = 1.2U_{ij}$ (eq) for the atom to which they are bonded] used for subsequent refinements.

- UV-Visible spectra were recorded using Schimadzu UV-1601 UV-Visible Spectrophotometer, data collected using UVPC Personal Spectroscopy Software v3.5, absorption recording range: -0.1 to 1.5 from 1000 nm to 200 nm, sampling interval: 0.5 nm, light source 360 nm.

- Emission spectra were recorded using a Hitachi F-2500 Fluorescence spectrophotometer, 220 V, 50/60 H with a Xe lamp. Software used: F L Solutions

8.2 Synthesis

Many of the structures reported in this thesis are known but the characterisation of the dyes and precursors is poorly documented in most cases. Novel compounds are noted. The reactions have been grouped together with general preparations with any variations stated below the reagents tables.

8.2.1 Dye Precursors

Three main procedures were used to prepare the dye precursors:

8.2.1.1 General experimental I for benzothiazolium salts

A mixture of 2-methylbenzothiazole (**X**) and alkyl halide (**Y**) were dissolved in MeCN (with a catalytic amount of NaI was added in some cases) and heated to reflux for 2-3 days. The reaction's progress was monitored by TLC. Upon completion, the reaction mixture was cooled to RT, resulting in the precipitation of a solid. This solid was isolated and washed with an appropriate solvent.

Synthesis of 3-benzyl-2-methyl-benzothiazolium bromide, **28**

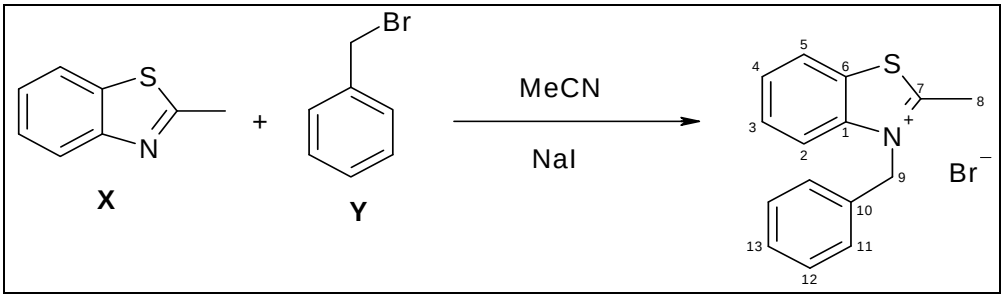

Reagent/solvent	**2-methylbenzothiazole, X**	**Benzyl bromide, Y**	MeCN
Mol	3.9 mmol	3.9 mmol	-
Mass/volume	0.5 mL, 0.587 g	0.47 mL, 0.672 g	5 mL

After 24 hrs, an off-white solid (0.289 g, 23%) was isolated by filtration and washed with ether (50 ml). The solid was then crystallised from hot MeCN producing off-white plates (0.20 g. Yield 16 %).

[Lab book reference code: 4205/79 & 4205/81]

Characterisation (known compound)

MP: 238 °C (Lit[108] 231-232 °C)

IR (ATR, υ/ cm^{-1}): 3334 (m), 3056 (w), 2929 (w), 2361 (m), 1744 (w), 1650 (w), 1581 (w), 1511 (m), 1495 (m), 1450 (m).

LRMS (ES^+, MeCN) *m/z*: 240, 241 & 242 [M^+] (100%){S^{32}: S^{34} 0.95:0.04}

LRMS (ES^-, MeCN) *m/z*: 79 & 81 [Br^-]{Br^{79}:Br^{80} 1:1}, 127 [I^-]

HRMS (ES^+) calcd for $C_{15}H_{14}N_1S_1$ 240.08469, found 240.0839 [M^+]

^{1}H NMR (300Hz, DMSO-d_6). δ: 8.54 (1H, dd, J= 2.2, 7.5 Hz, $H^{5/2}$), 8.22 (1H, dd, J= 1.5, 7.3 Hz, $H^{5/2}$), 7.86 – 7.76 (2H, m, H^{4+3}), 7.42 – 7.32 (5H, m, $H^{11,12\&13}$), 6.12 (2H, s, H^9), 3.29 (3H, s, H^8).

^{13}C NMR (300 Hz, DMSO-d_6). δ: 178.4 (q, C^7), 141.0 (q, C^1), 132.8 (q, C^{10}), 129.5 (Ar-**C**H), 129.2 (q, C^6), 129.1 (Ar-**C**H), 128.5 (Ar-**C**H), 128.2 (Ar-**C**H), 127.0 (Ar-**C**H), 124.9 (Ar-**C**H), 117.1 (Ar-**C**H), 51.9 (**C**H_2, C^9), 17.4 (**C**H_3, C^8)

Crystal structure: 05glh002

Synthesis of 3-(2-Bromo-benzyl)-2-methyl-benzothiazolium bromide, **29**

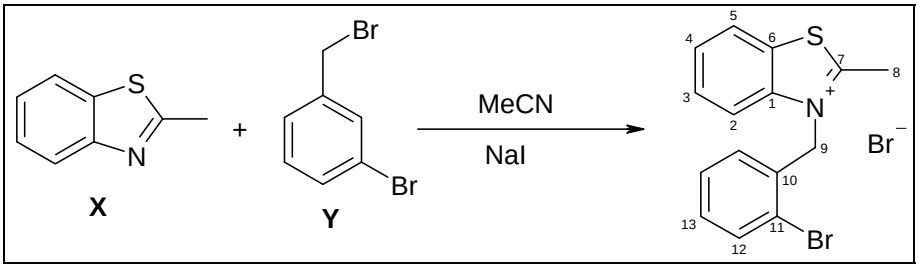

Reagent/solvent	**2-methylbenzothiazole, X**	**1-Bromo-2-bromomethyl-benzene Y**	MeCN
Mol	3.14 mmol	3.14 mmol	-
Mass/volume	0.4 mL, 0.47 g	0.79 g	7 mL

After 24 hours, an off-white solid (0.32 g, 26%) was isolated by filtration and washed with ether (50 ml). The solid was then crystallised from hot MeCN producing clear, colourless needles that turned opaque upon removal from solvent (0.186 g, Yield 15 %).

[Lab book reference code: 4205/87]

Characterisation (Novel compound):

MP: 204 °C

IR (ATR, υ/ cm^{-1}): 3330 (m), 3048 (m), 2999 (m), 2852 (w), 2365 (s), 2154 (w), 1998 (m), 1740 (w)

LRMS (ES^+, MeCN) *m/z*: 318 (100%), 319, 320 (100%), 321 & 322 $[M^+]\{Br^{79}:Br^{80}$ 1:1, S^{32}: S^{34} 0.95:0.04}

LRMS (ES^-, MeCN) *m/z*: 79 & 81 $[Br^-]\{Br^{79}:Br^{80}$ 1:1} (100%), 127 $[I^-]$ (75%)

HRMS (ES^+) calcd for $C_{15}H_{13}N_1S_1Br_1$ 317.9947, found 317.9943

^{1}H NMR (300Hz, DMSO-d_6) δ: 8.56-8.53 (1H, m, Ar-H), 7.99-7.96 (1H, m, Ar-H), 7.85-7.79 (3H, m, Ar-H), 7.37-7.30 (2H, m, Ar-H), 6.8 (1H, dd, J= 7.0, 1.7 Hz, Ar-H), 6.06 (2H, s, H^9), 3.21 (3H, s, H^8).

^{13}C NMR: Not sufficiently soluble.

Synthesis of 3-(4-Bromo-benzyl)-2-methyl-benzothiazolium bromide, **30**

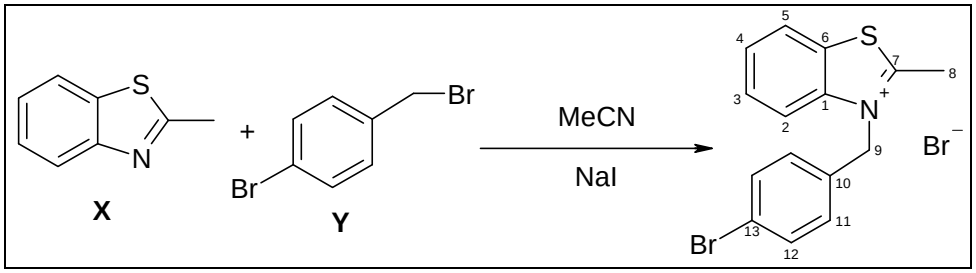

Reagent/solvent	**2-methylbenzothiazole, X**	**1-Bromo-4-bromomethyl-benzene, Y**	MeCN
Mol	23.5 mmol	23.6 mmol	-
Mass/volume	5.89 g	3 mL, 3.52 g	7 mL

After 24 hrs, a grey solid (5.92 g, 63%) was isolated by filtration and washed with ether (~80 ml). The solid was then crystallised from hot MeCN producing clear pale pink crystals that turned opaque upon removal from the solvent (5.71 g, Yield 61%). A small amount was recrystallised from MeOH resulting in crystals suitable for X-ray structural studies.

[Lab book reference code: 4205/89]

Characterisation (Novel Compound)

MP: 211-213 °C

IR (ATR, υ/ cm^{-1}): 3334 (m), 3052 (w), 2733 (w), 2370 (m), 1736 (w), 1642 (m), 1495 (s), 1332 (s), 1495 (m)

LRMS (ES^+, MeCN) *m/z*: 318 (100 %), 319, 320 (100 %), 322 & 321 $[M^+]\{Br^{79}:Br^{80}$ 1:1, S^{32}: S^{34} 0.95:0.04}

LRMS (ES^-, MeCN) *m/z*: 79 & 81 (100%) $[Br^-]\{Br^{79}:Br^{80}$ 1:1}

HRMS (ES^+) calcd for $C_{15}H_{13}Br_1N_1S_1$ 317.9947, found 317.9945 [M^+]

^{1}H NMR (300 HZ, DMSO-d_6). δ: 8.55 (1H, dd, J= 2.0, 7.3 Hz, $H^{5/2}$), 8.21 (1H, dd, J= 1.3, 9.0 Hz, $H^{5/2}$), 7.86 - 7.76 (2H, m, $H^{3\&4}$), 7.57 (2H, dd, J= 1.6, 8.4 Hz, $H^{11/12}$), 7.32 (2H, d, J= 8.4 Hz, $H^{11/12}$), 6.12 (2H, s, H^9), 3.29 (3H, s, H^8).

^{13}C NMR (300Hz, DMSO-d_2): δ: 178.6 (q, C^7), 140.9 (q, C^1), 132.2 (q, C^{10}), 131.9 (Ar-**C**H), 129.5 (Ar-**C**H), 129.4 (Ar-**C**H), 129.3 (q, C^6), 128.2 (Ar-**C**H), 124.9 (Ar-**C**H), 121.8 (q, C^{13}), 117.0 (Ar-**C**H), 51.33 (**C**H_2, C^9), 17.48 (**C**H_3, C^8)

Crystal structure: 07glh007

Preparation of 3-ethyl-5-fluoro-2-methyl-benzothiazolium iodide, **31**

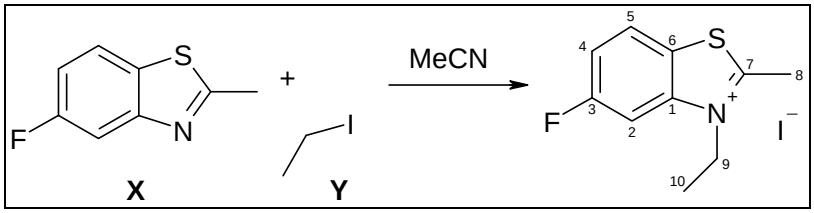

Reagent/solvent	**5-fluoro-2-methylbenzothiazole, X**	**Iodoethane, Y**	MeCN
Mol	7.5 mmol	11 mmol	-
Mass/volume	1 mL, 1.26 g	0.9 mL, 1.76 g	5 mL

No solid formed in RM. After 7 days cooled reaction to RT. Removed solvent in *vacuo* resulting in an off-white solid. This was washed with ether (~150 ml) resulting in a pure off-white solid (1.13 g. Yield of 47%). A small amount product crystallised from hot MeOH.

[Lab book reference code: 4981/08]

Characterisation (Known Compound)

MP: 200 °C (Lit[109]: 195 °C)

IR (ATR, υ/ cm^{-1}): 3062 (w), 3039 (w), 2992 (m), 2969 (m), 2930 (m), 2888 (w), 1589 (m), 1443 (s).

LRMS (ES^+, MeCN) *m/z*: 196(100%), 197, 198, 199 & 200 [M^+] {S^{32}: S^{34} 0.95:0.04}

HRMS (ES^+) calcd for $C_{10}H_{11}F_1N_1S_1$ 196.05962, found 196.0589 [M^+]

^{1}H NMR (300Hz, DMSO-d_6). δ: 8.52 (1H, d, J= 5.1, 9.1 Hz, H^5), 8.05 (1H, dd, J= 2.3, 9.5 Hz, H^2), 7.74 (1H, td, J= 2.3, 9.0 Hz, H^4), 4.74 (2H, q, J= 7.2 Hz, H^9), 3.23 (3 H, s, H^8), 1.44 (3H, t, J= 7.2 Hz, H^{10}).

^{13}C NMR (300Hz, DMSO-d_6) δ: 179.1 (q, C^7), 162.4 (q, d, J_{CF}= 981.0 Hz, C^3), 141.7 (q, d, J_{CF}= 50.1 Hz, C^1), 126.7 (Ar-**C**H, d, J_{CF}= 40.8 Hz, C^5), 125.2 (q, C^6), 116.8 (Ar-**C**H, d, J_{CF}= 99.9 Hz, $C^{2/4}$), 104.1 (Ar-**C**H, d, J_{CF}= 114.0 Hz,$C^{2/4}$), 45.1 (**C**H_2, C^9), 17.1 (**C**H_3, C^8), 13.1 (**C**H_3, C^{10}).

Preparation of 3-benzyl-5-fluoro-2-methyl-benzothiazolium bromide, **32**

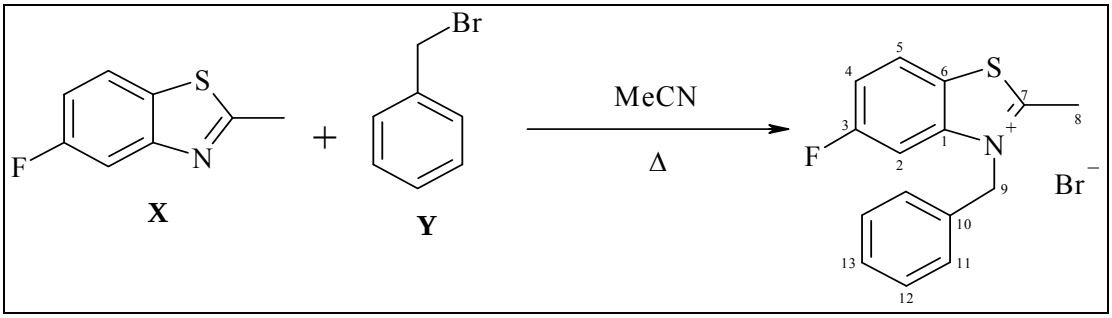

Reagent/solvent	**5-fluoro-2-methylbenzothiazole, X**	**Bromomethyl-benzene, Y**	MeCN
Mol	7.52 mmol	15.04 mmol	-
Mass/volume	1 mL, 1.2 g	1.7 mL, 2.57 g	5 mL

No solid formed in RM. After 7 days cooled reaction to RT. Removed solvent in *vacuo* resulting in an off-white solid. This was washed with ether (~150 mL) resulting in a pure sand-coloured crystalline solid (2.31 g. Yield of 91%). A small amount product recrystallised from hot MeOH.

[Lab book reference code: 4981/10]

Characterisation (Novel Compound)

MP: 189 °C

IR (ATR, υ/ cm^{-1}): 3028 (m), 2945 (m), 2605 (m), 1603 (m), 1588 (m), 1444 (s).

LRMS (ES^+, MeCN) *m/z*: 258 (100%), 259, 260, 261 & 262 [M^+] {S^{32}: S^{34} 0.95:0.04}

HRMS (ES^+) calcd for $C_{15}H_{13}F_1N_1S_1$ 258.07527, found 258.0742 [M^+]

^{1}H NMR (300Hz, DMSO-d_6). δ: 8.62 (1H, dd, J= 5.1, 9.0 Hz, H^5), 8.29 (1H, dd, J= 1.7, 9.3 Hz, H^2), 7.75 (1H, td, J= 1.9, 9.0 Hz, H^4), 7.40- 7.32 (5H, m, $H^{11\text{-}13}$), 6.10 (2H, s, H^9), 3.27 (3H, s, H^8).

^{13}C NMR (300Hz, DMSO-d_6) δ: 180.5 (q, C^7), 162.4 (q, d, J_{CF}= 981.9 Hz, C^3), 142.2 (q, d, J_{CF}= 50.7 Hz ,C^1), 132.5 (q, C^{10}), 129.1 (Ar-**C**H), 128.6 (Ar-CH), 127.1 (Ar-

CH, d, J_{CF}= 26.1 Hz ,C^5) 125.4 (q, C^6), 117.0 (Ar-**C**H, d, J_{CF}= 98.7 Hz, $C^{2/4}$), 104.3 (Ar- **C**H, d, J_{CF}= 114.3 Hz, $C^{2/4}$), 52.1 (**C**H_2, C^9), 17.7 (**C**H_3, C^8).

Preparation of 5-chloro-2-methyl-3-ethyl benzoxazolium iodide, **33**.

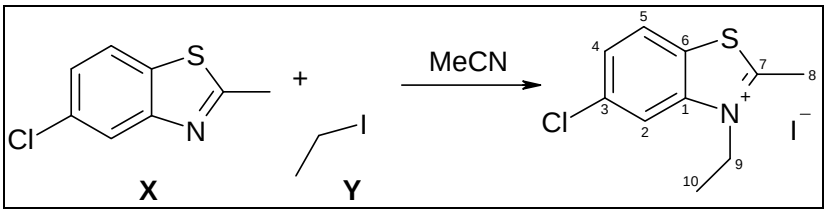

Reagent/solvent	**5-chloro-2-methylbenzothiazole, X**	**Iodoethane, Y**	**MeCN**
Mol	5.44 mmol	10.89 mmol	-
Mass/volume	1.00 g	0.87 mL, 1.70 g	10 ml

After 24 hrs, a pale green solid (0.27 g, 15%) was isolated by filtration and washed with ether (~80 ml). No further purification was required. A small amount was crystallised from MeOH in an attempt to result in crystals suitable for X-ray structural studies.

[Lab book reference code: 4409/50A]

Characterisation (Known Compound):

(Detailed searches resulted in no analytical data to be found)

MP: 219 °C

IR (ATR, υ cm^{-1}): 3039 (w), 2979 (w), 2937 (w), 2903 (w), 1567 (m), 1508 (m), 1441(s), 1423 (s).

LRMS (ES^+, MeCN) *m/z*: 212 (100%), 213, 214, 215 & 216 [M^+] {S^{32}: S^{34} 0.95:0.04, Cl^{35}:Cl^{37} 0.76:0.24}.

LRMS (ES^-, MeCN) *m/z*: 127 [I^-]

HRMS (ES^+) calcd for $C_{10}H_{11}Cl_1N_1S_1$ 212.03007, found 212.0293 [M^+]

^{1}H NMR (300Hz, D_2O). δ: 8.26 (1H, d, J= 1.6 Hz, H^2), 8.13 (1H, d, J= 8.8 Hz, H^5), 7.77 (1H, dd, J= 8.8, 1.73 Hz, H^4), 4.80 (2H, q, J= 7.4 Hz, H^9), 3.24 (2.6* H, s, H^8), 1.62 (3H, t, J= 7.37 Hz, H^{10}). (* Expect 3 H. Observe 2.6 H because proton readily lost)

^{13}C NMR (300Hz, DMSO-d_6) δ: 178.8 (q, C^7), 141.4 (q, C^1), 134.5 (q, C^3), 128.4 (Ar-**C**H), 128.1 (q, C^6), 126.2 (Ar-**C**H), 116.99 (Ar- **C**H), 45.0 (**C**H_2, C^9), 17.1 (**C**H_3, C^8), 13.2 (**C**H_3, C^{10}).

Preparation of 3-benzyl-5-chloro-2-methyl-benzothiazolium bromide, **34**.

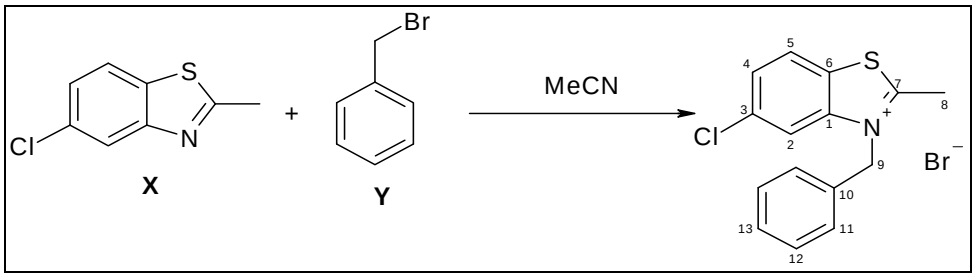

Reagent/solvent	**5-chloro-2-methylbenzothiazole X**	**Bromomethyl-benzene, Y**
Mol	4.4 mmol	2.9 mmol
Mass/volume	0.80 g	0.35 mL, 0.35 g

After 24 hrs, a pale green solid (0.32 g, 31%) was isolated by filtration and washed with ether (~80 ml). No further purification was required. A small amount was crystallised from MeCN resulting in large blocks suitable for X-ray structural studies. [Lab book reference code: 4632/09]

Characterisation (Known Compound)

(Detailed searches resulted in no analytical data to be found)

MP: 251-2 °C

IR(ATR, υ/ cm^{-1}): 3073 (w), 3047 (w), 3935 (m), 2873 (m), 1587 (m), 1569 (m), 1496 (m), 1438 (s).

LRMS (ES^+, MeCN) *m*/*z*: 274 (100%), 275, 276, 277 & 278 [M^+] {S^{32}: S^{34} 0.95:0.04, Cl^{35}:Cl^{37} 0.76:0.24}.

LRMS (ES^-, MeCN) *m*/*z*: 127 [I^-]

HRMS (ES^+) calcd for $C_{15}H_{13}Cl_1N_1S_1$ 274.04572, found 274.0452 [M^+]

^{1}H NMR (300Hz, DMSO-d_6). δ: 8.59 (1H, d, J= 8.8 Hz, H^5), 8.47 (1H, d, J= 1.6 Hz, H^2), 7.87 (1H, dd, J= 1.7, 8.8 Hz, H^4), 7.44 - 7.31 (5H, m, $H^{11\text{-}13}$), 6.12 (2 H, s, H^9), 3.26 (3H, s, H^8).

^{13}C NMR (300Hz, DMSO-d_6) δ: 180.3 (q, C^7), 141.9 (q, C^1), 134.5 (q, C^3), 132.6 (q, C^{10}), 129.1 (Ar-**C**H), 128.5 (Ar-**C**H), 128.5 (Ar-**C**H), 128.3 (q, C^6), 127.0 (Ar-**C**H), 126.5 (Ar-**C**H), 116.9 (Ar- **C**H), 52.0 (**C**H_2, C^9), 17.6 (**C**H_3, C^8).

Crystal structure: 07glh006

8.1.1.2 General procedure II for the Preparation of Benzothiazolium Salts

A mixture of 2-methylbenzothiazole (**X**) and **Y** was heated to 180 °C upon which a white solid formed. The reaction mixture was allowed cool to RT and acetone was added to the mixture. This was then filtered and washed with acetone and diethyl ether.

Preparation of 2,3-dimethyl-benzoxazolium Iodide, **35**.

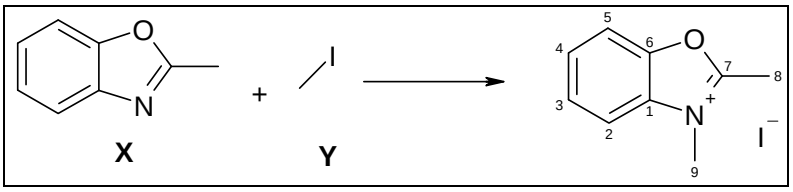

Reagent/solvent	**2-methylbenzoxazole, X**	**Iodomethane, Y**
Mol	16.8 mmol	8.4 mmol
Mass/volume	2 mL, 2.24 g	1 mL, 1.44 g

After 24 hrs, an off-white solid (1.16 g, 50%) was isolated by filtration and washed with ether (~80 ml). The solid was then crystallised from hot MeCN resulting in fine white needles (0.91 g, overall yield 39%).

[Lab book reference code: 4632/06].

Characterisation (Known compound)

MP: 187-9 °C (Lit[110]173 °C)

IR(ATR, υ/ cm^{-1}): 3085 (w), 3043 (w), 3020 (m), 2915 (w), 1739 (m), 1605 (m), 1476 (m), 1460 (s).

LRMS (ES^+, MeCN) *m*/*z*: 148 (64%), 148, & 149[M^+], 165 (100%), 166 & 167 [(M^+-H)+(NH_4)]$^+$.

HRMS (ES^+) calcd for $C_9H_{10}N_1O_1$ 148.07624, found 148.0754 [M^+]

LRMS (ES^-, MeCN) *m*/*z*: 127 [I^-] (100%).

^{1}H NMR (300Hz, D_2O). δ: 7.19- 7.14 (2H, m, Ar-**H**), 6.95 (1H, d, J= 7.5 Hz, Ar-**H**), 6.81 (1H, t, J= 7.5 Hz, Ar-**H**), 3.00 (3H, s, H^8), 1.67 (2.6 H, s, H^9).

^{13}C NMR (300Hz, DMSO-d_6) δ: 169.6 (q, C^7), 152.8 (q, C^1), 131.1 (q, C^6), 128.9 (Ar-**C**H), 128.8 (Ar-**C**H), 119.6(Ar- **C**H), 116.6 (Ar- **C**H), 35.2 (**C**H_3, C^9), 21.5 (**C**H_3, C^8).

Crystal structure: 07glh019

Synthesis of 2-methyl-3-phenethyl benzothiazolium bromide, **36**.

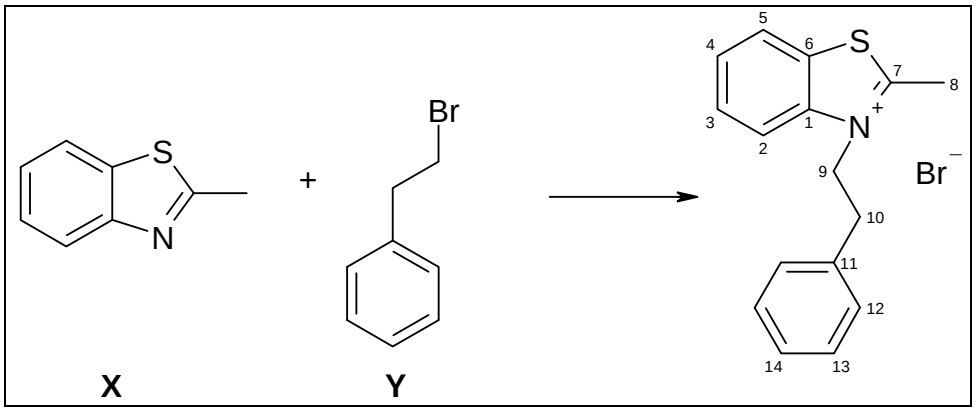

Reagent/solvent	**2-methylbenzothiazole, X**	**1-bromo-2-phenethane, Y**
Mol	16 mmol	16 mmol
Mass/volume	2 mL, 2.35 g	4.11 mL, 3 g

After 2 days, a pale brown solid (3.67 g, 69%) was isolated by filtration and washed with ether (150 ml). The solid was then crystallised from hot MeOH resulting in clear pale pink/brown crystals (3.26 g, yield 61%).

[Lab book reference code: 4409/07]

Characterisation (Known Compound):

MP: 196-197 °C (Lit: 200-201 °C[108])

IR (ATR, υ/ cm^{-1}): 3023 (w), 2917 (w), 2337 (w), 1585 (w), 1442 (m)

LRMS (ES^+, MeCN) *m*/*z*: 254 (100%), 255, 256 & 257 [M^+] {S^{32}: S^{34} 0.95:0.04}

LRMS (ES^-, MeCN) *m*/*z*: 79 & 81 (100%) [Br^-]{Br^{79}:Br^{80} 1:1}

HRMS (ES^+) calcd for $C_{16}H_{16}N_1S_1$ 254.0998, found 254.0994 [M^+]

^{1}H NMR (300Hz, DMSO-d_6). δ: 8.48 (1H, dd, J= 0.7, 7.7 Hz, $H^{5/2}$), 8.32 (1H, d, J= 7.9 Hz, $H^{5/2}$), 7.86 (1H, td, J= 7.3, 1.5 Hz, $H^{3/4}$), 7.79 (1H, td, J= 8.1, 1.3 Hz, $H^{3/4}$), 7.31 - 7.17 (5H, m, $H^{12,13\ \&\ 14}$), 5.00 (2H, t, J= 7.1 Hz, H^9), 3.23 (2H, t, J= 7.1 Hz, H^{10}), 2.93 (3H, s, H^8)

^{13}C NMR (300Hz, DMSO-d_6) δ: 177.3 (q, C^7), 140.6 (q, C^1), 136.5 (q, C^{11}), 129.4 (Ar-**C**H), 129.1 (Ar-**C**H), 128.9 (q, C^6), 128.6 (Ar-**C**H), 128.1 (Ar-**C**H), 127.2 (Ar-**C**H), 124.7 (Ar-**C**H), 117.0 (Ar-**C**H), 50.5 (**C**H_2, C^9), 33.40 (**C**H_2, C^{10}), 16.63 (**C**H_3, C^8).

Crystal structure: 05glh008

Synthesis of 2,2'-dimethyl-3,3'-hexanediyl-bis-benzothiazolium dibromide, **37**

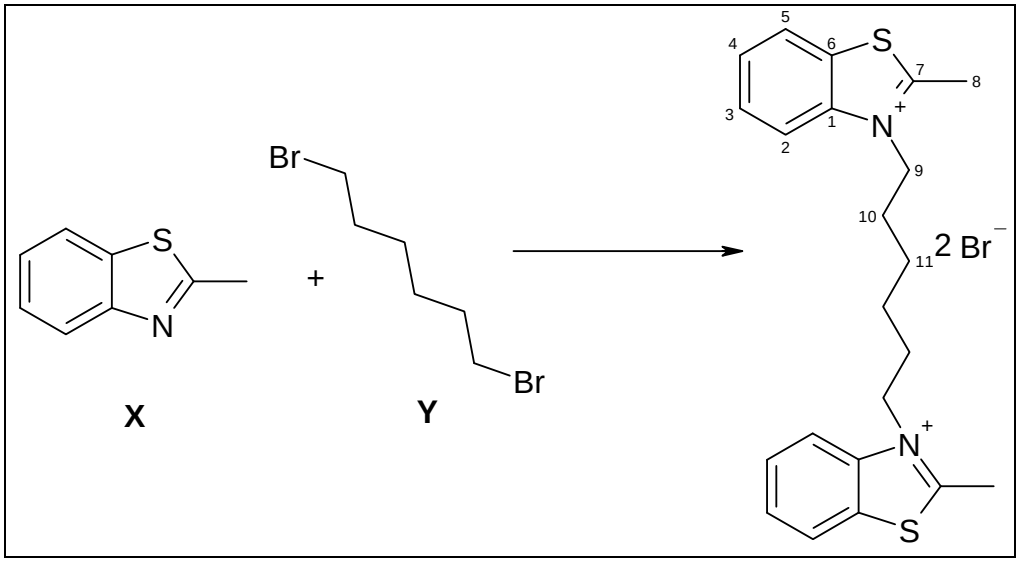

Reagent/solvent	**2-methylbenzothiazole, X**	**1,6-dibromo-hexane, Y**
Mol	7.8 mmol	1.9 mmol
Mass/volume	0.99 mL, 1.16 g	0.3 mL, 0.48 g

After 2 days, an off-white solid (1.34 g, 130%*) was isolated by filtration and washed with ether (100 ml). The solid was then crystallised from hot MeOH resulting in yellow/pink blocks (1.01 g. Yield 98%). [*Solvent could not be removed]

[Lab book reference code: 4409/01]

Characterisation (Known Compound):

(No data except combustion quoted in lit[111])

MP: > 270 °C

IR (ATR, υ/ cm^{-1}): 3542 (w), 3330 (w), 2942 (w), 2357 (m), 1994 (br), 1740 (w), 1634 (w), 1450 (m)

LRMS (ES^+, MeCN) *m/z*: 191 (100 %) & 192 [M^{2+}], 381 (20 %), 382, 383 & 384 [M^{2+}- H]$^+$ {S^{32}: S^{34} 0.95:0.04}

LRMS (ES^-, MeCN) *m/z*: 79 & 81 [Br^-]{Br^{79}:Br^{80} 1:1} (100%)

HRMS (ES) calcd 381.14591 for $C_{22}H_{26}N_2S_2$, found 381.1450 [M^{2+}-H], 191.0761 [M^{2+}]

^{1}H NMR (300Hz, D_2O) δ: 8.16 (2H, d, J= 7.9 Hz, $H^{5/2}$), 8.07 (2H, d, J= 8.6 Hz, $H^{5/2}$), 7.84 (2H, t, J= 7.3 Hz, $H^{3/4}$), 7.75 (2H, t, J= 7.9 Hz, $H^{3/4}$), 4.71 (4H, t, J= 7.3 Hz, H^9), 3.13 (6H, s, H^8), 2.01-1.91 (4H, m, $H^{10/11}$), 1.53-1.48 (4H, m, $H^{10/11}$)

^{13}C NMR (300Hz, D_2O) 175.8 (q, C^7), 141.0 (q, C^1), 129.7 (Ar-**C**H), 129.0 (q, C^6), 128.6 (Ar-**C**H), 123.9 (Ar-**C**H), 116.5 (Ar-**C**H), 49.5 (**C**H_2, C^9), 27.51 (**C**H_2, C^{10}), 25.57 (**C**H_2, C^{11}), 16.43 (**C**H_3, C^8).

Preparation of 2-methyl-3-(α-methylnaphthyl)benzothiazolium bromide, **38**.

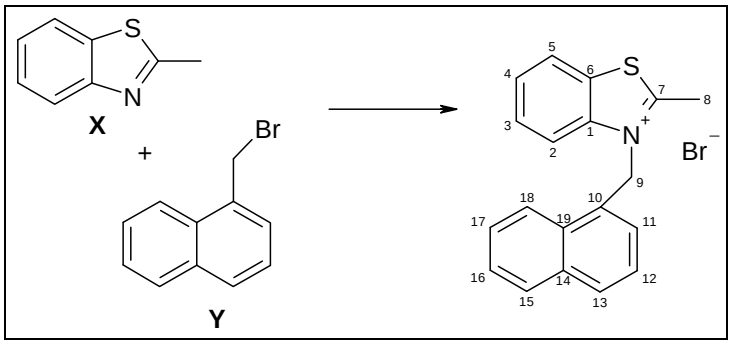

Reagent/solvent	**2-methylbenzothiazole, X**	**1-bromo-methylnaphthalene, Y**
Mol	3.6 mmol	7.24 mmol
Mass/volume	0.8 g	0.87 mL, 1.03 g

After 2 days, an off-white solid (1.34 g, 100%) was isolated by filtration and washed with ether (150 ml). The solid was then crystallised from hot EtOH resulting in pale lilac/brown crystals (1.04 g, yield 79%).

[Lab book reference code: 4409/54]

Characterisation (Novel Compound)

MP: 233 °C

IR (ATR, υ/ cm^{-1}): 3039 (w), 2960 (w), 2850 (w), 2752 (w), 1506 (m), 1429 (m).

LRMS (ES^+, MeCN) *m/z*: 290 (100%), 291, 292 & 293 [M^+] {S^{32}: S^{34} 0.95:0.04}

LRMS (ES^-, MeCN) *m/z*: 79 & 81 [Br^-]{Br^{79}:Br^{80} 1:1} (100%)

HRMS (ES^+) calcd for $C_{19}H_{16}N_1S_1$ 290.10034, found 290.0996 [M^+]

^{1}H NMR (300Hz, DMSO-d_6). δ: 8.59 (1H, dd, J= 1.7, 6.8 Hz, Np-**H**), 8.29 (1H, d, J= 8.4 Hz, $H^{2/5}$), 8.07- 8.03 (2H, m, Np-**H**), 7.94 (1H, d, J= 8.3 Hz, $H^{2/5}$), 7.85 - 7.74 (3H, m, Np-**H**), 7.69 (1H, td, J= 1.1, 8.1 Hz, Np-**H**), 7.33 (1H, t, J= 7.3 Hz, $H^{3/4}$), 26.63 (2H, s, H^9), 6.54 (1H, dd, J= 0.6, 7.1 Hz, $H^{3/4}$), 3.22 (3H, s, H^8).

^{13}C NMR (300Hz, DMSO-d_6) δ: 179.1 (q, C^7), 141.1 (q, C^1), 133.3 (q, C^{10}), 129.36 (Ar-**C**H), 129.6 (q, $C^{14/19}$), 129.3 (q, $C^{14/19}$), 128.7 (Ar-**C**H), 128.6 (Ar-**C**H), 128.3 (Ar-CH), 128.2 (q, C^6), 126.9 (Ar-**C**H), 126.7 (Ar- **C**H), 125.5 (Ar- **C**H), 124.9 (Ar-**C**H), 123.3 (Ar- **C**H), 121.7 (Ar-**C**H), 116.9 (Ar-**C**H), 50.1 (**C**H_2, C^9), 17.0 (**C**H_3, C^8).

8.1.1.3 General Preparation III dye for the Preparation of Benzothiazolium and Benzoselenazolium Salts

The heterocyclic amine, **X** and sultone, **Y** were dissolved in dry MeCN (dried over CaH_2) and heated to ~ 70 °C. The reaction was monitored by TLC. A white solid resulted after 24 – 36 hrs. The reaction was cooled to RT and the solid was isolated by vacuum filtration, washed with ice cold MeCN and ether. (Preparation adapted from Galin *et al.*[77])

Preparation of 2-methyl-3-(4-sulfopropyl)-benzothiazolium, **39**.

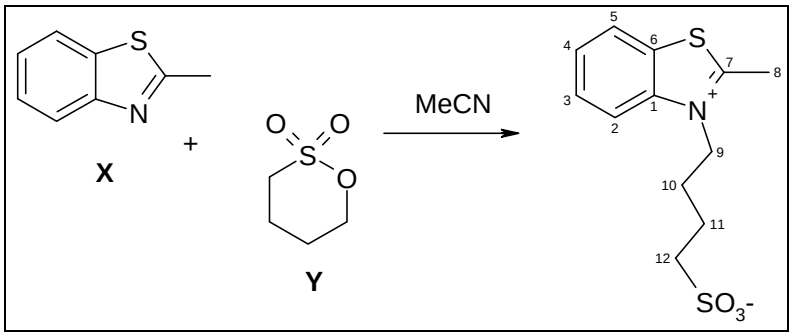

Reagent/solvent	**2-methylbenzothiazole, X**	**1,4-butane sultone, Y**	**MeCN**
Mol	14.1 mmol	11.7 mmol	-
Mass/volume	2.0 g, 1.7 ml	1.59 g, 1.2 mL	10 ml

After 24 hrs, a white solid (1.46 g, 44 % crude yield) was isolated from the reaction. A portion of this (1.42 g) was then crystallised from hot MeOH, resulting in clear, colourless block crystals (1.16 g, Crystallisation 82% efficient, overall yield 35%).

[Lab book reference code: 4409/94 & 4632/52]

Characterisation (Known Compound)

(Detailed searches resulted in no analytical data to be found)

MP: 282 - 83 °C

IR (ATR, υ/ cm^{-1}): 3077 (w), 2990 (w), 2956 (w), 2922 (w), 2973 (w), 1646 (m), 1578 (w) 1558 (w), 1541 (w), 1521 (m), 1507 (w) 1446 (m).

LRMS (ES^+, MeCN) *m/z*: 286 (100%), 287, 286 & 285 $[M+H]^+$ {S^{32}: S^{34} 0.95:0.04}

LRMS (ES^-, MeCN) *m/z*: 284(100%), 285, 286 & 287 $[M-H]^-$ {S^{32}: S^{34} 0.95:0.04}

^{1}H NMR (300Hz, D_2O) δ: 8.24 (2H, dd, J= 11.7, 8.4 Hz, $H^{5\&2}$), 7.96 (1H, td, J= 7.4, 1.0 Hz, $H^{3/4}$), 7.86 (1H, td, J= 7.4, 0.6 Hz, $H^{3/4}$), 4.84 (2H, t, J= 7.8 Hz, H^9), 3.25 (3 H, s, H^8), 3.05 (2H, t, J= 7.5 Hz, H^{12}), 2.21 (2H, qn, J= 7.3 Hz, $H^{10/11}$), 2.00 (2H, qn, J= 8.0 Hz, $H^{10/11}$).

^{13}C NMR (300Hz, D_2O) δ: 176.0 (q, C^7), 141.0 (q, C^1), 129.7 (Ar-**C**H), 129.0 (q, C^6), 128.5 (Ar-**C**H), 123.8 (Ar-**C**H), 116.5 (Ar-**C**H), 50.1 (**C**H_2, $C^{9/12}$), 49.1 (**C**H_2, $C^{9/12}$), 26.4 (**C**H_2, $C^{10/11}$), 21.5 (**C**H_2, $C^{10/11}$), 16.3 (**C**H_3, C^8).

Crystal structure 06glh010

Preparation of 2-methyl-3-(3-sulfopropyl)-benzothiazolium, **40**.

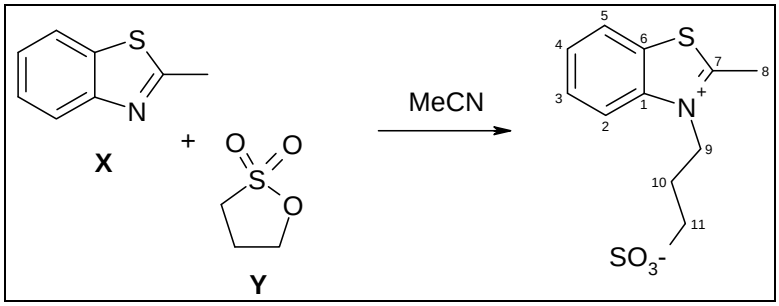

Reagent/solvent	**2-methylbenzothiazole X**	**1,3-propane sultone, Y**	**MeCN**
Mol	19 mmol	16 mmol	-
Mass/volume	2.73 g, 2.3 ml	1.4 mL, 2.0 g	10 ml

After 24 hrs, a white solid (2.29 g, 53 % yield) was isolated from the reaction. No need for further purification although a small portion of this was then crystallised from hot MeOH, resulting in an opaque, non-crystalline solid, unsuitable for X-ray structural studies.

[Lab book reference code: 4632/18, 4632/36, 4831/21]

Characterisation (Known Compound)

MP: 294-5 °C (Lit.: 283-84 °C[112])

IR (ATR, υ/ cm^{-1}): 3088 (w), 3009 (w), 2979 (w), 2937 (w), 2899 (w), 1521 (w), 1426 (w)

LRMS (ES^+, H_2O) *m/z*: 272 (100%) $[M+H]^+$, 294, 295, 296 & 297 $[M+Na]^+$ {S^{32}: S^{34} 0.95:0.04}

LRMS (ES^-, H_2O) *m/z*: 270, 271, 272 & 273 $[M-H]^-$ {S^{32}: S^{34} 0.95:0.04} (100%)

HRMS (ES^+) calcd for $C_{11}H_{13}N_1Na_1O_3S_2$ 294.02345, found 294.0229 $[M+Na]^+$

^{1}H NMR (300Hz, D_2O) δ: 8.23 (2H, t, J= 7.2 Hz, $H^{5\&2}$), 7.94 (1H, t, J= 7.4 Hz, $H^{3/4}$), 7.84 (1H, t, J= 7.7 Hz, $H^{3/4}$), 4.95 (2H, t, J= 8.1 Hz, H^9), 3.26 (3H, s, H^8), 3.19 (2H, t, J= 7.1 Hz, H^{11}), 2.45 (2H, qn, J= 7.2 Hz, H^{10}).

^{13}C NMR (300Hz, D_2O) δ: 176.4 (q, C^7), 140.9 (q, C^1), 129.9 (Ar-**C**H), 129.0 (q, C^6), 128.6 (Ar-**C**H), 123.8 (Ar-**C**H), 116.3 (Ar-**C**H), 47.8 (**C**H_2, $C^{9/11}$), 47.4 (**C**H_2, $C^{9/11}$), 23.2 (**C**H_2, C^{10}), 16.3 (**C**H_3, C^8).

Preparation of 5-chloro-2-methyl-3-(3-sulfopropyl)-benzothiazolium, **41**.

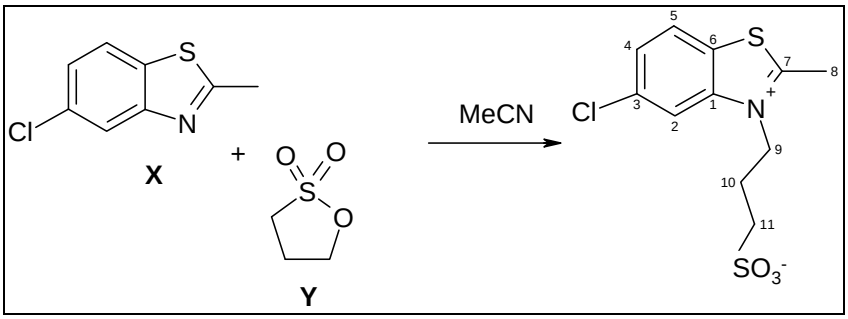

Reagent/solvent	**5-chloro-2-methylbenzothiazole X**	**1,3-propane sultone, Y**	**MeCN**
Mol	1.68 mmol	2.46 mmol	-
Mass/volume	0.31 g	0.3 g	4 ml

After 24 hrs, an off-white microcrystalline solid (0.13 g, 25% yield) was isolated from the reaction. No need for further purification.

[Lab book reference code: 4831/35]

Characterisation (Known Compound)

MP: 296 - 7 °C (Lit[113]: 291 °C)

IR(ATR, υ/ cm^{-1}): 3112 (w), 3072 (w), 3009 (w), 2972 (w), 2921 (w), 1641 (m), 1592 (w), 1571 (w), 1508 (w), 1475 (w), 1442 (m) 1424 (m).

LRMS (ES^+, H_2O) *m/z*: 328 (100%), 329, 330, 331, 332 & 333 $[M+Na]^+$ {S^{32}: S^{34} 0.95:0.04, Cl^{35}:Cl^{37} 0.76:0.24}

LRMS (ES^-, H_2O) *m/z*: 336(100%), 337, 338, 339 & 340 $[M+MeOH\ adduct]^-$ {S^{32}: S^{34} 0.95:0.04, Cl^{35}:Cl^{37} 0.76:0.24}

HRMS (ES^+) calcd for $C_{11}H_{13}N_1Cl_1O_3S_2Na_1$ 327.98448, found 327.9836 $[M+Na]^+$

^{1}H NMR (300Hz, D_2O) δ: 8.36 (1H, d, J= 1.7 Hz, H^2), 8.21 (1H, d, J= 8.8 Hz, H^5), 7.85 (1H, dd, J= 1.8, 8.8 Hz, H^4), 4.95- 4.89 (2H, m, H^9), 3.27 (3H, s, H^8), 3.19 (2H, t, J= 7.1 Hz, H^{11}), 2.50-2.40 (2H, m, H^{10}).

^{13}C NMR (300Hz, D_2O) δ: 178.2 (q, C^7), 141.8 (q, C^1), 136.0 (q, C^3), 129.2 (Ar-**C**H), 127.7 (q, C^6), 125.0 (Ar-**C**H), 116.5 (Ar-**C**H), 48.0 (**C**H_2, $C^{9/11}$), 47.4 (**C**H_2, $C^{9/11}$), 23.1 (**C**H_2, C^{10}). C^8 not seen.

Preparation of 2-methyl-3-(3-sulphopropyl)benzoselenazolium, **42**.

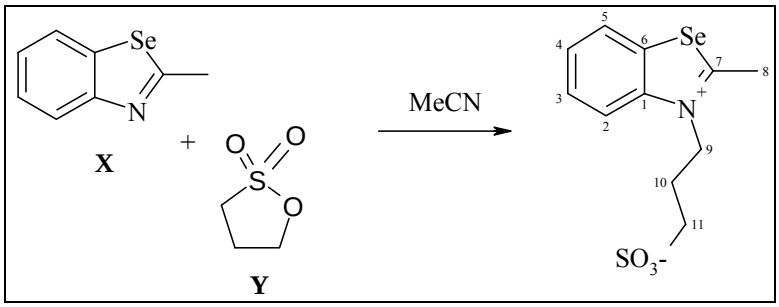

Reagent/solvent	**2-methylbenzoselenazole X**	**1,3-propane sultone, Y**	**MeCN**
Mol	2.75 mmol	3.68 mmol	-
Mass/volume	0.54 g	0.45 g	4 ml

After 24 hrs, an off-white microcrystalline solid (0.14 g, 16% yield) was isolated from the reaction. No need for further purification.

[Lab book reference code: 4831/41]

Characterisation (Known Compound)

(Detailed searches resulted in no analytical data to be found)

MP: 285-6 °C

IR(ATR, υ/ cm^{-1}): 3084 (w), 2989 (w), 2974 (w), 2937 (w), 2903 (w), 1521 (w)

LRMS (ES^+, H_2O) *m/z*: 338, 340, 342 (100%) & 344 $[M+Na]^+$ {S^{32}: S^{34} 0.95:0.04, Se^{74}:Se^{76}:Se^{77}:Se^{78}:Se^{80}:Se^{82} 0.87: 9.02: 7.58: 23.52: 49.82: 9.19}

LRMS (ES^-, H_2O) *m/z*: 312, 314, 316, 318(100%)& 320 $[M-H]^-$ {S^{32}: S^{34} 0.95:0.04, Se^{74}:Se^{76}:Se^{77}:Se^{78}:Se^{80}:Se^{82} 0.87: 9.02: 7.58: 23.52: 49.82: 9.19}

HRMS (ES^+) calcd for $C_{11}H_{13}N_1O_3S_1Se_1Na_1$ 341.9679, found 341.9670 $[M+Na]^+$

^{1}H NMR (300Hz, D_2O) δ: 8.27 (2H, t, J= 9.56 Hz, $H^{5\&2}$), 7.9 (1H, dt, J= 7.28, 1.19 Hz, $H^{3/4}$), 7.77 (1H, dt, J= 8.22, 0.98 Hz, $H^{3/4}$), 4.94-4.91 (2H, m, H^{9}), 3.26 (3H, S, H^{8}), 3.19, (2H, t, J= 7.03 Hz, H^{11}), 2.48- 2.38 (2H, m, H^{10}).
^{13}C NMR (300Hz, D_2O) δ: 141.9 (Q, C), 131.46 (Q, C), 129.24 (Ar-CH), 128.38 (Ar-CH), 126.54 (Ar-CH), 118.03 (Ar-CH), 48.78 (CH_2), 47.42 (CH_2), 22.99 (CH_2). C^{7} Does not show up.

8.2.2 General Preparation of Monomethine Dyes

To a solution of the activated methyl quaternary salt, **X**, in acetic acid, amyl nitrite was added. On addition of these reagents the solution turned brown getting progressively darker during the course of the reaction. This solution was left to reflux and was monitored using TLC. Once the reaction had gone to completion, the mixture was allowed to cool to room temperature and was added to water (~200ml) which resulted in an oily product which stuck to the glassware. The water was decanted off and ether was added resulting in a dark solid. If no solid formed, the oily product was triturated with ether. This solid was then isolated by vacuum filtration and then purified by crystallisation.

Preparation of 3,3'-diethyl benzothiacyanine triiodide/iodide, **3a/3f**.

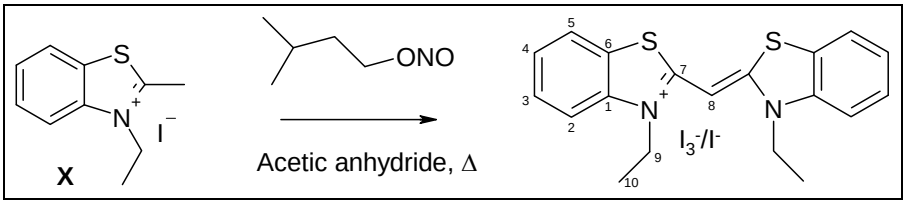

Reagent/solvent	3-ethyl-2-methyl-benzothiazolium iodide, X	Amyl nitrite	Acetic anhydride
Mol	3.3 mmol	3.3 mmol	-
Mass/volume	1 g	0.48 ml	10 mL

After 18 hrs, a purple solid (0.60g, 60% crude yield*) was isolated by filtration from the reaction. This was then crystallised from hot MeCN, resulting in dark purple needles (0.50 g, 51% yield*). [*Calculated assuming 50% triiodide and 50% iodide counterion occurrence].

[Lab book reference code: 4205/08]

Characterisation (Known Compound):

(Detailed searches resulted in no analytical data to be found of triiodide)

MP: 230-233 °C

IR (ATR, υ/ cm^{-1}) 3072 (m), 2984 (m), 2324 (w), 2465 (w), 1923 (w), 1463 (s)

LRMS (ES^+, MeCN) *m/z*: 339 (100 %), 340, 341, 340 [M^+]{S^{32}: S^{34} 0.95:0.04}

LRMS (ES^-, MeCN) *m/z:* 127 (100%) [I^-], 381 [I_3^-]

^{1}H NMR (300Hz, DMSO-d_6). δ: 8.2 (2H, dd, J= 1.1, 8.0 Hz, $H^{2/5}$), 7.88 (2H, d. J= 8.2 Hz, $H^{2/5}$), 7.67 (2H, td, J= 8.6, 1.3 Hz, $H^{3/4}$), 7.49 (2H, td, J= 8.1, 0.9 Hz, $H^{3/4}$), 6.72 (1H, s, H^8), 4.68 (4H, q, J= 7.0 Hz, H^9), 1.39 (6H, t, J= 7.0 Hz, H^{10}).

^{13}C NMR (300Hz, DMSO-d_6) δ: 161.4 (q, C^7), 139.7 (q, C^1), 128.6 (C^5), 125.0 (q, C^6), 125.0 (Ar-**C**H, C^3), 123.5 (Ar-**C**H, C^4), 113.6 (Ar-**C**H, C^2), 81.9 (**C**H, C^8), 41.6 (**C**H_2, C^9), 12.3 (**C**H_3, C^{10})

UV λ_{max}(MeOH): 423 nm (ε_{MeOH} : 66000 $M^{-1}cm^{-1}$)

Crystal structure 3f: 04jbo083

Preparation of 3,3'-diethyloxabenzocarbocyanine triiodide, **44a/44b**

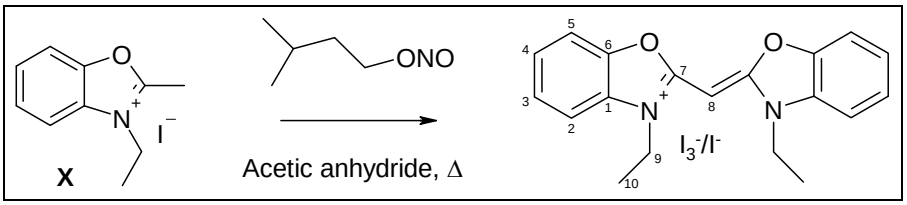

X

Reagent/solvent	3-ethyl-2-methyl-benzoxazolium iodide, X	Amyl nitrite	Acetic anhydride
Mol	3.46 mmol	3.46 mmol	-
Mass/volume	1.00 g	0.46 ml	~10 mL

After 18 hrs, a black solid (0.57 g, 59% crude yield*) was isolated by filtration from the reaction. This was then crystallised from hot MeCN, resulting in metallic-grey blocks (0.32 g, 33% yield*). [*Calculated assuming 50% triiodide and 50% iodide counterion occurrence].

[Lab book reference code: 4205/11]

Characterisation (Known Compound)

MP: 213-5 °C (Lit. >250 °C[58])

IR (ATR, υ/ cm^{-1}): 2975 (m), 2342 (w), 1752 (s), 1589 (m), 1478 (m)

LRMS (ES^+, MeCN) *m/z* 307.2 [M^+]

LRMS (ES^-, MeCN) *m/z* 127 [I^-], 381 [I_3^-]

^{1}H NMR (300Hz, DMSO-d_6). δ: 7.83 (2H, dd, J= 0.9, 7.3 Hz, $H^{2/5}$), 7.73 (2H, dd, J= 1.1, 8.1 Hz, $H^{2/5}$), 7.52 (2H, td, J= 7.7, 1.1 Hz, $H^{3/4}$), 7.45 (2H, td, J= 8.1, 1.5 Hz, $H^{3/4}$), 5.9 (1H, s, H^8), 4.41 (4H, q, J= 7.1, H^9), 1.40 (6H, t, J= 7.0 Hz, H^{10}).

^{13}C NMR (300Hz, DMSO-d_6) δ: 161.1 (q, C^7), 146.4 (q, C^6), 130.1 (q, C^1), 126.1 (Ar-**C**H), 125.0 (Ar-**C**H), 111.2 (Ar-**C**H), 111.1 (Ar-**C**H), 57.1 (**C**H_2, C^9), 12.6 (**C**H_3, C^{10}).

UV λ_{max} (MeCN) 374 nm (shoulder/peak 359 nm). Would not dissolve in MeOH therefore ε was not calculated.

Crystal structure 44b: 04jbo082

Preparation of 5,5'-chloro-3,3'-diethylbenzothiacyanine triiodide, **45a/45b**

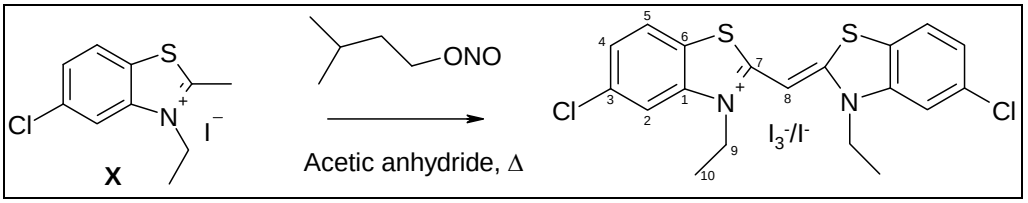

Reagent/solvent	5-chloro-3-ethyl-2-methyl-benzothiazolium iodide, X	Amyl nitrite	Acetic anhydride
Mol	1.27 mmol	1.4 mmol	-
Mass/volume	0.43 g	0.19 mL, 0.16 g	10 mL

After 24 hrs, a dark purple solid (0.17 g, 41% crude yield*) was isolated by filtration from the reaction. A portion of the crude solid (0.14 g) was then crystallised from hot MeCN, resulting in a mixture of dark purple needles and yellow needles (0.09 g, purification 66% efficient, overall yield 22%*). [*Calculated assuming 50% triiodide and 50% iodide counterion occurrence].

[Lab book reference code: 4981/06]

Characterisation (Known Compound):

(Detailed searches resulted in no analytical data to be found)

MP: 272 °C (melting point of triiodide dye, could not isolate iodide dye crystals)

IR (ATR, υ/ cm^{-1}) 3058 (w), 2990 (w), 2926 (w), 1507(s), 1456 (s)

LRMS (ES^+, MeCN) *m/z*: 407 (100%), 408, 409, 410, 411, 412 & 413 [M^+] {S^{32}: S^{34} 0.95:0.04, Cl^{35}:Cl^{37} 0.76:0.24}

LRMS (ES^-, MeCN) *m/z*: 127 (100%) [I^-]

HRMS (ES^+) calcd for $C_{19}H_{17}N_2S_2Cl_2$ 407.02102 found 407.0202 [M^+]

^{1}H NMR (300 Hz, DMSO-d_6). δ: 8.21 (2H, d, J= 8.6 Hz, H^5), 8.07 (2H, d, J= 1.6 Hz, H^2), 7.54 (2H, dd, J= 1.7, 8.5 Hz, H^4), 6.70 (1H, s, H^8), 4.66 (4H, q, J= 6.7 Hz, H^9), 1.36 (6H, t, J= 6.9 Hz, H^{10}).

^{13}C NMR (300Hz, DMSO-d_6) δ: 162.4 (q, C^7), 141.0 (q, C^1), 133.7 (q, C^3), 125.0 (Ar-**C**H), 124.0 (q, C^6), 113.7 (Ar-**C**H), 82.7 (**C**H, C^8), 41.8 (**C**H_2, C^9), 12.3 (**C**H_3, C^{10}).

UV λ_{max}(MeOH): 428 nm (ε_{MeOH} : 93000 $M^{-1}cm^{-1}$)

Crystal structure: Yellow needles (**45a**): 07glh010
Dark purple needles (**45b**): 07glh004

Preparation of 5,5'-fluoro-3,3'-diethylbenzothiacyanine triiodide/iodide, **46a/46b**

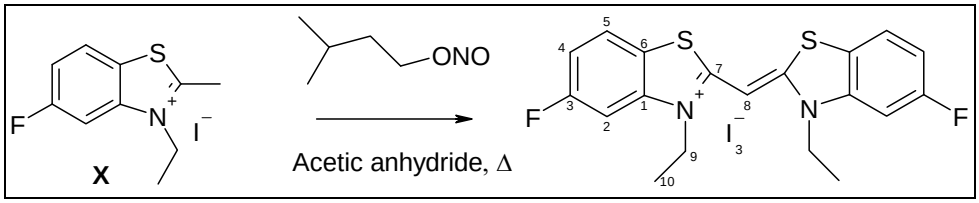

Reagent/solvent	3-ethyl-5-flouro-2-methyl-benzothiazolium iodide, X	Amyl nitrite	Acetic anhydride
Mol	0.93 mmol	1.11 mmol	-
Mass/volume	0.3 g	1.23 g, 0.15 mL	5 mL

After 24 hrs, a dark purple solid (0.16 g, 55% crude yield*) was isolated by filtration from the reaction. A portion of the crude solid (0.15 g) was then crystallised from hot MeCN, resulting in a mixture of large, dark grey blocks and small, yellow/green needles (0.14 g, purification 89 % efficient, overall yield 46%). [*Calculated assuming 50% triiodide and 50% iodide counterion occurrence].

[Lab book reference code: 4981/24]

Characterisation (**Novel Compound)**

MP: 298 °C

IR (ATR, υ/ cm^{-1}) 3077 (w), 3036 (w), 2983 (w), 2926 (w), 2877 (w), 1590 (m), 1514(s), 1476 (s), 1463 (m)

LRMS (ES^+, MeCN) *m/z*: 375 (100%), 376, 377, 378, & 379 [M^+] {S^{32}: S^{34} 0.95:0.04}

HRMS (ES^+) calcd for $C_{19}H_{17}F_1N_1S_1$ 375.08012, found 375.0791 [M^+]

^{1}H NMR (300 Hz, DMSO-d_6). δ: 8.26 (2 H, dd, J= 5.2, 8.6 Hz, H^5), 7.94 (2 H, dd, J= 2.1, 10.0, H^2), 7.41 (2H, td, J= 8.9, 2.1 Hz, H^4), 6.75 (1H, s, H^8), 4.66 (4 H, q, J= 6.8 Hz, H^9), 1.37 (6 H, t, J= 6.9 Hz, H^{10}).

^{13}C NMR (300Hz, DMSO-d_6) δ: 162.8 (q, C^7), 162.6 (q, d, J= 972 Hz, C^3), 141.2 (q, d, J= 48.9 Hz, C^1), 125.2 (Ar-**C**H, d, J= 40.2 Hz, C^5), 120.7 (q, C^6), 112.7 (Ar-**C**H, d, J= 97.8 Hz, $C^{2/4}$), 101.5 (Ar-**C**H, d, J= 116.4 Hz, $C^{2/4}$), 82.7 (**C**H, C^8), 41.5 (**C**H_2, C^9), 12.2 (**C**H_3, C^{10}).

UV λ_{max}(MeOH): 426 nm (ε_{MeOH} : 104000 $M^{-1}cm^{-1}$)

Crystal structures: Yellow needles(**46a**): 07glh008
Dark blocks (**46b**): 07glh011

8.2.3 Conversion of 3,3'-diethylbenzocyanine triiodide (45b) to 3,3'-diethylbenzocyanine iodide (45a)

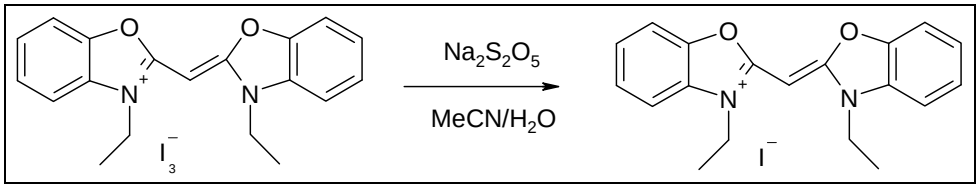

To a solution of the triiodide dye (0.024 g, 0.0356 mmol) in MeCN (~7 ml), the sodium metabisulfate (0.054 g, 0.284 mmol) was added. Drops of water were added until the salt had dissolved. As the reaction mixture was stirred at RT the brown colour disappeared. The RM was stirred for a further 10 mins. The solvent was removed in *vacuo*. The resulting off-white solid washed with H_2O (~30 mL) and crystallised from hot MeOH. Pale brown crystals resulted (0.013 g, 85 % yield). [Lab book reference code: 4831-87]

MP: > 300 °C (Lit[69]: 301 °C)

UV-Vis (MeOH): λ_{max} 362, 375.

Crystal structure 45a: 07pnh0005

8.2.4 General Procedure for Trimethine Dyes

A solution of activated methyl quaternary salt, **X**, in dry pyridine was heated to reflux under an atmosphere of N_2. After 5 mins an excess of triethyl orthoformate was added and refluxed overnight. The progress of the reaction was monitored by UV-vis and TLC, once the reaction had gone to completion the RM was cooled to RT. Ether was added to the solution which resulted in precipitation. This was then filtered and washed with ether until the filtrate ran colourless. The solid was purified by crystallisation. The reaction and products were shielded from light at all points possible.

Synthesis of 3,3'-diethylbenzothiadicarbocyanine iodide, **2a**

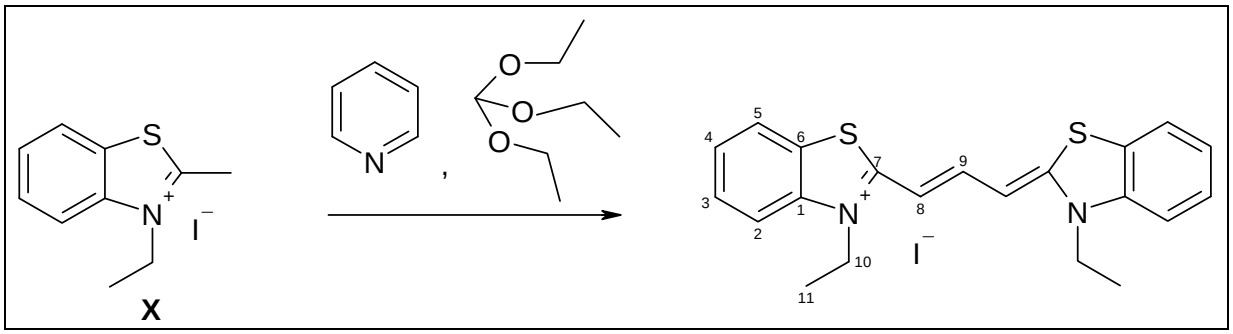

Reagent/solvent	**3-ethyl-2-methyl-benzothiazolium iodide, X**	**Triethyl orthoformate**	Pyridine
Mol	0.66 mmol	1.3 mmol	-
Mass/volume	0.2 g	0.21 mL, 0.19 g	5 mL

After 24 hrs, a dark purple/ brown solid (0.15 g, 94% crude yield) was isolated. The crude solid was then crystallised from hot MeCN, resulting in metallic grey blocks (0.14 g, yield 88%).

[Lab book reference code: 4205/58]

Characterisation (**Known Compound)**:

MP 282-4 °C (Lit[66]: 267 – 268 °C)

IR (ATR, υ/ cm^{-1}): 3330 (br), 2970 (w), 2365 (m), 1540 (s), 1458 (s)

LRMS (ES^+, MeCN) *m*/*z*: 365 (100 %), 366, 367 & 368 [M^+] {S^{32}: S^{34} 0.95:0.04}

LRMS (ES^-, MeCN) *m*/*z*: 127 (100%) [I^-]

^{1}H NMR (300Hz, DMSO-d_6). δ: 7.99 (2H, d, J= 7.5 Hz, $H^{5/2}$),7.79 (1H, t, J= 13.0 Hz, H^{11}), 7.76 (2H, d, J= 8.4 Hz, $H^{5/2}$), 7.57 (2H, td, J= 7.3, 1.1 Hz, $H^{3/4}$), 7.41 (2H, dt, J=

0.7, 7.3 Hz, $H^{4/3}$), 6.62 (2H, d, J= 12.6 Hz, H^{10}),4.38 (4H, q, J= 7.0 Hz, H^{9}), 1.35 (6H, t, J= 7.0 Hz, H^{8}).

^{13}C NMR (300 Hz, DMSO-d_6).δ: 164.2 (q, C^7), 146.6 (q, **C**^{1})*, 140.8 (q, C^6), 128.1 (Ar-**C**H), 125.2 (Ar-**C**H), 123.1 (Ar-**C**H), 113.3 (Ar-**C**H, C^2), 98.6 (**C**H, C^8), 41.4 (**C**H_2, **C**^{10}), 12.6 (**C**H_3, **C**^{11}). *C^9 missing- on another ^{13}C and DEPT spectrum the signal at ~46 ppm appears as a CH peak suggesting that C^9 and C^1 signals in the same place.

UV λ_{max} (MeOH) 556 nm (ε_{MeOH} : 126000 $M^{-1}cm^{-1}$)

Crystal structure: 06glh009

Preparation of 3,3'-diethyloxacarbocyanine iodide, **5a**.

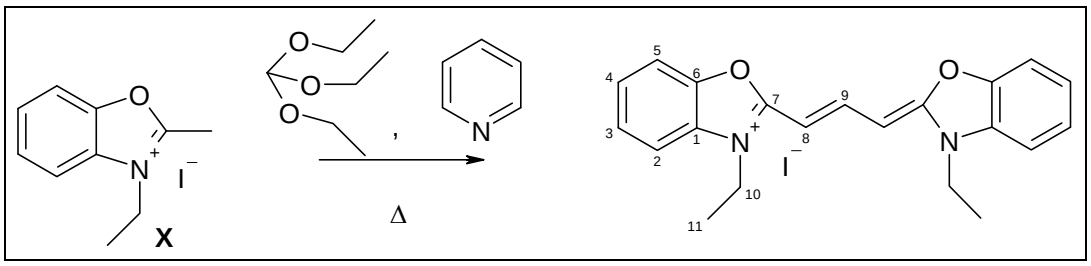

Reagent/solvent	3-ethyl-2-methyl-benzoxazolium iodide, X	Triethyl orthoformate	Pyridine
Mol	2.76 mmol	6.9 mmol	-
Mass/volume	0.8 g	1.1 mL, 0.98 g	10 mL

After 24 hrs, a purple crystalline solid (0.37 g, 58 % crude yield) was isolated by filtration from the reaction. The crude solid was then crystallised from hot MeCN, resulting in large metallic red/purple blocks (0.26 g, yield 42%).

[Lab book reference code: 4409/78]

Characterisation (Known Compound):

MP: 279-81 °C (Lit^{66}: 263 – 266 °)

IR (ATR, υ/ cm^{-1}): 3036 (w), 2990 (w), 2937 (w), 2869 (w), 1561 (s), 1506 (m), 1456 (m).

LRMS (ES^+, MeCN) *m/z*: 333 (100%), 334, 305 & 306 [M^+] {O^{16}:O^{18} 0.997:0.02}

LRMS (ES^-, MeCN) *m/z*: 127 (100%) [I^-]

HRMS (ES^+) calcd for $C_{21}H_{21}N_2O_2$ 333.16029, found 333.1595 [M^+]

^{1}H NMR (300Hz, MeOD-d_4). δ: 8.59 (1H, t, J= 13.3 Hz, H^9), 7.63 (2H, d, J= 8.2 Hz, $H^{5/2}$), 7.56 (2H, d, J= 7.5 Hz, $H^{5/2}$), 7.47 (2H, dt, J= 6.5, 1.1 Hz, $H^{3/4}$), 7.12 (2H, dt, J=

7.5, 1.4 Hz, $H^{3/4}$), 6.04 (2H, d, J= 13.3 Hz, H^{9}), 4.27 (4H, q, J= 7.3 Hz, H^{10}), 1.48 (6H, t, J= 7.2 Hz, H^{11}).

^{13}C NMR: No spectrum obtained because of solubility issues

UV λ_{max}(MeOH): 482 nm (ε_{MeOH} : 154000 $M^{-1}cm^{-1}$)

Crystal structure: 06glh004

Preparation of 3,3'-dimethyloxacarbocyanine iodide, **48**.

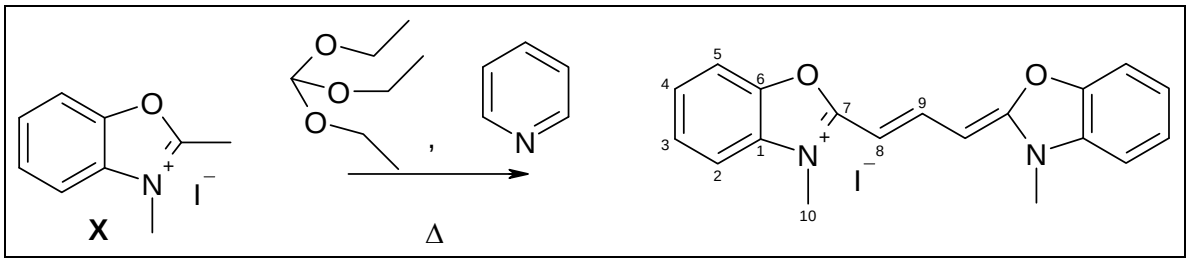

Reagent/solvent	2,3-dimethyl-benzoxazolium iodide, X	Triethyl orthoformate	Pyridine
Mol	1.1 mmol	2.7 mmol	-
Mass/volume	0.3 g	0.43 mL, 0.39 g	5 mL

After 1 hr, a purple/ red crystalline solid (0.28 g, 119 % crude yield*) was isolated. The crude solid was then crystallised from hot MeCN, resulting in small orange needles (0.16 g, yield 69%). [*could not remove solvent]

[Lab book reference code: 4632/07]

Characterisation (Known Compound)

MP: 281-2 °C (Lit.[114]: 275-277 °C)

IR (ATR, υ/ cm^{-1}): 3024 (w), 3005 (w), 2971 (w), 1560 (m), 1508 (m), 1478 (m), 1483 (m).

^{1}H NMR (300Hz, DMSO-d_6). δ: 8.27 (1H, t, J= 13.4 Hz, H^{9}), 7.75 (2H, d, J= 7.9 Hz, $H^{5/2}$), 7.65 (2H, d, J= 7.7 Hz, $H^{2/5}$), 7.46 (2H, t, J= 7.5 Hz, $H^{3/4}$), 7.39 (2H, t, J= 7.7 Hz, $H^{3/4}$), 6.01 (2H, d, J= 13.4 Hz, H^{8}), 3.73 (6H, s, H^{10}).

^{13}C NMR (300Hz, MeOD-d_4): δ 164.7 (q, C^{7}), 149.2 (**C**H, C^{9}), 148.7 (q, C^{1}), 133.8 (q, C^{6}), 127.7 (Ar-**C**H), 126.8 (Ar-**C**H), 112.4 (Ar-**C**H), 112.2 (Ar-**C**H), 86.4 (**C**H, C^{8}), 31.2 (**C**H_3, C^{10}).

LRMS (ES^+, MeCN) *m*/*z*: 305 (100%), 306, 307 & 308 [M^+] {O^{16}:O^{18} 0.997:0.02}

LRMS (ES^-, MeCN) *m*/*z*: 127 (100%) [I^-]

HRMS (ES^+) calcd for $C_{19}H_{17}O_2N_2$ 305.129, found 305.1280 [M^+]

UV λ_{max}(MeOH): 481 nm (ε_{MeOH} : 152000 $M^{-1}cm^{-1}$)

Synthesis of 3,3'-dibenzylbenzothiacarbocyanine bromide, **49**

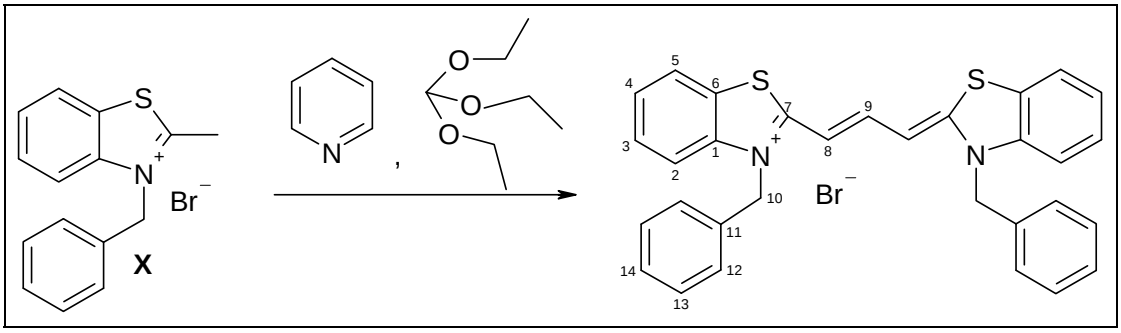

Reagent/solvent	**3-benzyl-2-methyl-benzothiazolium iodide, X**	**Triethyl orthoformate**	Pyridine
Mol	1.25 mmol	3.13 mmol	-
Mass/volume	0.4 g	0.5 mL, 0.45 g	5 mL

After 24 hrs, a dark brown solid (0.43 g, 120%* crude yield) was isolated. The crude solid was then crystallised from hot MeCN, resulting in metallic-green blocks (0.26 g, yield 74%). [*Could not removed all solvent from crude]

[Lab book reference code: 4205/85]

Characterisation (Known Compound):

MP 256 °C (Lit.[115]: 246 °C)

IR (ATR, υ/ cm^{-1}): 3027 (w), 2120 (Br), 1552 (s), 1461 (s)

LRMS (ES^+, MeCN) *m*/*z*: 489 (100%), 490, 491 & 492 [M^+] {S^{32}: S^{34} 0.95:0.04}

LRMS (ES^-, MeCN) *m*/*z*: 79& 81 (100%) [Br^-]{Br^{79}:Br^{80} 1:1}

HRMS (ES^+) calcd for $C_{31}H_{25}N_2S_2$ 489.1454 Da, found 489.1142 [M^+]

^{1}H NMR (300Hz, DMSO-d_6). 8.05 (2H, dd, J= 0.9, 7.9 Hz, $H^{5/2}$) 7.86 (1H, t, J= 12.6 Hz, H^9), 7.69 (2H, d, J= 8.2 Hz, $H^{5/2}$), 7.53 (2H, td, J= 7.1, 1.1 Hz, $H^{4/3}$), 7.43 (2H, td, J= 8.2, 0.7 Hz) 7.40-7.21 (6H, m, $H^{12,13\&14}$), 6.59 (2H, d, J= 13.2 Hz, H^8), 5.66 (4H, s, H^{10})

^{13}C NMR : Sample not soluble enough to produce concentrated solution: no spectrum even at extended scans

UV λ_{max} (MeOH) 560 nm (ε_{MeOH} : 168000 $M^{-1}cm^{-1}$)

Crystal structure: 05glh001

Synthesis of 3,3'-diphenethyl benzothiacarbocyanine bromide, **50**

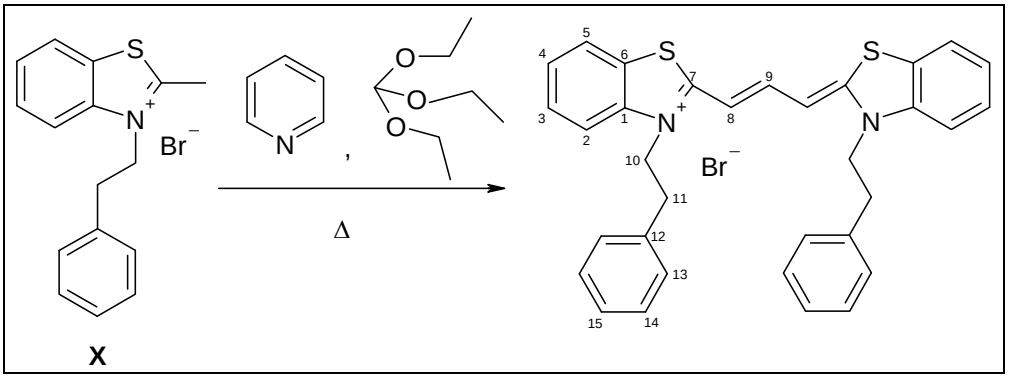

Reagent/solvent	**3-phenethyl-2-methyl-benzothiazolium iodide, X**	**Triethyl orthoformate**	Pyridine
Mol	2.99 mmol	5.99 mmol	-
Mass/volume	1 g	1 mL, 0.891 g	10 mL

After 24 hrs, a dark brown solid (1.24 g, 139%* crude yield) was isolated. The crude solid was then crystallised from hot MeCN resulting in metallic gold/green blocks (0.73 g, yield 82%). [*Could not remove all solvent from crude]

[Lab book reference code: 4409/08]

Characterisation (Known Compound):

(Detailed searches resulted in no analytical data to be found)

MP 130-132 °C

IR (ATR, υ/ cm^{-1}): 3367 (br), 3015 (w), 2353 (w), 1736 (w), 1536 (s), 1450 (m)

LRMS (ES^+, MeCN) *m/z*: 517 (100%), 518, 519 & 520 [M^+] {S^{32}: S^{34} 0.95:0.04}

LRMS (ES^-, MeCN) *m/z*: 79 & 81 [Br^-]{Br^{79}:Br^{80} 1:1} (100%)

HRMS (ES^+) calcd for $C_{33}H_{29}N_2S_2$ 517.1767, found 517.1766

^{1}H NMR (300Hz, DMSO-d_6). δ 7.95 (2H, d, J= 7.5 Hz, $H^{5/2}$) , 7.64 (1H, t, J= 12.6 Hz, H^9), 7.6 (2H, d, J= 8.1, $H^{5/2}$), 7.45 (2H, t, J= 7.3, $H^{3/4}$), 7.32 (2H, td, J= 8.2, 1.5 Hz, $H^{3/4}$), 7.26- 7.16 (10 H, m, $H^{13, 14 \& 15}$), 6.59 (2H, d, J= 12.5 Hz, H^8), 4.57 (4H, t, J= 7.1 Hz, H^{10}), 3.07 (4H, t, J= 7.1 Hz, H^{11})

^{13}C NMR (300 Hz, DMSO-d_6) δ 163.2 (q, C^7), 145.1 (**C**H, C^9), 139.8 (q, C^1), 135.8 (q, C^{12}), 128.0 (Ar-**C**H), 127.2 (Ar-**C**H), 126.7 (Ar-**C**H), 125.7 (Ar-**C**H), 123.8 (Ar-**C**H), 123.6 (q, C^6), 121.8 (Ar-**C**H), 112.4 (Ar-**C**H), 98.0 (**C**H_2, C^8), 46.1 (**C**H_2, C^{10}), 31.7 (**C**H_2, C^{11})

UV λ_{max} (MeOH) 561 nm (ε_{MeOH} : 140000 $M^{-1}cm^{-1}$)

Crystal Structure: 05glh007

Preparation of 3,3'-dinaphthylbenzothiacarbocyanine bromide, **51**

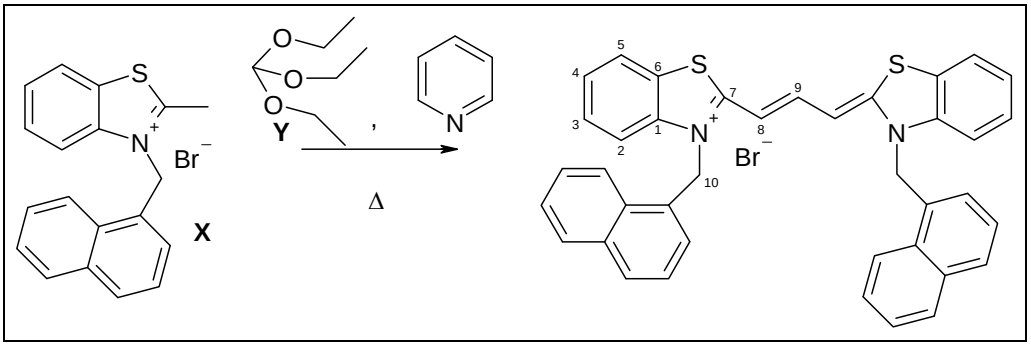

Reagent/solvent	**3-naphthyl-2-methyl-benzothiazolium iodide, X**	**Triethyl orthoformate**	Pyridine
Mol	0.5 mmol	1.4 mmol	-
Mass/volume	0.2 g	0.22 mL, 0.2 g	2 mL

After 1.5 hr a dark purple crystalline solid (0.16 g, 100%* crude yield) was isolated. The crude solid was then crystallised from hot EtOH resulting in metallic green blocks (0.12 g, overall yield 73%). [*Could not remove all solvent from crude]
[Lab book reference code: 4632/28]

Characterisation (Novel compound):

MP: 214 °C

IR (ATR, υ/ cm^{-1}): 3039 (w), 3002 (w), 2918 (w), 2877 (w), 1594 (m), 1556 (s), 1458 (m)

LRMS (ES^+, MeCN) *m/z*: 589 (100%), 590, 591, 592 & 593 [M^+] {S^{32}: S^{34} 0.95:0.04}

HRMS (ES^+) calcd for $C_{39}H_{29}N_2S_2$ 589.17721 found 589.1753 [M^+]

^{1}H NMR (400 Hz, DMSO-d_6). δ: 8.12 (2H, d, J= 8.0 Hz, $H^{2/3/4/5}$), 8.00 (2H, d, J= 8.0 Hz, $H^{2/3/4/5}$), 7.90 (2H, d, J= 7.7 Hz, $H^{2/3/4/5}$), 7.83 (1H, t, J= 12.8 Hz, H^9), 7.63 (2H, d, J= 8.2 Hz, $H^{2/3/4/5}$), 7.57 (4H, qn, J= 6.6 Hz, Np-**H**), 7.45- 7.34 (6H, m, Np-**H**), 7.26 (2H, t, J= 7.7 Hz, Np-**H**), 6.54 (2H, d, J= 7.0 Hz, Np-**H**), 6.34 (2H, d, J= 12.8 Hz, H^8), 6.00 (4H, s, H^{10}).

^{13}C NMR (400 Hz, DMSO-d_6). δ: 166.9 (q, C^7), 148.4 (CH, C^9), 142.6 (q, C^1), 134.6 (q, C^6), 131.2 (q, C^{15}), 129.9 (q, C^{20}), 129.8 (Ar-**C**H), 129.4 (Ar-**C**H), 129.3 (Ar-**C**H), 127.7 (Ar-**C**H), 127.6 (Ar-**C**H), 126.7 (Ar-**C**H), 126.5 (Ar-**C**H), 126.3 (q, C^{11}),

124.4 (Ar-**C**H), 124.3 (Ar-**C**H), 122.3 (Ar-**C**H), 114.7 (Ar-**C**H), 100.7 (CH, C^{8}), 49.0 (**C**H_2, C^{10}).

UV λ_{max} (MeOH) 561 nm ($\boldsymbol{\varepsilon_{MeOH}}$: 159000 $M^{-1}cm^{-1}$)

Crystal structure: 06glh011

Preparation of 3,3'-di(4-bromobenzyl)benzocarbocyanine bromide, **52**

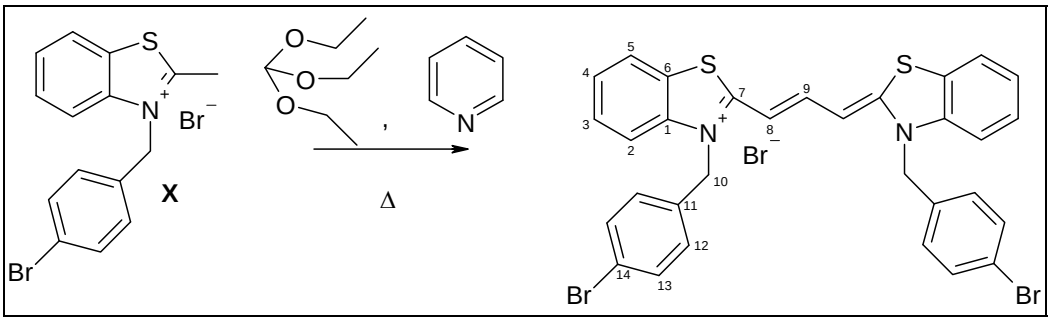

Reagent/solvent	**3-(4-bromo-benzyl)-2-methyl-benzothiazolium iodide, X**	**Triethyl orthoformate**	Pyridine
Mol	2.5 mmol	7.5 mmol	-
Mass/volume	1 g	1.25 mL, 1.11 g	10 mL

After 24 hrs, a metallic green crystalline solid (0.87 g, 95% crude yield) was isolated. The crude solid was then purified via slow extraction in MeCN (Soxhlet) resulting in large, metallic green blocks (0.68 g, yield 75%).

[Lab book reference code: 4409/63]

Characterisation (Novel Compound):

MP: 265-7 °C

IR (ATR, υ/ cm^{-1}): 3062 (w), 3028 (w), 2967 (w), 2896 (w), 1541 (s), 1458 (s)

LRMS (ES^{+}, MeCN) *m*/*z*: 645, 647 (100%), 648, 649, 650, 651 & 652 [M^{+}] {S^{32}: S^{34} 0.95:0.04, Br^{79}:Br^{81} 0.51:0.49}

HRMS (ES^{-}) calcd for $C_{31}H_{23}Br_2N_2S_2$ 644.96693, found 644.9652 [M^{+}]

^{1}H NMR (300Hz, DMSO-d_6). δ: 8.05 (2H, d, J= 7.8 Hz, $H^{5/2}$), 7.85 (1H, t, J= 12.7 Hz, H^{9}), 7.69 (2H, d, J= 8.0 Hz, $H^{2/5}$), 7.56 (4H, d, J= 8.4 Hz, H^{12}), 7.54 (2H, t, J= 7.8 Hz, $H^{3/4}$), 7.43 (2H, t, J= 7.6 Hz, $H^{3/4}$), 7.18 (4H, d, J= 8.3, H^{13}), 6.53 (2H, d, J= 12.6, H^{8}), 5.63 (4H, s, H^{10}).

^{13}C NMR (300Hz, DMSO-d_6), δ: 166.2 (q, C^{7}), 147.8 (**C**H, C^{9}), 141.5 (q, C^{1}), 133.2 (q, C^{6}), 132.4 (Ar-**C**H), 128.6 (Ar-**C**H), 126.0 (Ar-**C**H), 125.4 (q, C^{11}), 123.1 (Ar-

CH), 122.2 (q, C^{14}), 113.7 (**C**H, C^{2}), 99.6 (**C**H, C^{8}), 49.0 (**C**H_2, C^{10}). Ar-**C**H signal missing.

UV λ_{max} (MeOH) 561 nm ($\boldsymbol{\varepsilon_{MeOH}}$: 172000 $M^{-1}cm^{-1}$)

Crystal structure: 06glh002

Preparation of 5,5'-dichloro-3,3'-diethylbenzothiacarbocyanine Iodide, **53**.

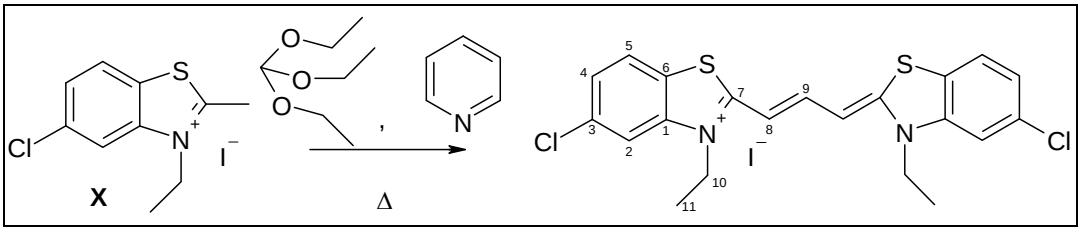

Reagent/solvent	**5-chloro-3-ethyl-2-methyl-benzothiazolium iodide, X**	**Triethyl orthoformate**	Pyridine
Mol	0.35 mmol	0.88 mmol	-
Mass/volume	0.12 g	0.15 mL, 0.13g	3 mL

After 24 hrs, a dark brown solid (0.07 g, 69% crude yield) was isolated. The crude solid was then purified via slow extraction in MeCN (Soxhlet) resulting in dark purple blocks (0.05 g, yield 54%).

[Lab book reference code: 4632/04]

Characterisation (Known Compound)

MP: >300 °C (Cf. Bromide counter ion Lit[116]: 289-291 °)

IR(ATR, υ/ cm^{-1}): 3073 (w), 3058 (w), 2971 (w), 2922 (w), 1542 (s), 1435 (m)

LRMS (ES^+, MeCN) *m/z*: 433 (100%), 436, 435, 437 & 438 [M^+] {S^{32}: S^{34} 0.95:0.04, Cl^{35}:Cl^{37} 0.76:0.24}

LRMS (ES^-, MeCN) *m/z*: 127 (100%) [I^-]

HRMS (ES^+) calcd for $C_{21}H_{19}N_2S_2Cl_2I$ 433.03667 found 433.0355 [M^+]

^{1}H NMR (400 Hz, DMSO-d_6). δ: 8.00 (2H, d, J= 8.5 Hz, H^5), 7.96 (2H, s, H^2), 7.78 (1H, t, J= 12.7 Hz, H^9), 7.46 (2H, d, J= 8.5 Hz, H^4), 6.64 (2 H, d, J= 12.6 Hz, H^8), 4.37 (4 H, q, J= 7.0 Hz, H^{10}), 1.32 (6 H, t, J= 6.9 Hz, H^{11}).

^{13}C NMR (400 Hz, DMSO-d_6) δ: 165.6 (q, C^7), 147.5 (CH, C^9), 142.4 (q, C^1), 133.6 (q, C^6), 125.5 (Ar-**C**H), 124.8 (Ar-**C**H), 124.6 (q, C^3), 113.8 (Ar-**C**H, C^2), 99.9 (**C**H, C^8), 42.1 (**C**H_2, C^{10}), 13.0 (**C**H_3, C^{11})

UV λ_{max} (MeOH) 561 nm (ε_{MeOH} : 188000 $M^{-1}cm^{-1}$)

Crystal structure: 06glh008

Preparation of 3,3'-dibenzyl-5,5'-dichlorobenzothiacarbocyanine bromide, **54**.

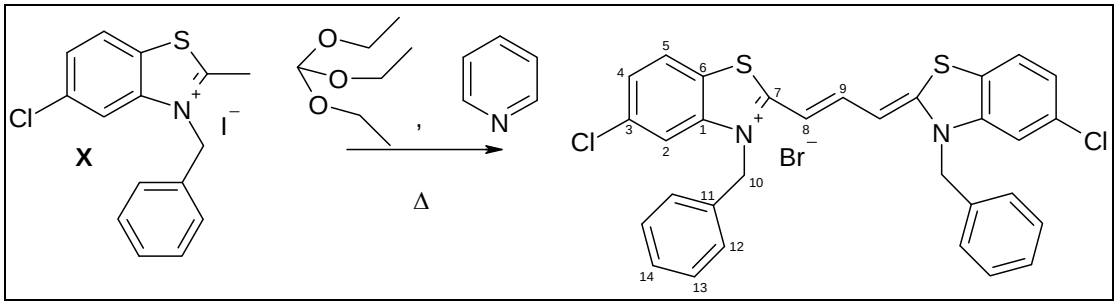

Reagent/solvent	**3-benzyl-5-chloro-2-methyl-benzothiazolium iodide, X**	**Triethyl orthoformate**	Pyridine
Mol	0.567 mmol	5.67 mmol	-
Mass/volume	0.2 g	0.94 mL, 0.84 g	7 mL

After 24 hrs, a dark purple solid (0.13 g, 73% crude yield) was isolated. A portion of the crude solid (0.11 g) was then crystallised from hot MeOH resulting in metallic green blocks (0.05 g, purification 46% efficient, overall yield 29%).

[Lab book reference code: 4831/97]

Characterisation (Known Compound)

MP: 271 °C (Lit[116]: 264-265 °)

IR(ATR, υ/ cm^{-1}): 3085 (w), 3024 (w), 3005 (w), 1541 (s), 1486 (m), 1432 (m)

LRMS (ES^+, MeCN) *m/z*: 557 (100%), 558, 559, 560 & 561 [M^+] {S^{32}: S^{34} 0.95:0.04, Cl^{35}:Cl^{37} 0.76:0.24}

HRMS (ES^+) calcd for $C_{31}H_{23}Cl_2N_2S_2$ 557.06796 found 557.0662 [M^+]

^{1}H NMR (400 Hz, DMSO-d_6). δ: 7.97 (2H, d, J= 8.5 Hz, H^5), 7.79 (2H, s, H^2), 7.75 (1H, t, J= 12.7 Hz, H^9), 7.40 (2H, dd, J= 1.6, 8.5 Hz, H^4), 7.4- 7.2 (6H, m, $H^{13\&14}$), 7.1 (4H, d, J= 7.3 Hz, H^{12}), 6.47 (2H, d, J= 12.6 Hz, H^8), 5.55 (4H, s, H^{10}).

^{13}C NMR (400Hz, DMSO-d_6): Sample not soluble enough to obtain spectrum. Extended scans (10 K) scans and mixed solvents attempted.

UV λ_{max} (MeOH) 566 nm (ε_{MeOH} : 166000 $M^{-1}cm^{-1}$)

Crystal structure: 07glh002

Preparation of 3,3'-diethyl-5,5'-fluoro benzothiacarbocyanine bromide, **55**.

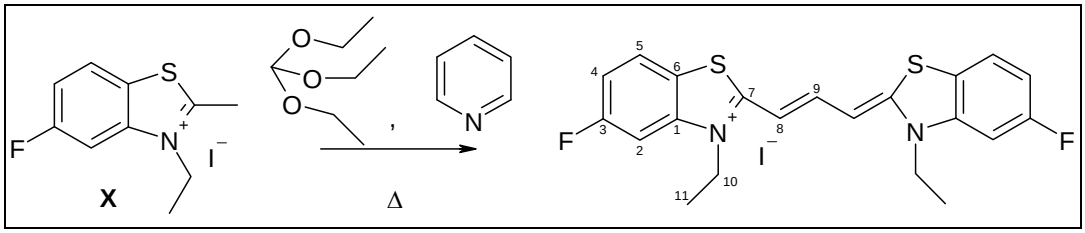

Reagent/solvent	**3-ethyl-5-fluoro-2-methyl-benzothiazolium iodide, X**	**Triethyl orthoformate**	Pyridine
Mol	0.929 mmol	4.6 mmol	-
Mass/volume	0.3 g	0.77 mL, 0.69 g	5 mL

After 12 hr a dark purple solid (0.33 g, 133%* crude yield) was isolated. The crude solid was then crystallised from hot EtOH resulting in metallic dark purple needles (0.15 g, overall yield 60%). [*Could not remove residual solvent from crude]
[Lab book reference code: 4981/22]

Characterisation (Known Compound)

MP: 298 °C (Lit[109] 288 – 289 °C)

IR (ATR, υ/ cm^{-1}): 3070 (w), 2994 (w), 1599 (w), 1553 (s), 1484 (m), 1442 (m).

LRMS (ES^+, MeCN) *m*/*z*: 401 (100%), 402, 403, 404 & 405 [M^+] {S^{32}: S^{34} 0.95:0.04}

LRMS (ES^-, MeCN) *m*/*z*: 127 (100%) [I^-]

HRMS (ES^+) calcd for $C_{21}H_{19}F_2N_2S_2$ 401.09577 found 401.0941 [M^+]

^{1}H NMR (400 Hz, DMSO-d_6). δ: 7.99 (2H, dd, J= 5.2, 8.7 Hz, H^5), 7.80 (1H, t, J= 12.8 Hz, H^9), 7.77 (2H, d, J= 8.1 Hz, H^2), 7.28 (2H, td, J= 8.9, 2.1 Hz, H^4), 6.62 (2H, d, J= 12.7 Hz, H^8), 4.35 (4H, q, J= 6.7 Hz, H^{10}), 1.33 (6H, t, J= 7.0 Hz, H^{11}).

^{13}C NMR (400 Hz, DMSO-d_6). δ: 163.8 (q, C^7), 160.4 (q, d, J_{C-F}= 986.4 Hz, C^3), 142.3 (q, d, J_{C-F}= 51.2 Hz,C^1), 124.6 (Ar-CH, d, J_{C-F}= 38.8 Hz, C^5), 120.9 (q, C^6), 112.8 (Ar-CH, d, J_{C-F}= 95.6 Hz, $C^{2/4}$), 101.4 (Ar-**C**H, d, J_{C-F}= 116.0 Hz, $C^{2/4}$), 99.4 (CH, C^8), 41.9 (**C**H_2, C^{10}), 12.5 (**C**H_3, C^{11}). C^9 Not shown up. Solubility issues even with mixed solvents (MeOH and DMSO).

UV λ_{max} (MeOH) 561 nm ($\boldsymbol{\varepsilon_{MeOH}}$: 177000 $M^{-1}cm^{-1}$)

Crystal structure: 07glh016

Preparation of 5,5'-Fluoro-3,3'-dibenzylbenzothiacarbocyanine bromide, **56**.

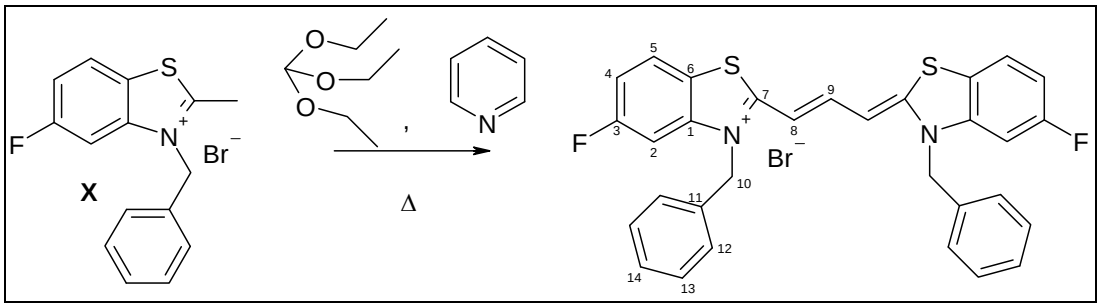

Reagent/solvent	**3-benzyl-5-fluoro-2-methyl-benzothiazolium iodide, X**	**Triethyl orthoformate**	Pyridine
Mol	1.89 mmol	9.47 mmol	-
Mass/volume	0.64 g	1.52 mL, 1.4 g	5 mL

After 12 hr a dark purple solid (0.72 g, 126%* crude yield) was isolated. A portion of the crude solid (0.69 g) was then crystallised from hot EtOH resulting in small, metallic-green blocks (0.28 g, purification 41% efficient, overall yield 49%). [*Could not remove residual solvent from crude]

[Lab book reference code: 4981/20]

Characterisation (Novel compound)

MP: 267-8 °C

IR (ATR, υ/ cm^{-1}): 3088 (w), 3017 (w), 2967 (w), 1541 (s), 1496 (m), 1460 (m)

LRMS (ES^+, MeCN) *m/z*: 525 (100%), 526, 527, 528 & 529 [M^+] {S^{32}: S^{34} 0.95:0.04}

HRMS (ES^+) calcd for $C_{31}H_{23}F_2N_2S_2$ 525.12706 found 525.1261 [M^+]

^{1}H NMR (400 Hz, DMSO-d_6). δ: 7.95 (2 H, dd, J= 5.1, 8.8 Hz, H^5), 7.85 (1H, t, J= 12.7 Hz, H^9), 7.58 (2H, d, J= 8.8 Hz, H^2), 7.37 – 7.18 (12 H, m, $H^{4, 12, 13 \& 14}$), 6.54 (2H, d, J= 12.7, H^8), 5.58 (4H, s, H^{10}).

^{13}C NMR (400 Hz, DMSO-d_6) δ: 167.5 (q, C^7), 162.8 (q, d, J_{C-F}= 975.2 Hz, C^3), 149.1* (Ar-CH), 147.6* (Ar-CH), 146.1 (Ar-CH, C^9), 143.1 (q, d, J_{C-F}= 47.6 Hz, C^1), 134.2 (q, C^{11}) 129.3 (Ar-**C**H, $C^{12/13}$), 129.0* (Ar-**C**H), 128.4 (Ar-**C**H, C^{14}), 126.7 (Ar-**C**H, $C^{12/13}$), 124.8 (Ar-**C**H, d, J_{C-F}= 38.4 Hz, C^5), 121.1 (q, C^6), 113.4 (Ar-CH, d, J_{C-F}= 98.4 Hz, $C^{2/4}$), 101.8 (Ar-CH, d, J_{C-F}= 114.4 Hz, $C^{2/4}$), 100.3 (Ar- **C**H, C^8), 49.5 (C^{10}). *solvent

UV λ_{max} (MeOH) 566 nm (ε_{MeOH} : 172000 $M^{-1}cm^{-1}$)

Crystal structure: 07glh009

Preparation of 3,3'- di(3-sulfobutyl)-benzothiacarbocyanine, **57**.

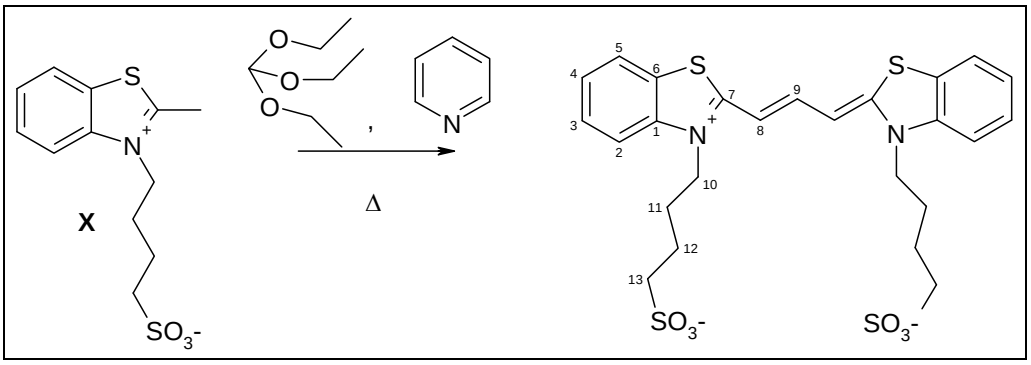

Reagent/solvent	**2-methyl-3-(3-sulfobutyl)-benzothiazolium, X**	**Triethyl orthoformate**	Pyridine
Mol	0.87 mmol	2.2 mmol	-
Mass/volume	0.25 g	0.37 mL, 0.33 g	mL

Precursor **X** was ground into a fine powder to increase solubility in pyridine. After 8.5 hrs a dark purple/brown solid (0.30 g, 120%* crude yield) was isolated. The crude product was purified by slow extraction in EtOH using Soxhlet apparatus resulting in metallic-green blocks (0.25 g, overall yield 98%). [*Could not remove residual solvent from crude]

[Lab book reference code: 4409/96]

Characterisation (Known Compound)

(Detailed searches resulted in no analytical data to be found)

MP: >300 °C

IR(ATR, v/ cm-1): 3063 (w), 2975 (w), 2945 (w), 2873 (w), 1548 (s), 1461 (m), 1410 (m).

LRMS (ES^-, H_2O) *m/z*: 579 (100%), 580, 581, 582 & 583 $[M^+]$ {S^{32}: S^{34} 0.95:0.04}

HRMS (ES^+) calcd for $C_{25}H_{27}N_2Na_2O_6S_4$ 625.05437, found 625.0527 $[M^-+2Na]^+$

^{1}H NMR (400 Hz, MeOD-d_4). δ: 6.25 (1H, t, J= 11.7 Hz, H^9), 6.22 (2H, d, J= 7.2 Hz, Ar-H), 6.00 – 5.94 (4H, m, Ar-H), 5.75 (2H, t(br)*, Ar-H), 2.73 (4H, s(br)*, $H^{10/13}$), 1.49 (4H, s(br)*, $H^{10/13}$), 0.5 (8H, s(br)*, $H^{11\ \&\ 12}$). * Broad signals probably because of aggregation within solution (At low concentrations MeOH would prevent aggregation but NMR sample concentration relatively high).

^{13}C NMR (400 Hz, MeOD-d_4) δ: 165.6 (q, C^7), 147.3 (Ar-CH, C^9), 144.7 (q, C^1), 141.7 (q, C^6), 128.6 (Ar-**C**H), 125.7 (Ar-**C**H) 123.0 (Ar-**C**H), 113.6 (Ar-**C**H), 99.1 (Ar-**C**H), 51.0 (**C**H_2, $C^{10/13}$), 46.6 (**C**H_2, $C^{10/13}$), 26.8 (**C**H_2, $C^{11/12}$), 22.5 (**C**H_2, $C^{11/12}$). Also EtOH peaks- solvent of crystallisation peaks.

UV λ_{max} (MeOH) 558 nm (ε_{MeOH} : 123000 $M^{-1}cm^{-1}$)

Crystal structure: 07glh003

Preparation of 3,3'-di(3-sulfopropyl)benzothiacarbocyanine, **58**.

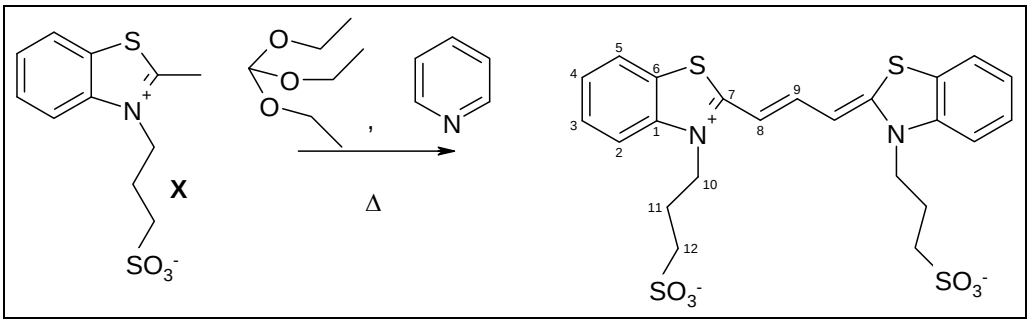

Reagent/solvent	**2-methyl-3-(3 -sulfopropyl)-benzothiazolium, X**	**Triethyl orthoformate**	Pyridine
Mol	1.47 mmol	3.69 mmol	-
Mass/volume	0.4 g	0.61 mL, 0.55 g	5 mL

Precursor **X** was ground into a fine powder to increase solubility in pyridine. After 2 hr a dark green/brown solid (0.46 g, 114%* crude yield) was isolated. The crude product was purified by slow extraction in EtOH using Soxhlet apparatus resulting in a dark purple microcrystalline product (0.25 g, overall yield 63%). [*Could not remove residual solvent from crude]

[Lab book reference code: 4632/22]

Characterisation (Known Compound)

(Detailed searches resulted in no analytical data to be found)

MP >300 °C

IR (ATR, υ/ cm^{-1}): 3081 (w), 3032 (w), 2949 (w), 1557 (s), 1460 (m)

LRMS (ES^-, H_2O) *m/z*: 551 (100%), 552, 553, 554 & 555 [M^+] {S^{32}: S^{34} 0.95:0.04}

HRMS (ES^+) calcd for $C_{23}H_{23}N_2O_6S_4Na_2$ 597.02343 found 597.0219 $[M^-+2Na]^+$

^{1}H NMR (400 Hz, D_2O). δ: 7.28 (2H, d, J= 7.3 Hz, Ar-H), 7.14 (1H, t, J= 12.7 Hz, H^{9}), 7.00- 6.93 (4H, m, Ar-H), 6.63 (2H, t, J= 7.1 Hz, Ar-H), 5.90 (2H, d, J= 12.7 Hz, H^{8}), 3.75 (4H, t (Br)*, H^{10}), 2.95 (4H, t, J= 7.2 Hz, H^{12}), 1.89 (4H, qn (Br)*, H^{11}). *No coupling constant attainable as broad signal probably because of aggregation within sample.

^{13}C NMR (400 Hz, D_2O): No carbon obtained. Solubility and aggregation issues.

UV λ_{max} (MeOH) 558 nm (ε_{MeOH} : 134000 $M^{-1}cm^{-1}$)

Synthesis of cyclic-bis(3,3'-dihexylthiacarbocyanine), **66**

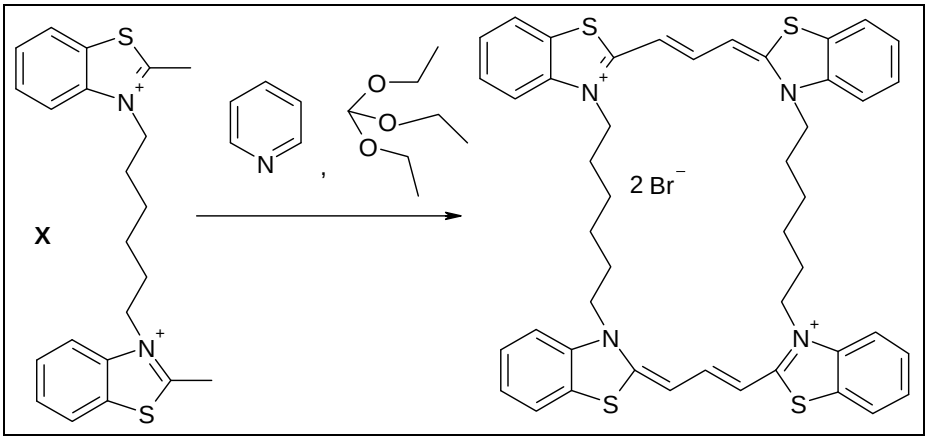

Reagent/solvent	**2,2'-dimethyl-3,3'-hexanediyl-bis-benzothiazolium dibromide, X**	**Triethyl orthoformate**	Pyridine
Mol	1.47 mmol	5.99 mmol	-
Mass/volume	0.8 g	0.95 mL, 0.84 g	20 mL

After 24 hrs a dark purple solid (1.57 g*) was isolated. The crude solid was purified by Soxhlet extraction using MeCN Resulting in purple powder (0.29 g, overall yield 21%). *A large amount of residual solvent

[Lab book reference code: 4409/04]

Characterisation (Novel compound)

Full Characterisation was not possible as product insoluble in a wide range of common solvents; purity therefore undetermined.

MP: >250 °C

SSNMR: Inconclusive

UV λ_{max} (H_2O): 522 nm, 548 nm

Preparation of 5,5'-dichloro-3,3'-di(3-sulphopropyl)benzothiacarbocyanine, **16**.

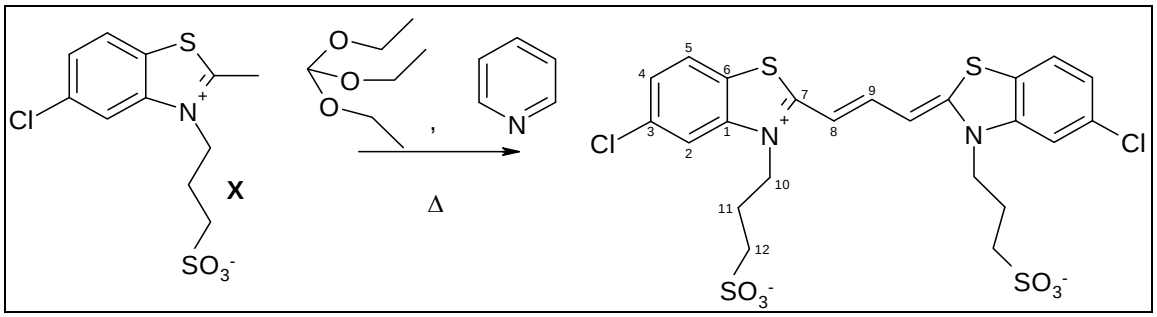

Reagent/solvent	**5-chloro-2-methyl-3-(3-sulfopropyl)-benzothiazolium, X**	**Triethyl orthoformate**	**Pyridine**
Mol	0.25 mmol	0.58 mmol	-
Mass/volume	0.08 g	0.1 mL, 0.09 g	~2 mL

Precursor **X** was ground into a fine powder to increase solubility in pyridine. After 24 hrs a dark brown solid (0.08 g, 100%* crude yield) was isolated. The crude product could not be purified as only soluble in water and MeOH where concentrated solutions resulted in aggregation and ultimately precipitation [*Mixture of product, starting material and residual solvent].

[Lab book reference code: 4831/43]

Characterisation (Known Compound)

(Detailed searches resulted in no analytical data to be found)

NMR and MS showed mixtures of starting material and product

Preparation of 3,3'-di(3-sulphopropyl)benzoselenacarbocyanine, **65**.

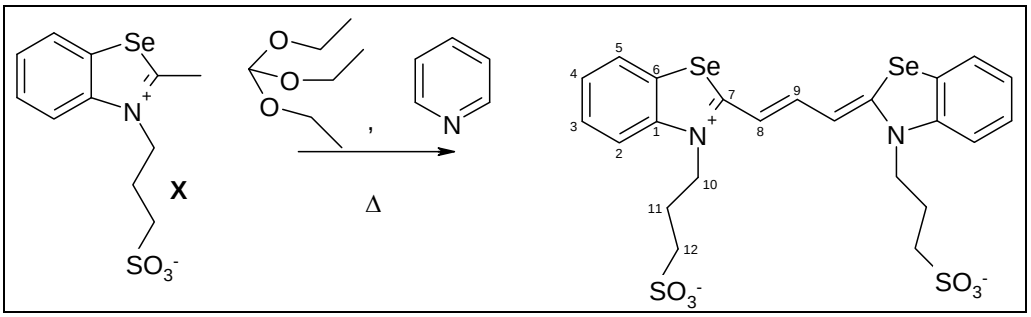

Reagent/solvent	**2-methyl-3-(3-sulfopropyl)-benzoselenazolium, X**	**Triethyl orthoformate**	Pyridine
Mol	0.23 mmol	0.58 mmol	-
Mass/volume	0.07 g	0.1 mL, 0.09 g	~2 mL

Precursor **X** was ground into a fine powder to increase solubility in pyridine. After 24 hrs a dark brown solid (0.08 g, 109%* crude yield) was isolated. The crude product could not be purified as only soluble in water and MeOH where concentrated solutions resulted in aggregation and ultimately precipitation [*Mixture of product, starting material and residual solvent]

[Lab book reference code: 4831/45]

Characterisation (Known Compound)

(Detailed searches resulted in no analytical data to be found)

NMR and MS showed mixtures of starting material and product

8.2.5 General Procedure for Meso-Substituted Trimethine Dyes

The activated methyl quaternary salt, **X**, was dissolved in dry pyridine, in the presence of molecular sieves, under an inert atmosphere and heated to reflux. After approx. 3 mins the orthoester, **Y**, was added. The reaction was monitored by TLC and UV-vis. After ~ 1 hour the reaction mixture was hot filtered to remove the molecular sieves and washed with copious amounts of EtOH and MeOH. The solvent was then removed in *vacuo* and the resulting solid washed with ether. The crude solid was then purified by crystallisation.

Preparation of 3,3'-di(3-sulfopropyl)-9-ethyl-benzothiacarbocyanine, **11**.

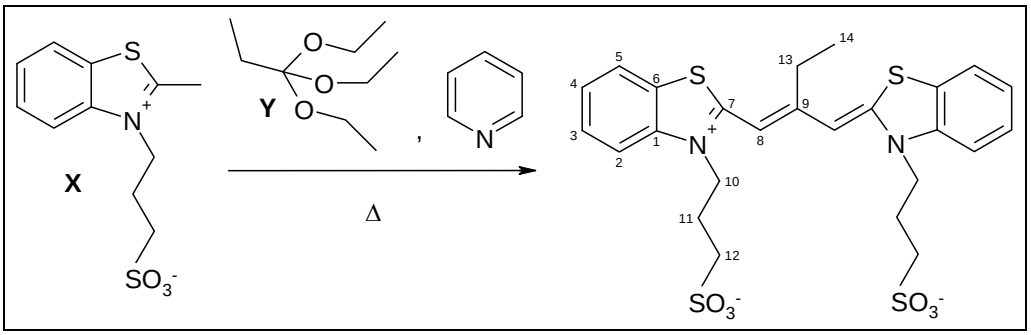

Reagent/solvent	**2-methyl-3-(3-sulfopropyl)-benzothiazolium, X**	**Triethyl orthoformate, Y**	**Pyridine**
Mol	1.85 mmol	9.23 mmol	-
Mass/volume	0.5 g	1.85 mL, 1.6 g	5 mL

The dye precursor was ground up into a fine powder to increase solubility. After 1 hr 15 mins a dark purple/brown solid (0.61 g, 114%* crude yield) was isolated. The crude product was crystallised from a dilute EtOH/toluene mixed solvent system taking only the first crop. This resulted in a dark purple microcrystalline solid (0.02 g, overall yield 4%). Any solid after the first crop tended to be majority starting material with a very small percentage of dye. [*Mixture of SM, product and residual solvent] [Lab book reference code: 4831/75]

Characterisation (Known Compound)

(Detailed searches resulted in no analytical data to be found)

MP: 252 °C

IR (ATR, υ/ cm^{-1}): 3070 (w), 3028 (w), 3009 (w), 2971 (w), 2926 (w), 1508 (s), 1458 (m).

LRMS (ES^-, H_2O) *m/z*: 579 (100%), 581& 582 [M^-] {S^{32}: S^{34} 0.95:0.04}

HRMS (ES^+) calcd for $C_{25}H_{27}N_2Na_2O_6S_4$ 625.05473, found 625.0529 $[M^-+2Na]^+$

^{1}H NMR (300Hz, MeOD-d_4). δ: 7.92 (2H, d, J= 7.9 Hz, $H^{5/2}$), 7.68 (2H, d, J= 8.3 Hz, $H^{5/2}$), 7.49 (2H, t, J= 7.4 Hz, $H^{3/4}$), 7.29 (2H, t, J= 7.6 Hz, $H^{3/4}$), 6.45 (2H, s, H^8), 4.54 (4H, t, J= 8.1 Hz, H^{10}), 2.99 (4H, t, J= 6.8 Hz, H^{12}), 2.90 (2H, q, J= 7.6 Hz, H^{13}), 2.32-2.22 (4H, m, H^{11}), 1.31 (3H, t, J= 7.4, H^{14})

^{13}C NMR. Not obtained because of limited amount of pure sample and solubility difficulties.

UV λ_{max} (MeOH) 548 nm (ε_{MeOH} : 90000 $M^{-1}cm^{-1}$)

Preparation of 3,3',9-triethylbenzocarbocyanine iodide, **59**.

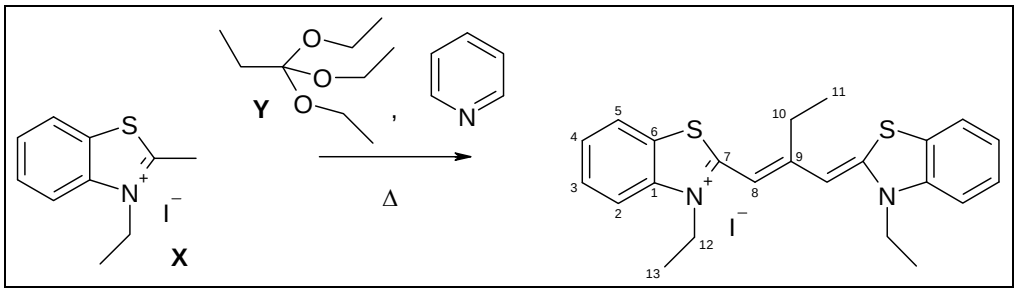

Reagent/solvent	**3-ethyl-2-methyl-benzothiazolium iodide, X**	**Triethyl orthopropinate, Y**	Pyridine
Mol	1.7 mmol	4.2 mmol	-
Mass/volume	0.52 g	0.85 mL, 0.75 g	6 mL

After 1 hr a dark purple solid (0.64 g, 145%* crude yield) was isolated. The crude product was crystallised from MeCN by slow evaporation process resulting in large metallic grey blocks (0.15 g, overall yield 35%). [*Could not remove residual solvent from crude]

[Lab book reference code: 4409/55]

Characterisation (Known Compound)

MP: 227-8 °C (Lit [71]: 236-237 °C)

IR (ATR, υ/ cm^{-1}): 2967 (w), 2922 (w), 2869 (w), 1500 (s), 1480 (s), 1456 (s).

^{1}H NMR (300Hz, MeOD-d_4). δ: 7.94 (2H, d, J= 8.0 Hz, $H^{5/2}$), 7.73 (2H, d, J= 8.3 Hz, $H^{5/2}$), 7.64 (2H, t, J= 7.3 Hz, $H^{3/4}$), 7.45 (2H, t, J= 7.3 Hz, $H^{3/4}$), 6.50 (2H, s, H^{8}), 4.55 (4H, q, J= 7.1 Hz, H^{12}), 3.05 (2H, q, J= 7.6 Hz, H^{10}), 1.53 (6H, t, J= 7.2 Hz, H^{13}), 1.43 (3H, t, J= 7.5 Hz, H^{11}).

^{13}C NMR: Not obtained; compound not soluble enough to obtain decent spectra.

LRMS (ES^+, MeCN) *m*/*z*: 393 (100%), 394, 395 & 396 [M^-] {S^{32}: S^{34} 0.95:0.04}

LRMS (ES^-, MeCN) *m*/*z*: 127 (100%) [I-].

HRMS (ES^+) calcd for $C_{23}H_{25}N_2S_4$ 393.14591, found 393.1453 [M^+]

UV λ_{max} (MeOH) 546 nm (ε_{MeOH} : 137000 $M^{-1}cm^{-1}$)

Crystal structure: 06glh001

8.2.6 Undesired Dyes as a Result of the Presence of Water

In an attempt to produce meso-substituted dyes, the following reactions were carried out. Instead of yielding the desired dye, the reaction resulted in the following cyanine dyes in small quantities using the following procedure:

General Procedure:

The dye precursor, **X**, was dissolved in dry pyridine under an inert atmosphere and heated to reflux. After ~ 3 mins the orthoester, **Y**, was added. The reaction was monitored by TLC and UV-vis. After ~ 1 hour the reaction was allowed to cool to RT and ether added to the RM, resulting in a precipitate. The resulting solid isolated by vacuum filtration and washed with ether until the filtrate ran colourless. The crude solid was then purified by crystallisation.

Preparation of 3,3'-diethylbenzothiacyanine iodide, **3a,** and 3,3'-diethyl-9-methylbenzothiacarbocyanine, **61**

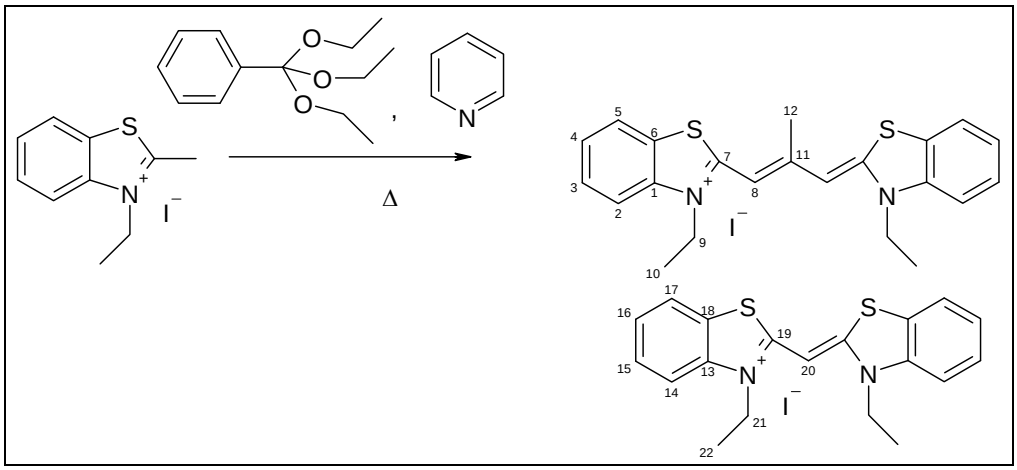

Reagent/solvent	**3-ethyl-2-methyl-benzothiazolium iodide, X**	**Triethyl orthobenzoate, Y**	**Pyridine**
Mol	3.28 mmol	8.2 mmol	-
Mass/volume	1 g	1.86 mL, 1.8 g	5 mL

After 2 hr a dark purple solid (0.99 g) was isolated. The crude product was crystallised from hot MeCN resulting in a mixture of large metallic purple needles and small yellow needles (0.24 g, 23% overall yield). The major product was trimethine, **61**, and the minor product was the monomethine, **3a** with a ratio of 1:0.3 respectively (identified by NMR). Dyes **3a** and **61** could not be separated by

chromatography or crystallisation resulting in any characterisation/analysis showing both products.

[Lab book reference code: 4205/05]

Characterisation (Known Compounds)

MP V: 205 °C

MP M: > 300 °C (Lit[68]: 312 °C)

LRMS (ES^+, MeCN) *m/z*: 339 [Dye **3a**$^+$], 379 [Dye **61**$^+$]

^{1}H NMR (300Hz, DMSO-d_6). δ: 8.22 (0.6 H,dd, J= 1.11, 7.9 Hz, $H^{14/17}$), 8.08 (2H, dd, J= 0.9, 7.9 Hz, $H^{5/2}$), 7.90 (0.6H, d, J= 8.2 Hz, $H^{14/17}$), 7.83 (2H, d, J= 8.0 Hz, $H^{5/2}$), 7.69 (0.6H, dt, J= 1.3, 7.3 Hz, $H^{15/16}$), 7.63 (2H, dt, J= 1.3, 7.5 Hz, $H^{4/3}$), 7.51 (0.6H, dt, J= 1.1, 7.3 Hz, $H^{15/16}$), 7.44(2H, dt, J= 0.9, 8.0 Hz, $H^{4/3}$), 6.74(0.3H, s, H^{20}), 6.6 (2H, s, H^8), 4.69 (1.2H, q, J= 6.9 Hz, H^{21}), 4.52 (4H, q, 7.3 Hz, H^9), 2.62 (3H, s, H^{12}), 1.41 (7.8H, t, J=7.13, $H^{22\&10}$).

Crystal structure of 61: 05jbo006

Crystal Structures of 3a: 05jbo001 and 05glh006 (polymorphs). Molecules crystallised from same solvent, only variable rate of evaporation.

Preparation of 3,3'-dibenzyl-benzothiacyanine, **47**

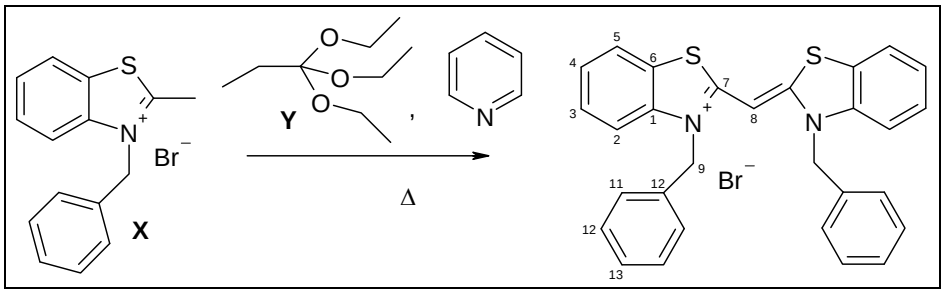

Small amount of dark brown residue resulted. This was crystallised from hot MeCN resulting in dark brown blocks (0.002 g). Because very few crystals were isolated there is only limited characterisation. Remaining crude product could not be characterised.

[Lab book reference code: 4409/37]

Characterisation (Novel Compound)

MP: 265-7 °C

Crystal Structure: 05glh010

Preparation of 3,3'-diethyl benzoselenacyanine iodide, **64a**

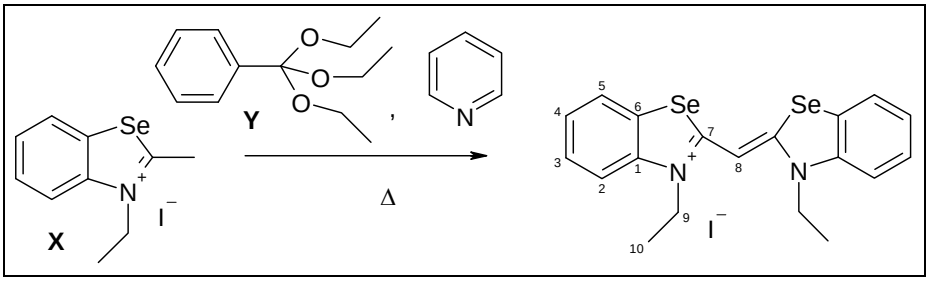

Small amount of dark brown crystalline solid resulted (0.027 g). This was crystallised from hot MeCN resulting in small lime-green needles (0.004 g). Because very few crystals were isolated there is only limited characterisation. Remaining crude product could not be characterised.

[Lab book reference code: 4205/53]

Characterisation (Known Compound)

MP: 299 °C (Lit.: 273 °C[70])

IR (ATR, υ/ cm^{-1}) 3077 (w), 3047 (w), 3020 (w), 2964 (w), 2865 (w), 1584 (m), 1504 (s), 1459 (s)

LRMS (ES^+, MeCN) *m*/*z*: 425, 426, 427, 428, 429, 430, 431 (51 %), 432, 433 (89 %), 434, 435 (100%), 436, 437, 438, 439 & 440 [M^+] {Se^{74}: Se^{76}: Se^{77}: Se^{78}: Se^{80}: Se^{82} 0.01: 0.09: 0.08: 0.24: 0.50: 0.09}

LRMS (ES^-, MeCN) *m*/*z*: 127 (100%) [I-]

UV λ_{max}(MeOH): 430 nm (ε_{MeOH} : 73000 $M^{-1}cm^{-1}$)

Crystal structure: 2007pnh0003

8.2.7 General Procedure for Pentamethine Dyes

In the presence of molecular sieves, activated methyl quaternary salt, **X**, and dry pyridine (dried over CaH_2) were heated to reflux, at which point and 1,1,3,3-tetramethoxypropane was added. The reaction mixture continued to be heated for 30-45 mins whilst being monitored by UV-Vis. At the point when the λmax ceases to increase compared to other absorbances (λmax at ~650 nm for oxadicarbocyanine and ~750 nm for thiadicarbocyanines) the reaction was removed from the heat and the reaction mixture hot filtered to remove the molecular sieves and washed with copious

amounts of EtOH, DCM and MeOH. The solvent was then removed in *vacuo* and the resulting solid washed with copious amounts of ether (until the ether ran colourless). The crude solid was isolated and in all cases purification was attempted but starting material was found in all cases. The reaction conditions are described below but no characterisation has been shown because at the detection limits of the common techniques, starting material was the only the species to shown. UV-vis was the only method to readily detect up the dyes.

Preparation of 3,3'-diethylbenzothiadicarbocyanine iodide, **4**.

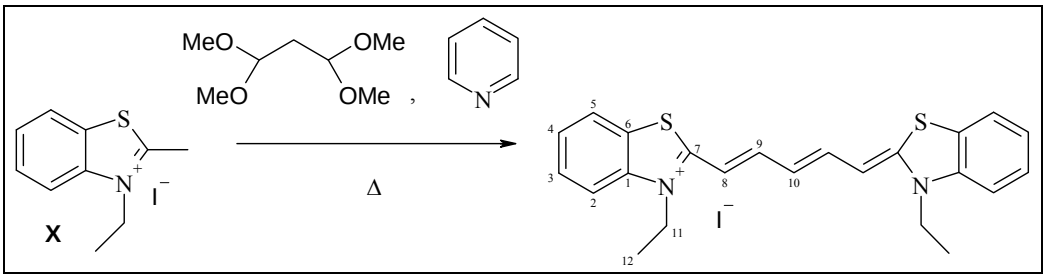

Reagent/solvent	**3-ethyl-2-methyl-benzothiazolium iodide, X**	**1,1,3,3-tetramethoxypopane**	**Pyridine**
Mol	1.05 mmol	2.6 mmol	-
Mass/volume	0.32 g	0.43 mL, 0.43g	6 mL

After 1.25 hrs a dark yellow/green crystalline solid (0.26 g, 94% crude yield) was isolated. The crude solid was then crystallised from hot EtOH, resulting in a mixture of metallic green needles and starting material(0.01 g, approx. yield 5%).

[Lab book reference code: 4409/67]

UV λ_{max} (MeOH) 650 nm

Preparation of 3,3'-diethylbenzoxadicarbocyanine iodide, **67**

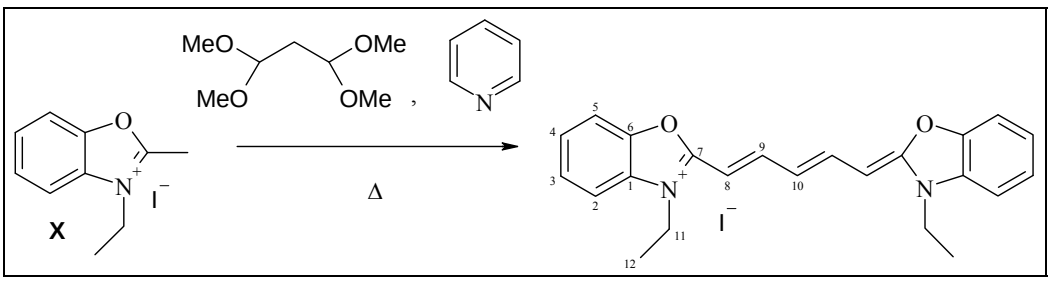

Reagent/solvent	3-ethyl-2-methyl-benzoxazolium iodide, X	1,1,3,3-tetramethoxypopane	Pyridine
Mol	4 mmol	8 mmol	-
Mass/volume	0.6 g	1.3 mL, 1.31 g	5 mL

After 0.5 hrs a purple/red oily residue was isolated. The crude product was then crystallised from hot EtOH, resulting in a mixture of large, red/purple block and starting material(0.06 g, approx. yield 6%).

[Lab book reference code: 4409/90]

UV λ_{max} (MeOH) 584 nm

Preparation of 3,3'-dibenzylbenzothiadicarbocyanine iodide, **68**.

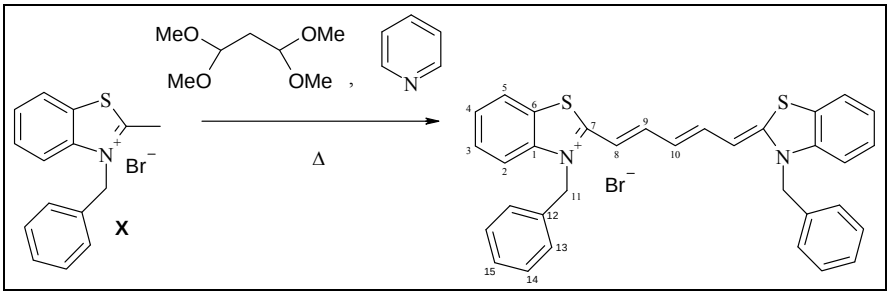

Reagent/solvent	3-benzyl-2-methyl-benzothiazolium iodide, X	1,1,3,3-tetramethoxypopane	Pyridine
Mol	1.23 mmol	3.1 mmol	-
Mass/volume	0.41 g	0.51 mL, 0.5 g	5 mL

After 45 mins a dark purple solid (0.21 g, 58% yield) was isolated. The crude product was purified by slow extraction in EtOH using Soxhlet apparatus resulting in a mixture of metallic, lime-green needles and starting material(0.10 g, approx. yield 22%).

[Lab book reference code: 4409/76]

UV λ_{max} (MeOH) 658 nm

Preparation of 3,3'-diphenethyl-benzothiadicarbocyanine iodide, **69**

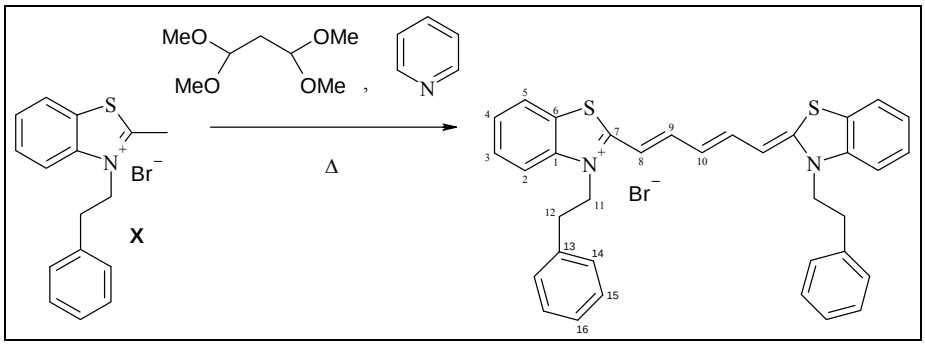

Reagent/solvent	**3-phenethyl-2-methyl-benzothiazolium iodide, X**	**1,1,3,3-tetramethoxypopane**	Pyridine
Mol	1.23 mmol	3.1 mmol	-
Mass/volume	0.41 g	0.51 mL, 0.5 g	5 mL

After 45 mins a dark purple residue was isolated. The crude product was then crystallised from hot EtOH, resulting in a mixture of dark green blocks and starting material (0.11 g, approx. yield 30%).

[Lab book reference code: 4409/69]

UV λ_{max} (MeOH) 658 nm

Preparation of 3,3'-di(4-bromobenzyl)benzothiabiscarbocyanine bromide, **70**

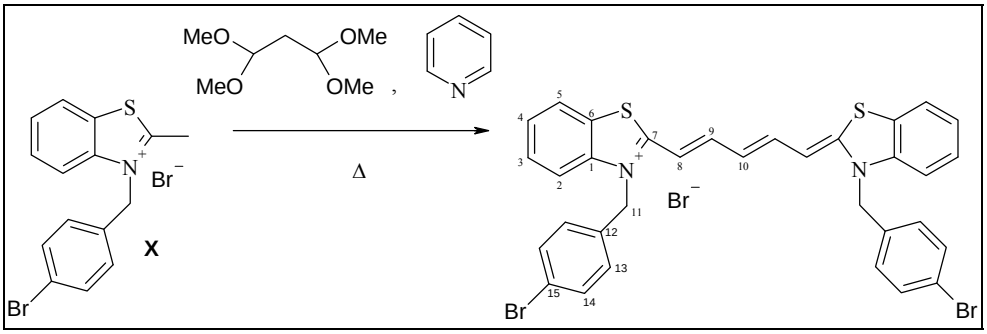

Reagent/solvent	**3-(4-bromo-benzyl)-2-methyl-benzothiazolium iodide, X**	**1,1,3,3-tetramethoxypopane**	Pyridine
Mol	1.8 mmol	4.7 mmol	-
Mass/volume	0.75 g	0.77 mL, 0.77 g	6 mL

After 30 mins a dark purple residue was isolated. The crude product was purified by slow extraction in EtOH using Soxhlet apparatus resulting in a mixture of metallic, dark-green blocks (0.196 g, Approx. yield 29%).

[Lab book reference code: 4409/85]:

UV λ_{max} (MeOH) 659 nm

8.3 X-Ray Structural Studies

In this section the most basic crystal structure details are presented along with a diagram of the asymmetric unit for each crystal structure solved. Full details are available on the compact disc attached to the back of this thesis.

8.3.1 Quaternary Salt Crystal Data

Crystal data of 3-benzyl-2-methyl-benzothiazolium bromide, **28**

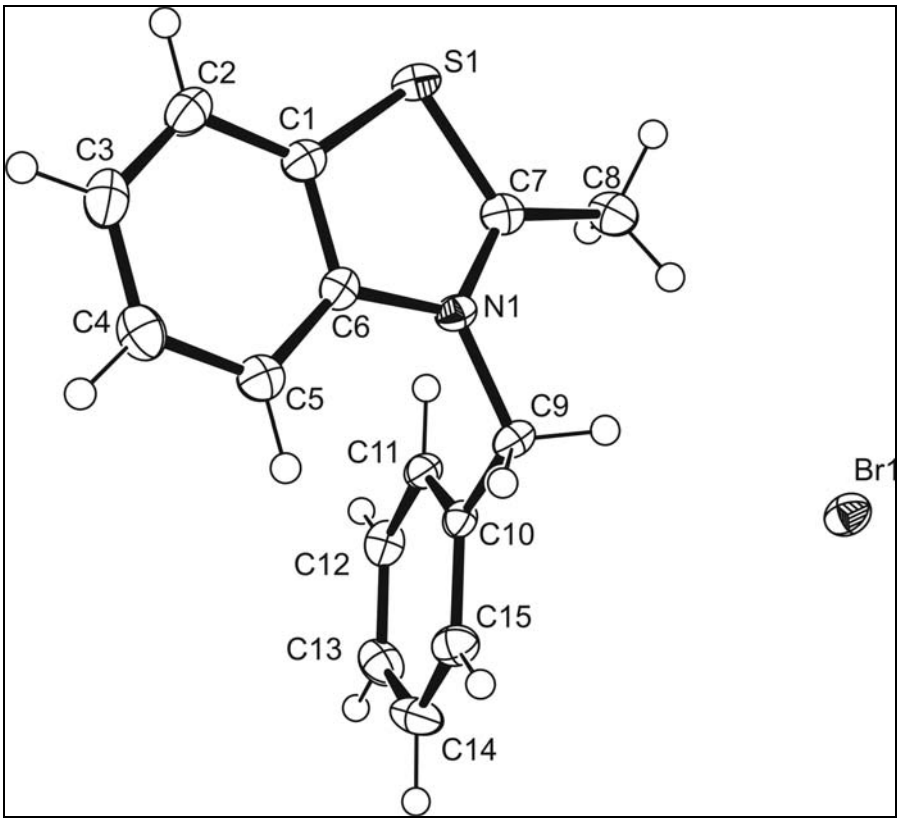

*Figure 8.1. Graphical representation of **28** from X-ray structural studies. Ellipsoids represent greater than 50% probability level.*

05glh002	$C_{15}H_{14}BrNS$, FW 320.24	Volume: 2685.17 (17) $Å^3$
a= 9.5178 (3) Å	b= 16.6744 (6) Å	c= 16.9194 (7) Å
α= 90 °	β= 90 °	γ= 90 °
Orthorhombic	Pbca	R = 5.5%, GoOF= 1.048
Clear Colourless	Cut Plate	0.48 x 0.4 x 0.08 mm
Z= 8, μ= 3.198 mm^{-1}	λ = 0.71073 Å	120 K

*Table 8.1. X-ray structural data of **28**. Data collected and structure solved by G. Hallworth.*

Crystal data of 3-(4-Bromo-benzyl)-2-methyl-benzothiazolium bromide, **30**.

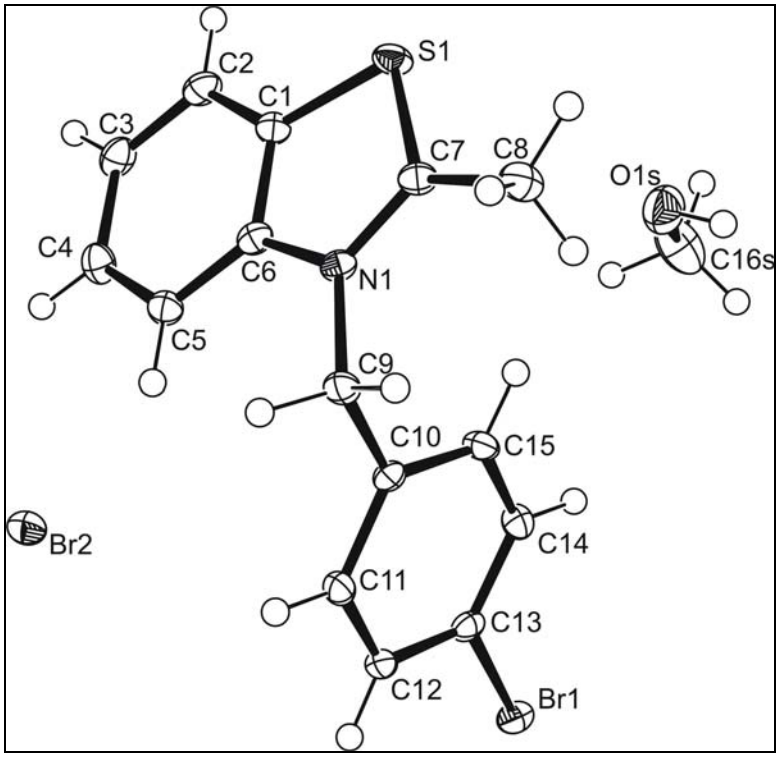

Figure 8.2. Graphical representation of **30** *from X-ray structural studies. Ellipsoids represent greater than 50% probability level.*

07glh007	$C_{16}H_{17}Br_2NOS$, FW 431.19	Volume: 1655.56 (4) $Å^3$
a= 9.08020 (10) Å	b= 11.3700 (2) Å	c= 16.1163 (2) Å
α= 90 °	β= 95.7300 (10) °	γ= 90 °
Monoclinic	$P2_1/c$	R = 3.92%, GoOF= 1.206
Clear Colourless	Cut Block	0.50 x 0.40 x 0.02 mm
Z= 4, μ= 5.020 mm^{-1}	λ = 0.71073 Å	120 K

Table 8.2. X-ray structural data of **30**. *Data collected and structure solved by G. Hallworth*

Crystal data of 3-benzyl-5-chloro-2-methyl-benzothiazolium bromide, **34**.

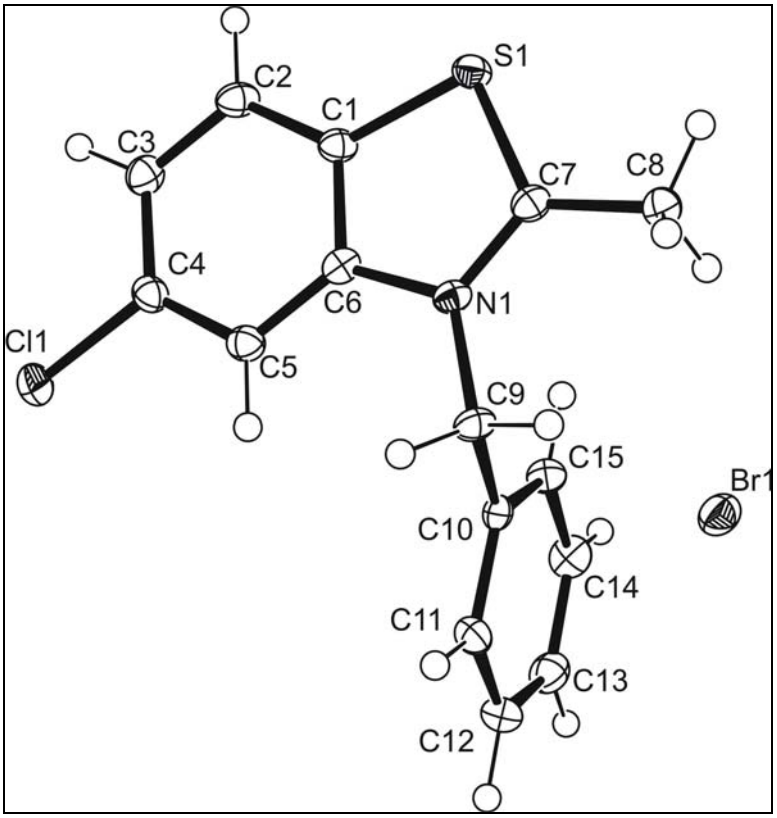

Figure 8.3. Graphical representation of **34** *from X-ray structural studies. Ellipsoids represent greater than 50% probability level.*

07glh006	$C_{15}H_{13}BrClNS$, FW 354.68	Volume: 2882.22 (7) $Å^3$
a= 9.50000 (10) Å	b= 16.6578 (2) Å	c= 18.2132 (3) Å
α= 90 °	β= 90 °	γ= 90 °
Orthorhombic	Pbca	R = 3.80%, GoOF= 1.050
Clear Colourless	Cut Block	0.60 x 0.50 x 0.40 mm
Z= 8, μ= 3.167 mm^{-1}	λ = 0.71073 Å	120 K

Table 8.3. X-ray structural data of **34**. *Data collected and structure solved by G. Hallworth*

Crystal data of 2,3-dimethyl-benzoxazolium Iodide, **35**.

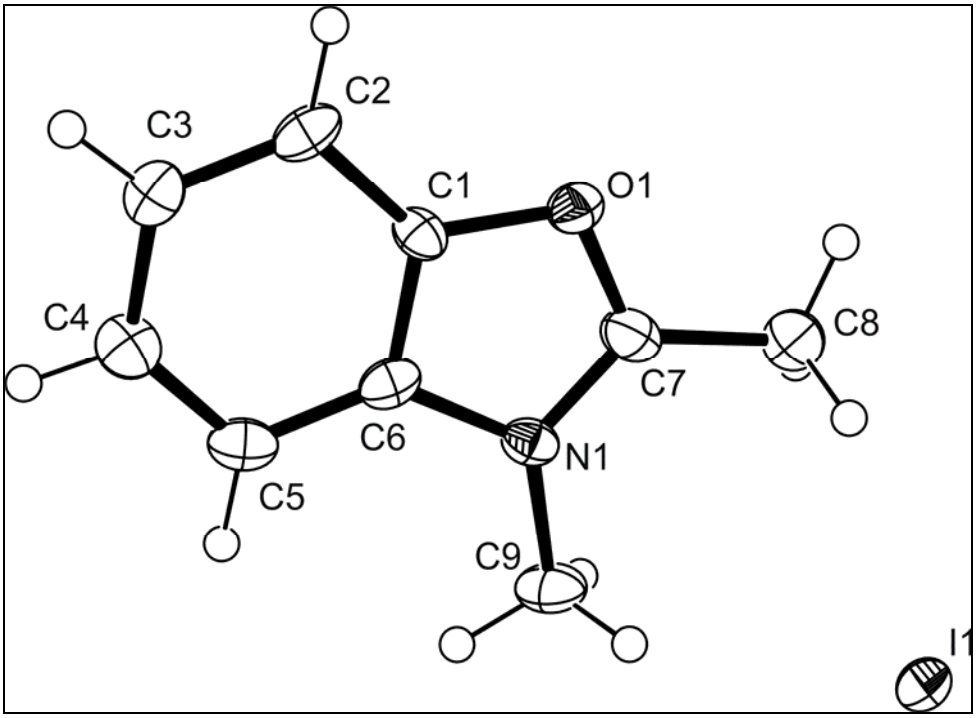

*Figure 8.4. Graphical representation of **35** from X-ray structural studies. Ellipsoids represent greater than 50% probability level.*

07glh019	$C_9H_{10}INO$, FW 274.74	Volume: 2005.2 (3) $Å^3$
a= 7.1307 (5) Å	b= 11.5666 (9) Å	c= 24.3122 (19) Å
α= 90.00 °	β= 90.00 °	γ= 90.00 °
Orthorhombic	Pbca	R = 8.42%, GoOF= 1.126
Clear Colourless	Cut Block	0.08 x 0.05 x 0.02 mm
Z= 9, μ= 3.149 mm^{-1}	λ = 0.71073 Å	120 K

*Table 8.4. X-ray structural data of **35**. Data collected and structure solved by G. Hallworth*

Crystal data of 2-methyl-3-phenethyl benzothiazolium bromide, **36**.

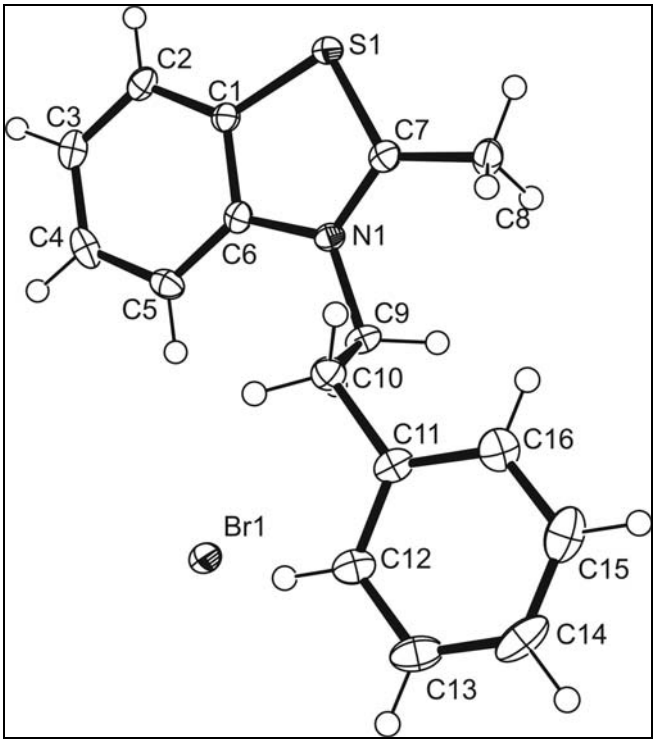

*Figure 8.5. Graphical representation of **36** from X-ray structural studies. Ellipsoids represent greater than 50% probability level.*

05glh008	$C_{16}H_{16}BrNS$, FW 334.27	Volume: 360.51 (2) $Å^3$
a= 7.3829 (2) Å	b= 7.5709 (3) Å	c= 7.5934 (2) Å
α= 82.382 (2) °	β= 67.322 (2) °	γ= 67.037 (2) °
Triclinic	P-1	R = 3.23%, GoOF= 0.861
Clear Colourless	Needle	0.30 x 0.08 x 0.04 mm
Z= 1, μ= 2.981 mm^{-1}	λ = 0.71073 Å	120 K

*Table 8.5 X-ray structural data of **36**. Data collected and structure solved by G. Hallworth*

Crystal data of 2-methyl-3-(4-sulfopropyl)-benzothiazolium, **39**.

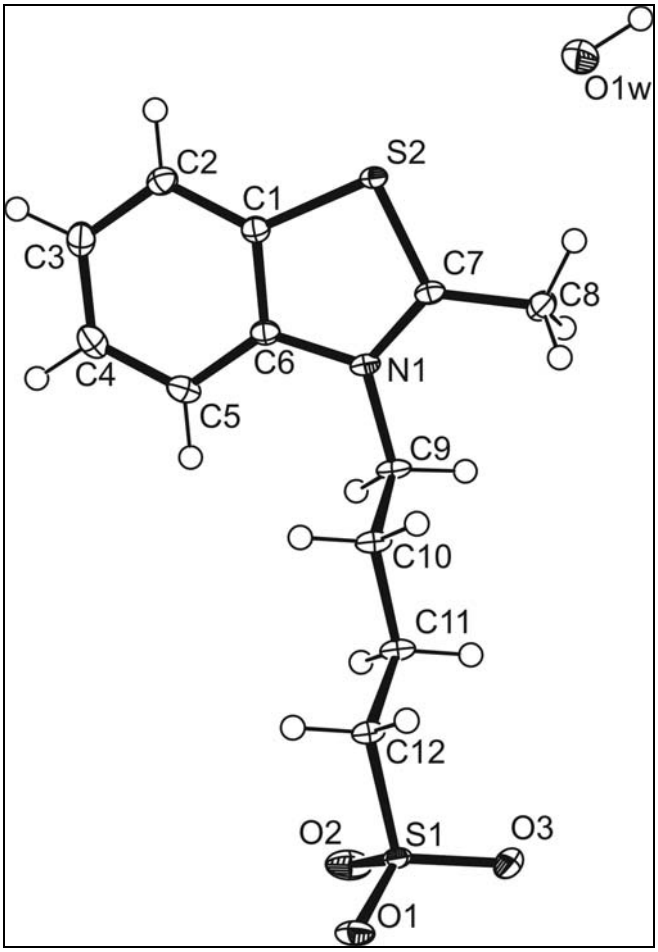

Figure 8.6. Graphical representation of **39** *from X-ray structural studies. Ellipsoids represent greater than 50% probability level.*

06glh010	$C_{10}H_{17}N_1O_4S_2$, FW 303.39	Volume: 1343.83 (5) Å^3
a= 9.5013 (2) Å	b= 11.4302 (2) Å	c= 12.3935 (3) Å
α= 90 °	β= 93.2230 (10) °	γ= 90 °
Monoclinic	$P2_1/c$	R = 2.88%, GoOF= 1.055
Clear Colourless	Block	1.00 x 0.70 x 0.40 mm
Z= 4, μ= 0.405 mm^{-1}	λ = 0.71073 Å	120 K

Table 8.6. X-ray structural data of **39**. *Data collected and structure solved by G. Hallworth*

Crystal data of 2-methyl-3-ethyl-benzothiazolium, **62a**.

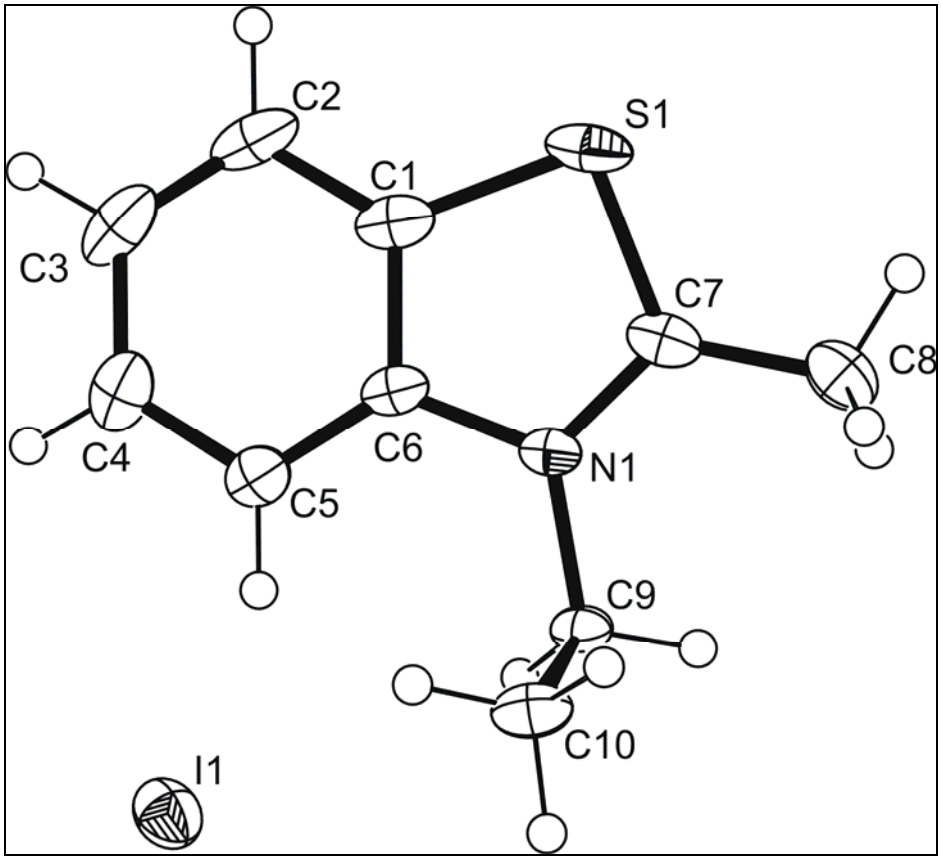

Figure 8.7. Graphical representation of **62a** *from X-ray structural studies. Ellipsoids represent greater than 50% probability level.*

05jbo002	$C_{10}H_{12}INS$, FW 610.33	Volume: 1128.75 (13) $Å^3$
a= 7.0300 (3) Å	b= 15.5690 (12) Å	c= 10.3760 (8) Å
α= 90 °	β= 96.323 (5) °	γ= 90 °
Monoclinic	$P2_1/c$	R = 2.23%, GoOF= 1.087
Dark Purple	Cut Block	0.1 x 0.08 x 0.06 mm
Z= 2, μ= 2.978 mm^{-1}	λ = 0.71073 Å	120 K

Table 8.7. X-ray structural data of **62a**. *Data collected and structure solved by G. Hallworth*

Crystal data of 2-methyl-3-ethyl-benzoselenazolium, **71**.

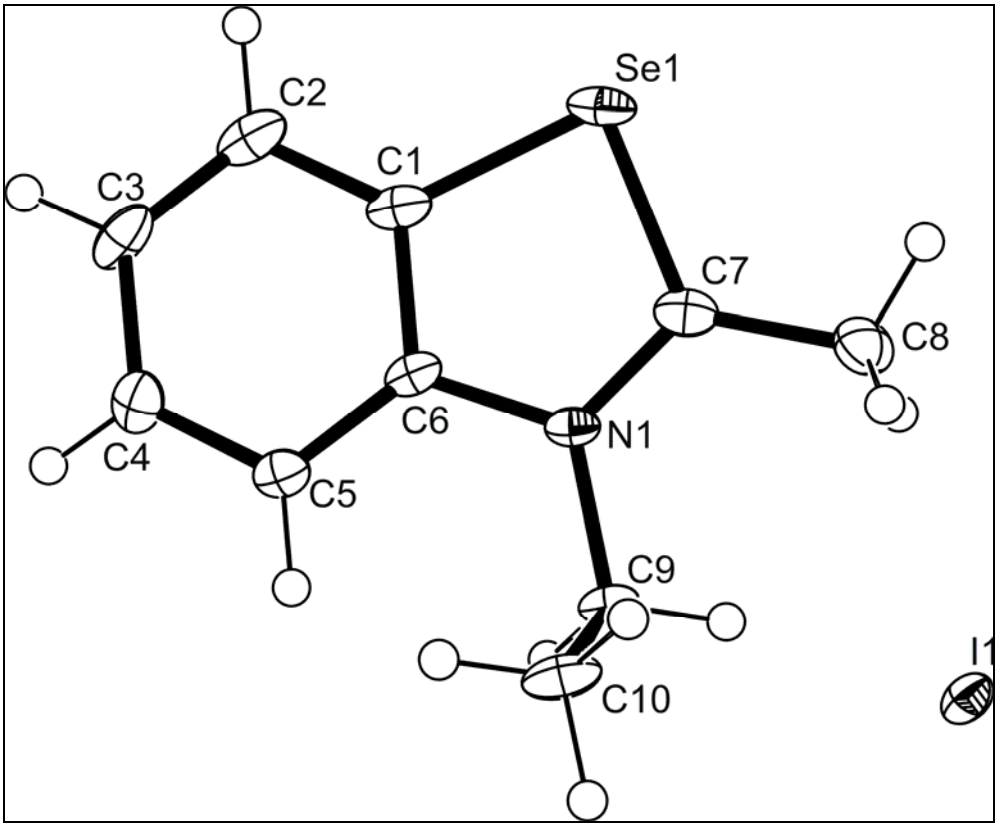

Figure 8.8. Graphical representation of **71** *from X-ray structural studies. Ellipsoids represent greater than 50% probability level.*

07glh013	$C_{10}H_{12}INSe$, FW 352.07	Volume: 1137.99 (2) $Å^3$
a= 7.13490 (10) Å	b= 15.6009 (2) Å	c= 10.26240 (10) Å
α= 90 °	β= 94.9890 (10) °	γ= 90 °
Monoclinic	$P2_1/c$	R = 2.55%, GoOF= 1.185
Clear Pale Brown	Cut Block	0.50 x 0.40 x 0.3 mm
Z= 4, μ= 5.969 mm^{-1}	λ = 0.71073 Å	120 K

Table 8.8. X-ray structural data of **71**. *Data collected and structure solved by G. Hallworth*

8.3.2 Monomethine Crystal Data

Crystal data of 3,3'-diethylbenzothiacyanine iodide, **3a**

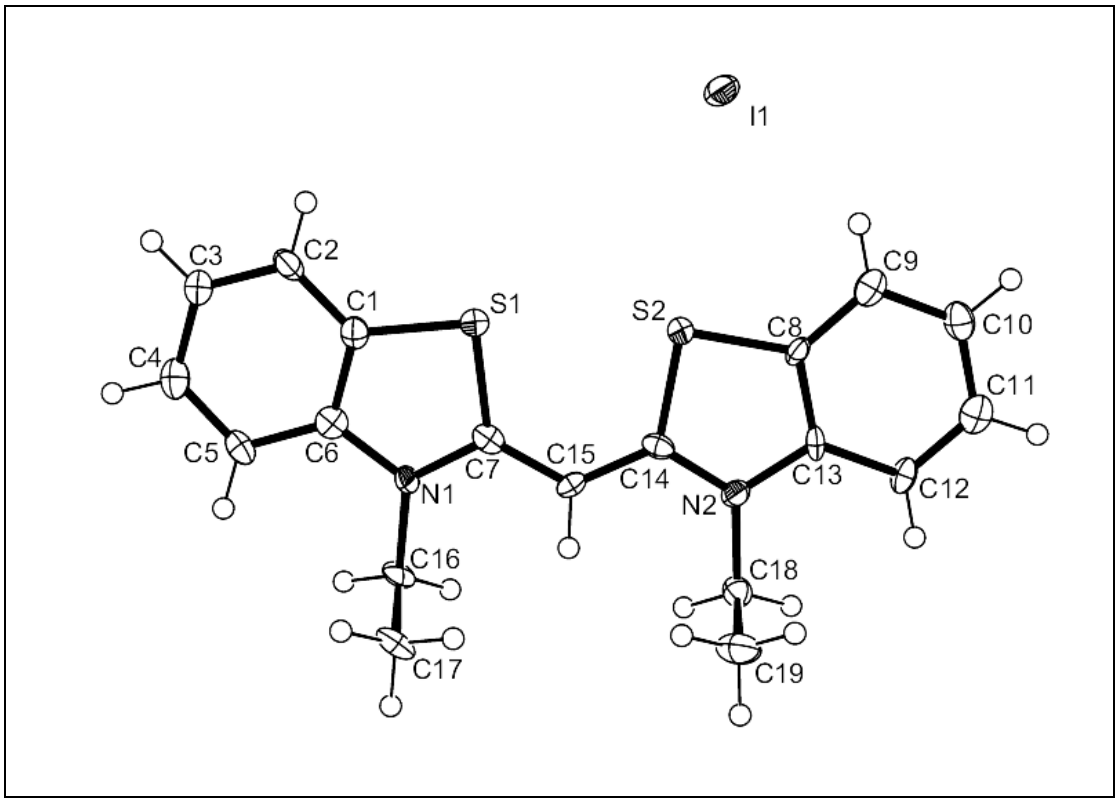

*Figure 8.9. Graphical representation of **3a** from X-ray structural studies. Ellipsoids represent greater than 50% probability level.*

05glh006	$C_{19}H_{19}IN_2S_2$, FW 466.38	Volume: 1851.29(17) $Å^3$
a= 7.2097(3) Å	b= 25.5797(15) Å	c= 10.0386(6) Å
α= 90 °	β= 90.410(4) °	γ= 90 °
Monoclinic	$P2_1/n$	R = 16.36 %, GoOF= 1.172
Clear Light Brown	Needle	0.22 x 0.04 x 0.01 mm^3
Z= 4, μ= 1.958 mm^{-1}	λ = 0.71073 Å	120 K

*Table 8.9. X-ray structural data of **3a**. Data collected and structure solved by G. Hallworth*

Crystal data of 3,3'-diethylbenzothiacyanine iodide, **3a**

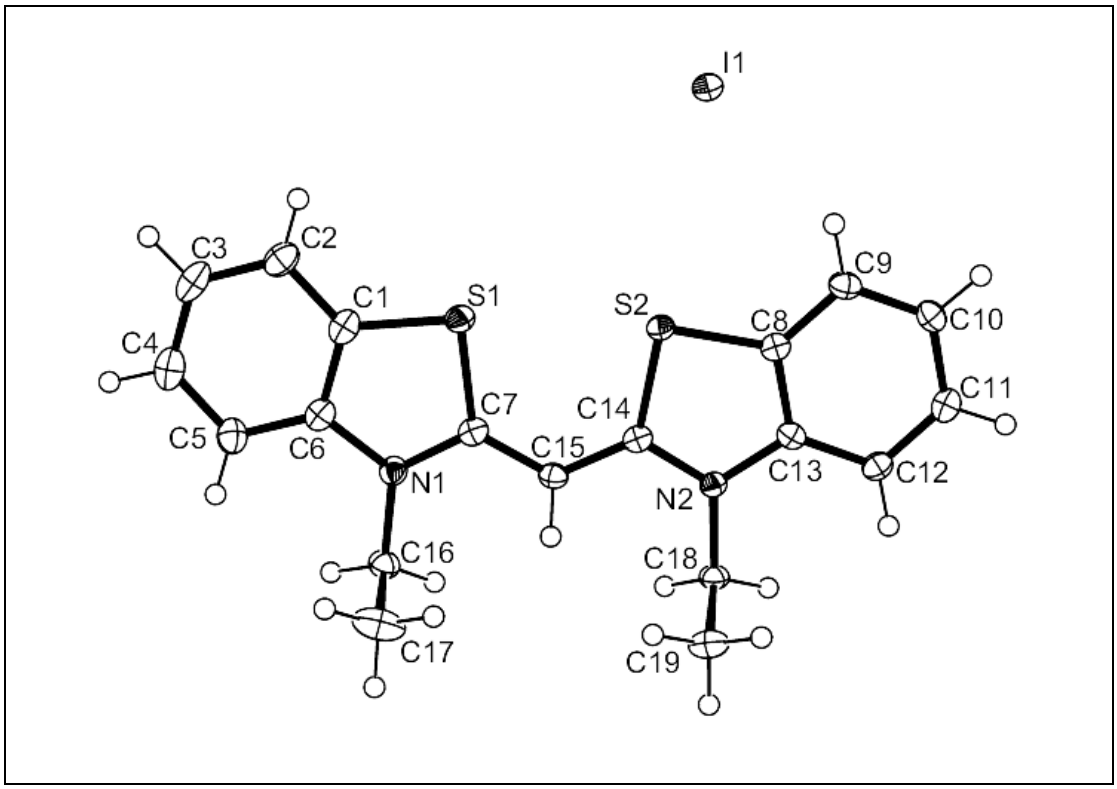

*Figure 8.10. Graphical representation of **3a** from X-ray structural studies. Ellipsoids represent greater than 50% probability level.*

05jbo001	$C_{19}H_{19}IN_2S_2$, FW 466.38	Volume: 920.97(11) $Å^3$
a= 8.1070(6) Å	b=10.2154(6) Å	c=12.0360(9) Å
α= 103.572(6) °	β= 97.192(2) °	γ= 104.305(4) °
Triclinic	P-1	R = 3.82%, GoOF= 1.076
Dark Brown	Needle	0.25 x 0.10 x 0.04 mm
Z= 2, μ= 1.968 mm^{-1}	λ = 0.71073 Å	120 K

*Table 8.10. X-ray structural data of **3a**. Data collected by J. Orton and structure solved by G. Hallworth*

Crystal data of 3,3'-diethyl benzothiacyanine triiodide, **3f**.

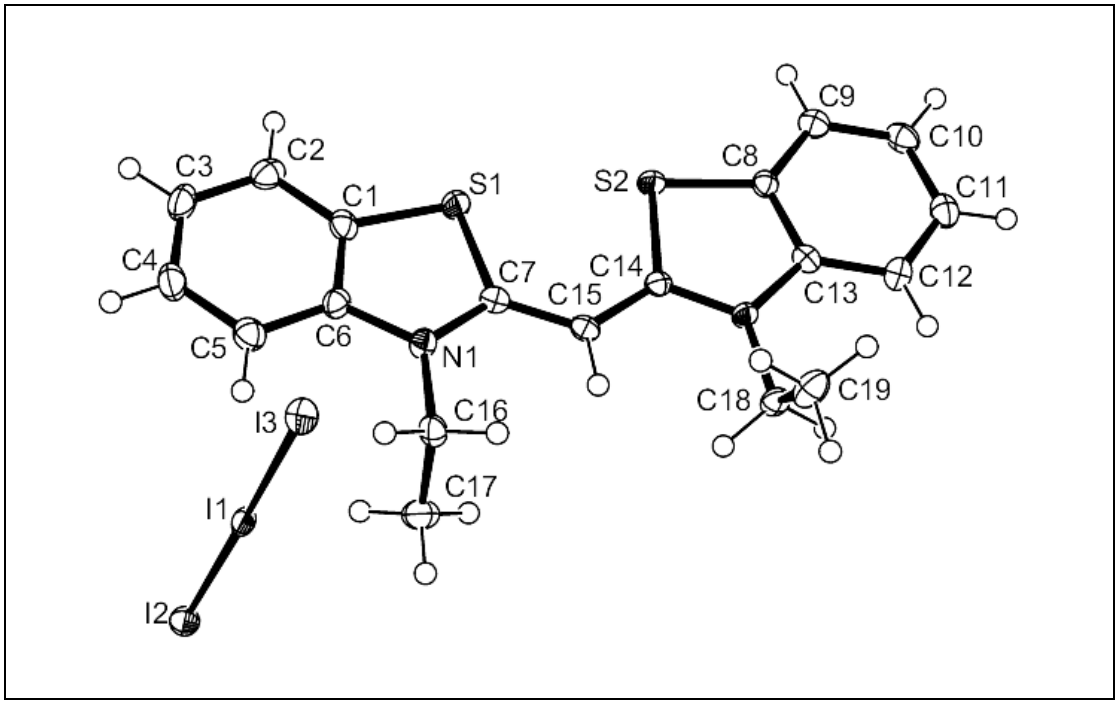

*Figure 8.11. Graphical representation of **3f** from X-ray structural studies. Ellipsoids represent greater than 50% probability level.*

04jbo083	$C_{19}H_{19}I_3N_2O_2$, FW 720.18	Volume: 1121.10(9)Å^3
a= 8.702(5) Å	b= 10.626(5) Å	c= 12.799(5) Å
α= 76.133(5) °	β= 81.496(5) °	γ= 78.901(5) °
Triclinic	P-1	R = 2.80%, GoOF= 1.078
Dark Orange	Cut plate	0.24 x 0.10 x 0.02 mm
Z= 2, μ= 4.375 mm^{-1}	λ = 0.71073 Å	120 K

Table 8.11. *X-ray structural data of **3f**.* Data collected J. Orton and structure solved by G. Hallworth

Crystal data of 3,3'-diethylbenzocyanine iodide, **45a**

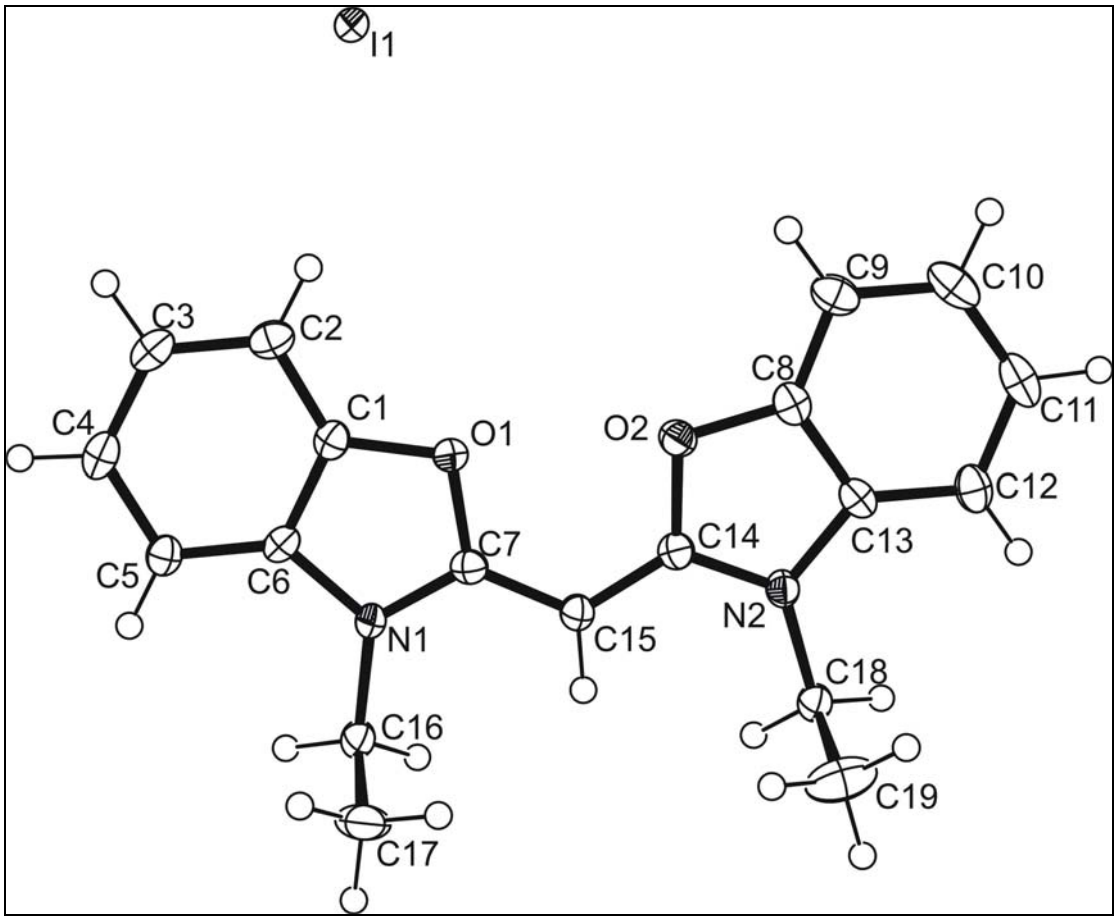

*Figure 8.12. Graphical representation of **44a** from X-ray structural studies. Ellipsoids represent greater than 50% probability level.*

07pnh0005	$C_{19}H_{19}IN_2O_2$, FW 434.26	Volume: 9.14.87 (4) Å^3
a= 17.8820 (2) Å	b= 10.8178 (3) Å	c= 12.0902 (3) Å
α= 110.3640 (10) °	β= 98.4390 (10) °	γ= 102.5900 (10) °
Triclinic	P-1	R = 2.15%, GoOF= 1.062
Pale Yellow	Block	0.10 x 0.09 x 0.04 mm
Z= 2, μ= 1.763 mm^{-1}	λ = 0.71073 Å	120 K

*Figure 8.12. X-ray structural data of **44a**. Data collected by P. N. Horton and structure solved by G. Hallworth*

Crystal data of 3,3'-diethyloxabenzocarbocyanine triiodide, **44b**

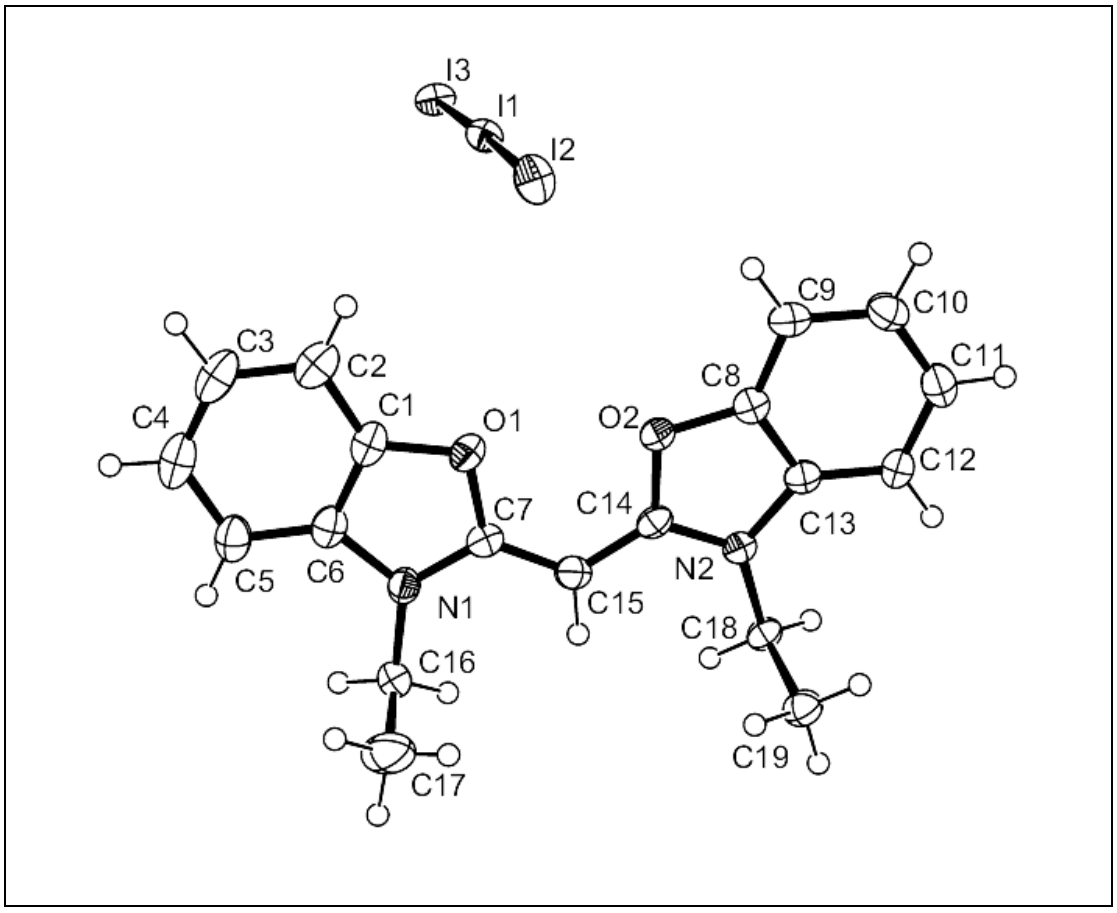

*Figure 8.13. Graphical representation of **44b** from X-ray structural studies. Ellipsoids represent greater than 50% probability level.*

04jbo082	$C_{19}H_{19}I_3N_2O_2$, FW 688.06	Volume: 2155.4(5) $Å^3$
a= 12.6648(14) Å	b= 14.3580(15) Å	c= 12.7020(19) Å
α= 90 °	β= 111.066(11) °	γ= 90 °
Monoclinic	$P2_1/n$	R = 3.97%, GoOF= 1.301
Dark Purple	Block	0.22 x 0.18 x 0.08 mm
Z= 4, μ= 4.366 mm^{-1}	λ = 0.71073 Å	120 K

*Table 8.13. X-ray structural data of **44b**. Data collected by J. Orton and structure solved by G. Hallworth*

Crystal data of 5,5'-chloro-3,3'-diethylbenzothiacyanine iodide, **45a**

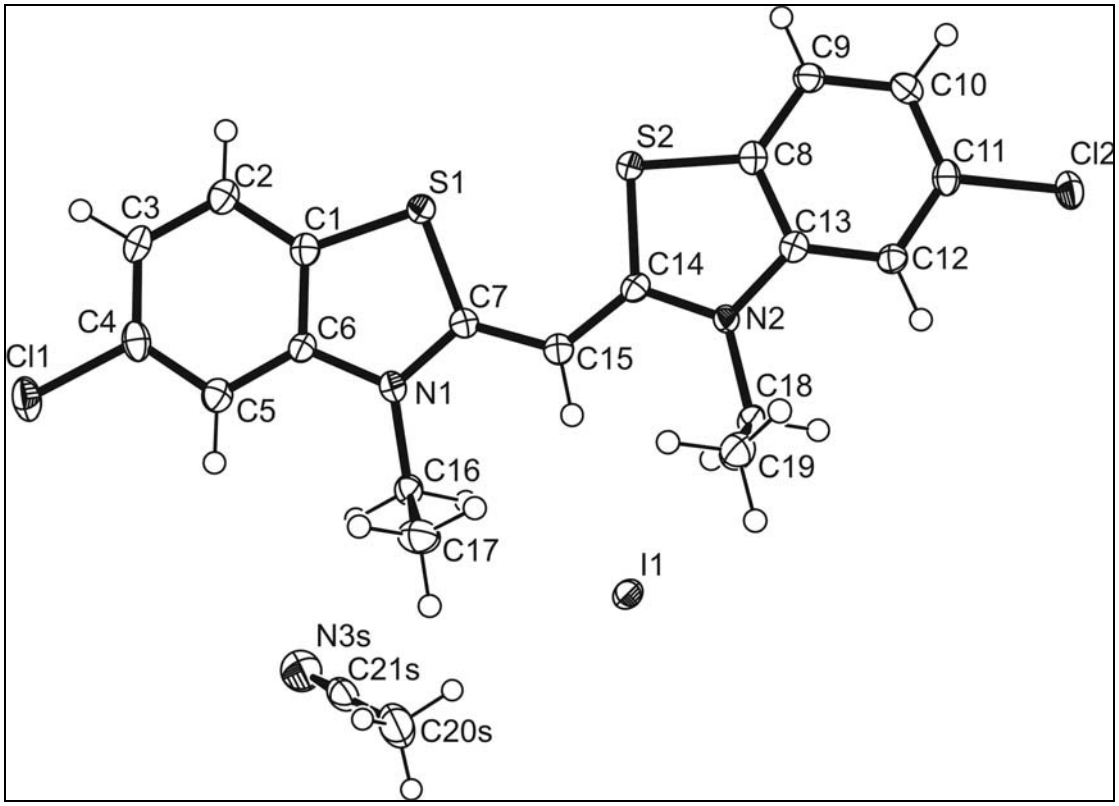

*Figure 8.14. Graphical representation of **45a** from X-ray structural studies. Ellipsoids represent greater than 50% probability level.*

07glh010	$C_{21}H_{20}Cl_2IN_3S_2$, FW 576.32	Volume: 1137.10 (5) $Å^3$
a= 7.3266 (2) Å	b= 10.0136 (3) Å	c= 15.7987 (4) Å
α= 95.313 (2) °	β= 98.922 (2) °	γ= 93.287 (2) °
Triclinic	P-1	R = 4.81%, GoOF= 1.190
Intense Yellow	Needle	0.2 x 0.02 x 0.01 mm
Z= 2, μ= 1.840 mm^{-1}	λ = 0.71073 Å	120 K

*Table 8.14. X-ray structural data of **45a**. Data collected and structure solved by G. Hallworth*

Crystal data of 5,5'-chloro-3,3'-diethylbenzothiacyanine triiodide, **45b**

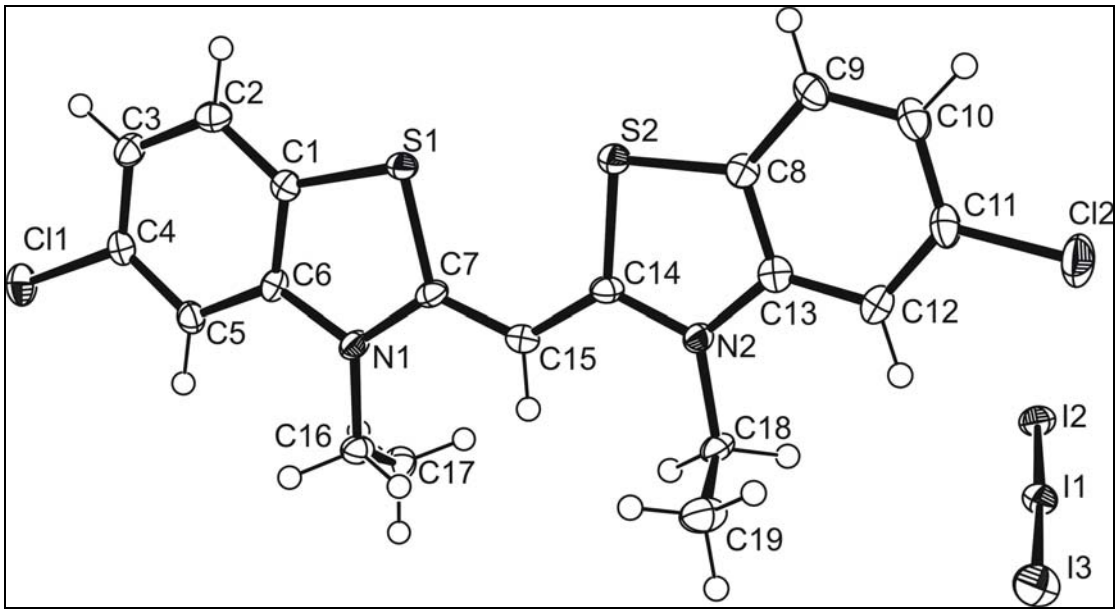

*Figure 8.15. Graphical representation of **45b** from X-ray structural studies. Ellipsoids represent greater than 50% probability level.*

07glh004	$C_{19}H_{17}Cl_2I_3N_2S_2$, FW 789.07	Volume: 2413.59 (11) Å^3
a= 9.0859 (2) Å	b= 25.5888 (7) Å	c= 10.5194 (3) Å
α= 90 °	β= 99.299 (2) °	γ= 90 °
Monoclinic	$P2_1/n$	R = 4.08%, GoOF= 1.137
Dark Red	Needle	0.6 x 0.03 x 0.02 mm
Z= 4, μ= 4.289 mm^{-1}	λ = 0.71073 Å	120 K

*Table 8.15. X-ray structural data of **45b**. Data collected and structure solved by G. Hallworth*

Crystal data of 5,5'-fluoro-3,3'-diethylbenzothiacyanine iodide, **46a**

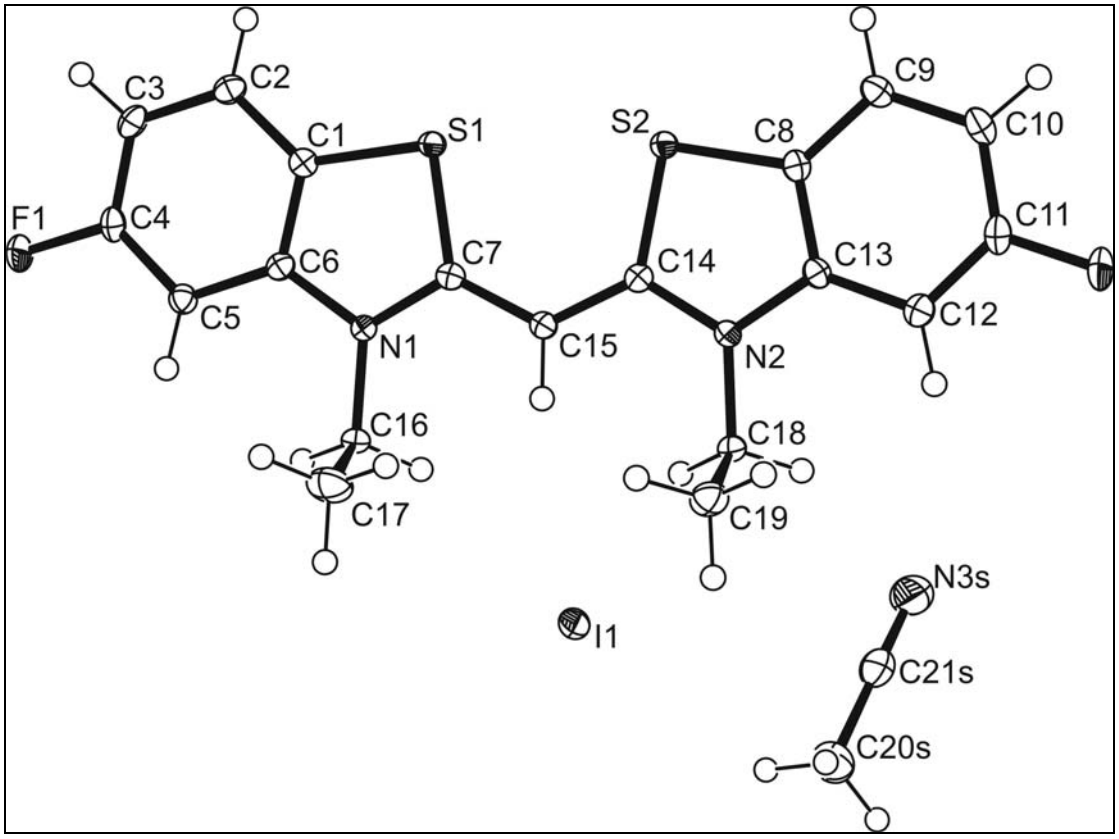

*Figure 8.16. Graphical representation of **46a** from X-ray structural studies. Ellipsoids represent greater than 50% probability level.*

07glh008	$C_{21}H_{20}F_2IN_3S_2$, FW 543.42	Volume: 1087.55(3)Å^3
a= 8.34700(10) Å	b= 11.7934(2) Å	c= 12.0323(2) Å
α= 70.3570(10)°	β= 83.8000(10) °	γ= 77.3160(10) °
Triclinic	P-1	R = 1.88%, GoOF= 1.210
Clear Intense Yellow	Cut block	0.1 x 0.08 x 0.04 mm
Z= 2, μ= 1.694 mm^{-1}	λ = 0.71073 Å	120 K

*Table 8.16. X-ray structural data of **46a**. Data collected and structure solved by G. Hallworth*

Crystal data of 5,5'-fluoro-3,3'-diethylbenzothiacyanine triiodide, **46b**

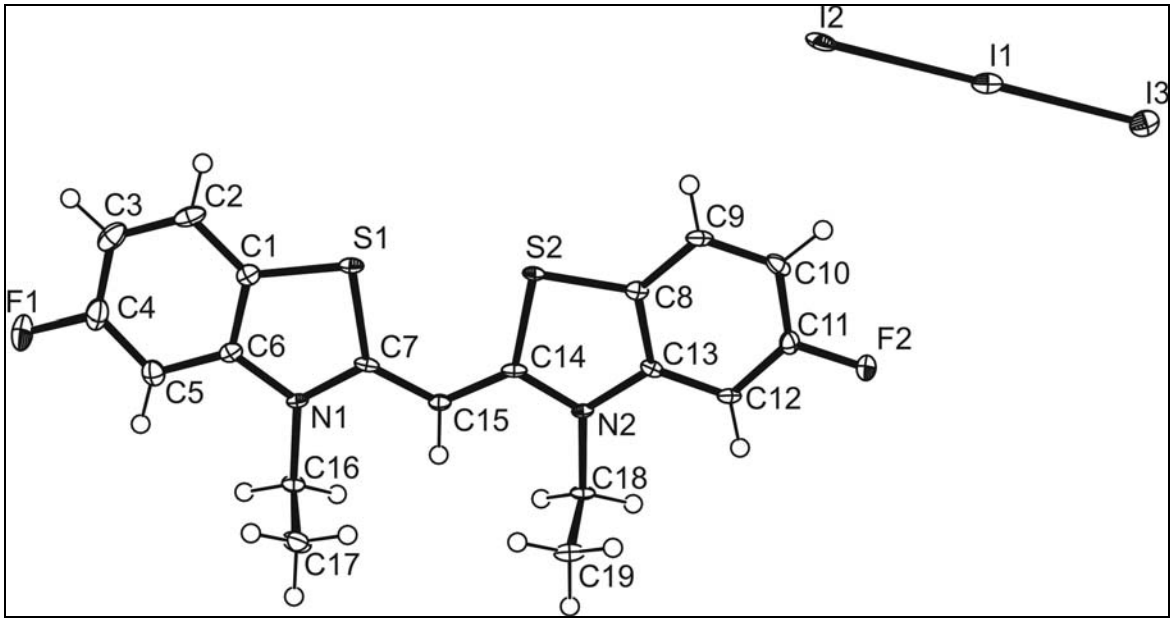

*Figure 8.17. Graphical representation of **46b** from X-ray structural studies. Ellipsoids represent greater than 50% probability level.*

07glh014	$C_{19}H_{17}F_2I_3N_2S_2$, FW 756.17	Volume: 4569.86(13)Å^3
a= 18.2364(3) Å	b= 10.9260(2) Å	c= 23.5612(3) Å
α= 90 °	β= 103.2370(10) °	γ= 90 °
Monoclinic	C2/c	R = 5.45%, GoOF= 1.134
Brown	Block	1.00 x 0.80 x 0.60 mm
Z= 8, μ= 4.311 mm^{-1}	λ = 0.71073 Å	120 K

*Table 8.17. X-ray structural data of **46b**. Data collected and structure solved by G. Hallworth*

Crystal data of 3,3'-dibenzyl-benzothiacyanine, **47**

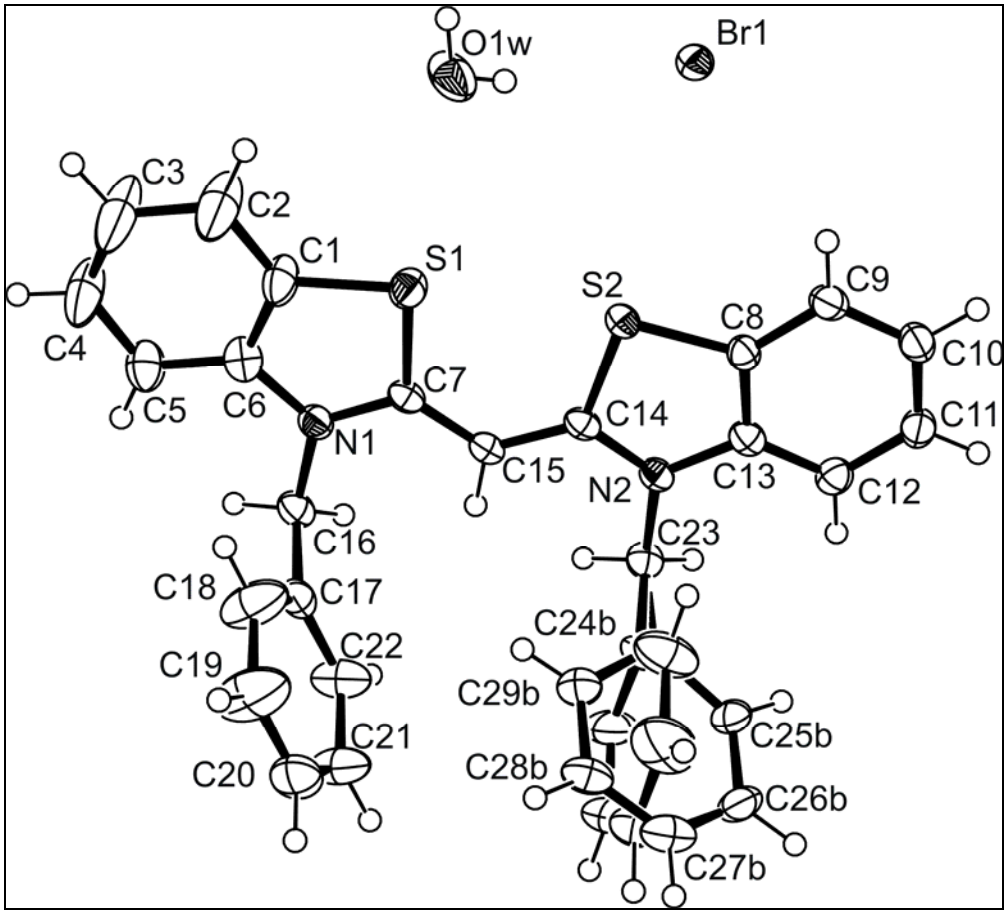

Figure 8.18. Graphical representation of ***47*** *from X-ray structural studies. Ellipsoids represent greater than 50% probability level.*

05glh010	$C_{29}H_{25}Br_1N_2O_1S_2$, FW 561.54	Volume: 4935.6(2)Å^3
a= 18.2891(4) Å	b= 14.5389(4) Å	c= 18.9775(4) Å
α= 90 °	β= 102.016(2) °	γ= 90 °
Monoclinic	C2/c	R = 5.12%, GoOF= 1.066
Clear Dark Orange	Cut block	0.60 x 0.40 x 0.40 mm
Z= 8, μ= 1.862 mm^{-1}	λ = 0.71073 Å	120 K

Table 8.18. *X-ray structural data* of **47**. Data collected and structure solved by G. Hallworth

Crystal data of 3,3'-diethyl benzoselenacyanine iodide, **64a**

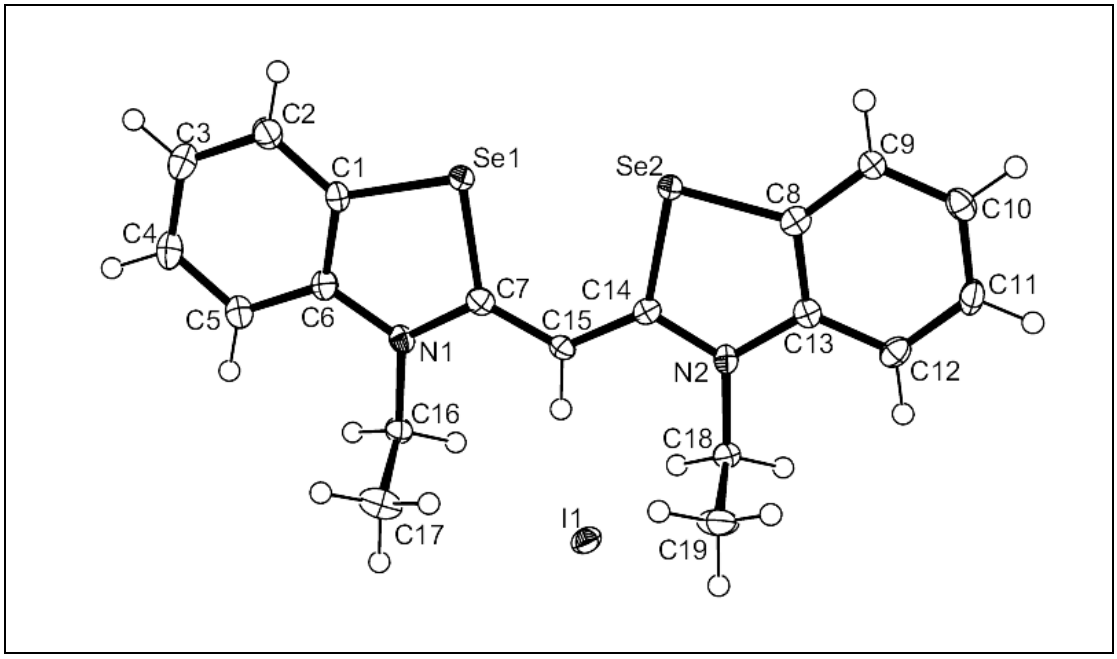

*Figure 8.19. Graphical representation of **64a** from X-ray structural studies. Ellipsoids represent greater than 50% probability level.*

2007pnh0003	$C_{19}H_{19}IN_2Se_2$, FW 560.18	Volume: 1912.81 (16) $Å^3$
a= 7.3143 (3) Å	b= 26.090 (13) Å	c= 10.0238 (5) Å
α= 90 °	β= 90.596 (2) °	γ= 90 °
Monoclinic	$P2_1/n$	R = 3.65%, GoOF= 1.253
Yellow	Needle	0.18 x 0.02 x 0.02 mm^3
Z= 4, μ= 5.483 mm^{-1}	λ = 0.71073 Å	120 K

*Table 8.19. X-ray structural data of **64a**. Data collected by P. N. Horton and structure solved by G. L. Hallworth*

8.3.3 Trimethine Dye Crystal Data

Crystal data of 3,3'-diethylbenzothiadicarbocyanine iodide, **2a**

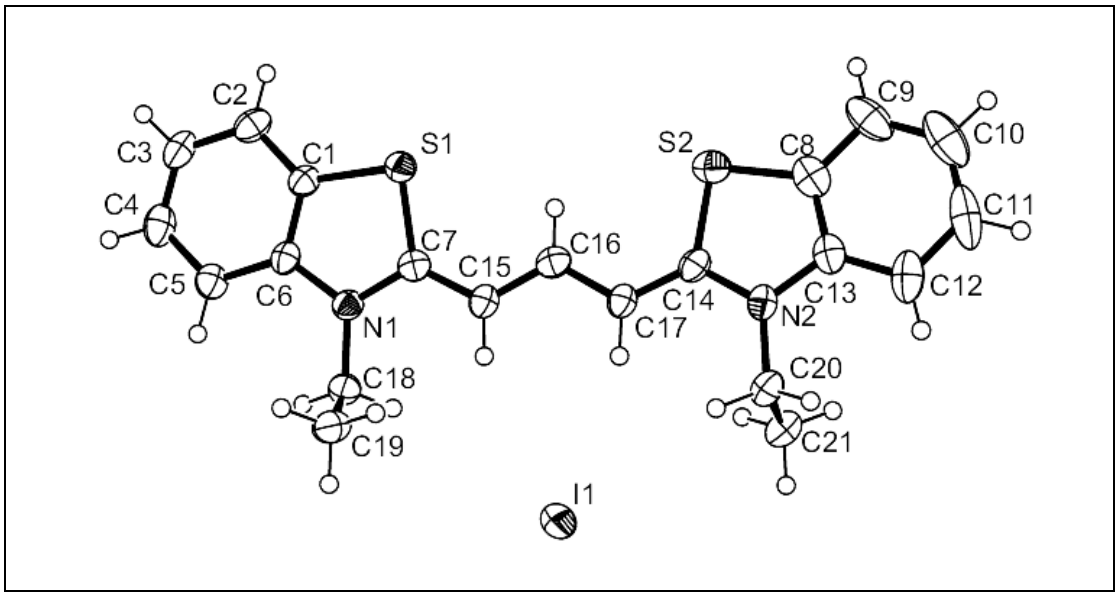

*Figure 8.20. Graphical representation of **2a** from X-ray structural studies. Ellipsoids represent greater than 50% probability level.*

06glh009	$C_{21}H_{21}IN_2S_2$, FW 492.42	Volume: 4544.3 (6) $Å^3$
a= 17.5779 (12) Å	b= 18.3422 (13) Å	c= 15.1370 (6) Å
α= 90 °	β= 111.389 (13) °	γ= 90 °
Monoclinic	C2/c	R = 4.31%, GoOF= 1.028
Clear Red	Split Plate	0.4 x 0.2 x 0.02 mm
Z= 8, μ= 1.606 mm^{-1}	λ = 0.71073 Å	120 K

*Table 8.20. X-ray structural data of **2a**. Data collected and structure solved by G. Hallworth*

Crystal data of 3,3'-diethyloxacarbocyanine iodide, **5a**.

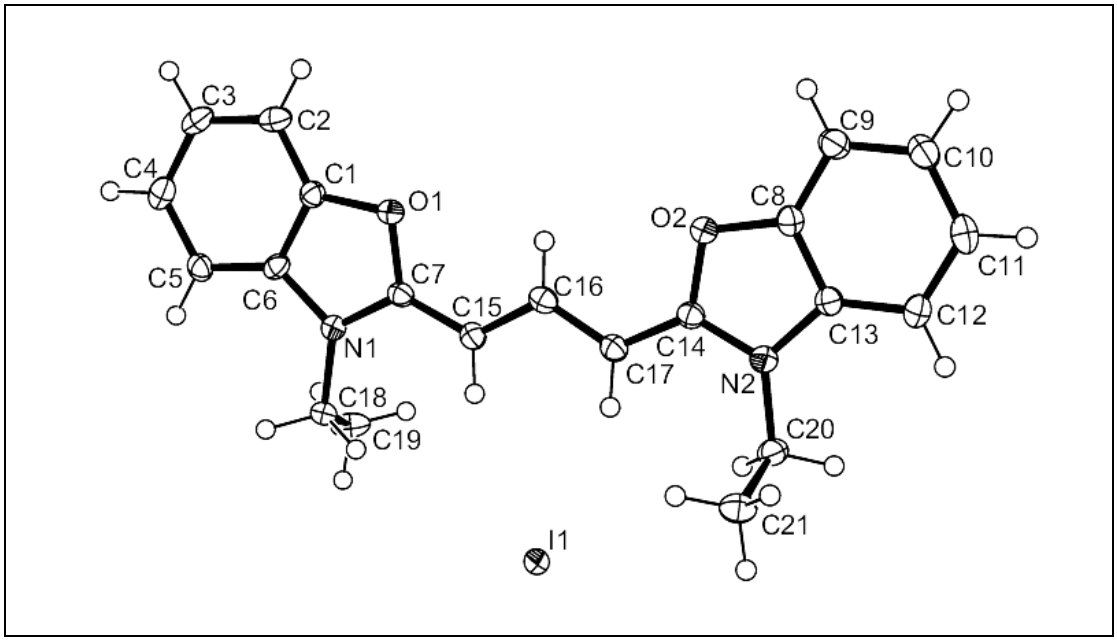

Figure 8.21. Graphical representation of ***5a*** *from X-ray structural studies. Ellipsoids represent greater than 50% probability level.*

06glh004	$C_{21}H_{21}IN_2O_2$, FW 460.30	Volume: Å^3
a= 8.82200 (10) Å	b= 10.3432 (2) Å	c= 21.7052 (4) Å
α= 90 °	β= 98.7450 (10) °	γ= 90 °
Monoclinic	$P2_1/n$	R = 7.9%, GoOF= 1.411
Clear Red	Block	0.3 x 0.12 x 0.12 mm
Z= 4, μ= 1.653 mm^{-1}	λ = 0.71073 Å	120 K

Table 8.21. X-ray structural data of ***5a****. Data collected and structure solved by G. Hallworth*

Crystal data of 3,3'-dibenzylbenzothiacarbocyanine bromide, **49**

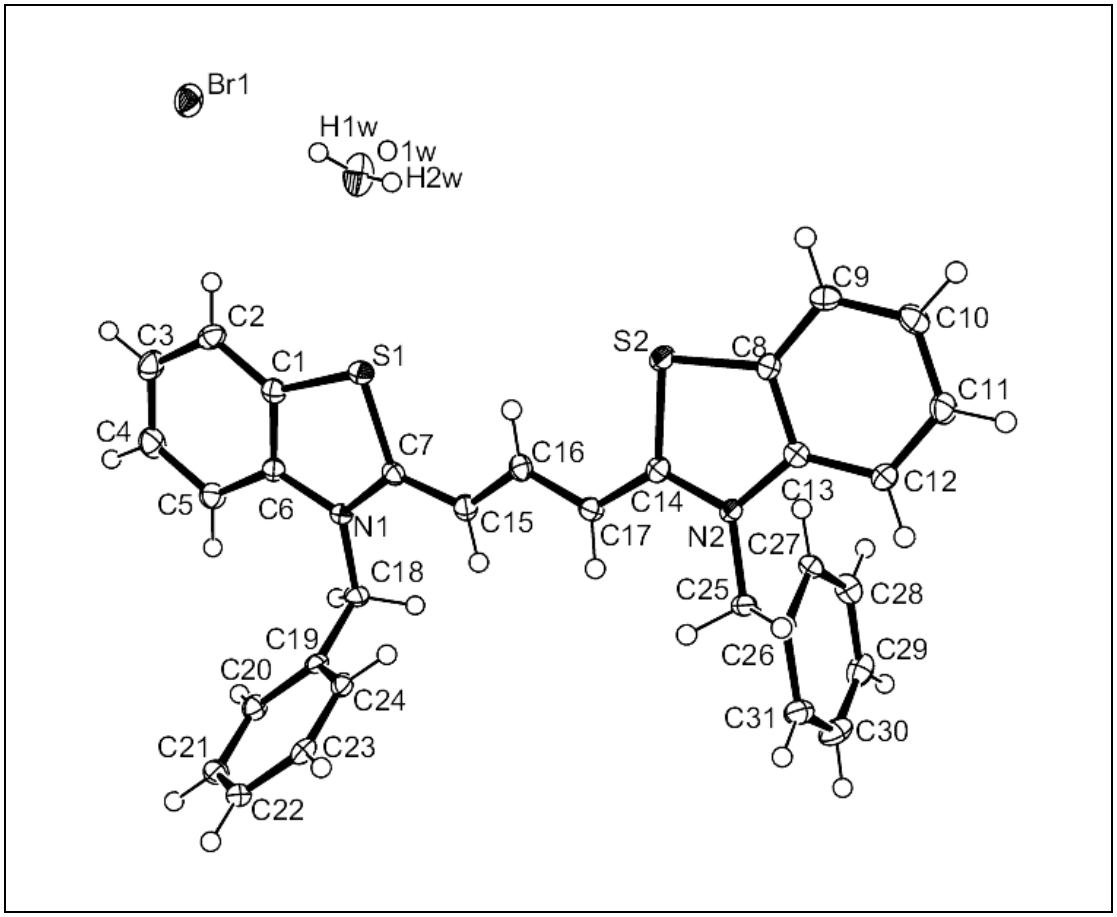

*Figure 8.22. Graphical representation of **49** from X-ray structural studies. Ellipsoids represent greater than 50% probability level.*

05glh001	$C_{31}H_{27}BrN_2OS_2$, FW 587.58	Volume: 1305.86 Å^3
a= 11.2043 (3) Å	b= 11.2786 (3) Å	c= 12.1458 (2) Å
α= 67.048 (2) °	β= 79.551 (2) °	γ= 67.6140 (10) °
Triclinic	P-1	R = 3.43%, GoOF= 1.045
Metallic Green	Block	0.31 x 0.19 x 0.17 mm
Z= 2, μ= 1.763 mm^{-1}	λ = 0.71073 Å	120 K

*Figure 8.22. X-ray structural data of **49**. Data collected and structure solved by G. Hallworth*

Crystal data of 3,3'-diphenethyl benzothiacarbocyanine bromide, **50**

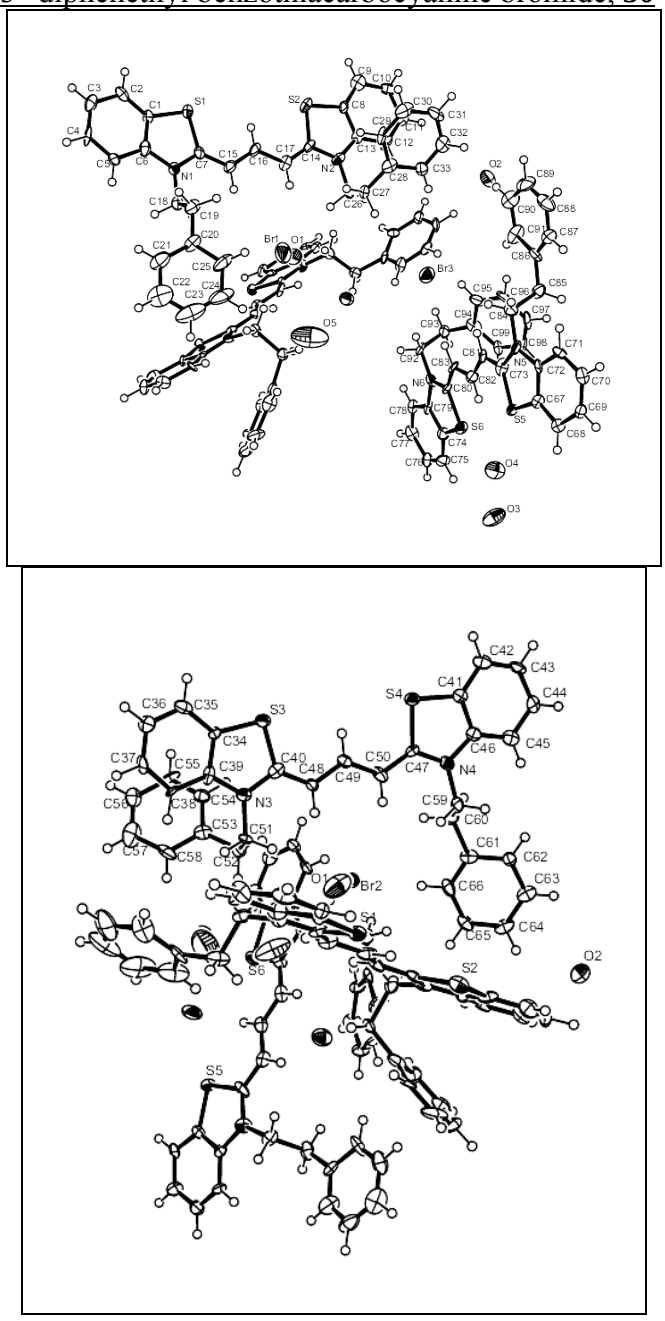

*Figure 8.23. Graphical representation of **50** from X-ray structural studies. Ellipsoids represent greater than 50% probability level.*

05glh007	$C_{33}H_{32.33}Br_1N_2O_{1.67}S_2$, FW 627.64	Volume: 4427.8 (5) $Å^3$
a= 13.6122 (8) Å	b= 18.5564 (11) Å	c= 19.2134 (12) Å
α= 73.562 (2) °	β= 74.592 (3) °	γ= 76.965 (4) °
Triclinic	P-1	R = 17.6%, GoOF= 1.080
Metallic Red	Needle	0.26 x 0.04 x 0.01 mm
Z= 6, μ= 1.566 mm^{-1}	λ = 0.71073 Å	120 K

*Table 8.23. X-ray structural data of **50**. Data collected and structure solved by G. Hallworth*

Crystal data of 3,3'-dinaphthylbenzothiacarbocyanine Bromide, **51**

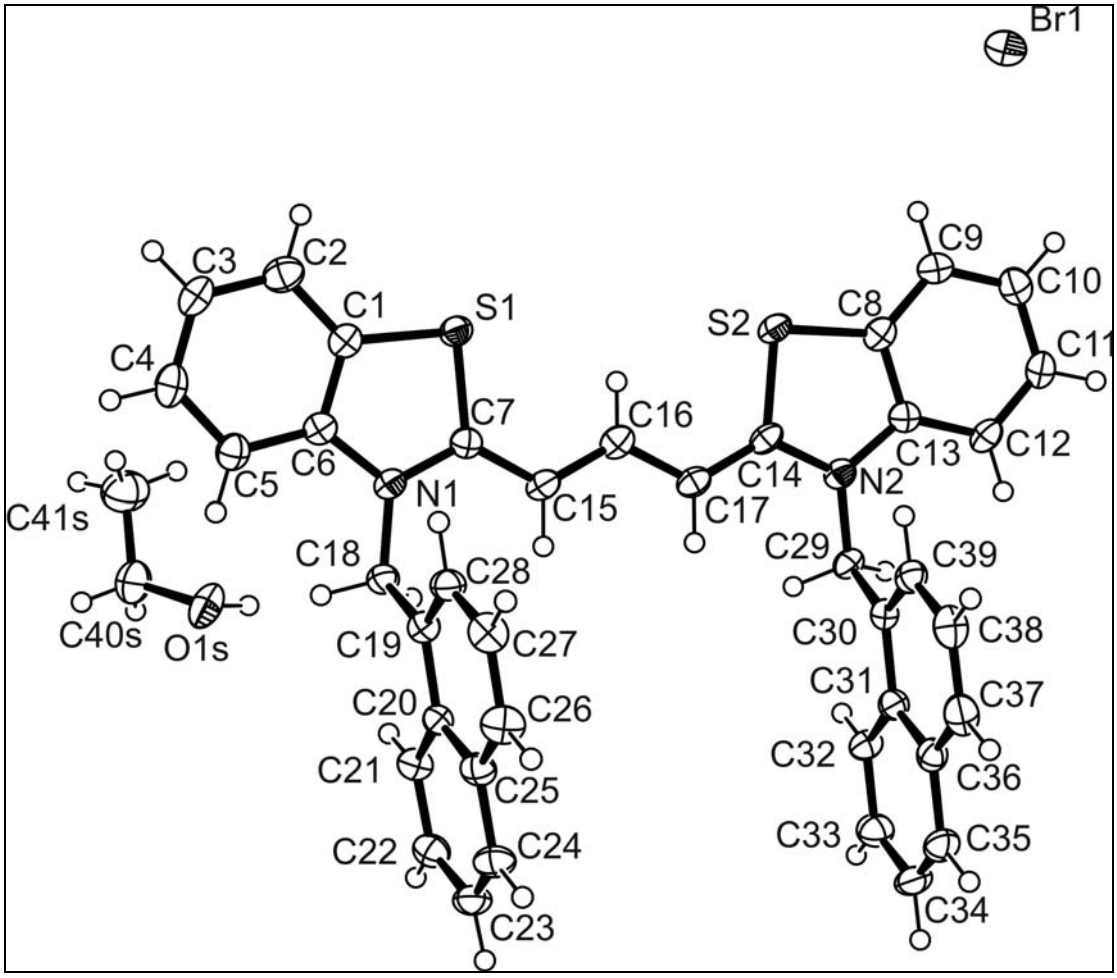

*Figure 8.24. Graphical representation of **51** from X-ray structural studies. Ellipsoids represent greater than 50% probability level.*

06glh011	$C_{41}H_{35}BrN_2OS_2$, FW 715.74	Volume: 1754.77 (11) Å^3
a= 9.0565 (4) Å	B= 12.6289 (3) Å	c= 15.4844 (6) Å
α= 96.735 (2) °	β= 90.565 (2) °	γ= 93.738 (2) °
Triclinic	P-1	R = 7.45%, GoOF= 1.059
Clear Dark Red	Slab	0.4 x 0.26 x 0.04 mm
Z= 2, μ= 1.325 mm^{-1}	λ = 0.71073 Å	120 K

*Table 8.24. X-ray structural data of **51**. Data collected and structure solved by G. Hallworth*

Crystal data of 3,3'-di(4-bromobenzyl)benzocarbocyanine bromide, **52**

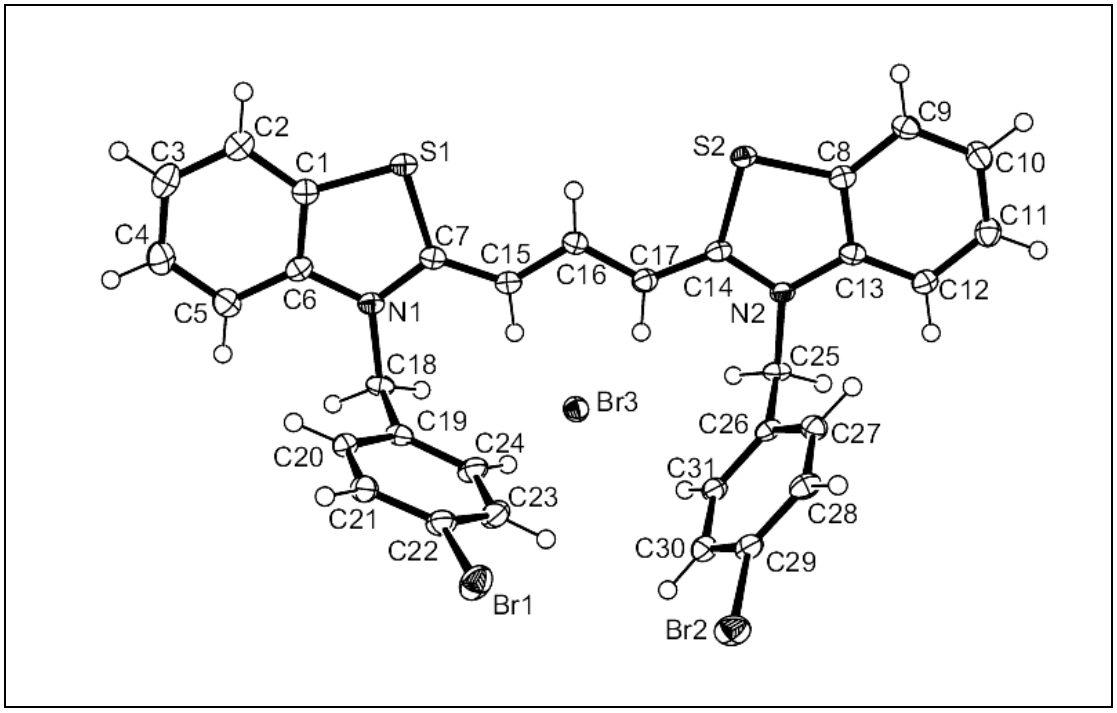

*Figure 8.25. Graphical representation of **52** from X-ray structural studies. Ellipsoids represent greater than 50% probability level.*

06glh002	$C_{31}H_{23}Br_3N_2S_2$, FW 727.36	Volume: 139.03 Å^3
a= 9.7946 (2) Å	b= 10.2816 (2) Å	c= 14.5811 (3) Å
α= 90.2900 (10) °	β= 103.5830 (10) °	γ= 101.7880 (10) °
Triclinic	P-1	R = 3.95%, GoOF= 1.275
Metallic Green	Cut Block	0.2 x 0.2 x 0.1 mm
Z= 2, μ= 4.512 mm^{-1}	λ = 0.71073 Å	120 K

*Table 8.25. X-ray structural data of **52**. Data collected and structure solved by G. Hallworth.*

Crystal data of 5,5'-dichloro-3,3'-diethylbenzothiacarbocyanine Iodide, **53**.

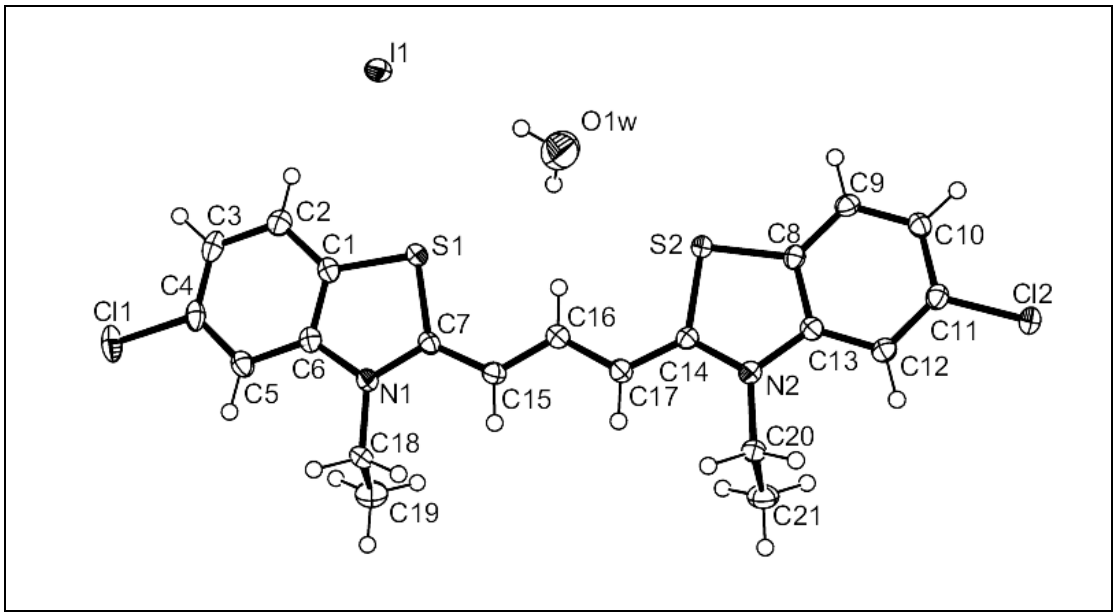

*Figure 8.26. Graphical representation of **53** from X-ray structural studies. Ellipsoids represent greater than 50% probability level.*

06glh008	$C_{21}H_{21}Cl_2IN_2OS_2$, FW 579.32	Volume: 1123.73 (8) Å^3
a= 7.4805 (3) Å	b= 9.7932 (4) Å	c= 16.6109 (7) Å
α= 90.962 (2) °	β= 101.006 (2) °	γ= 109.222 (3) °
Triclinic	P-1	R = 3.38%, GoOF= 1.071
Clear Dark Red	Block	0.4 x 0.2 x 0.02 mm
Z= 2, μ= 1.865 mm^{-1}	λ = 0.71073 Å	120 K

*Table 8.26. X-ray structural data of **53**. Data collected and structure solved by G. Hallworth.*

Crystal data of 3,3'-dibenzyl-5,5'-dichlorobenzothiacarbocyanine bromide, **54**.

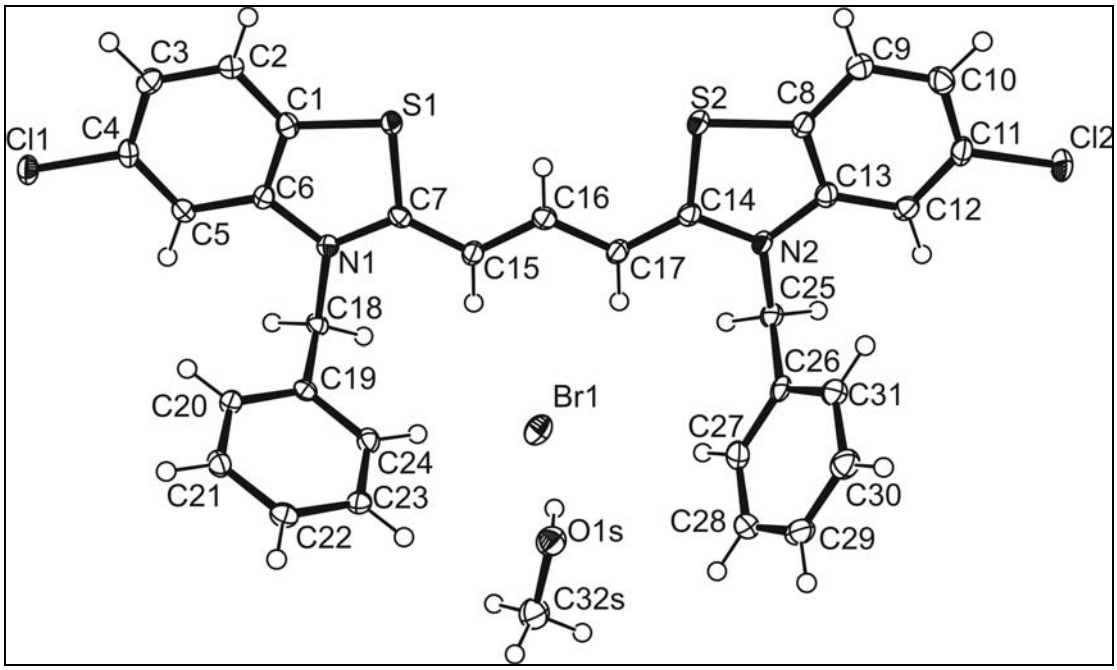

*Figure 8.27. Graphical representation of **54** from X-ray structural studies. Ellipsoids represent greater than 50% probability level.*

07glh002	$C_{32}H_{27}Br_1Cl_2N_2O_1S_2$, FW 670.69	Volume: 1412.25 (10) $Å^3$
a= 9.4922 (4) Å	b= 10.7683 (4) Å	c= 15.5649 (6) Å
α= 109.891 (3) °	β= 97.429 (2) °	γ= 103.975 (3) °
Triclinic	P-1	R = 4.07%, GoOF= 1.084
Metallic Dark Red	Block	0.2 x 0.2 x 0.06 mm
Z= 2, μ= 1.824 mm^{-1}	λ = 0.71073 Å	120 K

*Table 8.27. X-ray structural data of **54**. Data collected and structure solved by G. Hallworth*

Crystal data of 3,3'-diethyl-5,5'-fluoro benzothiacarbocyanine bromide, **55**.

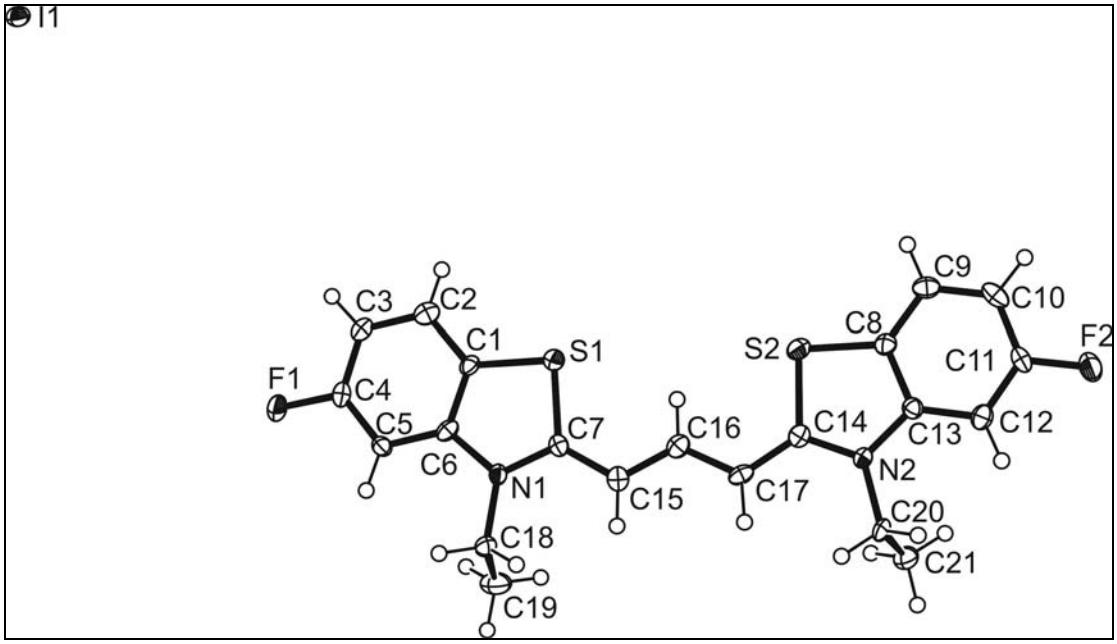

Figure 8.28. Graphical representation of ***55*** *from X-ray structural studies. Ellipsoids represent greater than 50% probability level.*

07glh016	$C_{21}H_{19}F_2I_1N_2S_2$, FW 528.40	Volume: 2054.41 (9) Å^3
a= 7.6018 (2) Å	b= 16.7063 (4) Å	c= 16.5917 (4) Å
α= 90 °	β= 102.842 (2) °	γ= 90 °
Monoclinic	$P2_1/n$	R = 5.77%, GoOF= 1.218
Clear Brown	Needle	0.08 x 0.02 x 0.01 mm
Z= 4, μ= 1.789 mm^{-1}	λ = 0.71073 Å	120 K

Table 8.28. X-ray structural data of ***55****. Data collected and structure solved by G. Hallworth*

Crystal data of 5,5'-Fluoro-3,3'-dibenzylbenzothiacarbocyanine bromide, **56**.

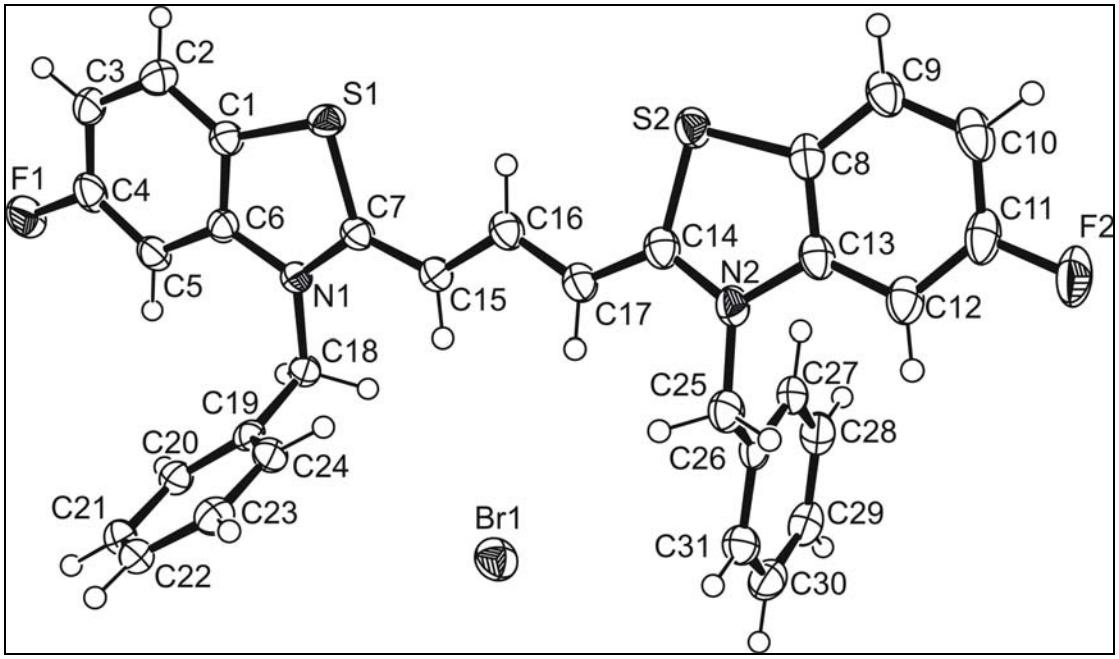

Figure 8.29. Graphical representation of ***56*** *from X-ray structural studies. Ellipsoids represent greater than 50% probability level.*

07glh009	$C_{31}H_{23}BrF_2N_2S_2$, FW 605.54	Volume: 1493.12 (14) $Å^3$
a= 10.7320 (6) Å	b= 11.2346 (6) Å	c= 13.2519 (7) Å
α= 108.265 (4) °	β= 98.564 (3) °	γ= 92.607 (4) °
Triclinic	P-1	R = 5.05 %, GoOF= 1.014
Metallic Dark Blue	Block	0.40 x 0.26 x 0.16 mm
Z= 2, μ= 1.551 mm^{-1}	λ = 0.71073 Å	120 K

Table 8.29. X-ray structural data of ***56****. Data collected and structure solved by G. Hallworth*

Crystal data of 3,3'- di(3-sulfobutyl)-benzothiacarbocyanine, **57**.

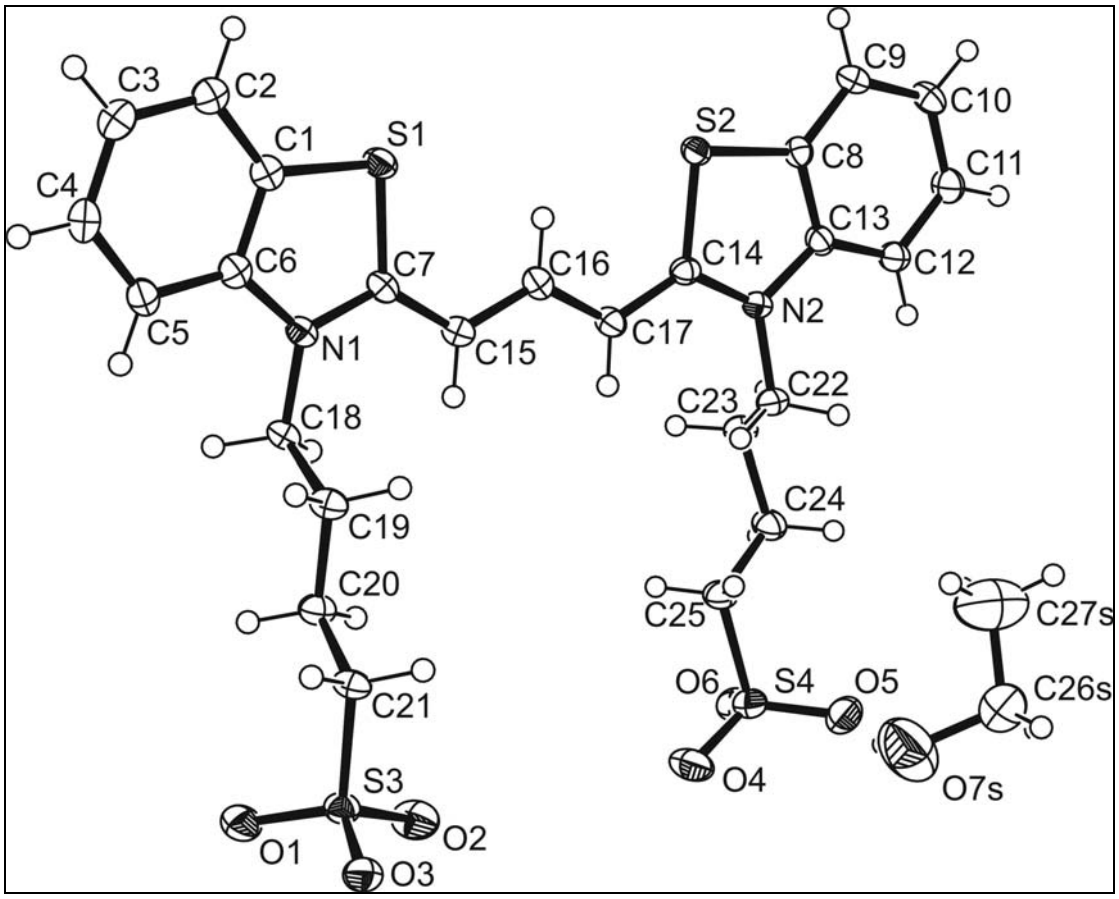

*Figure 8.30. Graphical representation of **57** from X-ray structural studies. Ellipsoids represent greater than 50% probability level.*

07glh003	$C_{27}H_{33}N_2O_7S_4$, FW 625.79	Volume: 1439.75 (6) Å^3
a= 10.0034 (3) Å	b= 12.1643 (3) Å	c= 13.5663 (3) Å
α= 64.2170 (10) °	β= 89.0060 (10) °	γ= 76.6460 (10) °
Triclinic	P-1	R = 6.33%, GoOF= 1.130
Metallic Dark Red	Block	0.08 x 0.06 x 0.03 mm
Z= 2, μ= 0.379 mm^{-1}	λ = 0.71073 Å	120 K

*Table 8.30. X-ray structural data of **57**. Data collected and structure solved by G. Hallworth*

Crystal data of 3,3',9-triethylbenzocarbocyanine iodide, **59**.

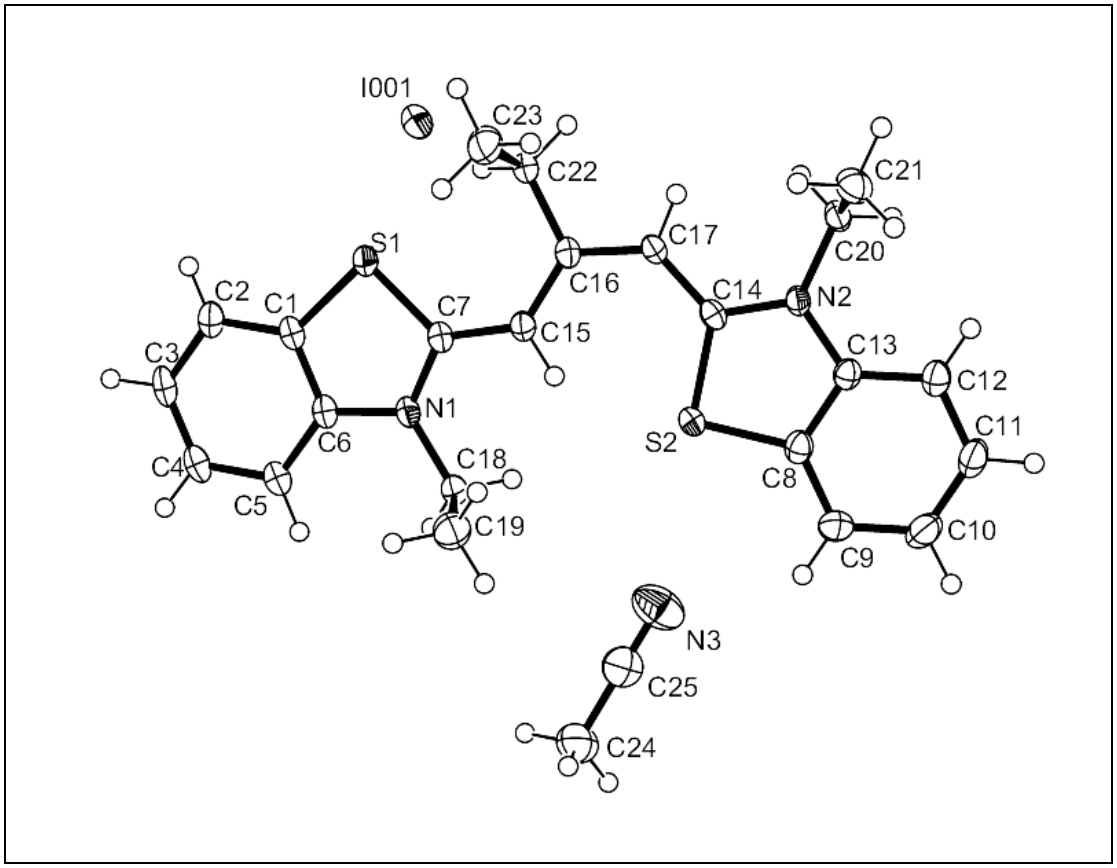

*Figure 8.31. Graphical representation of **59** from X-ray structural studies. Ellipsoids represent greater than 50% probability level.*

06glh001	$C_{25}H_{28}IN_3S_2$, FW 561.54	Volume: 1242.00 Å^3
a= 11.1569 (2) Å	b= 11.3741 (2) Å	c= 12.1218 (2) Å
α= 103.8150 (10) °	β= 116.6450 (10) °	γ= 102.2030 (10) °
Triclinic	P-1	R = 4.09%, GoOF= 1.404
Dark Red	Cut Block	0.2 x 0.16 x 0.12 mm
Z= 2, μ= 1.475 mm^{-1}	λ = 0.71073 Å	120 K

*Table 8.31. X-ray structural data of **59**. Data collected and structure solved by G. Hallworth*

Crystal data of 3,3'-diethyl-9-methylbenzothiacarbocyanine, **61**

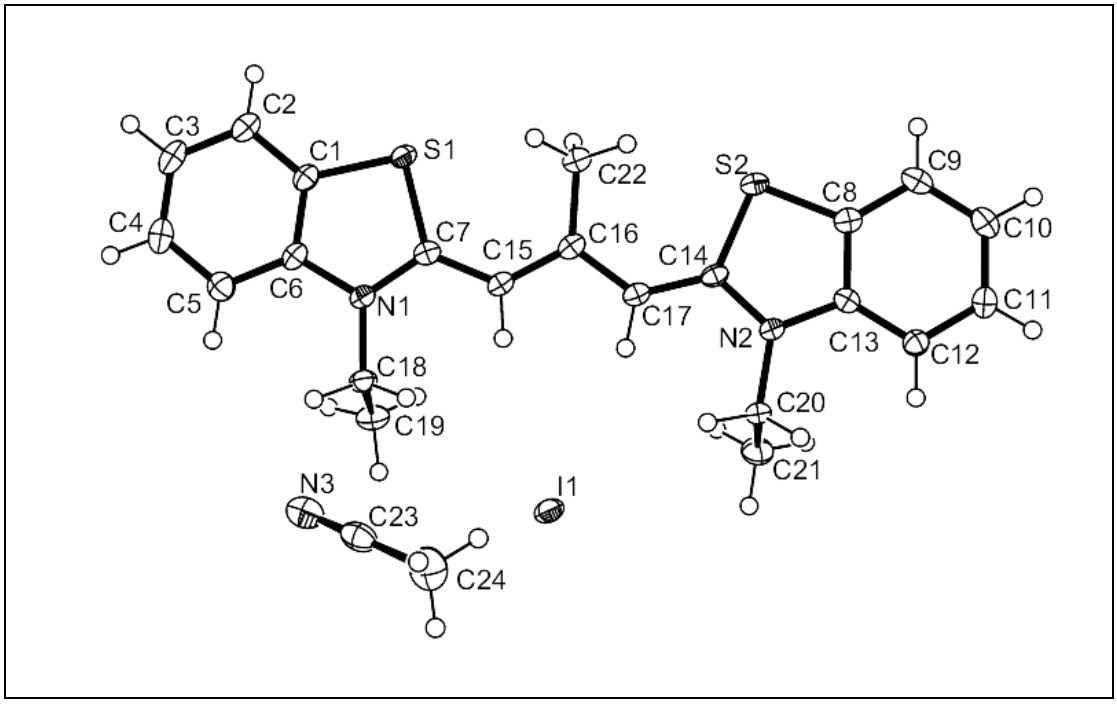

*Figure 8.32. Graphical representation of **61** from X-ray structural studies. Ellipsoids represent greater than 50% probability level.*

05jbo006	$C_{24}H_{26}IN_3S_2$, FW 547.4	Volume: 1161.7 (10) $Å^3$
a= 7.600 (5) Å	b= 11.993 (5) Å	c= 12.894 (5) Å
α= 91.524 (5) °	β= 93.524 (5) °	γ= 97.758 (5) °
Triclinic	P-1	R = 2.63%, GoOF= 1.089
Dark Red	Needle	0.37 x 0.02 x 0.02 mm
Z= 2, μ= 1.54 mm^{-1}	λ = 0.71073 Å	120 K

*Table 8.32. X-ray structural data of **61**. Data collected by J Orton and structure solved by G. Hallworth.*

8.4. Physical Experiments

8.4.1 Extinction coefficients

The dyes were initially dissolved in MeOH resulting in a bulk solution. Aquilots of the bulk solution were diluted further to produce the sample solutions with concentrations shown below. A UV-visible spectrum was then obtained for each sample from which the λ_{max} was extracted and the extinction coefficient (ε) calculated using equation:.

$\varepsilon = A/Cl$ (where A= absorbance, C= concentration and l= pathlength)

Molecule	Concentration Range/ M	Y-intercept	ε/ $M^{-1}cm^{-1}$	λ_{max}
2a	5.02×10^{-6}- 2.51×10^{-5}	0.1868	126460	556
3f	4.08×10^{-6}- 1.21×10^{-5}	0.0032	66484	423
5a	4.02×10^{-6}- 1.21×10^{-5}	0.0402	154150	482
11	3.92×10^{-6}- 1.20×10^{-5}	0.0074	90060	548
45b	4.03×10^{-6}- 1.21×10^{-5}	-0.0122	93000	428
46b	4.06×10^{-6}- 1.20×10^{-5}	0.0088	104162	426
48	4.05×10^{-6}- 1.20×10^{-5}	0.0268	151744	481
49	3.98×10^{-6}- 1.22×10^{-5}	0.0104	168272	560
50	4.12×10^{-6}- 1.21×10^{-5}	0.0234	139754	561
51	3.96×10^{-6}- 1.20×10^{-5}	0.0342	159380	561
52	3.88×10^{-6}- 1.19×10^{-5}	0.0044	171558	561
53	4.00×10^{-6}- 1.20×10^{-5}	0.0018	187502	561
54	3.96×10^{-6}- 1.19×10^{-5}	0.051	166054	566
55	4.03×10^{-6}- 1.20×10^{-5}	0.05	176662	561
56	3.93×10^{-6}- 1.21×10^{-5}	0.0438	172112	566
57	3.95×10^{-6}- 1.16×10^{-5}	0.0094	122758	558
58	3.92×10^{-6}- 1.21×10^{-5}	0.0142	133616	558
59	4.06×10^{-6}- 1.19×10^{-5}	0.06	136696	546
64a	4.01×10^{-6}- 1.20×10^{-5}	-0.0058	73080	430
67	3.91×10^{-6}- 1.20×10^{-5}	0.0648	222880	584
68	3.95×10^{-6}- 1.21×10^{-5}	0.1182	260492	658
70	3.79×10^{-6}- 1.16×10^{-5}	0.0606	239220	659

8.4.2. Fluorescence studies of non-aggregating dyes

The dyes were dissolved in MeOH resulting in a bulk solution. Aquilots of the bulk solution were then diluted further to produce the sample solutions. The emission spectrum of each sample was then measured enabling the data shown below to be extracted.

[Lab notebook reference: 4981-31]

Dye	Concentration Range	Excitation λ/ nm	Shift λ_{max}/ nm	Max emission/ A.U
2a	8.20×10^{-7}- 7.99×10^{-6}	556	7	501
5a	8.13×10^{-7}- 8.13×10^{-6}	482	5	1570
11	7.96×10^{-7}- 5.53×10^{-6}	561	8.5	71
48	8.10×10^{-7}- 8.00×10^{-6}	482	5	1218
49	8.10×10^{-7}- 8.01×10^{-6}	560	6.5	726
50	8.05×10^{-7}- 8.00×10^{-6}	561	7	485
51	7.90×10^{-7}- 8.00×10^{-6}	561	7	883
52	8.18×10^{-7}- 7.79×10^{-6}	561	6	778
53	8.00×10^{-7}- 8.00×10^{-6}	561	7	649
54	7.76×10^{-7}- 8.02×10^{-6}	566	7.5	833
55	7.64×10^{-7}- 8.00×10^{-6}	560	7	498
56	7.83×10^{-7}- 8.02×10^{-6}	560	6.5	700
57	8.70×10^{-7}- 1.16×10^{-5}	558	7	675
58	8.15×10^{-7}- 8.92×10^{-6}	556	6	638
59	8.29×10^{-7}- 8.00×10^{-6}	556	10.5	69

8.4.3 Solvent Effects

A bulk solution of **57** was prepared in water (**X** M). Aquilots of the bulk solution were diluted further with aqueous-MeOH (**Y**%) solution. A UV-visible spectrum was obtained for each sample to observe the effect of the increasing MeOH concentration had on the aggregation.

[Lab book reference code: 4632/62-A]

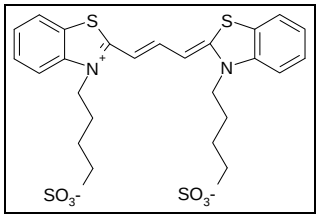

Solution	**Y**: % MeOH	**X**: [Dye]/ mM
A	10	0.025
B	20	0.025
C	30	0.025
D	40	0.025
E	50	0.025
F	60	0.025
G	70	0.025
H	80	0.025

8.4.4 Varying concentration of water-soluble dyes- UV-Visible spectroscopy studies

A bulk solution was prepared(**X** M) in water. Samples were prepared by dissolving **Y** mL of the bulk solution into 5 mL of solvent resulting in a sample concentration of **A** M. Various pathlengths were used.

Dye **11** concentration profile

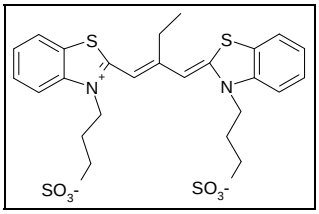

Bulk solution. **X**: 0.119 M (0.69 mg in 10 mL H_2O).

1 mm cuvette used

[Lab book reference code: 4831/86]

Solution	**Y** (Volume bulk/ ml)	**A** ([**11**]/ M)
A	0.084	2.00E-06
B	0.210	5.01E-06
C	0.315	7.51E-06
D	0.420	1.00E-05
DI	0.800	1.91E-05
E	1.000	2.38E-05
F	2.097	5.00E-05
G	3.000	7.15E-05
H	5.000	1.19E-04

Dye **11** concentration profile

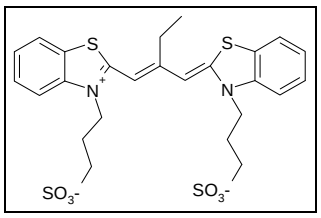

Bulk solution. **X**: 0.0898 M (0.52 mg in 10 mL H_2O).

5 mm cuvettes used

[Lab book reference code: 4831-91]

Solution	**Y** (Volume bulk/ ml)	**A** ([**11**]/ M)
A	0.111	2.00E-06
B	0.334	6.00E-06
C	0.557	1.00E-05
D	0.835	1.50E-05
E	1.113	2.00E-05
F	1.670	3.00E-05
G	2.227	4.00E-05
H	2.784	5.00E-05
I	3.340	6.00E-06

Dye **58** concentration profile

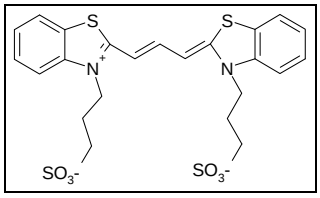

Bulk solution. **X**: 1.07 mM (0.52 mg in 10 mL H_2O).

1 mm cuvettes used

[Lab notebook reference: 4831-11]

Solution	**Y** (Volume bulk/ ml)	**A** ([**58**]/ M)
A	0.1*	5.00E-07
B	0.2*	1.00E-06
C	1.00*	5.00E-06
D	2.00*	1.00E-05
E	0.152	2.50E-05
F	0.234	5.00E-05
G	0.351	7.50E-05
H	0.468	1.00E-04
I	1.17	2.50E-04
J	2.34	5.00E-07
K	3.51	1.00E-06

*Diluted from 2.50E-05 bulk solution

Dye **57** concentration profile

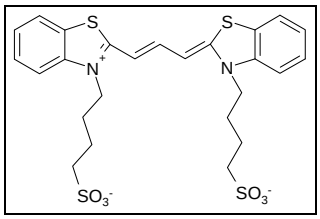

Bulk solution. **X**: 1.07 mM (0.52 mg in 10 mL H_2O).

5 mm cuvettes used

[Lab notebook reference: 4632-33]

Solution	**Y** (Volume bulk/ ml)	**A** ([**57**]/ M)
A	5	9.74E-05
B	3.637	7.09E-05
C	2.425	4.72E-05
D	2.425*	2.36E-05
E	0.970*	9.45E-06
F	0.727*	7.09E-06
G	0.485*	4.72E-06
H	0.2422*	2.36E-06
I	0.097*	9.45E-07

* 10 mL solutions

8.4.5 Varying concentration of water-insoluble dyes- UV-Visible spectroscopy studies

The bulk solution (**A** M in **B** % MeOH/water solution) was diluted further (**C** mL into 5 mL) by **B** % MeOH/water and made up with water resulting in an overall concentration of **D** M and 10 % MeOH sample. Various cuvette pathlengths were used. It is important to note that concentrations are approx. as dye tended to stick to glass.

Concentration profile of **49**

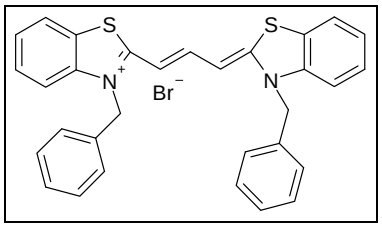

Bulk solution. **A**: 0.17 mM (0.96 mg in 10 mL MeOH/H_2O). **B**: 25% MeOH solutions
Samples: **X**: 10% MeOH, 5 mm cuvettes used.
[Lab notebook reference: 4981-43D]

Solution	C: Volume bulk solution used/ mL	Amount 25% MeOH solution used/ mL	D: [49]/M
A	0.12	1.88	$4.05x10^{-06}$
B	0.24	1.76	$8.10x10^{-06}$
C	0.36	1.64	$1.21x10^{-05}$
D	0.53	1.47	$1.79\ x10^{-05}$
E	0.65	1.35	$2.19\ x10^{-05}$
F	1.19	0.81	$4.02\ x10^{-05}$

Concentration profile of **54**

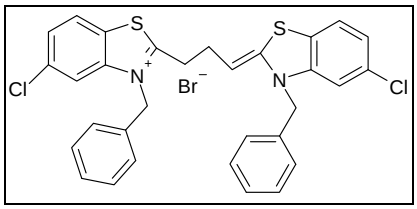

Bulk solution. **A**: 0.11 mM (0.68 mg in 10 mL MeOH/H_2O). **B**: 25% MeOH solutions
Samples: **X**: 10% MeOH, 5 mm cuvettes used,
[Lab notebook reference: 4981-43E]

Solution	C: Volume bulk solution used/ mL	Amount 25% MeOH solution used/ mL	D: [54]/M
A	0.19	1.81	$4.06x10^{-06}$
B	0.37	1.63	$7.9x10^{-06}$
C	0.56	1.44	$1.2x10^{-05}$
D	0.84	1.16	$1.79\ x10^{-05}$
E	1	1	$2.14\ x10^{-05}$
F	1.87	0.13	$3.99\ x10^{-05}$

Concentration profile of **56**

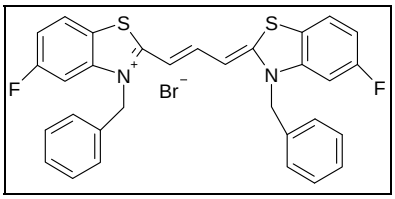

Bulk solution. **A**: 0.13 mM (0.81 mg in 10 mL MeOH/H_2O). **B**: 25% MeOH solutions
Samples: **X**: 10% MeOH, 5 mm cuvettes used.
[Lab notebook reference: 4981-43F]

Solution	C: Volume bulk solution used/ mL	Amount 25% MeOH solution used/ mL	D: [56]/M
A	0.15	1.85	$4.02x10^{-06}$
B	0.3	1.7	$8.03x10^{-06}$
C	0.45	1.55	$1.2x10^{-05}$
D	0.67	1.33	$1.79\ x10^{-05}$
E	0.82	1.18	$2.2\ x10^{-05}$
F	1.49	0.51	$3.99\ x10^{-05}$

Concentration profile of **52**

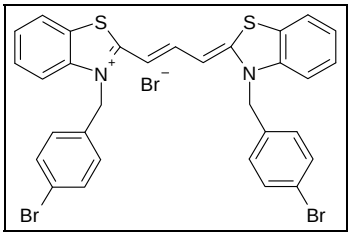

Bulk solution. **A**: 0.07 mM (0.54 mg in 10 mL MeOH/H_2O). **B**: 25% MeOH solutions
Samples: **X**: 10% MeOH, 5 mm cuvettes used.
[Lab notebook reference: 4981-46I]

Solution	C: Volume bulk solution used/ mL	Amount 25% MeOH solution used/ mL	D: [52]/M
A	0.27	1.73	$4.01\ x10^{-06}$
B	0.54	1.46	$8.02\ x10^{-06}$
C	0.81	1.19	$1.2\ x10^{-05}$
D	1.21	0.79	$1.80\ x10^{-05}$
E	1.48	0.52	$2.2\ x10^{-05}$
F	2	0	$2.97\ x10^{-05}$

8.4.6. Salt-induced aggregation - UV-visible spectroscopy studies

A bulk dye solution of **X** M was prepared. Salt solutions were prepared with a range of concentrations in volumetric flasks but were not made up to the mark to allow for the dye solution to be added. **Y** mL of bulk solution was added to each of the salt solutions and water added make up to the mark resulting in a **Z** M sample solution. This solution was then shaken by hand and the spectra obtained at 60 secs. Each spectrum was recorded the same time after addition of dye. It was important to add the dye to a salt solution because of varying solubilities.

Dye **11** in the presence of Na_2SO_4

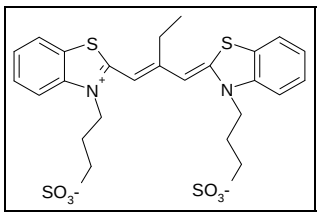

Bulk solution. **X**: 0.122 M (1.76 mg in 25 mL H_2O)
Sample solutions. **Y**: 0.411 mL bulk solution in 5 ml volumetric. **Z**: 1 x 10^{-5} M, 1 cm cuvettes used.
[Lab notebook reference: 4981-83]

Solution	Amount Na_2SO_4/ g	$[Na_2SO_4]$/ M
AA	0	0.0000
AB	0.24	0.3380
AC	0.33	0.4648
AD	0.43	0.6056
AE	0.52	0.7324
AF	0.61	0.8592
AG	0.71	1.0000
AH	0.82	1.1549
AI	0.91	1.2817
AJ	1.05	1.4789
AK	1.23	1.7324
AL	1.36	1.9155

Dye **11** in the presence of Na_2SO_4 of varying concentrations

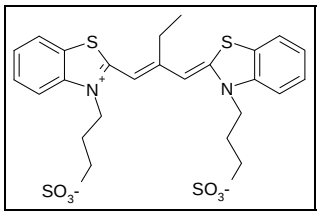

1 cm cuvettes used.

[Lab notebook reference: 4831-66]

Z: [11]/ M	$2.25x10^{-5}$	$1x10^{-5}$	$1x10^{-6}$
Solution	**$[Na_2SO_4]$/ M**		
A	0.000	0.000	0.000
B	0.136	0.141	0.162
C	0.289	0.281	0.306
D	0.424	0.423	0.414
E	0.716	0.562	0.575
F	0.980	0.708	0.725
G	1.258	0.846	0.841
H	1.542	0.983	1.005
I	1.683	1.132	1.136
J	1.844	1.391	1.288
K	2.110	1.423	1.530
L	-	-	1.685
M	-	-	1.856

Dye **11** in the presence of NaCl

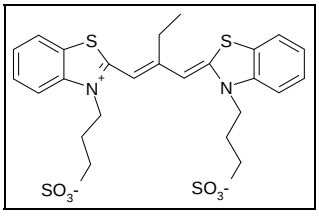

Bulk solution. **X**: 0.122 M (1.76 mg in 25 mL H_2O)

Sample solutions. **Y**: 0.411 mL bulk solution in 5 ml volumetric. **Z**: 1 x 10^{-5} M, 1 cm cuvettes used.

[Lab notebook reference: 4831-83]

Solution	Amount NaCl/ g	[NaCl]/ M
BA	0	0.000
BB	0.2	0.690
BC	0.41	1.414
BD	0.63	2.172
BE	0.84	2.897
BF	1	3.448
BG	1.2	4.138
BH	1.38	4.759
BI	1.54	5.310

Dye **11** in the presence of NaCl and Na_2SO_4

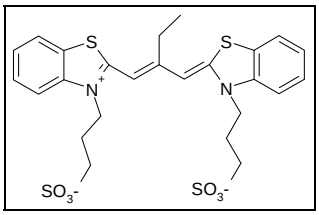

Bulk solution. **X**: 0.122 M (1.76 mg in 25 mL H_2O)
Sample solutions. **Y**: 0.411 mL bulk solution in 5 ml volumetric. **Z**: 1 x 10^{-5} M, 1 cm cuvettes used.
[Lab notebook reference: 4831-83]

Solution	Amount NaCl/ g	[NaCl]/ M	Amount Na_2SO_4/ g	[Na_2SO_4]/ M
CA	0	0.000	1.36	1.915
CB	0.22	0.759	1.09	1.532
CC	0.44	1.517	0.82	1.149
CD	0.67	2.310	0.54	0.766
CE	0.89	3.069	0.27	0.383
CF	1.11	3.828	0	0.000

Comparison of **2a** and **5a** in the presence of Na_2SO_4

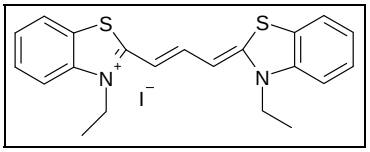

Bulk solution. **X**: 0.485 mM (2.39 mg in 10 mL 20% MeOH/H_2O)
Sample solutions. **Y**: 0.103 mL bulk solution in 5 ml volumetric. **Z**: 1 x 10^{-5} M [overall 3% MeOH].
1 cm cuvettes used.
[Lab notebook reference: 4632-69A]

Solution	Amount Na_2SO_4 added/ g	$[Na_2SO_4]$/ M
AA	0.206	0.290
AB	0.389	0.547
AC	0.505	0.712
AD	0.597	0.840
AE	0.706	0.994
AF	0.796	1.121
AG	0.908	1.279
AH	1.082	1.524

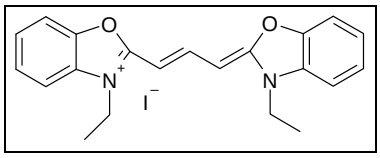

Bulk solution. **X**: 0.513 mM (2.36 mg in 10 mL 20% MeOH/H_2O)

Sample solutions. **Y**: 0.097 mL bulk solution in 5 ml volumetric. **Z**: 1 x 10^{-5} M [overall 3% MeOH]

1 cm cuvettes used.

[Lab notebook reference: 4632-69B]

Solution	Amount Na_2SO_4 added/ g	$[Na_2SO_4]$/ M
BA	0.202	0.284
BB	0.416	0.586
BC	0.506	0.713
BD	0.604	0.851
BE	0.699	0.985
BF	0.796	1.121
BG	0.895	1.261
BH	1.082	1.524

Dye **51** in the presence of $(NH_4)_2SO_4$

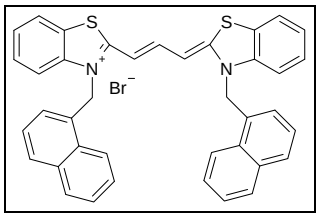

Bulk solution. **X**: 0.175 mM (1.17 mg in 10 mL 25% MeOH/H_2O)

Sample solutions. **Y**: 0.29 mL bulk solution in 5 ml volumetric. **Z**: 1 x 10^{-5} M [Overall 5% MeOH], 1 cm cuvettes used

[Lab notebook reference code: 4981-63]

Solution	Amount $(NH_4)_2SO_4$ / g	$[(NH_4)_2SO_4]$/ M
A	0	0
B	0.11	0.167
C	0.22	0.333
D	0.3	0.455
E	0.43	0.652
F	0.54	0.818
G	0.73	1.106
H	0.85	1.288
I	1.06	1.606
J	1.2	1.818

8.4.7 Emission Spectroscopy Studies

A bulk dye solution of **X** M in MeOH/water was prepared. Salt solutions were prepared with a range of concentrations in volumetric flasks but were not made up to the mark to allow for the dye solution to be added. **Y** mL of bulk solution was added to each of the salt solutions and water added make up to the mark resulting in a **Z** M sample solution. This solution was then shaken by hand and the spectra obtained at 60 secs. Each spectrum was recorded the same time after addition of dye. It was important to add the dye to a salt solution because of varying solubilities.

Dye **51** in the presence of NH_4Cl – Fluorescence study

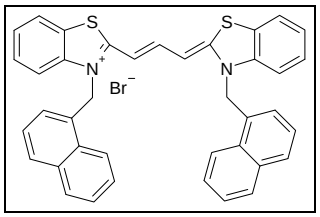

Bulk solution. **X**: 0.181 mM (1.21 mg in 10 mL 25% MeOH/H_2O)

Sample solutions. **Y**: 0.28 mL bulk solution in 5 ml volumetric.

Z: 1.01 x 10^{-5} M [overall 5% MeOH].

Excitation λ: 561 nm, scan range 400- 800 nm

[Lab notebook reference code: 4981-66B]

Solution	Amount NH_4Cl/ g	[NH_4Cl]/ M
BA	0	0
BB	0.05	0.188679
BC	0.1	0.377358
BD	0.2	0.754717
BE	0.3	1.132075
BF	0.43	1.622642
BG	0.5	1.886792
BH	0.68	2.566038
BI	0.93	3.509434

Concentration profile of Dye **58**- Fluorescence study

A bulk solution was prepared(**X** M) in water. Samples were prepared by dissolving **Y** mL of the bulk solution into 5 mL of solvent resulting in a sample concentration of **A** M. Various pathlengths were used.

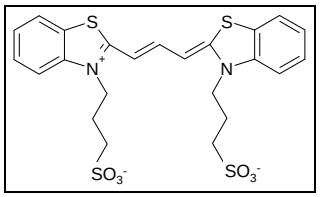

Bulk solution. **X**: 0.114 mM (0.63 mg in 10 mL H_2O)

Excitation λ: 556 nm, scan range 500- 800 nm

[Lab notebook reference code: 4981-54B]

Solution	Y: Vol bulk soln / ml	A: [Dye]/ M
BA	0.17	3.89E-06
BB	0.35	8E-06
BC	0.52	1.19E-05
BD	0.7	1.6E-05
BE	0.87	1.99E-05
BF	1	2.29E-05
BG	5	0.000114

Chapter 9

References

1 Beer, P. D., P. A. Gale, et al. Supramolecular Chemistry, 1999, Oxford, Oxford University Press.

2 Hunter, C. A. and J. K. M. Sanders, *J. Am. Chem. Soc*. 1990, **112**, 5525 - 5534.

3 Dixon, D. W. and V. Steullet. *J. Inorg. Biochem*., 1998, **69**, 25 - 32.

4 Mishra, A., R. K. Behera, et al. *Chem. Rev.*, 2000, **100**, 1973 - 2011.

5 Shklyarevskiy, I. O., M. I. Boamfa, et al., *J. Chem. Phys.,*, 2002, **116**(19), 8407 - 8410.

6 Xiang, J., X. Yang, et al., *J. Colloid Interf.*, 2003, **258**, 198 - 205.

7 Yagai, S., T. Kinoshita, et al.. *J. Am. Chem. Soc.*, 2007, **129**(43): 13277-13287.

8 Huang, T. J., B. Brough, et al., *Appl. Phys. Lett.*, 2004, **85**(22), 5391 - 5393.

9 Langhals, H. and R. Ismael, *Eu. J. Org. Chem.*, 1998, 1915 - 1917.

9a Berna, J., D. A. Leigh, et al., *Nature Materia*ls, 2005, **4**, 704 - 710.

10 Deng, W. Q., A. H. Flood, et al. (2005). *J. Am. Chem. Soc.,* 2005, **127**: 15994 - 15995.

11 Sturmer, D. M. (1977). Syntheses and Properties of Cyanine and Related Dyes. Special Topics in Heterocyclic Chemistry. A. Weissberger and E. C. Taylor. New York, Wiley.

12 Harrison, W. H., D. L. Mateer, et al., *J. Phys. Chem.*, 1966, **100**, 2310 - 2321.

13 West, W. and S. Pearce, *J. Phys. Chem.*, 1965, **69**(6), 1894 - 1903.

14 Scheibe, G., *Angew. Chem. Int. Ed.,* 1936, **49**, 563.

15 Jelly, E. E., *Nature*, 1936, **138**, 1009.

16 Beckers, E. H. A., S. C. J. Meskers, et al., *J. Am. Chem. Soc,* 2006, **128**, 649-657.

17 Mees, C. E. K., The Theory of the Photographic Process. New York, Macmillan, 1946

18 Mal'tsev, E. I., D. A. Lypenko, et al., *Appl. Phys. Lett*., 1999, **75**(13) 1896 - 1898.

19 Chibisov, A. K., H. Gorner, et al., *Chem. Phys. Lett*., 2004, **390**, 240 - 245.

20 Nuesch, F., A. Faes, et al., *J. Mater Sci*., 2004, **40**, 1353 - 1357.
21 Knudtson, J. T. and E. M. Eyring., *J. Phys. Chem.*, 1974, **78**(23), 1974.
22 Sahyun, M. R. V. and J. T. Blair. *J. Photochem. Photobio.* A, 1997, **104**, 179 - 187.
23 Zhang, Y., J. Xiang, et al., *Dyes and Pigments*, 2006, **76**(1), 88 -93.
24 Baraldi, I., M. Caselli, et al., *Chem. Phys*., 2002, **275**, 149 -165.
25 Slavnova, T. D., A. K. Chibisov, et al., *J. Phys. Chem.* A, 2005, **109**, 4758 - 4765.
26 Chibisov, A. K., T. D. Slavnova, et al., *Chem. Phys. Lett.,* 2006, **424**, 307 - 311.
27 Takahashi, D., H. Oda, et al., *Dyes and Pigments*, 2005, **66**, 1 - 6.
28 Reich, C., W. D. Pandole, et al., *Photogr. Sci. Eng.*, 1973, **17**(3), 334 - 341.
29 Honda, C. and H. Hada, *Photogr. Sci. Eng.*, 1977, **21**(2), 97 - 102.
30 Berlepsch, H. v., S. Kirstein, et al., *Langmuir*, 2002, **18**(20), 7699 -7705.
31 Chen, X., J. Guo, et al., *J. Photochem. Photobio. A*, 2005, **171**, 231 - 236.
32 Chen, X. and Z. G. Yao, *Chem. J. Chin. Univ.*, 1966, **17**, 1613 - 1616.
33 Kabatc, J. and J. Paczkowski, *Dyes and Pigments*, 2004, **61**, 1 - 16.
34 West, W., S. Pearce, et al. *J. Phys. Chem.*, 1967, **71**(5), 1316 - 1326.
35 Khairutdinov, R. F. and N. Serpone, *J. Phys. Chem.* B, 1997, **101**, 2602 - 2610.
36 Struganova, I. A., M. Hazell, et al., *J. Phys. Chem.* A, 2003, **107**, 2650 -2656.
37 Herz, A. H., *Photogr. Sci. Eng.*, 1974, **18**(3), 323 - 335.
38 Zhang, Y., J. Xiang, et al., *Chem. Lett*., 2006, **35**(11), 1316 - 1317.
39 Mukerjee, P. and A. K. Ghosh,. *J. Am. Chem. Soc.,* 1970, **92**(22), 6403 - 6407.
40 Struganova, I. *J. Phys. Chem.* A, 2000, **104**, 9670 - 9674.
41 Yamaguchi, A., N. Kometani, et al., *J. Phys. Chem. B*, 2005,109: 1408 - 1414.
42 Atkins, D. L., S. Ozcelik, et al., *J. Phys. Chem.* A, 1997, **101**, 3251 - 3259.
43 Pasterneck, R. F., C. Fleming, et al., *Biophysical Journal*, 2000, **79**, 550 - 560.
44 Kopainsky, B., J. K. Hallermeier, et al., *Chem. Phys. Lett*., 1982, **87**(1), 7 - 10.
45 Caselli, M., L. Latterini, et al., *Phys. Chem. Chem. Phys*., 2004, **6**, 3857 - 3863.
46 Kopainsky, B., J. K. Hallermeier, et al., *Chem. Phys. Lett*., 1981, **83**(3), 498 - 502.

47 Hannah, K. C. and B. A. Armitage, *Accounts of Chemical Research*, 2004, **37**, 845 - 853.

48 Koner, A. L. and W. M. Nau, *Supramolecular Chemistry*, 2007, **19**(1-2), 55 - 66.

49 Chibisov, A. K., G. V. Zakharova, et al., *Phys. Chem. Chem. Phys.*, 1999, **1**, 1455 - 1460.

50 Slavnova, T. D., A. K. Chibisov, et al. (2002). *J. Phys. Chem.*, A 106: 10985 - 10990.

51 Das, S., K. G. Thomas, et al., *J. Chem. Soc. Trans.,* 1992, **88**(23), 3419 - 3422.

52 Mohanty, J. and W. M. Nau, *Angew. Chemie Int. Ed*., 2005, **44**, 3750 - 3754.

53 Huang, W., S. Wang, et al., *J. Chem. Phys*., 2002, **117**(14), 6614 - 6617.

54 Buston, J. E. H., J. R. Young, et al., *Chem. Comm*., 2000, 905 - 906.

55 Arunkumar, E., C. C. Forbes, et al., *J. Am. Chem. Soc.,* 2005, **127**, 3288 - 3289.

56 Allen, F. H., *Acta Cryst. B*, 2002, **58**, 380- 388.

57 Smith, D. L, *Photogr. Sci. Eng.,* 1974, **18**(3), 309 - 322.

58 P Horton, *PhD Thesis*, University of Southampton, 2001.

59 Nakatsu, K., H. Yoshioka, et al., *Chem. Lett*, 1972, 339 - 340.

60 Czikklely, V., H. D. Forsterling, et al., *Chem. Phys. Lett*, 1970, **6**(1), 11 - 14.

61 Kim, J. S., R. Kodagahally, et al., *Talanta*, 2005, **67**, 947 - 954.

62 Czikklely, V., H. D. Forsterling, et al., *Chem. Phys. Lett*., 1970, **6**(3).

63 Chen, C., X. Qi, et al., *J. Photochem. Photobio.* A,1997, **109**, 155 - 158.

63a Meng, F., K. Chen, et al., *Appl. Phys. Lett*., 2003, **82**(21), 3788 - 3790.

64 Gil, A., D. Mobius, et al., *Langmuir*, 2003, **19**, 6430 -6435.

65 Vranken, N., M. V. d. Auweraer, et al., *Langmuir*, 2000, **16**, 9518 - 9526.

66 Klanderman, B. H. and D. C. Hoesterey, *J. Phys. Chem.*, 1969, **51**(1): 377 - 382.

67 Ficken, G. E., Cyanine Dyes. The Chemistry of Synthetic Dyes. K. Venkataraman. London, Academic Press. 1971, 4th edition.

68 Fisher, N. I. and F. M. Hamer, *J. Chem. Soc*., 1930, 2502 - 2510.

69 Fisher, N. I. and F. M. Hamer, *J. Chem. Soc*, 1934, 962 - 965.

70 Koral, M., A. Leifer, et al., *J. Chem. Eng. Data*, 1965, **10**(1), 67 - 70.

71 Brooker, L. G. S. and F. L. White, *J. Am. Chem. Soc., 1935,* **57**, 2480 - 2488.

72 Mushkalo, I. L., G. G. Dyadyusha, et al., *Tet. Lett*. 1980, **21**, 2977 - 2980.

73 Ibrayev, N. K., A. A. Ishchenko, et al., *J. Lumin*., 2000, **90**, 81 - 88.

74 Kazymov, A. V. and E. P. Shchelkina, *J. Org. Chem. USSR*-Eng. Trans., 1971, **7**, 2038 - 2039.

75 Koral, M., D. Bonis, et al. *J. Chem. Eng. Data*., 1964, **9**(3), 406 - 407.

76 Clark, L. M., *J. Chem. Soc*., 1928, 2313.

77 Galin, M., A. Chapoton, et al. (1993). *J. Chem. Soc*.,Perkin Transactions 2, 1993, **3**, 545- 553.

78 Herz, A. H., *Adv. Colloid Interface Science*, 1977, **8,** 237 - 298.

79 Henrichs, P. M. and S. Gross, *J. Am. Chem. Soc.,* 1976, **98**(23), 7169 - 7175.

80 Weist, R. C., CRC Handbook of Chemistry and Physics. Florida, CRC Press. 1978

81 Renikuntla, B. R., H. C. Rose, et al., *Org. Lett*., 2004, **6**(6), 909- 912

82 Skoog, D. A., D. M. West, et al. Fundamentals of Analytical Chemistry, Saunders College Publishing. 1997

83 Frey, J. G. *Private Communication*. 2008

84 Howard, A. G. Aquatic Environmental Chemistry. Oxford, Oxford University Press. 1998

85 Rowe, E. L. *J. Pharm. Sci,* 1972, **61**(5): 781-782.

86 Srenger, E. M. *Acta Cryst. B.,* 1970, **30**, 1911 -1914.

87 Desiraju, G. R. Crystal Engineering: The Design of Organic Solids (Materials Science Monograph). 1989, Amsterdam, Elsevier..

88 Sheldrick, G. M. SHELXL-97 - A Program for Crystal Structure Refinement WinGX Version. 1997, University of Goettingen, Germany..

89 Macrea, C. F., I. J. Bruno, et al*., J. Appl. Cryst*., 2008, **41**, 466- 470.

90 Wells, A. F. *Struct. Inorg. Chem.,* Claredon Press. 1984.

91 Kazheva, O. N., G. G. Alexsandrov, et al., *Russ. J. Coord. Chem*., 2004, **30**(8), 599-603.

92 Hallworth, G., P. Horton, et al. *In Press*, 2008

93 Halper, S. R. and S. M. Cohen, *Inorg. Chem*., 2005, **44**, 4319 - 4141.

93a Tsuzki, S., T. Uchimaru, et al., *J. Phys. Chem.*, A, 2003, **107**, 7962 - 7968.

94 Gelbrich, T. and M. B. Hursthouse, *Cryst. Eng. Comm*., 2005, **7**(53), 324 - 336.

95 Muro, N. H., L. R. Hanton, et al., *Acta. Cryst*., 2008, **E64** M574.

96 Butler, D. *Nature*, 2005, **436**, 20 - 21.

97 http://www.scientific-computing.com/scwjunjul06elns.html (2006). 29/06/08(20:21).

98 http://www.idbs.com/ELN/ (15/09/05 10:28).

99 Hughs, G., H. Mills, et al., *Org. Bio. Chem*., 2004, **2**, 3284 - 3293.

100 Eikeren, P. v., *Org. Process Res. Dev.,* 2004, **8**(6), 1015 - 1023.

101 Prilusky, J., E. Ourillet, et al., *Acta Crystallogr. D*, 2005, **61**, 671 - 678.

102 Coles, S., *D-Lib Magazine.* 2007, **13**.

103 Coles, S. (http://R4L.eprints.org. 01-07-2008, 21:21).

104 Hooft, R. Data Collection Software. Nonius BV. 1998

105 Otwinowski, Z. and W. Minor, *Methods in Enzymology*. 1997, **276**, 307-326.

106 Mackay, S., C. J. Gilmore, et al. MaXus: a Computer Program for the Solution and Refinement of Crystal Structures from Diffraction Data. B.V. Nonius, Delft, The Netherlands and MacScience Co. Ltd, Yokohama, Japan,1988.

107 Farrugia, L. J. *J. App, Crystallogr.,* 1999, **32**, 837.

108 Brooker, L. G. S. and L. A. Smith, US Application No. 22335511, 1937.

109 Anon, *Zh. Obshch. Khim*. 1952, **22**, 2209 - 2214.

110 Clark, L. M., *J. Chem. Soc*., 1926, 232.

111 Wilson, C. D. and N. J. Metuchen, U. S. Application No. 2425774, 1947.

112 Kitzing, R., G. E. Ficken, et al. Application No. 24299/77, 1977.

113 Riester, O. Application No. DE929080, 1951

114 Gulland, J. M., G. J. Virden, *J. Chem. Soc*., 1928, 1478.

115 Brooker, L. G. S., *J. Am. Chem. Soc*., 1945, **67**, 1875 - 77.

116 Brooker, L. G. S., G. H. Keyes, et al., *J. Am. Chem. Soc*., 1951, **73**, 5350 - 5356.

Appendix

Key to Quaternary Salts

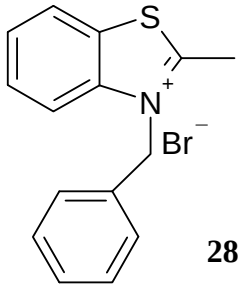 **28**	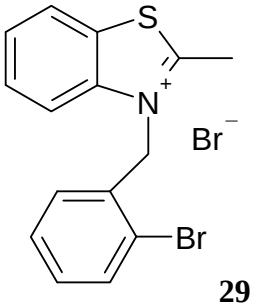 **29**	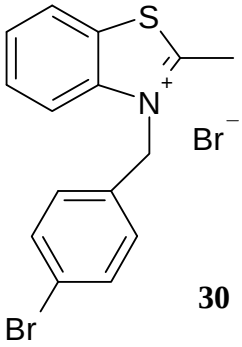 **30**
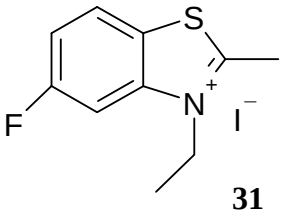 **31**	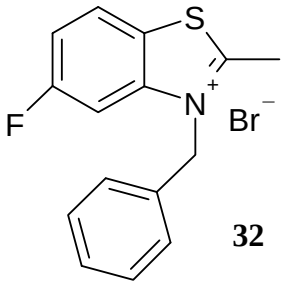 **32**	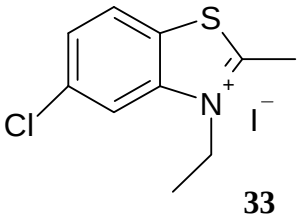 **33**
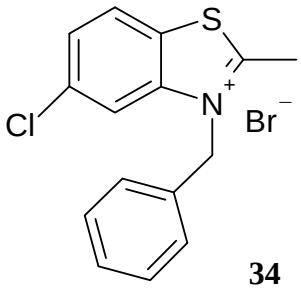 **34**	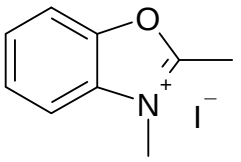 **35**	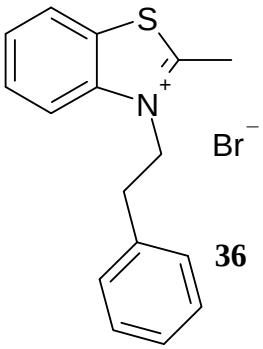 **36**
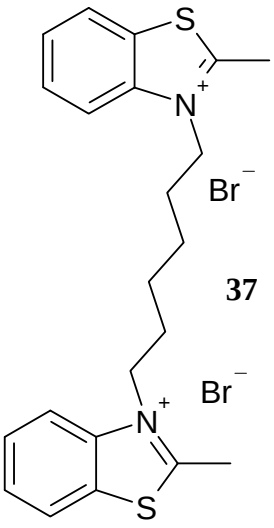 **37**	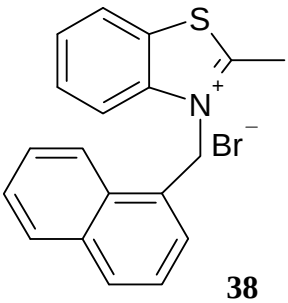 **38**	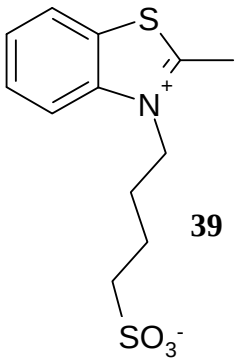 **39**

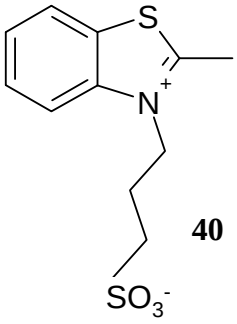 **40**	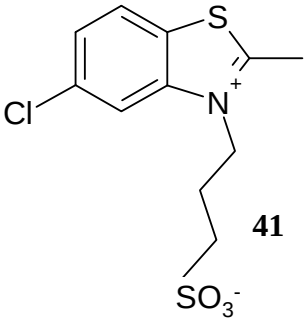 **41**	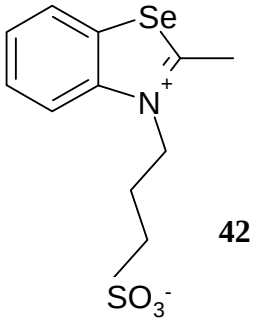 **42**
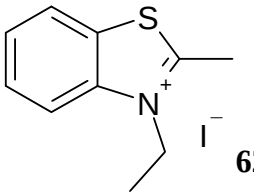 **62a**	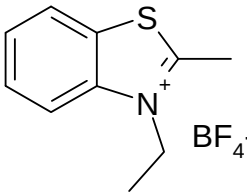 **62b**	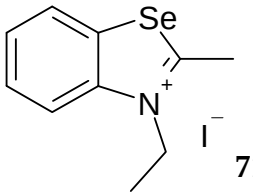 **71**

Key to Monomethine Dyes

Dye	Counterions		
	I^-	I_3^-	Br^-
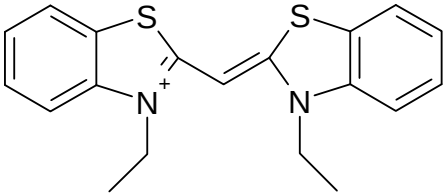	**3a**	**3f**	**3c**
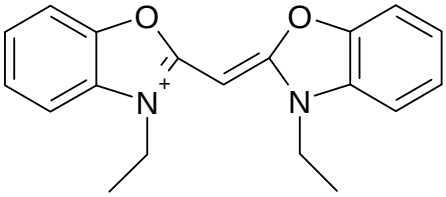	**44a**	**44b**	**-**
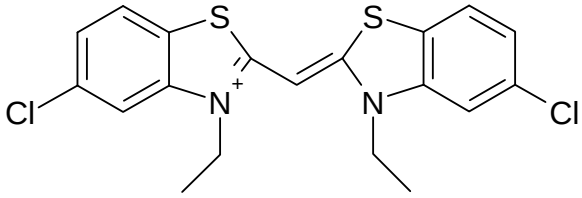	**45a**	**45b**	**-**
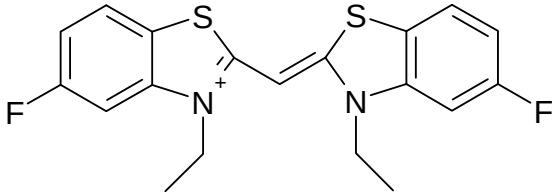	**46a**	**46b**	**-**
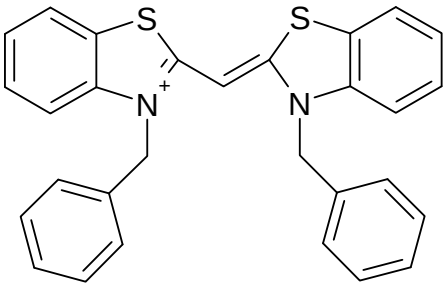	**-**	**-**	**47**
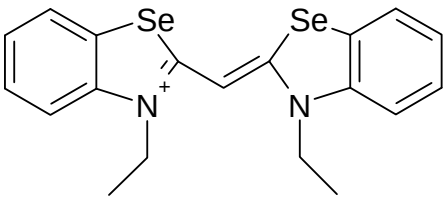	**64a**	**64b**	

Key to Trimethine Dyes

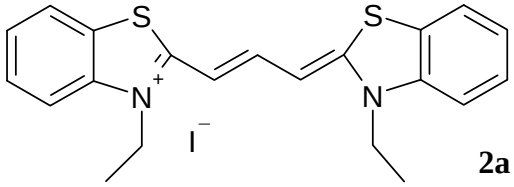

2a

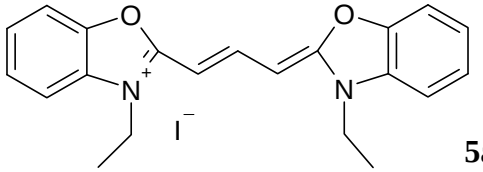

5a

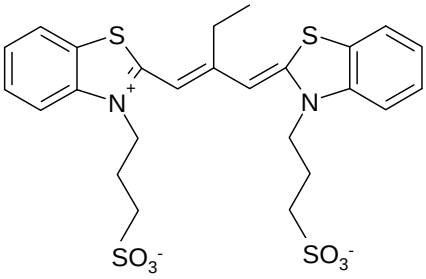

11

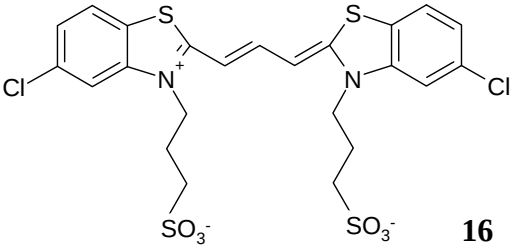

16

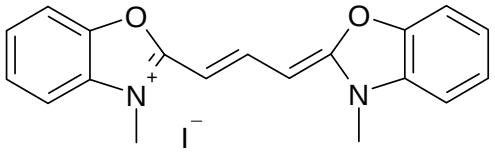

48

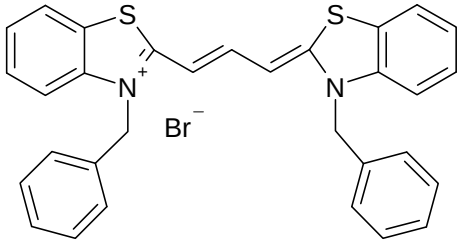

49

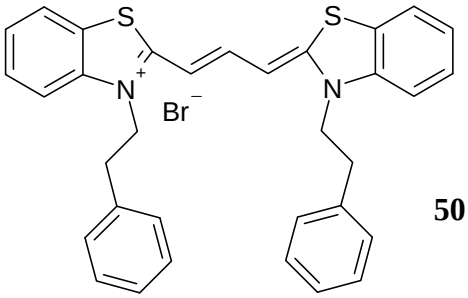

50

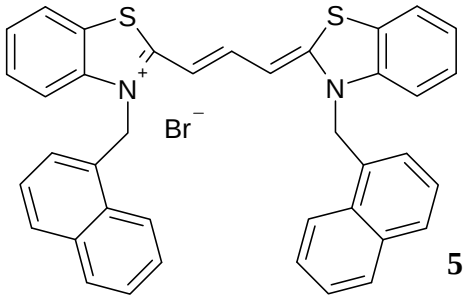

51

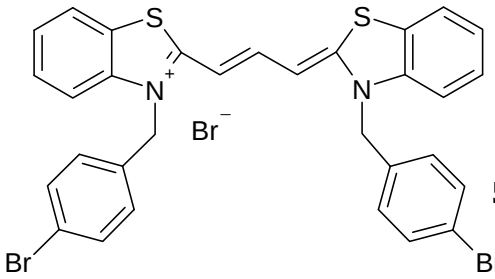

52

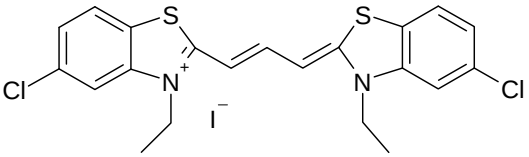

53

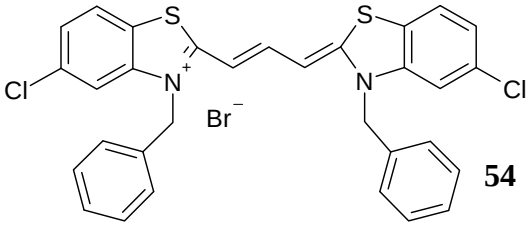

54

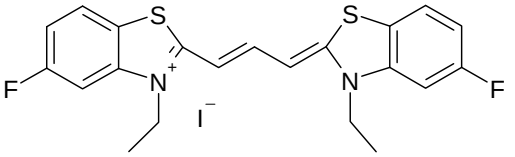

55

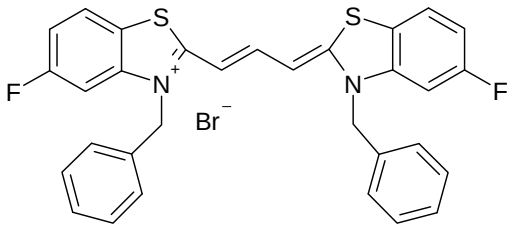

56

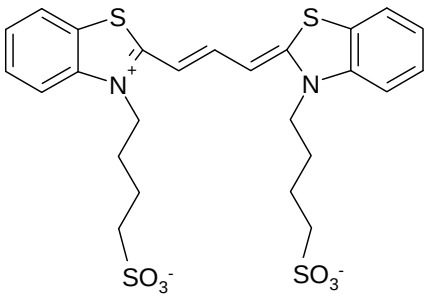

57

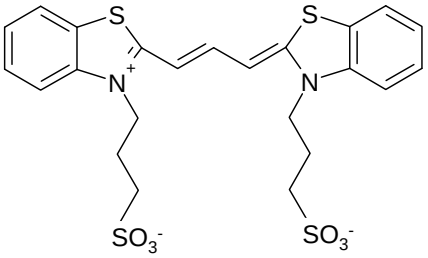

58

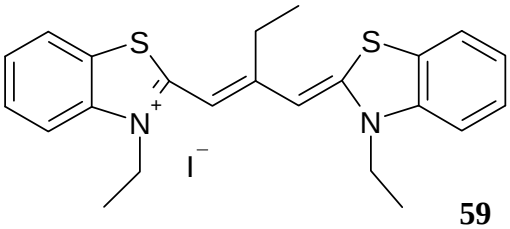

59

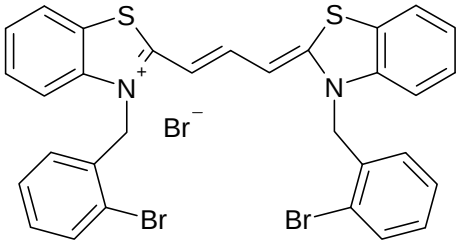

60

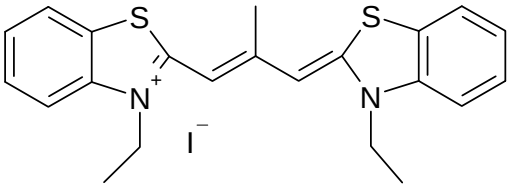

61

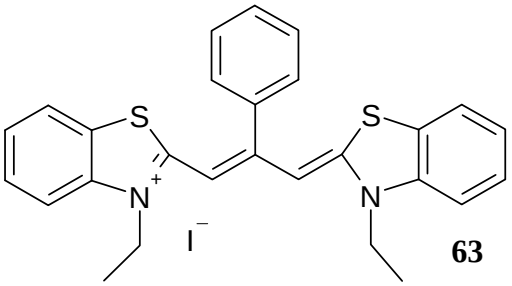

63

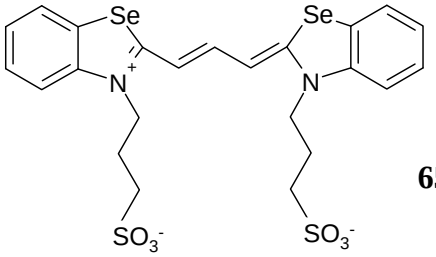

65

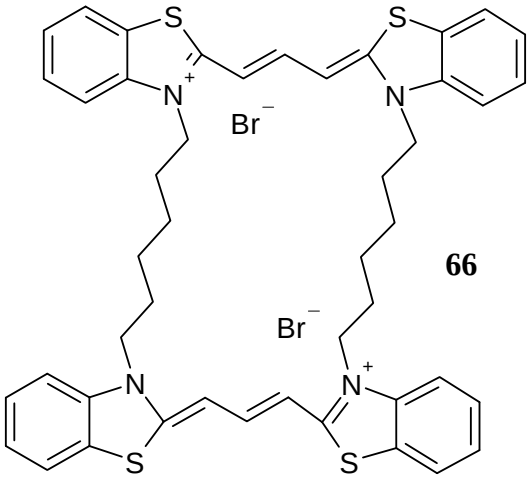

66

Key to Pentamethine Dyes